ME398 Final Product Report – AMPL Team

March 19, 2026

TRIPLE

Tri-Process Reconfigurable Integrated Platform for Lean Engineering

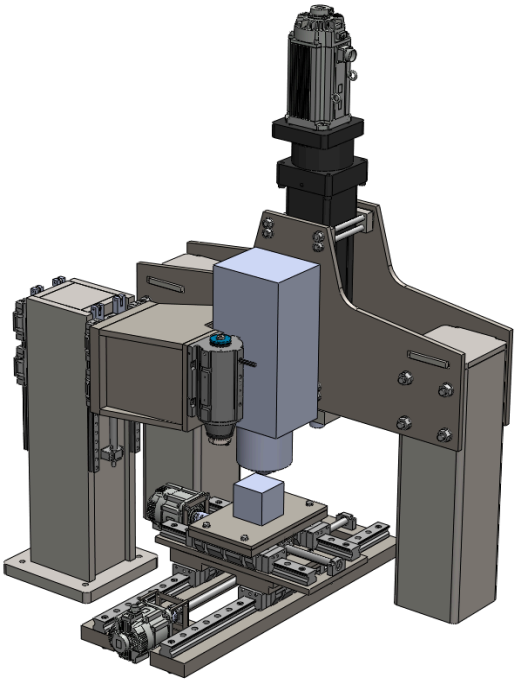

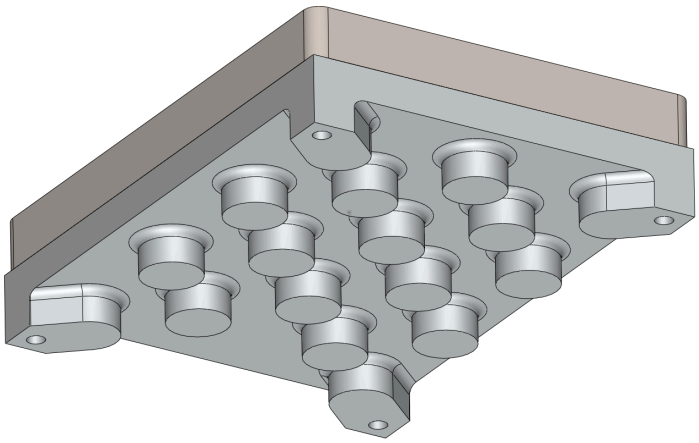

Submitted to

Professor David Gatchell, Professor Jeremy Keys

Submitted by

AMPL Capstone Team:

Adela Mihaela Jianu, Griffin Braunreiter, Jack Sokol, Joshua Hershey,

Michael Bayer, Ryan Kalgreen, Ryan Kelly, Santiago Rodriguez

Sponsored by

Northwestern University Advanced Manufacturing Processes Laboratory (AMPL)

Principal Investigator: Professor Jian Cao

Executive Summary

Hybrid manufacturing systems integrate multiple manufacturing processes into a single platform, allowing their advantages to compound. Northwestern University's Advanced Manufacturing Processes Lab (AMPL) is developing a hybrid manufacturing center that combines additive, subtractive, and forming processes into one machine to enable the production of complex geometries, reduce material waste, improve material properties, and increase manufacturing efficiency. The system incorporates laser wire directed energy deposition (DED), press forging, and conventional machining, with the long-term goal of producing functional Inconel 718 components within a compact, desktop-scale platform.

The team was tasked with designing a subsystem to support this effort. Because the project began in the early stages of development, and the primary challenge lies in integrating multiple processes into a single machine, the focus was placed on establishing a strong foundation for future system integration. This included defining system-level needs and metrics to guide design decisions.

During the first half of the project, a machine layout was developed based on these needs and metrics, and key frame and motion system components were designed using SolidWorks CAD and validated with ANSYS finite element analysis (FEA). Given the early stage of development, this area was selected as the project's focus to appropriately scope the work. Needs and metrics were iteratively refined to align with the lab's evolving objectives.

Due to the cost and lead time associated with full frame and motion system components, the team focused effort in the second half of the project on the development of a functional build plate as a critical, testable subsystem while still supporting design and simulation work on the previous work. The workpiece fixturing system interfaces directly with all three manufacturing processes and must simultaneously withstand high DED temperatures, forming compressive forces, and machining loads while protecting sensitive motion system components. Thermal simulations were conducted in ANSYS to evaluate heat transfer and inform design iterations, followed by experimental validation.

Testing was performed on scaled designs to ensure compatibility across all three processes. Results demonstrated that the build plate subsystem can withstand thermal exposure and mechanical loading while maintaining structural integrity and isolating critical components.

Final deliverables include a developed frame and motion system design with supporting FEA validation and selected components, as well as a validated workpiece fixturing subsystem supported by engineering analysis and testing data. This report documents the project background, design methodology, analysis, experimental results, and recommendations for future work. Accompanying CAD models and simulation files will also be provided to support continued development and implementation of the hybrid manufacturing system.

Table of Contents

List of Figures

List of Tables

Project Background

Mission Statement

We will develop a compact hybrid manufacturing machine that integrates additive, forming, and subtractive processes to support Northwestern's AMPL group. AMPL aims to enable efficient fabrication of high-performance metal parts. We will design the machine layout and frame components to support the needs of the processes. We will also design the motion system to provide the stiffness and multi-axis coordination needed to transition smoothly between them while ensuring precise, high-quality, and reliable results. Additionally, we will develop a workpiece holding system that keeps motion system components within their specified operating temperature ranges and withstands the required forming and subtractive forces without major deflection.

Problem Statement

To meet growing demands, the manufacturing industry is continually seeking ways to reduce lead times, streamline supply chains, and minimize material waste. One emerging solution is hybrid manufacturing, which integrates multiple processes into a single machine to enable the production of complex geometries—such as rocket engine nozzles or propellers—while improving efficiency and reducing waste. At Northwestern University's Advanced Manufacturing Processes Laboratory (AMPL), researchers are advancing this technology with support from the National Science Foundation's Hybrid Autonomous Manufacturing, Moving from Evolution to Revolution Engineering Research Center (NSF HAMMER-ERC).

AMPL is developing a system that integrates Direct Energy Deposition (DED), high-force compressive forming, and conventional machining into a unified platform. Each of these processes has inherent limitations when used independently: additive manufacturing can introduce porosity and poor surface finish, subtractive manufacturing generates significant material waste and limits geometric complexity, and forming lacks precision and flexibility. However, these shortcomings are complementary: each process can address the weaknesses of the others. Forming can densify and refine additively deposited material, machining can restore precision and surface finish, and additive manufacturing enables geometries unattainable by subtractive or forming methods alone. By integrating these processes into a single system, the hybrid approach leverages their combined strengths while mitigating individual limitations. This eliminates the need for part transfer between operations, preserves datums, and enables a level of part quality and manufacturing efficiency that exceeds what any single process can achieve.

The sequence begins with DED, which rapidly builds complex, near-net-shape geometries layer-by-layer with high material utilization. Crucially, the process involves the in-situ application of high-force compressive pressing after each deposited layer, a critical step designed to mitigate DED's common metallurgical flaws, such

as internal porosity, high residual thermal stress, and coarse-grain structure[1,2]. By applying high mechanical energy immediately following deposition, the forming process acts like an inter-layer hot isostatic press, significantly increasing material density, closing defects, and refining the microstructure. This results in final components possessing superior, often wrought-like, mechanical properties[1]. Finally, the conventional milling stage converts this structurally sound, near-net-shape part into a finished product, achieving the high dimensional accuracy and superior surface quality required for critical mating features—specifications that remain a primary limitation of both the DED and forming processes[3]. This single-setup, in-situ approach eliminates costly material transfer, re-fixturing, and alignment errors, fundamentally optimizing the production of robust, complex, and structurally sound components[4].

The commercial viability of integrating DED, forging, and milling on one platform hinges on balancing their radically opposed functional requirements within a shared operational space[5]. The system's core synergy stems from a shared, highly rigid base platform, the reliance on a CNC/robotic multi-axis gantry for precise tool-head positioning, and the essential need for a unified control interface for path sequencing and real-time feedback[5]. However, the machine design must resolve significant functional divergences, shown below in Table 1. The system must manage the high-precision thermal dynamics of the DED head and its associated environmental requirements (like an inert argon atmosphere) while the same machine structure must withstand and isolate the high dynamic loads generated by the in-situ press forging[6]. This engineering challenge requires a revolutionary machine architecture that successfully combines the structural rigidity necessary for high-force impact with the thermal and mechanical stability essential for high-precision subtractive finishing.

Table 1: Manufacturing Process Functions

Functional Category	Direct Energy Deposition (DED)	Press Forging	Conventional Milling
Material Type	Wire feed system	Solid workpiece	Solid workpiece
Thermal Requirements	A high-powered laser to melt the metal wire	Heated workpiece reduces the required forging force	Coolant is needed to cool the part and cutting tool

[1] Meiners et al., "New Hybrid Manufacturing Routes Combining Forging and Additive Manufacturing to Efficiently Produce High Performance Components from Ti-6Al-4V"

[2] Freitas et al., "A Review of Hybrid Manufacturing: Integrating Subtractive and Additive Manufacturing"

[3] Strong et al., "Hybrid manufacturing – integrating traditional manufacturers with additive manufacturing (AM) supply chain"

[4] Richhariya et al., "A Review of Hybrid Manufacturing: Integrating Subtractive and Additive Manufacturing"

[5] Sebbe et al., "Hybrid Manufacturing Processes Used in the Production of Complex Parts: A Comprehensive Review"

[6] Boivie et al., "Development of a Hybrid Manufacturing Cell; Integration of Additive Manufacturing with CNC Machining"

Motion Control	CNC motion system	High-force press	CNC motion system
Tooling	Deposition head with wire feed and laser	Forging press head(s)	Endmills, ballmills, and other cutting tools
Force Requirements	Low forces required to melt and deposit wire	High vertical force requirements to sustain consistent pressure	Medium axial force requirements to sustain machining forces
Environmental Needs	Inert environment or localized inert gas shielding	No specific environment needed, but a heated part is helpful	Method of clearing chips and containing coolant
Precision	High precision is needed for all axes	Overall, medium precision is likely needed. The precision needed in the z-axis will depend on the type of force application.	High precision is needed to achieve tight-tolerance parts
Safety & Shielding	Laser shielding and argon containment are necessary	Noise dampening and closed barriers to prevent hands from being in the forging area	Enclosed space to separate the operator from spinning tool, coolant, and chip spray

Subtractive manufacturing is the standard for many parts within the aerospace, energy, and defense industries, including examples like airframe brackets, steam turbine rotors, and missile housings. Computer Numerical Control (CNC) milling and turning are the most prominent subtractive processes. They allow for both high-mix low-volume manufacturing, where small quantities of a wide variety of products are made, and bulk manufacturing, where large quantities of a few products are made. However, both styles have high material waste and long lead times, up to six weeks for complex parts[7].

Inconel 718, a high-performance, nickel-chromium superalloy, is a popular choice for critical components in these industries due to its toughness, fatigue resistance, and high strength at elevated temperatures. Due to its expensive raw material composition, waste becomes extremely costly, and attempting to recycle such scrap is energy-intensive, with both Inconel and titanium (another popular material) having melting temperatures over

[7] DeBoer et al., "Additive, subtractive, and formative manufacturing of metal components: a life cycle assessment comparison"

1300 °C[8]. Subtractive processes are also unable to produce internal features and struggle with topologically optimized parts, requiring multiple axes and setups, where the single axis is only able to machine the top faces of the part. These restrictions limit designs in complexity and optimizations.

Additive manufacturing aims to remove some of those restrictions, allowing for more complex designs while eliminating most of the scrapped material. Currently, companies such as DMG Mori and Meltio have added direct energy deposition (DED) heads to conventional milling machines to allow for hybrid processes. But additive manufacturing also has its own limitations; specifically, the deposited material has disadvantageous properties, such as poorer accuracy and surface finish, where the layers can be seen on the outside faces, as well as increased porosity and anisotropy. While the accuracy and surface finish can be improved by post-processing with subtractive manufacturing, the other limitations cannot. The metal additive process desired for this machine is laser wire direct energy deposition (Laser Wire DED). Laser DED is more cost and material-efficient than other additive processes, and wire DED allows for quicker deposition than powder DED[9].

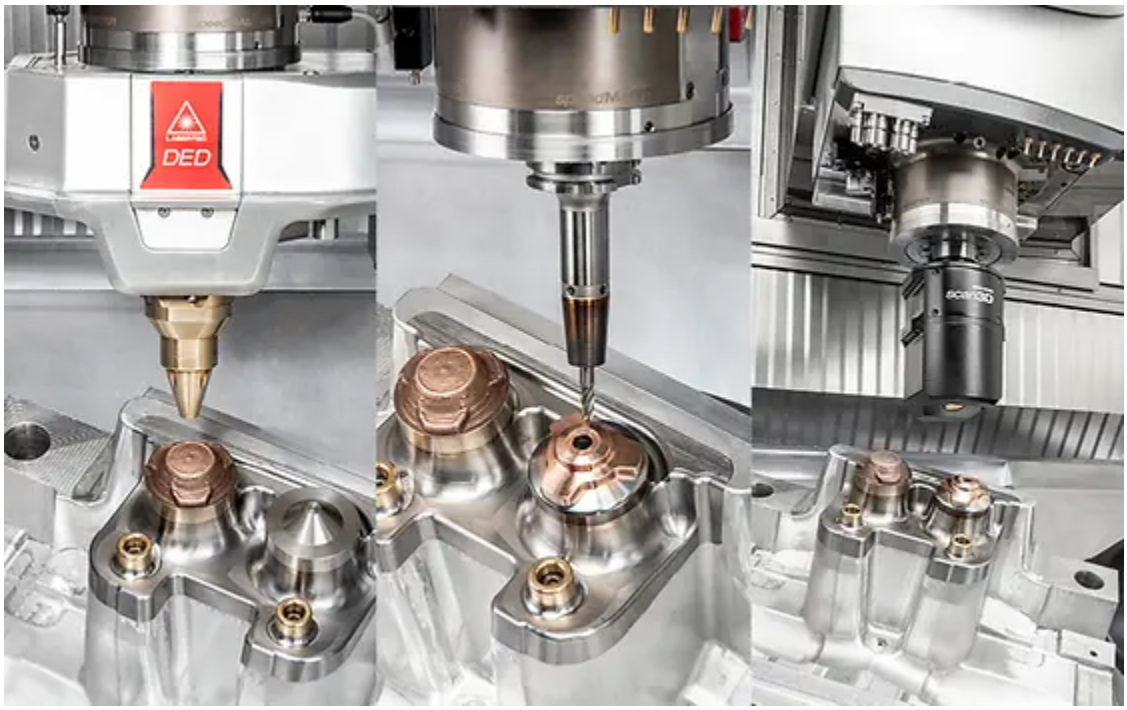

Figure 1: DMG Mori LASERTECH Hybrid Manufacturing Machine[10]

Currently, most industry examples of hybrid machines only integrate additive and subtractive manufacturing like DMG Mori's LASERTECH machine in Figure 1. AMPL aims to add forming to improve material properties and increase geometric accuracy. By incorporating forming immediately after additive manufacturing,

[8]American Elements, "Melting point of common metals, alloys, & other materials"

[9] Sciaky, "Benefits of Wire vs. Powder Metal 3D Printing"

[10] Image from DMG Mori

porosities can be eliminated, and the grain structure and alignment can be improved. Based on our client's requests, the desired forming process is open-die press forging. Press forging uses high forces and low to moderate strain rates to deform a hot or cold workpiece. Compared to subtractive processes, forging provides advantageous mechanical properties for parts in high-stress applications[11].

Of the three processes discussed, forging generally, and open-die forging in particular, are the most challenging processes to automate. Material handling has been the main focus for industry, in particular for the automotive and aerospace sectors[12]. Six-axis robot arms provide consistency and speed in material handling for closed-die applications, in addition to consistency of part geometry and quality in open-die applications[13]. Robot arms also remove people from the hazards of hot material handling in hot forging applications. There are several examples of fully automated forging lines in industry, but few, if any, at our intended scale.

Stakeholders

There are many individuals and groups associated with this project. The key stakeholders and considerations we are taking into account for each of them are listed below in Table 2.

Table 2: Primary, Secondary and Tertiary Stakeholders

Level	**Stakeholder**	**Key Considerations and Interests**
Primary	Professor Jian Cao, Carter Taylor, AMPL	Focused on creating a hybrid machine combining additive, subtractive, and forming methods. Primarily exploring how integrating forming can change metal microstructure to mimic true material properties and produce complex geometries, which is a novel area of research compared to traditional additive/subtractive machines.
	Machine Operators	Responsible for the physical loading, monitoring, and maintenance of the hybrid system to produce parts for both laboratory research and commercial clients.
	National Science Foundation (NSF)	Oversee the HAMMER-ERC grant; ensuring funds effectively advance hybrid manufacturing research.
Secondary	HAMMER-ERC Core Partners	Includes OSU, CWRU, UT, and NC A&T. Collaborate by focusing on different research areas and methods, allowing the NSF to distribute funds across a diverse range of goals.

[11] Groover, "Fundamentals of Modern Manufacturing," 5th Ed.

[12] Harrison, "A review of automation in manufacturing illustrated by a case study on mixed-mode hot forging"

[13] Yan et al., "Coordinated kinematic modelling for motion planning of heavy-duty manipulators in an integrated open-die forging centre"

	Academic Researchers	Utilize AMPL's published findings to advance the broader field of manufacturing science.
Tertiary	Northwestern University	Maintain institutional prestige and status as a premier global research hub, attracting researchers.
	Major Industries (eg. Aerospace, Medical, Auto)	Gain the ability to design stronger, more complex components through integrated forging capabilities.
	Machine Manufacturers (eg. DMG Mori, Additec, etc.)	Potential opportunity to commercialize a first-to-market machine combining all three manufacturing methods.

Competition and IP

Existing Implementations

Hybrid machining is a growing industry and a major focus of development in the manufacturing sector. Prior to beginning design on the TRIPLE we researched existing implementations. We used Google searches and ChatGPT to identify current commercial hybrid machining products. We found multiple that allow the combination of additive manufacturing, usually in the form of DED, and conventional subtractive machining. However, none of these products incorporates any sort of forming technique, a key piece of the problem that the AMPL team wants to address. The benchmarking matrix featured below compares existing products in the space.

Table 3: Review of Existing Commercial Hybrid Machines

Machine	Additive Process	Subtractive Process	Forming/ Forging Process	Details	Primary Benefit
DMG Mori *-LASERTEC 65 CNC Hybrid*	✓	✓		Integrates laser DED and 5-axis milling in one machine. 735 x 650 x 560 mm build envelope; Max laser power 3,000 W, max	Combines directed energy deposition (DED) with 5-axis milling in a single setup. Allows parts to be built and machined in one process, improving surface accuracy and reducing post-processing time

				workpiece weight 600kg 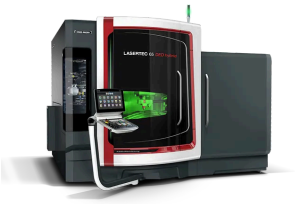	for complex metal components.
Romi *-Romi D Hybrid Series*	✓	✓		5-axis vertical machining center that combines additive metal deposition and 5-axis machining in a single setup to avoid re-fixturing. 	Uses laser metal deposition alongside 5-axis CNC machining. Suited for medium-sized parts where quick transitions between additive and subtractive steps help maintain alignment and dimensional precision.
Promation *-Dual Robotic Hybrid AM & SM Cell*	✓	✓		Multi-robot cell where one robot performs additive printing and another performs post-processing (machining). 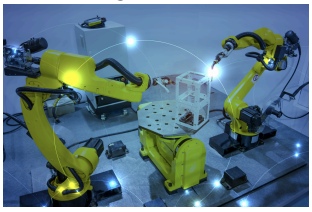	Robotic cell that integrates metal deposition with precision machining, and offers integration with localized mechanical forming.
Additec *-Hybrid 3*	✓	✓		Multi-tech platform combining LMJ, LDED, and CNC machining.	Compact hybrid system combining wire- and powder-fed DED with CNC control. Designed for small-scale production, multi-material work, and component repair with fine control over

				Minimum slice 0.24 mm. 	deposition parameters.
Matsuura *-Lumex Avance 60*	✓	✓		Integrates laser sintering and milling, building layer-by-layer. Build envelope up to 600 x 600 x 500 mm, layer build speeds: ~16 cc/h. 	Combines metal laser sintering with high-speed milling after each layer. Produces smooth surfaces and tight tolerances, making it effective for precision molds, dies, and conformal cooling geometries.
Meltio *-Meltio Engine CNC Integration*	✓	✓		Modular wire-laser DED unit designed to retrofit existing CNCs. Modular options available include dual-wire. 	Modular wire-laser DED head that can be mounted on CNC machines or robotic arms. Enables hybrid manufacturing or repair on existing equipment with multi-axis motion and lower system cost.

As seen in the table above, the ability to use forming processes is missing in all machines on the market. To find inspiration, our group turned to patents and published research articles for knowledge on the current approaches taken to including forming processes in hybrid machining.

Current Research

The research focus in this area has been on material properties and the grain structure of materials fabricated using DED and layer-by-layer (in situ) forming. When parts are created using DED, the grains are oriented in the direction orthogonal to the deposition layer plane. This results in anisotropic properties that can be detrimental to part functionality. Research laboratories have used forging to recrystallize the workpiece's grains and create isotropic properties, along with improved strength in all directions. To accomplish these tests, multiple groups have built machines that combine DED and forging techniques.

In one study, researchers applied forging methods simultaneously with material deposition from DED. A circular-crowned hammer applied strikes to the freshly laid bead of the material as the deposition head continued printing its layer of material (Figure 2)[14] . The benefits of this approach are that the material is still hot from the laser DED process, and therefore requires significantly less force in the forging process compared to if the workpiece were cooled to baseline temperature.

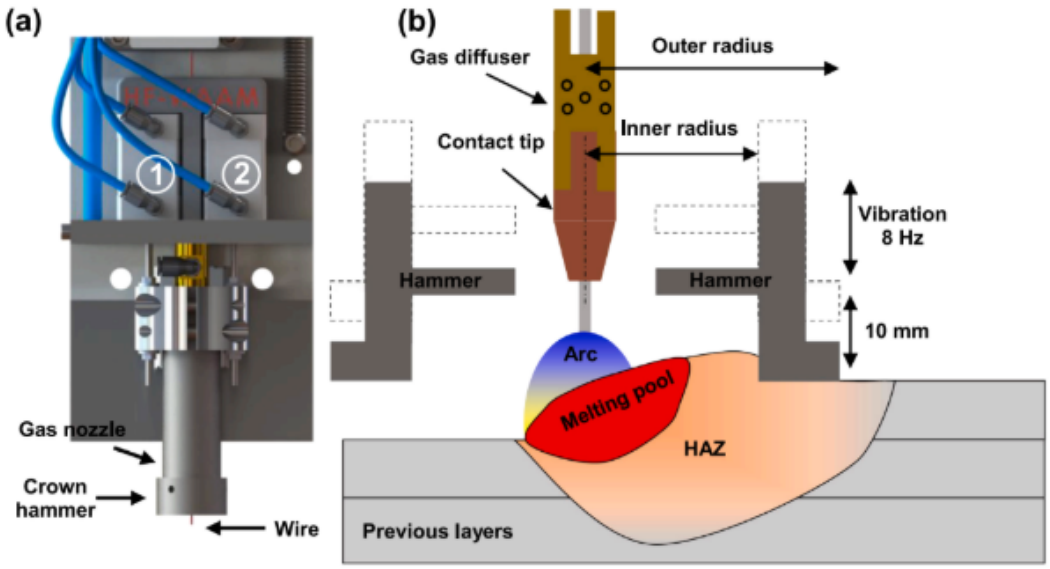

Figure 2: Schematic representation of arc-based DED and in situ forging.

Another research group took a similar approach, applying forging impacts shortly after laying down the material. However, rather than a circular-crowned hammer, theirs was a solid cylinder that followed the deposition head in the direction of deposition (Figure 3)[15].

[14] Farias et al., 2023

[15] Duarte et al., 2020

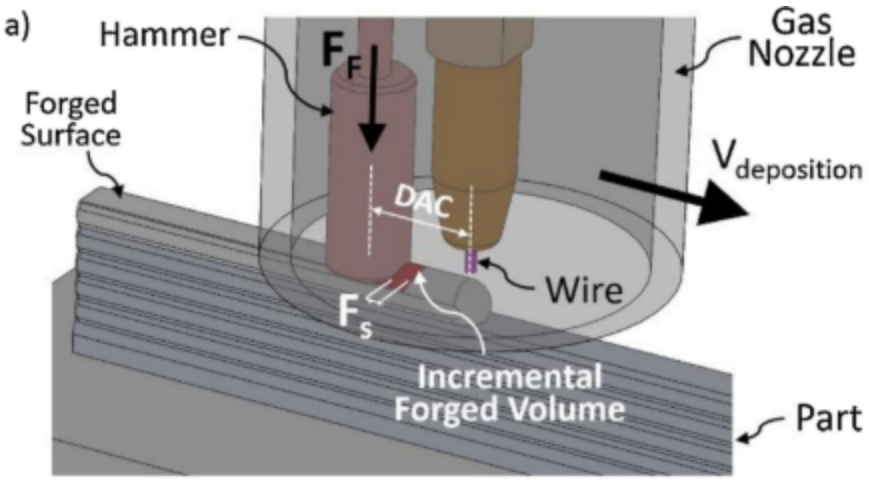

Figure 3: Schematic representation of forged area at each step.

Lastly, a research group in China tried a different approach to forging. Their group allowed each deposited layer to cool down to 50 ℃ before coming in with a separate forging head (Figure 4)[16]. Similar to the previously mentioned experiments, this resulted in the restructuring of material grains and an increase in maximal tensile and yield strength.

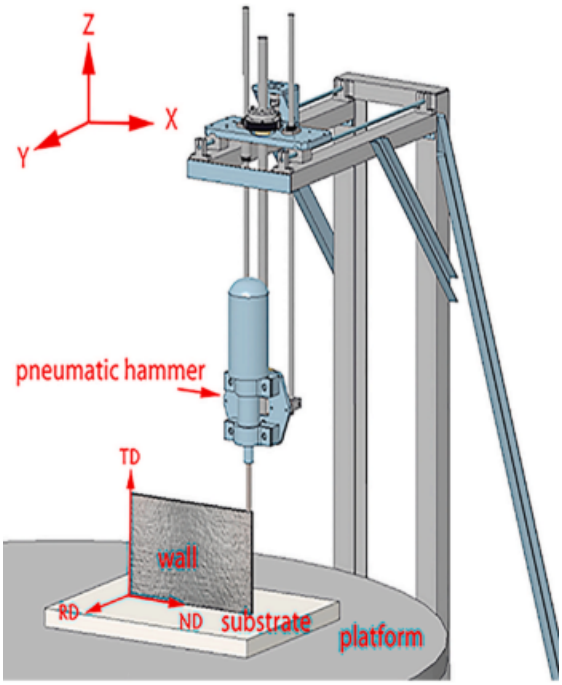

Figure 4: Schematic diagram of laboratory hammering equipment.

[16] Fang et al., 2021

Patents

Most machines that people have used to research hybrid manufacturing aren't patented, as they are primarily designed to study how different techniques and processes affect the material structure of parts, rather than to serve as commercial products. The focus in the industry has been on optimizing and comparing different forming/additive processes.

One patent presented a forging device that uses ultrasonic micro forging to improve the microstructure and mechanical properties of additively manufactured metal parts (Figure 5)[17].

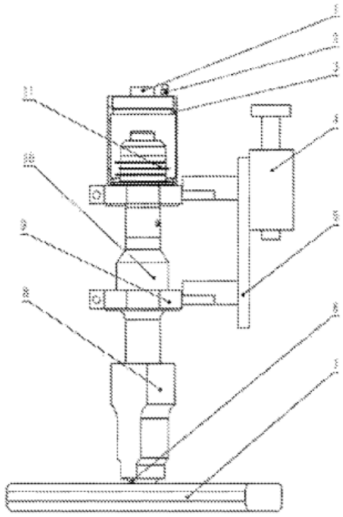

Figure 5: Combined Ultrasonic Micro-Forging Device

The device applies high-frequency ultrasonic vibrations through a small roller tool head that contacts each deposited layer during manufacturing. This process refines grains and improves uniformity in the metal deposition layer. Key components include a transducer, an amplitude transformer, a tool head with a roller, and a pneumatic sliding table that provides continuous downward pressure while also transmitting ultrasonic vibrations to the part. With respect to our project, this technique shows promising results for its use case, but does not directly align with our vision or specific goals. Our focus is on targeted press forging of very specific regions to alter the overall geometry of a part, a use case that does not appear well-suited to a roller-type forging system.

Another patent we reviewed described a system and method to perform dissimilar manufacturing operations (AM + SM primarily) in a single machine (Figure 6)[18].

[17] US11,110,513 B2
[18] WO2023004155A2

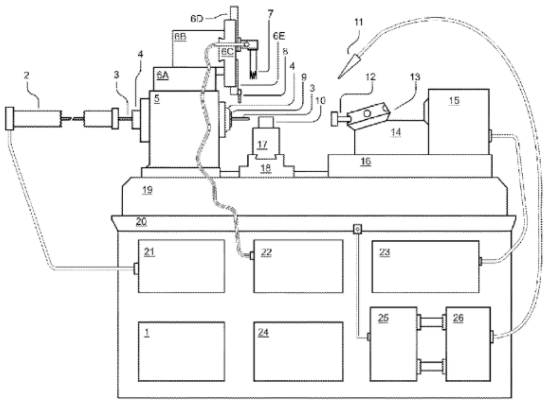

Figure 6: Single Machine Capable of Performing Dissimilar Manufacturing Operations

The machine uses modular tool heads, including a forming unit, machining spindle, and heating element, to transition between processes without removing the part. This approach improves alignment and accuracy by avoiding repositioning between steps.

In our case, the patent's idea of combining different operations in one system is interesting, but it doesn't align directly with our goals. It focuses on overall process coordination and efficiency, while our project is aimed at controlled, localized deformation of specific regions to adjust part geometry. The forming in this patent is more general and large-scale, not the targeted press forging approach we're developing.

As mentioned above, there are not many patents related to the project space that this team is tackling. This means that much of the design will have to be self-inspired and created from research into the specific manufacturing processes themselves, but also that patent infringement is unlikely for the TRIPLE.

Needs, Metrics, and Specifications

For this project, we worked to define three sets of needs, requirements, and specifications. Machine-level needs and specs are dictated by the processes involved and design direction from the lab. Motion system-level needs and metrics pertain to the structures and motion components of the motion system, and are derived from machine-level needs and metrics, additional research, and additional design direction from our client. Lastly, workpiece holding system-level needs and metrics drive structural and thermal design of our workpiece holding system, informed by the previous two sets of needs, component selections from our motion system prototype, and additional design input from our client. There is overlap between the needs of the different systems, so the needs tables restate needs from the machine level and maintain that need number

Machine Needs, Metrics, and Specifications

As a basis for our work, we created and continually updated needs and metrics for the entire machine, shown in Tables 4 and 5, respectively.

Table 4: Machine Level Needs

Category	Need Number	Need	Importance
Client Request	1	Machine can build a sufficiently sized part	5
	2	Combines desired manufacturing processes - laser wire DED, metal forming, subtractive manufacturing	5
DED/Additive Manufacturing	3	Environment protects against oxidation	1
	4	Capable of depositing desired material wire	5
	5	Compatible with existing laser wire DED head	4
	6	Material is accurately deposited	4
Forming Process	7	Press can deform workpiece	5
	8	Press head is durable	3
	9	Deformation size can vary	2
	10	Press heads can be changed automatically	1
	11	Workpiece is accurately deformed	4
Subtractive Manufacturing	12	Tooling can be cooled	3
	13	Chips can be cleared	2
	14	Cutting tool rotates at sufficient speeds	4
	15	Tooling is durable	3

	16	Workpiece is accurately machined	5
Integration	17	Tooling can be accurately positioned relative to the workpiece	5
	18	Part can be monitored while in progress	3

Table 5: Machine Level Metrics

Need	Metric	Marginal Value	Ideal Value	Units	Source/Comments
1	Build Volume	422	3375	cm^3	Client request (75mm and 150mm side length cube)
2	Number of Processes	2	3	processes	Client request
3	Environment Oxygen Content	0.2	0.1	% concentration	Client estimate
4	DED Head Heating Temperature	1345	1345	Celsius	Inconel 718 Melting Temps ASM Database High Temp Metals
4	Material Deposition Rate for laser wire DED	4.4	14.6	g/min Inconel	Laser Wire DED of Inconel 718
8, 11	Press Fatigue Life	$1.5*10^5$	$3.3*10^7<$	cycles to failure	Based on press size and build volume (rough calc)
9	Press Size	5	15	⌀ mm	Client estimate, and pressing force calculations
10	User input Needed for Tool Change	Yes	No	boolean	Client request
14	Air Flow Test	100	150	psi	Compressed air for chip clearing
15	Max Spindle Speed	6000	10000	RPM	Matching Shop CNC

Motion System Needs, Metrics, and Specifications

Additionally, we created needs and metrics for the motion system. The motion system, which includes frame components and machine layout, was chosen because any other critical system would rely heavily on how the machine was laid out and how it would move between the processes. Needs and metrics for the motion system are outlined below in Tables 6 and 7, respectively.

Table 6: Motion System Needs

Category	Need Number	Need	Importance
Client Requests	1	Machine can build a sufficiently sized part	5
	2	Combines desired manufacturing processes - laser wire DED, metal forming, subtractive manufacturing	5
Movement Control	17	Tooling can be accurately positioned relative to the workpiece	5
	19	Motion system provides each process with 3 axes of motion	5
	20	Axes movements are repeatable	5
	21	Axes movements are controlled	4
	22	Axes can move with sufficient linear velocity	4
	23	Motion system operates for duration of designed machine life	5
	24	Motion system can be maintained and repaired	3
	25	Motion system withstands vibrations from all processes	4
Subtractive	26	Axes can provide sufficient force for cutting	5
	27	Motion system operates with coolant present	2
	28	Motion system is unaffected by chips	2
Forming	29	Pressing force is effectively transmitted to part	5
	30	Motion system can withstand repeated loading	5

Table 7: Motion System Metrics

Need	Metric	Marginal Value	Ideal Value	Units	Source/Comments
1, 19	Linear Working Range per axis	150	300	mm	Client Request
2, 19	Number of Integrated Processes	2	3	processes	Client request, marginal is forming and additive processes only.
17, 30	Position Accuracy	10	5	μm	ISO 230-2, based on milling data
20	Position Variation (Repeatability)	5	2	μm	ISO 230-2
21	Velocity Error	5	1	%	Ward, 2022, depends on type of move
22	Maximum Velocity	6.5	21.5	m/min	Based off HAAS mini mill and super mini mill speeds, but may reevaluate lower for inconel cutting speeds
23, 30	Loading cycles to Failure	10^6	10^8	cycles	Criteria for infinite life
30	Pressing load at failure	21	224	Kilonewtons	Based off our press forming calculations for inconel 718 with a 5-15mm forming head here
23, 24	Working Life	5000	10000	Working Hours	Client Request
23, 24	Service Interval	100	500	Hours	Client Request
25	Resonant frequencies outside of ranges	1k-6k	1k-20k	Hz	Based off milling spindle speed
25	Machine Vibration Amplitude (from machine to environment)	0.9	1.1	mm/s RMS	ISO VC curves

26	X and Y Axis Drive Force	2520	8896	Newtons	Ideal based off HAAS mini mill, marginal off inconel machining calculations done here
26	Subtractive Z Axis Drive Force	2520	6000	Newtons	Pervais and Samad
29	Forming Z Axis Drive Force	21	224	Kilonewtons	Based off our press forming calculations for inconel 718 with a 5-15mm forming head here
27, 28	Interior Equipment Ingress Protection rating	66	67	IP	Based on coolant, chip and debris environment and ingress protection rating standards
29	Deflection of forming system during forming	1	0.5	mm	Working off of assumptions for deformation per press, 2mm layer height for DED, goal of 5% strain per blow, client request is this but it can be relaxed
30	System stiffness during subtractive machining	40	50	N/m	Based off of high-end of values for precision subtractive machines,

Workpiece Holding System Needs, Metrics, and Specifications

Our second critical system was the workpiece holding system. Our selected motion components had a limited operating temperature range, and controlling the heat that transferred from the build plate to the motion components is a critical task. The needs and metrics we developed for this critical system are below, in Tables 8 and 9 respectively.

Table 8: Workpiece Fixturing Needs

Category	Need Number	Need	Importance
General	1	The largest possible workpiece can be printed on the build plate	5
	31	The workpiece can be removed from the top build plate	4
DED/Additive Manufacturing	4	The top build plate surface allows commonly printed materials to be deposited	5
	32	The workpiece holding system does not let linear motion components exceed service temperature	5
	33	The temperature at the carriage plate can be monitored	3
	34	The plate can function under high temperatures	5
	35	The plate can be heated (stretch goal)	1
Forming	36	The workpiece holding system remains functional following repeated pressing operations	5
Subtractive	37	The workpiece holding system does not deflect excessively during machining	5
	38	The workpiece holding system can withstand vibrational loads	5
Ease of Use	39	The top build plate is easy to insert and remove from the machine	3
	40	The top build plate can be purchased/easily fabricated	4
	41	The top build plate can be reused	3

Table 9: Workpiece Fixturing Metrics

Needs	Metric	Marginal Value	Ideal Value	Units	Source/Comments
1	Build Area	$2.25*10^4$ (150^2)	$9*10^5$ (300^2)	mm^2	Client request
4	Number of compatible materials	3	5	#	Client request: must do Inconel, stainless steel, Ti alloys. Al alloys, tool steel nice to have
32	Temperature at Carriage Plate	80	60	Celsius	THK rails spec
33	Number of temperature sensors	1	2	#	Client Request
34	Minimum working temperature	1345	1345	Celsius	Inconel 718 Melting Temps ASM Database High Temp Metals
35	Active temperature at the top of the build plate	30	360	Celsius	Client Request
36	System Deflection	50	20	Micron	Ansys simulation results, deflection budget
36	Fatigue cycle life, forming	$1x10^7$	$1x10^8$	Cycles	Estimate for forming cycles for 100 (marginal) and 1000 (ideal) full-volume parts
37	Combined stiffness of workpiece holding + subtractive process	40	50	N/micron	Machine metrics
39	Number of nonstandard tools required to remove build plate	0	0	Binary	Client request
39	Time to remove build plate after print	5	1	Minutes	Client request
40	Cost of top build plate	500	350	$	Rough estimate from lab of current cost of consumable build plates, scaled up to our size.

40, 41	Machining setups to fabricate/prepare top build plate	3	2	#	Rough estimate of what may be feasible

Product Architecture

Our team was brought on board very early in the development of this machine, so our most pressing concern was outlining a project scope that would be achievable given our timeline, approximate budget, and collective skills. This process started by diagramming the high-level system functions, inputs, and outputs, informed by our background research and initial meetings with our client.

A solution-independent flow diagram of our client's hybrid manufacturing concept is shown in Figure 7 on the next page. It maps the high-level sequence of functions, with their respective inputs and outputs. We also created an expanded section that details the unique steps of each of the three manufacturing processes our client is looking to incorporate and the anticipated cyclic interactions between them.

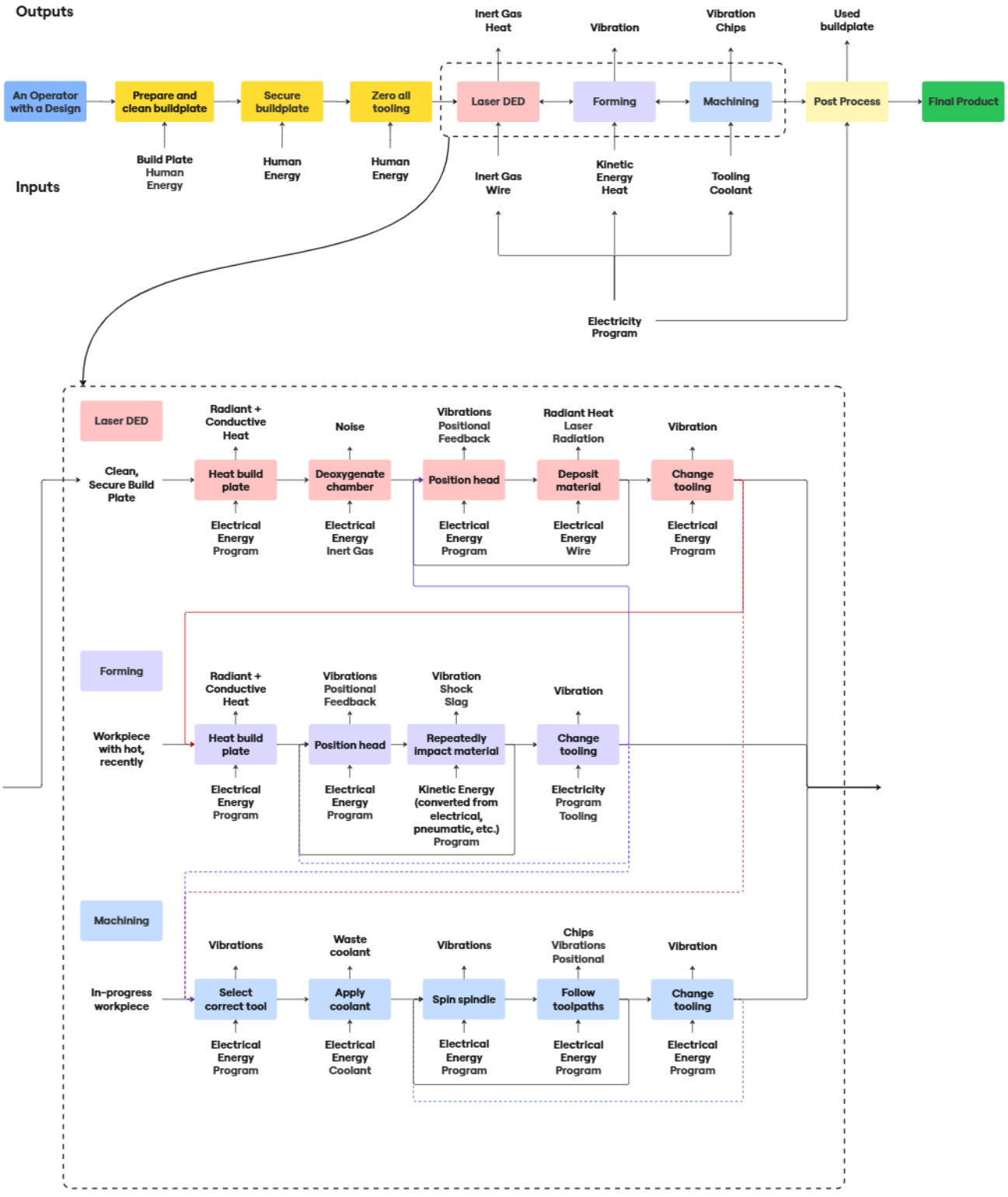

Figure 7: Functional Flow Diagram, Entire System

Workpiece Holding Architecture

The chart in Figure 8 follows the lifecycle of a build plate as it goes through the part creation process within the TRIPLE machine. Use this link for a clearer view: Build Plate Lifecycle Chart

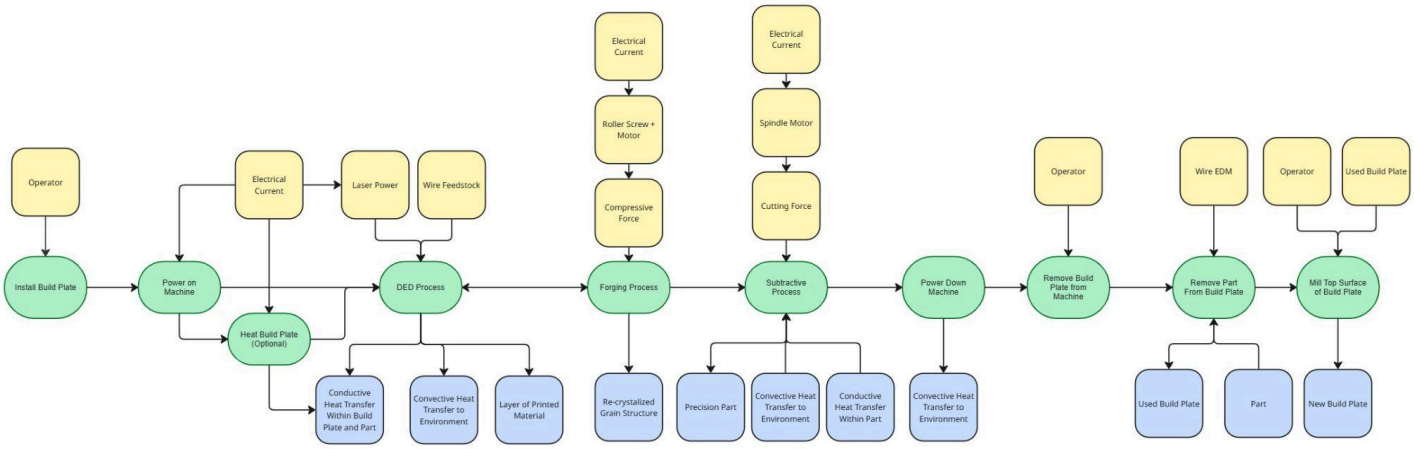

Figure 8: Build Plate Lifecycle Chart with processes (green), inputs (yellow), and outputs (blue)

Contextual Analysis

Global, Societal, Environmental and Economic Considerations

Hybrid manufacturing has shown potential for lower environmental and economic impacts compared with conventional CNC machining. In a lifecycle impact analysis done by Liu, Z.; Islam, F.; Era, I. Z.; Grandhi, M.,[19] the environmental impacts of CNC machining were compared to a hybrid manufacturing process that consisted of a DED base part followed by a CNC finishing process. The life cycle analysis was done during the manufacturing of a stainless steel 316 turbine blade. Five impact categories were considered: Global Warming, Acidification, Eutrophication, Ozone Depletion, and Photochemical Ozone Creation. Shown below in Table 10 are the initial results for each of the categories.

Table 10: Environmental Impacts Comparison

Impact Measure	Measurement	Hybrid Additive	CNC
Global Warming	Kilograms of CO_2	9.31	19.6
Acidification	Kilograms of SO_2	0.109	0.206
Eutrophication	Kilograms of NO_3	3.33E-3	4.12E-3
Ozone Depletion	Kilograms of CFC II	3.5E-9	9.35E-9
Photochemical Ozone Creation	Kilograms of C_2H_4	4.91E-3	1.43E-2

A normalization was performed to put the results on the same scale. The results are graphed below in Figure 9.

[19] Liu, Z.; Islam, F.; Era, I. Z.; Grandhi, M.

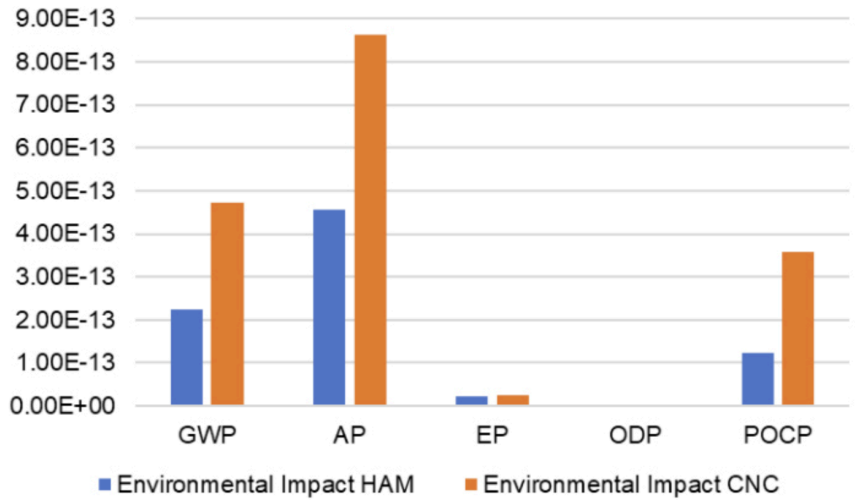

Figure 9: Environmental Impact Comparison Hybrid Additive vs CNC

GWP: Global Warming Potential; **AP**: Acidification Potential; **EP**: Eutrophication Potential; **ODP**: Ozone Depletion Potential; **POCP**: Photochemical Ozone Creation Potential

The hybrid manufacturing setup performs much better than conventional CNC machining in three of the categories; Global Warming, Acidification, and Photochemical Ozone Creation; while the other two categories are negligible for both setups. A large contributor to the difference is the energy inputs needed for the processes, shown below in Figure 10. The energy inputs for each setup are included in the below equations.

$$E_{HAM} = E_{Material} + E_{Pre-process} + E_{DED} + E_{Post-process}$$

$$E_{CNC} = E'_{Material} + E_{CNC-roughing} + E_{CNC-finishing}$$

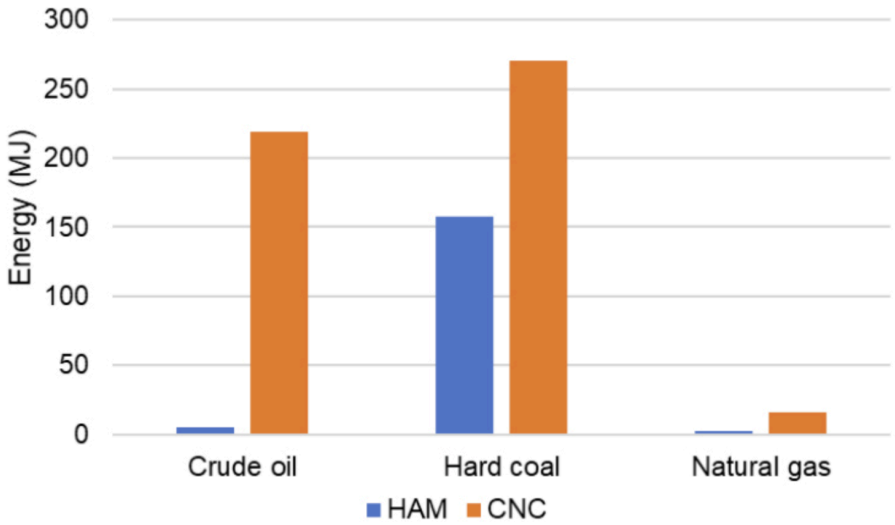

Figure 10: Required Energy Inputs, Hybrid Additive vs CNC

Much of the difference can be attributed to the higher transportation costs for CNC machining, with larger, heavier raw material needed compared to DED. Additionally, during the analysis, the paper took note that the buy-to-fly ratio, which measures the mass of the raw material compared to the finished product, was much higher for CNC machining than for the hybrid additive. CNC machining had a ratio of 5.53:1, while hybrid additive had a ratio of 1.34:1, representing a much lower material waste. They also noted that the hybrid setup took a total of 54 min to complete a single part compared to 60 min for the CNC program. While this is a small single part difference, this will stack over a mass production run, saving hours over thousands of parts.

This machine and similar hybrid manufacturing setups will also have societal and global impacts. Globally, they will increase the manufacturing gap between the world leaders and the rest of the world. Already, countries such as the United States, Germany, Japan, and China have a large lead on manufacturing capabilities, and hybrid machines will only serve to further that gap as the rest of the world does not have the resources to build their own. Sociologically, they will remove jobs. Where companies once needed three sets of operators to run the three separate machines, now one set of better trained operators will be able to function just as quickly.

Design Considerations

While the combination of wire DED, forming, and machining has the potential to reduce material waste compared with traditional manufacturing techniques, the costs and complexity of designing, building, and operating a tri-process hybrid machine will likely limit its efficiency. Our team's work supports the AMPL group in investigating how such a hybrid machine can create high-quality, high-precision metal parts. The goal is that this machine can be used as a starting point for research intended to address key challenges in hybrid manufacturing, including motion control, thermal management, grain structure, and other challenges. By creating a machine that can be used to study and refine these aspects, the project contributes to the long-term goal of making hybrid manufacturing machines more widely usable in high-precision manufacturing industries (such as aerospace) where they could eventually produce complex, high-strength parts. With a tri-process hybrid manufacturing machine, parts could be made with significantly reduced material waste and time, which is especially important for expensive alloys like Inconel. By creating the part's overall geometry through additive manufacturing, strengthening it with forging, and then refining dimensions through machining, a high-precision, strong part can be produced using a fraction of the material that would be required if it were machined from a solid block. Additionally, such parts could be produced very quickly without having to transfer them between machines specialized in one manufacturing process.

In the long term, hybrid machines like this have the potential to enable more sustainable and efficient high-performance manufacturing. However, significant research and development are still required before the material and time savings can fully offset the initial cost and complexity of building and operating such systems. We think that the work we've done designing this machine will contribute to these efforts and link our technical work to broader societal, economic, and environmental impacts.

Design Approach & Solutions

Concept Selection - Motion System

Once the function diagrams were created, and our needs and metrics were defined, the team progressed on to ideation. Ideation involved each team member sketching up various layout ideas for the machine, specifying the workpiece movement axes, tool head locations for manufacturing processes, and the general frame design. All sketches were then grouped by similarity, and six unique layout ideas were identified (Figure 11). The ideas ranged from designs where the workpiece was fixed (all movement coming from the tool heads) to those where the tool heads were fixed on a static frame (employing a tool-changing system akin to the HAAS CNC mills in the Ford shop). Many other combinations of tool and workpiece movement were considered in between these two extremes. After revising the sketches and considering which drive system to use for each axis, the six ideas were ranked in an alternative matrix (Table 11) to identify the best layouts. The selection criteria and their corresponding weights were provided to us by the client.

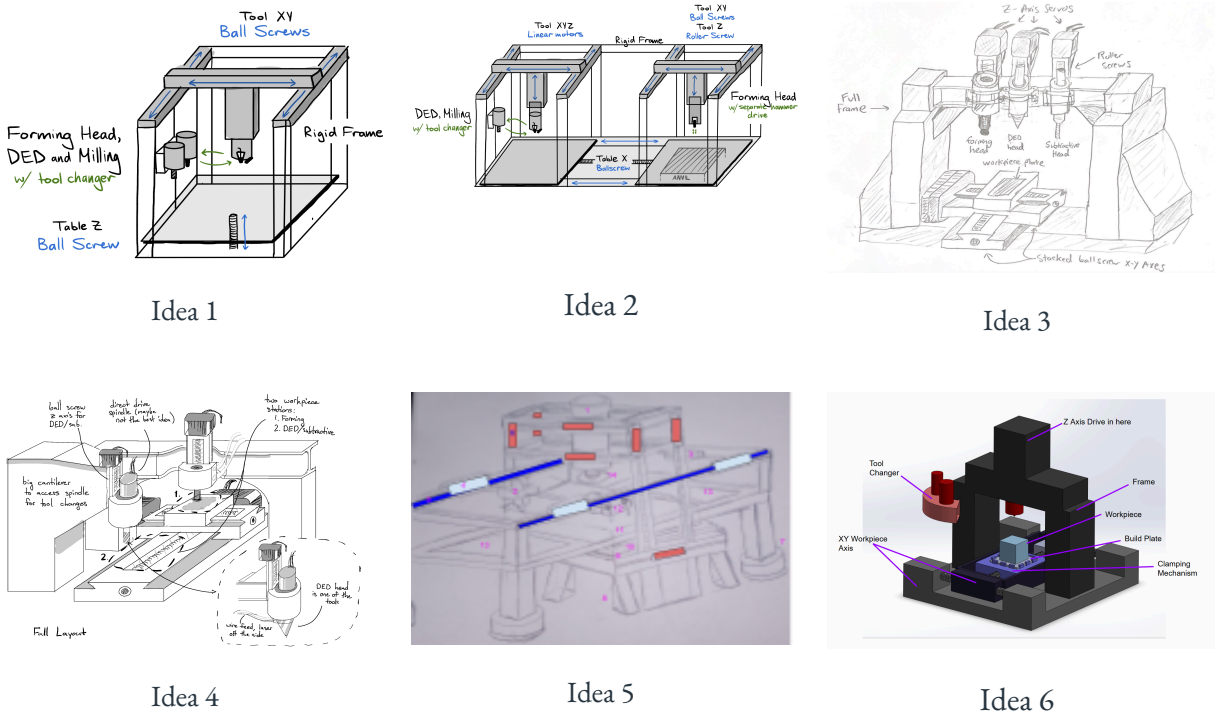

Idea 1 | Idea 2 | Idea 3

Idea 4 | Idea 5 | Idea 6

Figure 11: Initial Design Sketches

Table 11: Initial Layout Alternatives Matrix

LAYOUT IDEAS [1, 0, -1]							
		Idea 1	**Idea 2**	**Layout 3**	**Idea 4**	**Idea 5**	**Idea 6**
Selection	**Weight**						

Criteria	(%)	Score	Weighted	Score	Weighted	Score	Weighted	Score	Weighted	Score	Weighted	Score	Weighted
Cost	5	0	0	-1	-0.05	0	0	0	0	0	0	0	0
Simplicity	10	0	0	-1	-0.1	-1	-0.1	1	0.1	-1	-0.1	-1	-0.1
Workpiece Rigidity	20	1	0.2	1	0.2	1	0.2	1	0.2	1	0.2	1	0.2
Forming Head Rigidity	20	-1	-0.2	1	0.2	1	0.2	1	0.2	1	0.2	1	0.2
DED Head Rigidity	5	1	0.05	1	0.05	1	0.05	0	0	1	0.05	1	0.05
Sub Head Rigidity	10	1	0.1	1	0.1	1	0.1	0	0	1	0.1	1	0.1
Process Transition	20	1	0.2	0	0	1	0.2	1	0.2	0	0	1	0.2
Footprint	10	1	0.1	-1	-0.1	0	0	0	0	0	0	1	0.1
Total Score		0.45		0.3		0.65		0.7		0.45		0.75	
Rank		4		6		3		2		4		1	

Ideas 3, 4, and 6 received the highest ranking in the alternatives matrix. However, we ultimately selected Ideas 4, 5, and 6 for continued development. This adjustment was made because Ideas 3 and 4 feature similar moving build plates. To ensure a broader exploration of options, we decided to replace Idea 3 with Idea 5, offering a distinct layout with a stationary workpiece, thus diversifying the layouts carried into the next phase.

As we continued with our design process, it became clear that Idea 5 was far too complex. Each axis of movement required twice as many linear rails, ball screws, motors, etc., compared to the other designs, and the complexity and interference concerns between different sections were significant deterrents. This left us with two designs: the two-station design, with separate forming and additive/subtractive stations, and the single-station design with a toolchanger for each process. We made rough CAD models for both designs (Figure 12).

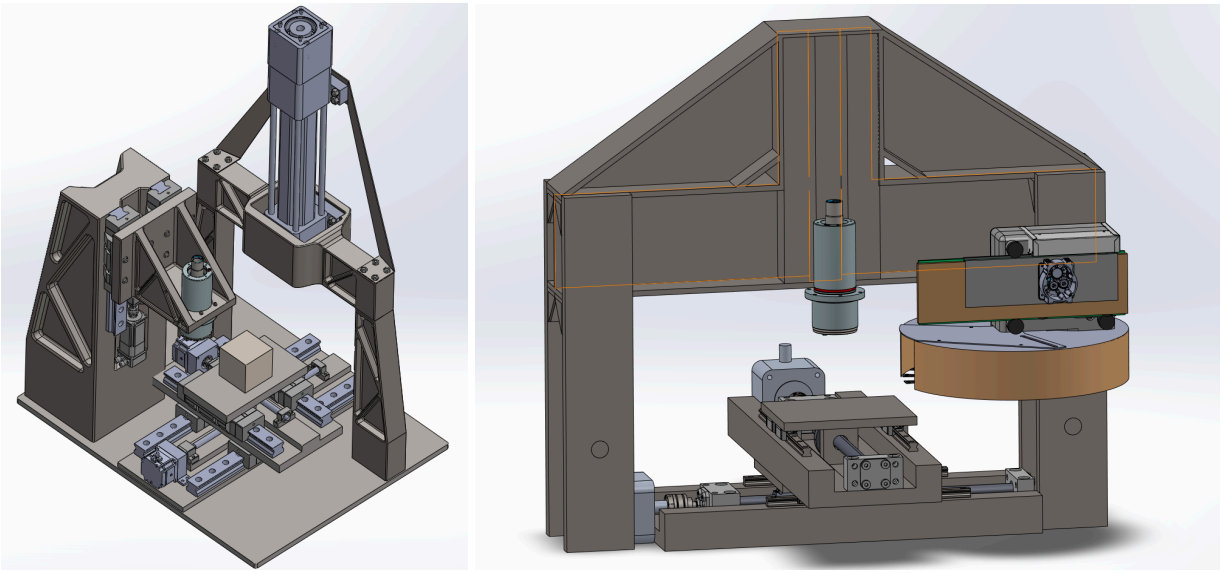

Figure 12: Initial Two-Station Design (left) and Single-Station Design (right)

The following alternatives matrix was filled out by all members of the team during a team meeting to decide on the final machine layout.

Table 12: Final Layout Alternatives Matrix

FINAL LAYOUT IDEAS [1, 0, -1]					
Selection Criteria	**Weight (%)**	Idea 4 **Two Station**		Idea 6 **One Station with Toolchanger**	
		Score	Weighted	Score	Weighted
Cost	5	0	0	0	0
Simplicity	10	0	0	-1	-0.1
Workpiece Rigidity	20	0	0	0	0
Forming Head Rigidity	20	1	0.2	-1	-0.2
DED Head Rigidity	5	1	0.05	0	0
Sub Head Rigidity	10	1	0.1	0	0
Process Transition	20	1	0.2	1	0.2
Footprint	10	-1	-0.1	1	0.1
Total Score		0.45		0	

Rank	1	2
Continue?	Yes	No

Based on the alternative matrix shown above in Table 12, the Two-Station layout was chosen over the Single-Station layout with a tool changer. The Two-Station is much simpler and has better rigidity in each of the three process heads. Additionally, the Two-Station design makes more sense in order to isolate the precision-dependent subtractive and DED heads on a separate frame from the high force and deflection forming head.

Final Design Overview - Motion System

Before going into detailed engineering analysis, here is an overview of the current motion system prototype developed from the two-station layout.

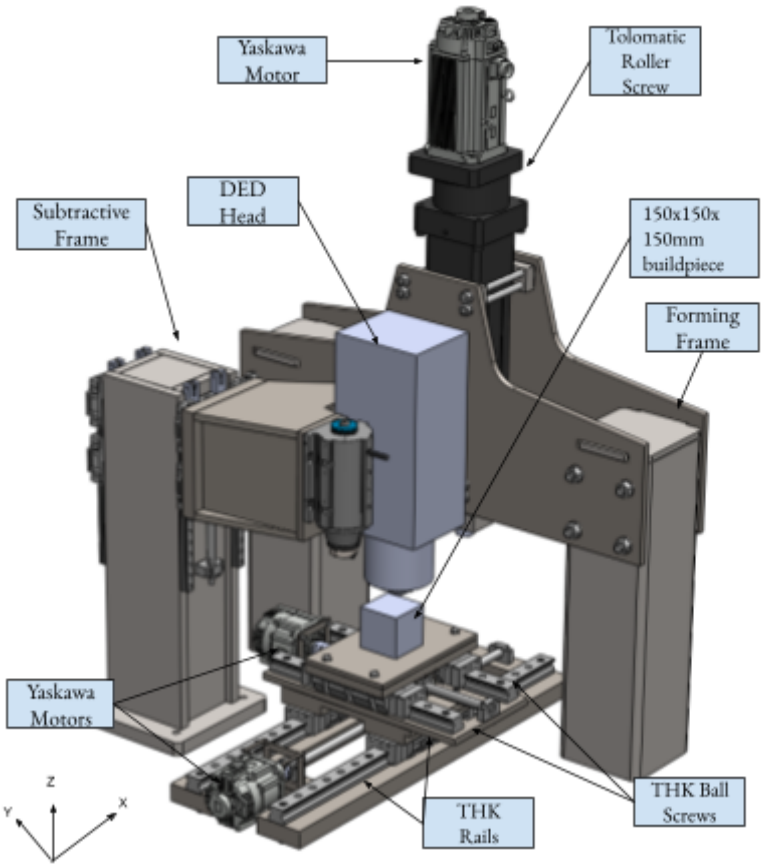

Figure 13: The TRIPLE

The TRIPLE (Tri-Process Reconfigurable Integrated Platform for Lean Engineering) is a manufacturing hub that combines additive, subtractive, and forming processes into one hybrid machine. There are two stations in the machine, a press forging station and a DED/subtractive station, connected by a single XY gantry. The press forging station includes two hollow, square steel uprights with two steel cross-member plates spanning them.

Mounted in the center of the frame is a roller screw that will drive our forming tool into the workpiece, capable of producing 294 kN of compressive force and inducing a 10% strain on a layer of Inconel 718 deposited by our DED head. The forming tool geometry is being designed by other members of AMPL.

The other station is for subtractive machining and laser wire DED. This station consists of a square steel tube filled with granite epoxy and reinforced with steel plate, and mounted to it is a cantilevered beam with a mill spindle and retractable DED head. The beam is mounted to vertical linear guide rails and a ball screw, allowing it to deposit and mill at any height of the 150mm cube workpiece. The mill spindle and DED head are being sourced by other members of AMPL.

An XY gantry system transports the buildplate between both stations. Each axis has an independent baseplate sliding on two rail/carriage pairs and driven by a ball screw. Fixed above the top baseplate is the part buildplate. This is where a part will be built by the laser DED system, and then subsequently moved to either the forging station or subtractive machining.

XY Gantry System

Similar to most conventional CNC machines, the basis for the design of this XY gantry system is two stacked ball screw assemblies, which was chosen to compactly fit within the forming frame uprights. The X axis extends between the forming frame and the subtractive frame, allowing for full range of motion for each of the three processes. The Y axis is mounted to the X axis carriages, and allows for the second degree of freedom in the XY plane. Everything is mounted together using 4130 steel.

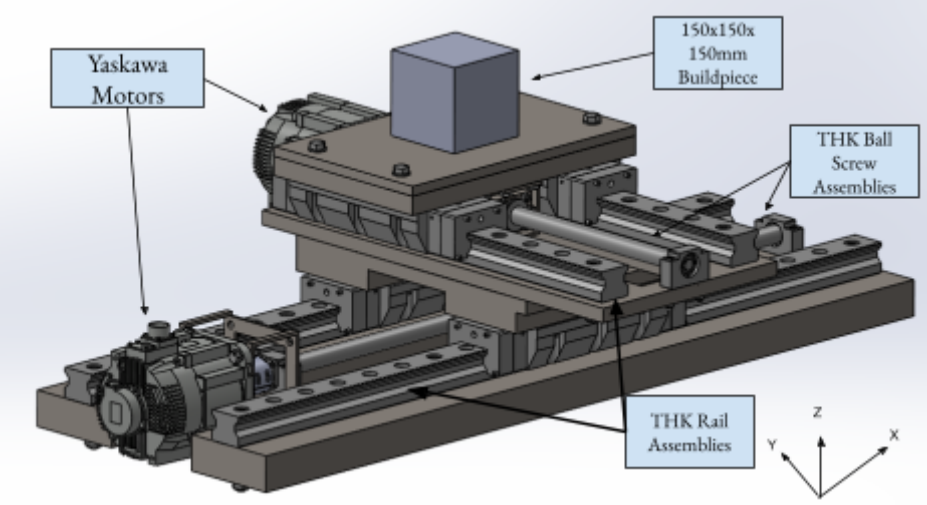

Figure 14: XY Gantry Design, End of Q1

The entire system weighs ~650kg (~1430lbs), which includes a full 150mm by 150mm by 150mm buildpiece. It fits in a 1600mm by 1000mm footprint. The top of the build piece sits 535mm above the bottom of the baseplate, though this does not include mounting bolts that extend below the plate.

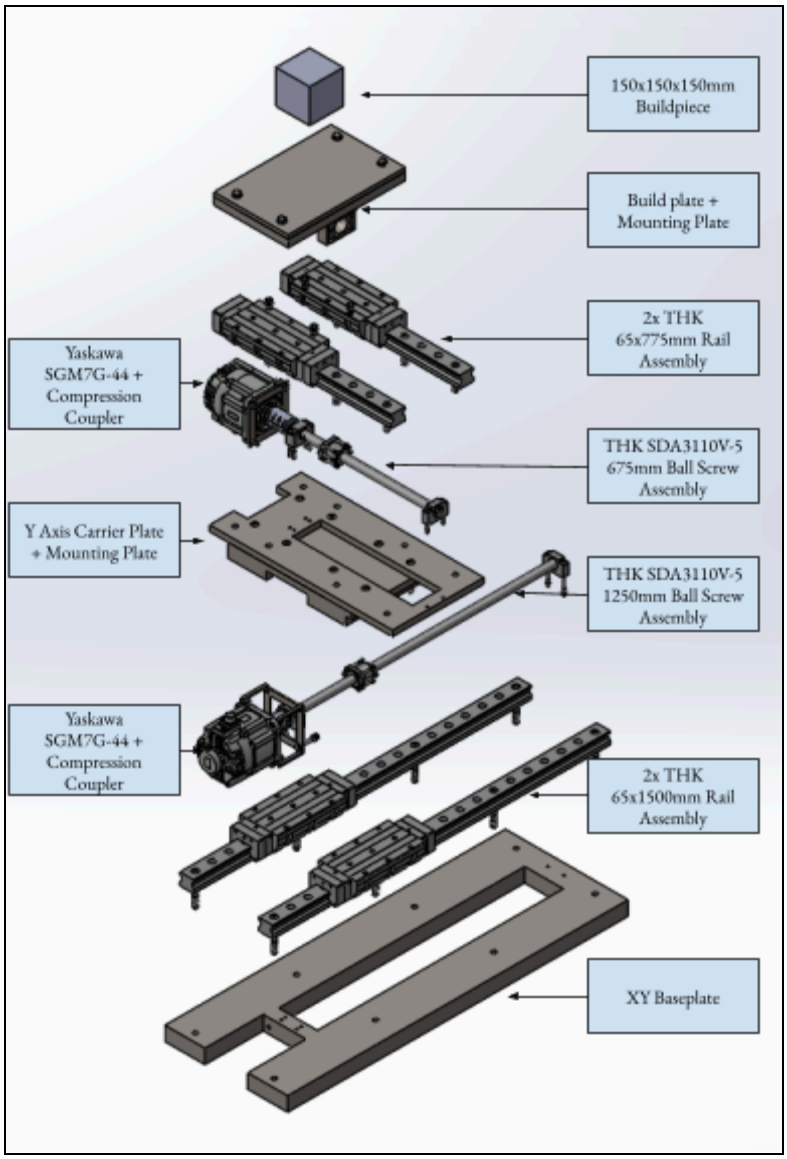

Figure 15: XY Gantry Exploded View

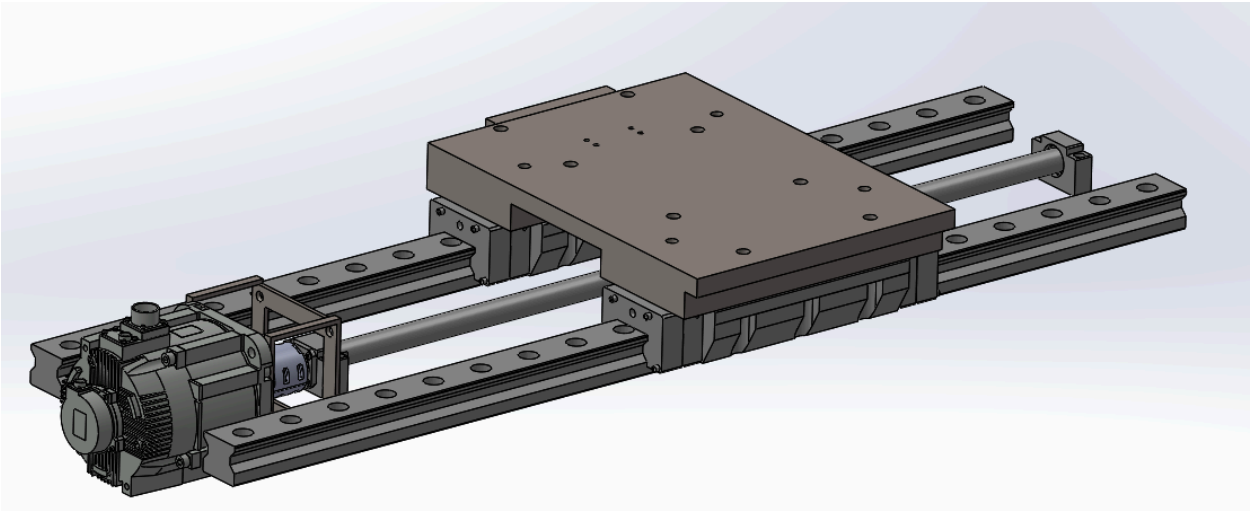

Figure 16: X Axis Assembly

The X axis is centered on the heads of both frames, with the ball screw directly below the heads, pushing at the center of mass of the mounting plate. The mounting plate is attached to the carriages using M16 socket head screws, using the pre-tapped holes in the carriages. The Y axis baseplate is mounted on top of the X axis carriage mounting plate. The Y axis is similarly designed to the X axis, though the rails are mounted closer together to reduce deflection of the build plate and its mounting.

The ball screws are attached to the mounting plates using custom deflection adapters, shown in green below in Figure 17. This adapter is designed to reduce the amount of force that the ball screw receives due to deflection of other components under full forming loads. The thin tabs that connect the center ball nut mount to the outer body are 1/16" thick and are designed to intentionally deflect when the outer body is forced downwards.

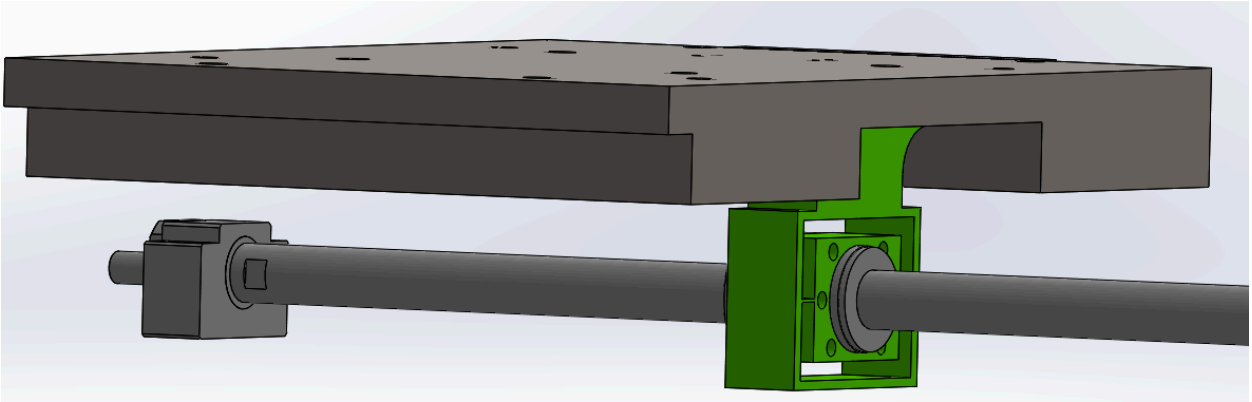

Figure 17: Ball Screw Adapter (green)

The Yaskawa SGM7G-44 motors are coupled to the ball screws using stepped compression couplers (Figure 18), which transmit torque through friction. The motors and ball screws are designed with machined ends with the motor output being 35mm and the ball screw being 17mm. Because of the large size difference, a keyed coupler is not used, as broaching a keyway would be impossible with the shoulder that is introduced with the step down

in size. This coupler would have to be custom made as suppliers do not sell couplers with such a specific, large size difference, with the largest step down that McMaster sells being 35mm to 19mm.

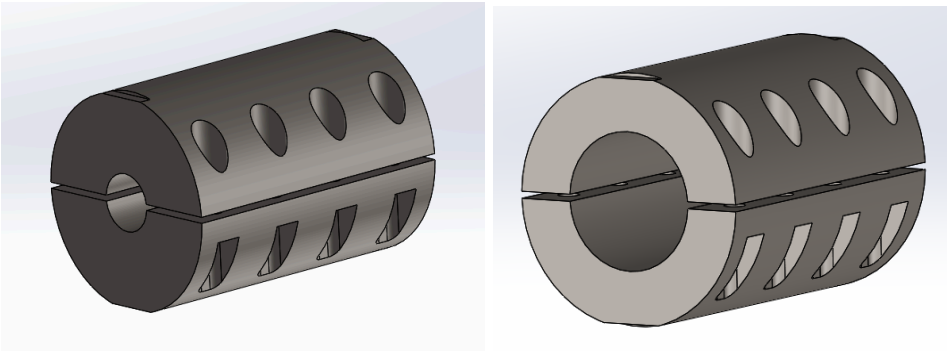

Figure 18: Compression Coupler: 17 mm Side (left), 35 mm Side (right)

Forming Frame

Drawing inspiration from commercially available presses, the forming frame design utilizes 1018 mild steel square tubing (320x320mm profile, 12.5mm wall thickness) for a pair of uprights and 25mm thick A36 steel plate for a pair of crossmembers. The roller screw is mounted between the crossmember plates, and the uprights would have provisions at their base to attach to the machine base plate/table. See Figures 19 and 20 below for a labeled diagram and exploded view.

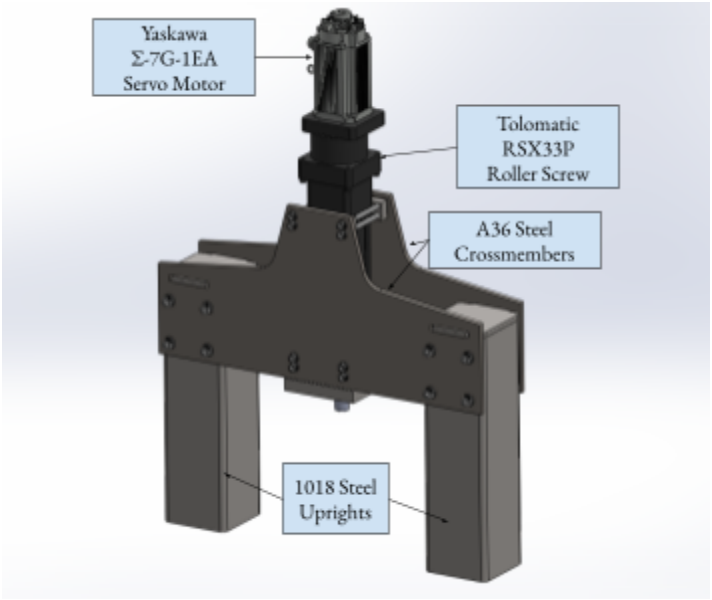

Figure 19: Forming Frame Design, End of Q1

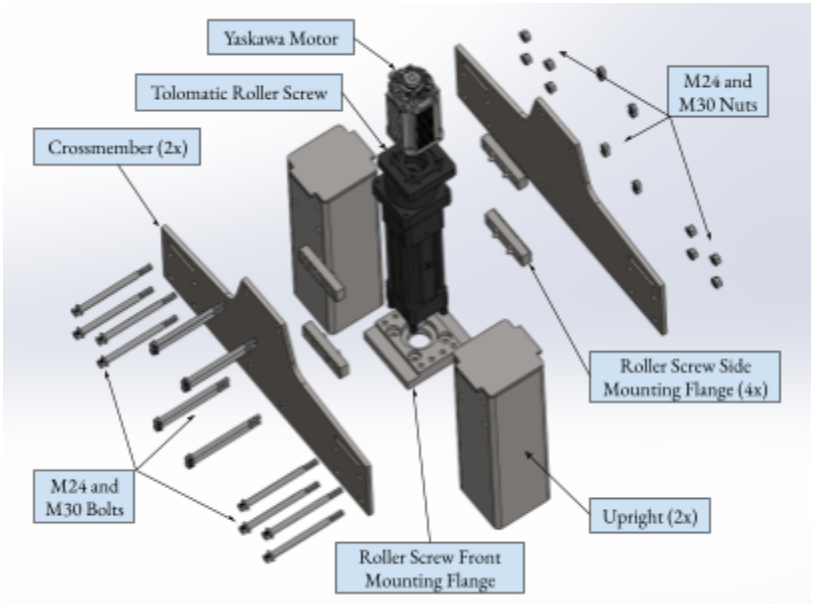

Figure 20: Forming Frame Exploded View

The roller screw is secured to the crossmember plates by eight Class 12.9 M24 bolts, and the crossmembers are secured to each uprights by four Class 8.8 M30 bolts. Full stress analysis was conducted on these joints, to be detailed further, and design details highlighted below in Figure 21 relieve some of the shear load off of the bolted connections. The assembly weighs 940kg (~2070lbs), and stands just over 2.5m (8'2") tall.

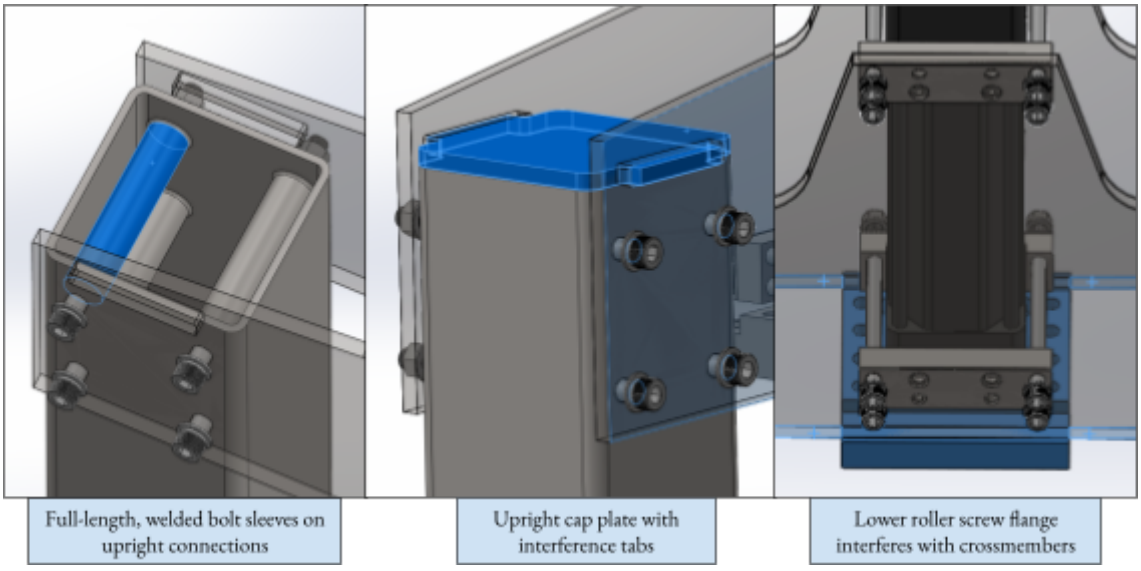

Figure 21: Shear Relief Design Features

The crossmember and upright designs are intentionally simple. Necessary holes are added for the hardware, and the crossmember slowly grows taller near the center to accommodate all of the required roller screw mounting. The lower roller screw flange is designed to be the point of adjustment for aligning the screw; it can be adjusted to square up the screw axis before the other mounting bolts are secured (see Figure 22).

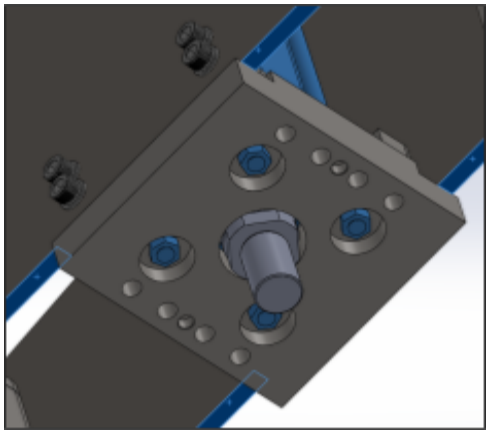

Figure 22: Four Flange Bolts Provide Adjustment

Subtractive Frame

Drawing inspiration from commercial and DIY C-frame vertical axis mills, the subtractive frame is made from a stationary vertical post supporting a moving Z axis cantilever. While both the subtractive and additive toolheads are mounted at the distal end of this cantilever, we have named this part the subtractive frame because it is primarily designed to withstand the subtractive process forces while machining with precision, and if it can do that it will be able to achieve the precision for the additive process. Currently the frame weighs 1497 kg and is 127cm tall.

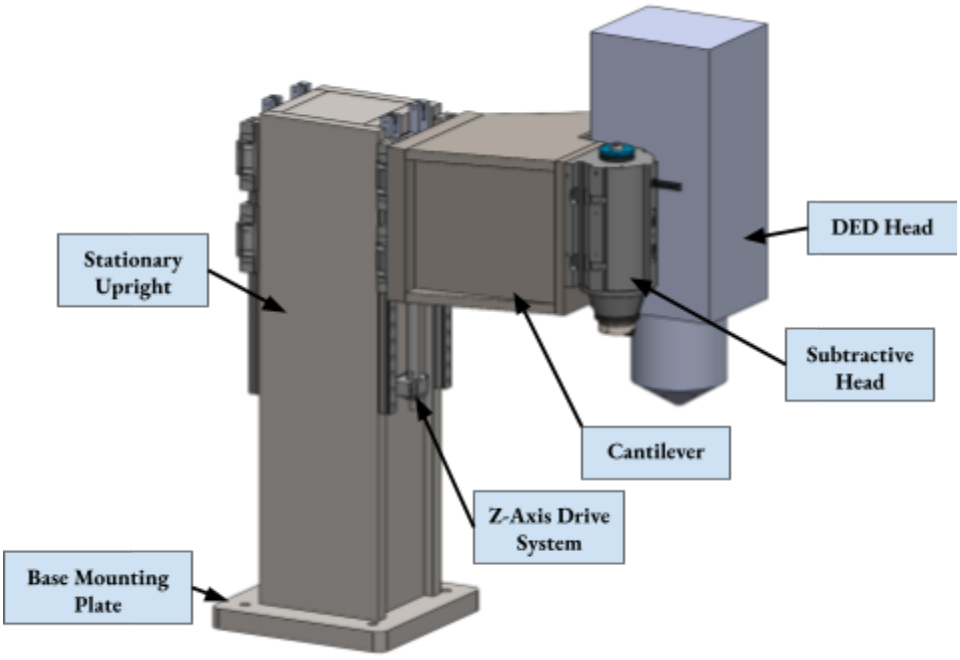

Figure 23: Subtractive Frame Design

The upright column is built from 1.5 inch thick welded A500 grade B steel plates and filled with a granite epoxy. The steel plates provide the torsional stiffness required for machining, but a solid steel beam is impractical due to cost, weight, and manufacturing difficulty. The epoxy granite filling means it is easier to assemble the frame and epoxy granite is commonly used in CNC machines to add mass and dampen vibrations.

The Z-axis cantilever beam is also constructed from welded ½-1.5 inch A500 grade B steel plates and filled with a granite epoxy. AMPL is still working on procuring the DED head and milling spindle so a potential candidate for each is displayed in the CAD and only generic mounting points are designed.

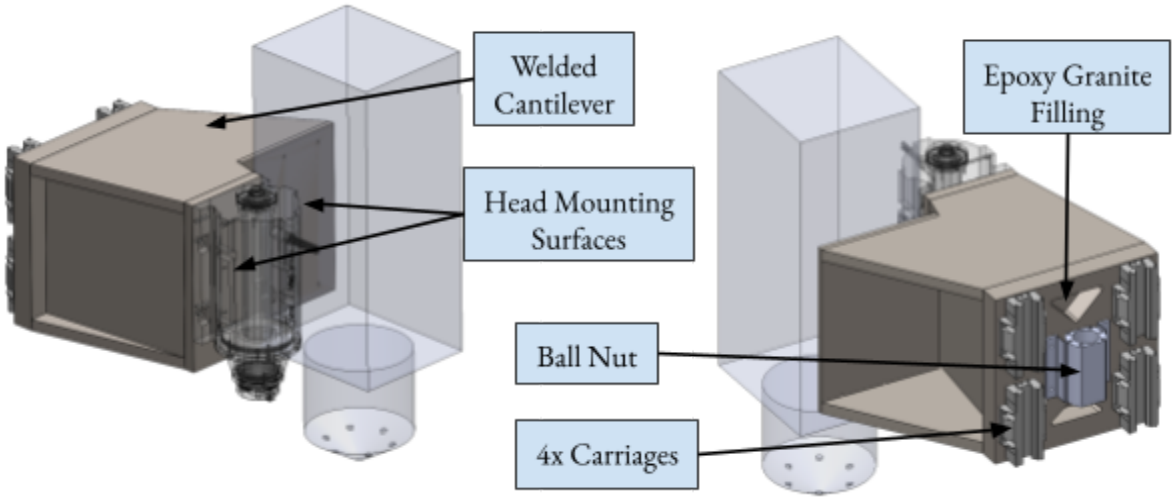

Figure 24: Subtractive Frame Cantilever

On the back of the cantilever are four carriages that attach to rails on the upright. These take the XY loads and moments from machining while allowing translation in Z. The Z translation is transferred to the cantilever through a ball nut adapter that prevents machining forces other than Z forces from being transferred to the ball screw that drives it.

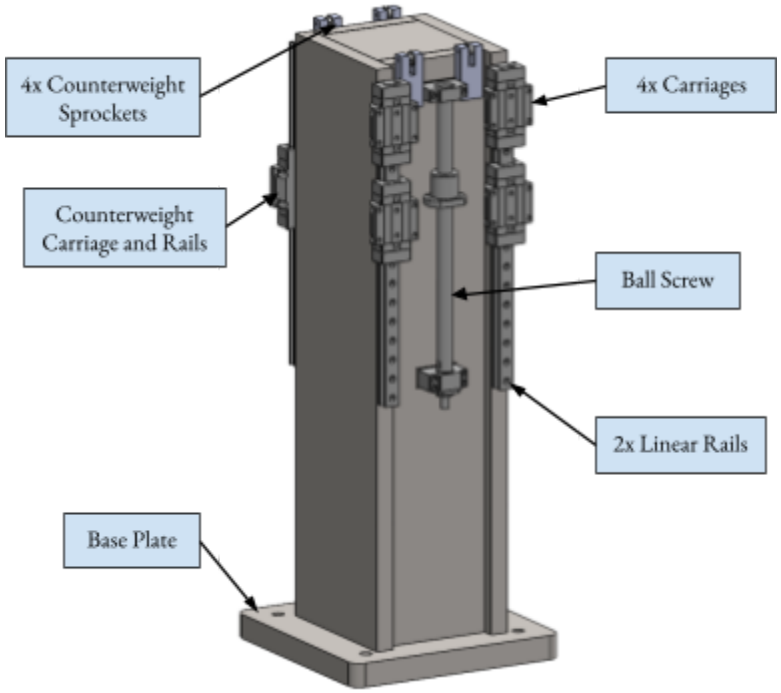

Figure 25: Subtractive Frame Z-Axis Movement

The Z axis translation is driven by a ball screw attached to the upright, and guided by two linear rails. To avoid the cantilever crashing down when unpowered and relieving some of the forces on the ball screw, a counterweight will be attached to rails on the back of the upright and connected with chains running over sprockets to the cantilever.

Final geometry will depend heavily on the process heads chosen by AMPL due to their weight and dictating where forces are applied. Currently the subtractive spindle is the heavy Gilman 400-3H-40-LC series and the DED head is the retracting Meltio DED head.

Concept Selection - Workpiece Fixturing System

Our main objective for the workpiece fixturing system is to isolate the carriages from the heat of the laser wire DED process so they don't exceed their 80 °C maximum operating temperature. We brainstormed different initial designs with passive and active cooling systems.

The first idea is similar to the setup on AMPL's Meltio DED machine; A build plate is secured to a block of material with an air gap between it and the linear motion carriages. Standoffs support the block, and active air cooling blows through the standoffs. The challenge with this design is ensuring effective cooling/insulation while deflecting less than 20 microns.

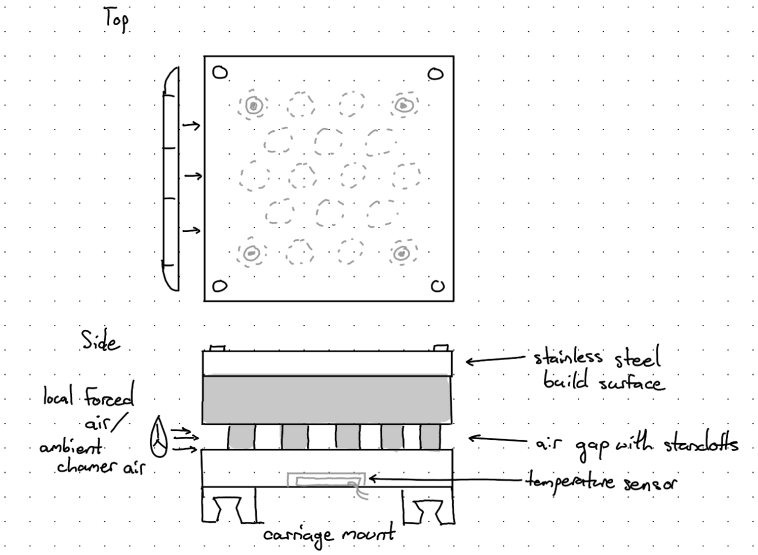

Figure 26: Air gap with standoffs/pillars, ambient or forced air cooling

The second idea is a large insulating layer of material between the build surface and the carriages (Figure 27). This is similar to the implementation in AMPL's ADDiTEC DED machine, which currently uses two inches of mica insulation. The challenge with this design is selecting an insulator that can withstand the compressive stress from forming and shear stress from machining.

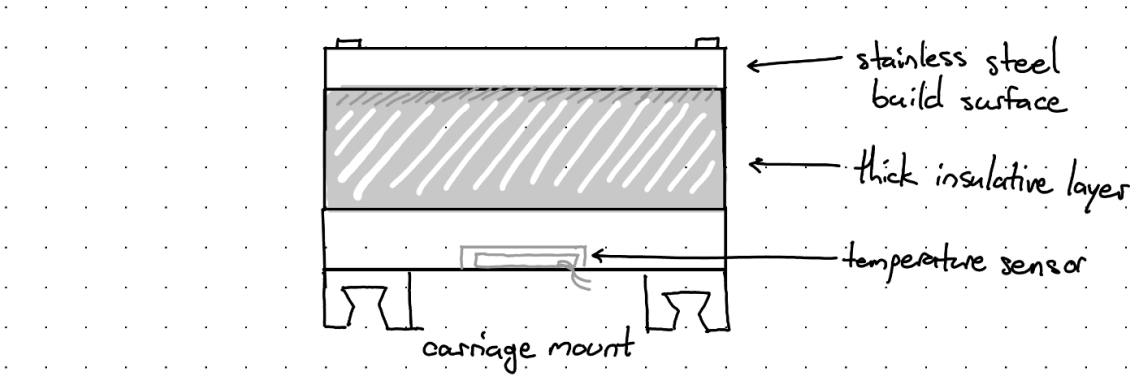

Figure 27: Thick insulative layer

For our stretch goal of adding a mechanism to heat the build plate, a resistive heating element could be added just below the build plate (Figure 28) in any design. A design similar to this is currently being developed by AMPL. However, AMPL's efforts have been stalled by the Office of Research Safety disallowing them to test their own heated buildplate, and it is unclear whether the heated buildplate will improve printing conditions and material properties.

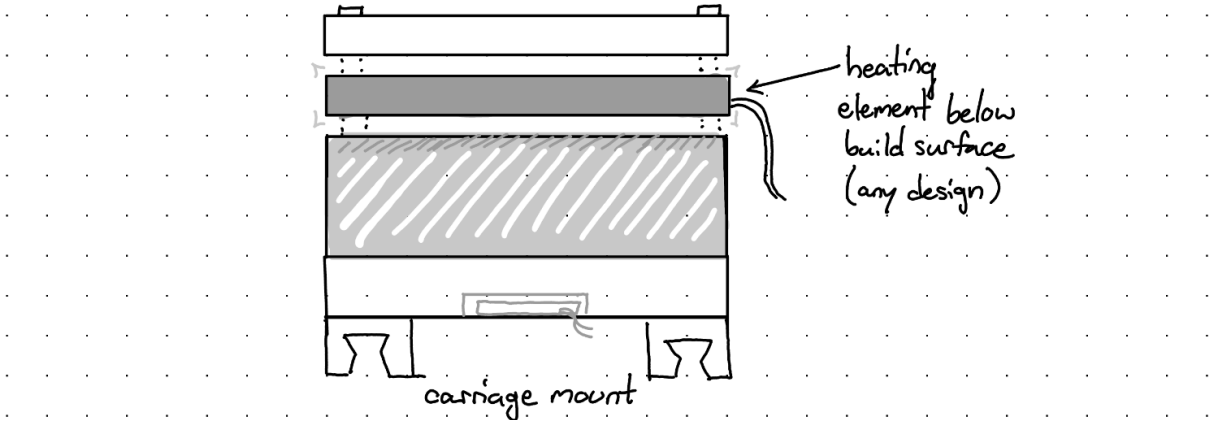

Figure 28: Resistive heating element under build plate

If active air cooling was not adequate, liquid cooling through standoffs (Figure 29) or cutting water channels through an aluminum plate be used. This would add significant complexity, and both our team and AMPL want to avoid liquid cooling if possible.

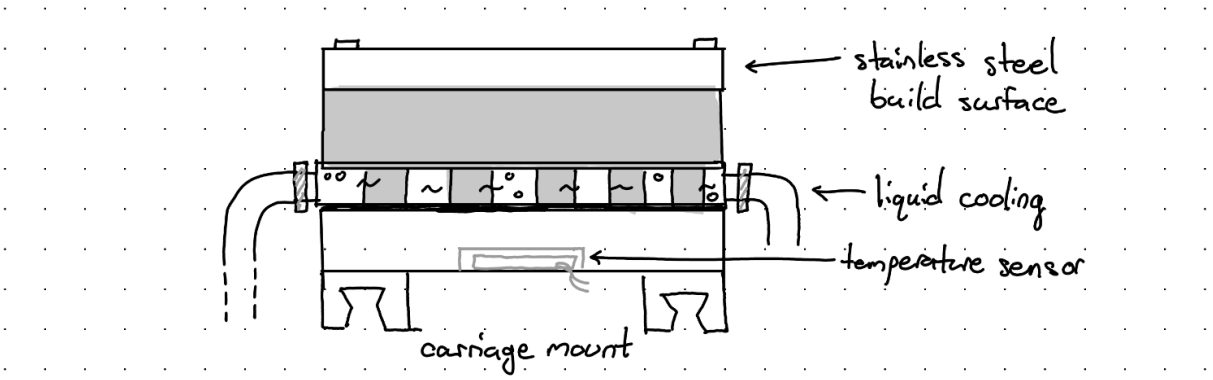

Figure 29: Liquid cooling with standoffs

Instead of holding the workpiece with bolts a magnetic fixturing was also considered. This would provide uniform support across the entire surface, distributing clamping force more evenly than standard bolts and decreasing the risk of part warping. The most resilient Samarium Cobalt (Sm_2Co_{17}) magnets only have a maximum working temperature of roughly 550°C[20]. The Curie temperature of SmCo is approximately 800°C where it loses all magnetism permanently. Considering peak temperature is unknown, and values above 800°C were being discussed at the lab meeting, this is not a reasonable solution. Vacuum clamps could provide a similar effect, but further investigation would be needed. Regardless, magnets and vacuum forces that would be required for this application could pose a significant safety risk. The immense attractive pressures/forces could lead to severe pinch or crush injuries during handling, and powerful magnetic fields may interfere with other sensitive electronic equipment.

From the concept selection we have determined that the four most promising ideas we would like to pursue further investigation into are the solid layer, standoffs without active air cooling, water cooling, and active air cooling through standoffs.

Alternatives Matrix

To evaluate our different potential buildplate layouts, we developed an alternatives matrix to compare the designs. The most important aspects of the buildplate are its ability to keep the carriages cool and to withstand the high forces sustained during the forming operation. We also wanted to compare the complexity of the plate and its cooling system, the total cost of the plate, and continual maintenance and upkeep required. Weights were assigned to our selection criteria and each design was given a score of 1, 0, or -1 based on how it would perform.

[20] Electron Energy Corporation

Table 13: Alternatives Matrix for Buildplate Designs

Selection Criteria	Weight (sum to 100)	Solid Insulation Layer	Standoffs	Water Cooling	Active Air Cooling
		Score	Score	Score	Score
Complexity	20	1	1	-1	0
Rigidity	30	1	0	0	-1
Cooling	30	-1	0	1	1
Cost	10	0	1	-1	0
Maintenance	10	1	1	-1	0
Total Score		0.3	0.4	-0.1	0
Rank		**2**	**1**	**4**	**3**
Continue?		Yes	Yes	Yes	Yes

The solid insulation layer and standoffs win based on their simplicity and ease to implement. They are low cost and require no external power or material source. They have no maintenance needs except replacing after potential warping, and would be much simpler to do so compared to the active cooling systems. While the active cooling systems perform much better at actual cooling, their increased performance is offset by their cons and the fact that the standoffs or solid layer can be improved by adding material until our optimal temperature dissipation is achieved.

While this alternatives matrix shows a clear “winning” and “losing” design, the difference is not that large. We decided that it would be very important to explore all four options based on simulation results and other design testing. As we explore each idea more thoroughly, we may find that decisions made in the alternative matrix are incorrect or were completely disregarded altogether.

Final Design Overview - Workpiece Fixturing System

Before reviewing the analysis and testing that validate our selection, here is a summary of the final workpiece fixturing design.

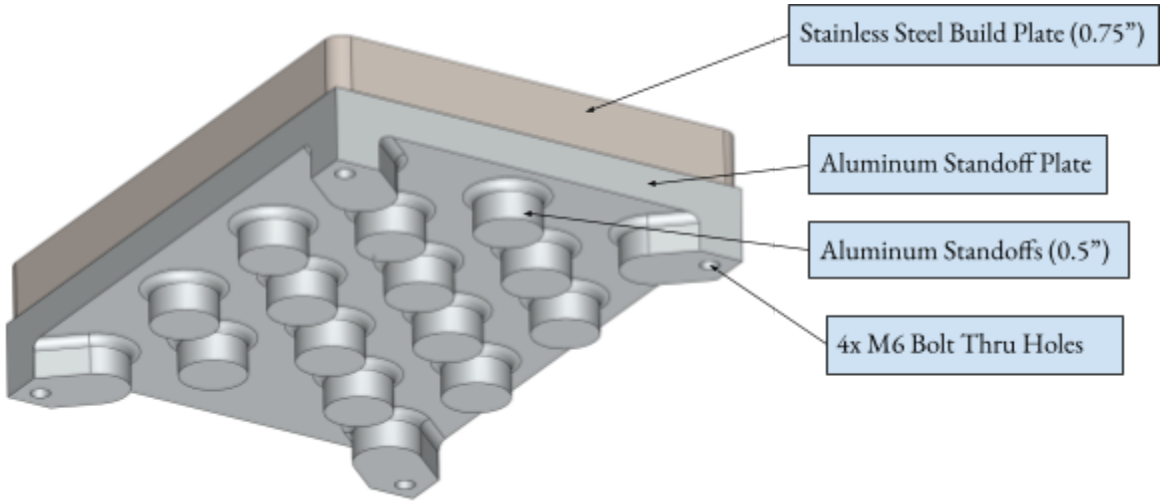

Figure 30. Final Workpiece Fixturing System CAD, viewed from underneath

The final workpiece fixturing system is a stack of two plates, secured in all four corners by M6 bolts to the motion system's mounting plate. On top is a ¾" 304 Stainless Steel build plate, identical to the build plates currently used by AMPL. Beneath it is a 1" 6061 Aluminum standoff plate. This plate has ½" of solid aluminum and ½" high standoffs with ⅞" diameter and ¼" fillets. These standoffs allow air circulation to cool the buildplate from underneath while supporting the forming forces.

The maximum build area provided by this design is 150mm x 150mm. It is smaller than the TRIPLE's full build area of 300mm x 300mm, but it is the largest that can be currently tested in the lab's Meltio M450 DED printer. Scaling this design for the TRIPLE will only require increasing the length and width of the plates and patterning out the standoffs.

Design & Engineering Analysis

Engineering Analysis - Motion System

Design Inputs and Criteria

To begin design work for the motion system, we needed to rigorously define our driving design inputs and criteria. Of the numerous metrics for the motion system touched on earlier, the forming force and subtractive machining forces are those that most directly impact the design and selection of subsystems and components, with rigidity being the primary objective with precision machine design. This section covers the rationale behind the chosen values for these metrics.

Heat Transfer

Because the temperature of the workpiece affects the force required to press it, our first objective was to estimate the temperature of deposited material during pressing. We initially performed simplified heat transfer calculations to approximate the cooling of deposited melted Inconel 718 immediately after deposition using Newton's Law of Cooling. In this model the heated build plate was treated as an infinite heat sink, because the deposited Inconel volume is much smaller than the thermal mass of the build area. Having derived a thermal conductivity constant k based on Inconel 718's material properties[21], estimated bead contact area, and deposited volume, the following model estimates the time t for a single bead to cool to a temperature T_{target}.

$$k = \frac{hA}{\rho Vc},\ t = -\frac{1}{k} ln \frac{T_{target} - T_{\infty}}{T_0 - T_{\infty}}$$

Table 14: Constants for Inconel 718, cooling model

Parameter	T_0 (°C)	T_∞ (°C)	ρ (kg/m^3)	c (J/kg°K)	A (m^2)	V (m^3)	h (W/m^{2}K
Value	1400	200	8193.25	435	7.85e-7	1e-9	1000
Description	Deposition Temp	Heated Buildplate Temp	Inconel 718 Property	Inconel 718 Property	Estimated bead contact area	Estimated bead volume	Inconel 718 Property

These calculations gave us a rough sense of cooling behavior, and we were later provided with more accurate thermal data by the client in a paper which included both simulated temperatures and experimental measurements for Inconel 718 deposition and cooling[22] (see Figure 31).

[21] ASM Material Database

[22] Goa et al., "An operando synchrotron study on the effect of wire melting state on solidification microstructures of Inconel 718 in wire-laser directed energy deposition"

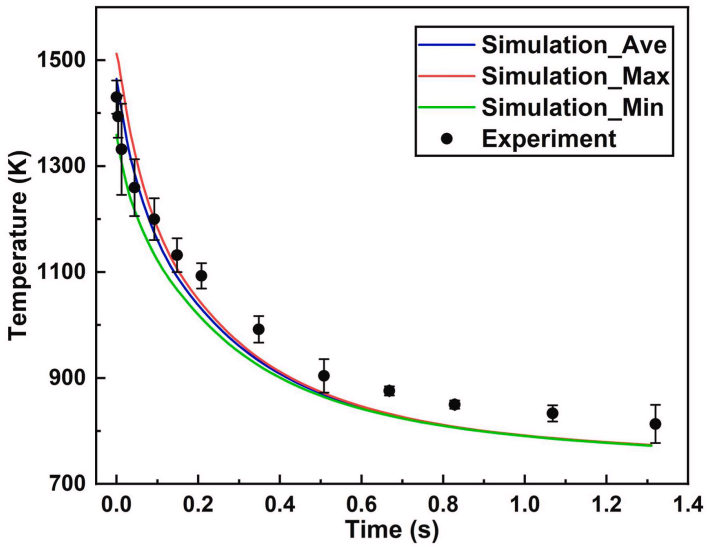

Figure 31: Inconel temperature over time after deposition, both simulated and experimentally measured[17]. Inconel heated to liquidus temperature (1609 K) and deposited onto a room temperature substrate (298 K).

This data provides us with better temperature estimates over time after deposition. Consistent with expectations for a small molten volume in contact with a large heat sink, the deposition material cools very quickly. As shown above during the initial cooling phase (1500-1250K), the temperature drops rapidly at a rate of approximately 3800 K/s. The cooling rate gradually decreases to approximately 80 K/s in the final stage of the measured cooling data.

Forming Force

The forming process is the biggest individual input force into our system. The press forming process our client desires is open-die press forging, which is well-established and documented. We used the following equations for open-die pressing force to determine our required forming force[23]:

$$F = K_f Y_f A$$

$$K_f = 1 + \frac{0.4\mu D}{h}$$

K_f is the forging shape factor, influenced by the friction coefficient μ, the diameter of the pressed area D, and the workpiece height h. Y_f is the flow stress, which represents the stress needed to continue deforming a material after it has yielded. A is the cross-sectional area of the pressing.

The flow stress of any given material is dependent on strain, strain rate, and temperature, and is typically found empirically via tensile testing[24]. We were able to find two good models for the flow stress of Inconel 718 in

[23] Groover, "Fundamentals of Modern Manufacturing," 5th Ed.
[24] ScienceDirect, "Engineering Topics: Flow Stress"

literature; for temperatures up to 400°C, a Khan–Huang–Liang (KHL) constitutive model developed by Gauri Mahalle et al[25] was utilized. See the equation and Table 15 below.

$$Y_f = \left[A + B\left(1 - \frac{ln\,\dot{\varepsilon}}{D_p^{\,0}}\right)^{n1} \varepsilon_p^{\,n0}\right]\left(\frac{\dot{\varepsilon}}{\dot{\varepsilon}^*}\right)^{C}\left(\frac{T_m - T}{T_m - T_{ref}}\right)^{m}$$

Table 15: Material constants for Inconel 718, KHL model

Parameter	A (MPa)	B (MPa)	n0	n1	C	m
Inconel 718	828.9	580.06	0.62	1.3417	0.0135	1.385

The listed parameters are the model fit parameters. ε is the true strain and $\dot{\varepsilon}$ is the strain rate. Per Gauri Mahalle,

> "T_m, T, T_{ref} are melting, current, and reference temperatures, respectively. $D_p^{\,0} = 10^6 s^{-1}$ known as deformation rate (arbitrarily chosen upper bound strain rate) and $\dot{\varepsilon}^* = 0.01\ s^{-1}$ (reference strain rate, at a reference temperature of T_{ref}, usually room temperature, at which material constants A, B and $n0$ are determined) ... For Inconel alloys, the melting temperatures were taken to be 1350°C (for Inconel 625) and 1336°C (for Inconel 718)."

Using this model, we calculated the flow stress for Inconel at 30°C (slightly over room temp) and 200°C (what our client had previously said was necessary to prevent workpiece warping). We also wanted an estimate that assumed we were forming at higher temperatures (950°C, just over 70% of melting temperature), if the workpiece was somehow heated or the process transition was really fast. Finding the flow stress at 950°C required a different model capable of handling high temperatures, one more typically used for material forming analysis. This equation is the Hansel-Spittel (HS) equation with optimized parameters found by Park et al[26], valid from 900°C to 1200°C. See the equation and Table 16 for more details.

$$Y_f = A \cdot exp(m_1 T)\varepsilon^{m2}\dot{\varepsilon}^{m3} \cdot exp\left(\frac{m_4}{\varepsilon}\right)$$

Table 16: Material parameters for Inconel 718, HS model after optimization

Parameter	A	m1	m2	m3	m4
Inconel 718	2640.9	-0.00196	-0.1036	0.15	-0.023

Again, the listed parameters are the model fit parameters, ε is the true strain, and $\dot{\varepsilon}$ is the strain rate. T is the material temperature. Although we are missing a flow stress model for the intermediate temperature range from 400°C to 900°C, these models were sufficient to give us an upper and lower bound for what our flow stress and forming force was going to be.

[25] Gauri Mahalle et al 2018 *J. Phys.: Conf. Ser.* 1063 012037

[26] Park et al., "Flow Stress Optimization of Inconel 718 Based on a Coupled Simulation of Material-Forming Analysis and Joule Heating Analysis"

To find flow stress and pressing force, we also made a couple of assumptions based on the processes involved and design direction from the lab:

1. The largest potential press diameter is 15mm, and the smallest is 5mm.
2. The DED layer thickness is 2mm.[27]
3. Total target strain is 10%, with a strain rate of 10%/s (1 second of pressing).
4. The friction coefficient was assumed to be 0.1.

Working from the above assumptions and equations, we calculated pressing force estimates at 30°C, 200°C, and 950°C for both the largest and smallest press heads, shown in Table 17.

Table 17: Flow stress and pressing force at different temperatures

Press Tool Size (mm)	Temperature (°C)	Flow Stress (MPa)	Required Pressing Force (kN)
15	30	977	224
	200	951	218
	950	230	40.6
5	30	977	21.1
	200	951	20.5
	950	230	4.52

These results span several orders of magnitude, and would drastically influence component design and selection depending on what values we choose. Great uncertainty remained surrounding the factors that influence the workpiece temperature, namely:

1. The cooling rate means the material quickly recrystallizes and the part falls out of the temperature range where flow stress is considerably diminished. Based on heat transfer data, the part cools to 950 °C in less than 0.1s.
2. The maximum service temperature of our preliminary selections of linear motion components was 80°C, which brings up the concern of thermally isolating the linear motion components from any mechanism that would heat up the workpiece.
3. The process transition time is still uncertain. We have estimates detailed in the subsequent subsection, but those assume perfect control and do not account for material cooling as the remainder of the layer is deposited. The same issue is present when the workpiece transitions to pressing; it will take considerable time to ensure that the entire area of a layer gets pressed.

With these uncertainties, we selected the worst-case scenario of 224kN for the large press tool at 30°C as our ideal specification and the 21.1kN corresponding to the small press tool at 30°C as our marginal specification.

[27] Duarte et al., "Hot forging wire and arc additive manufacturing (HF-WAAM)"

Process Transition Time

Ensuring minimal transition time is an important design goal when integrating several processes into a machine. Based on a general trapezoidal motion profile, shown below in Figure 32, three distinct sections exist: an acceleration period, a max velocity period, and a deceleration period.

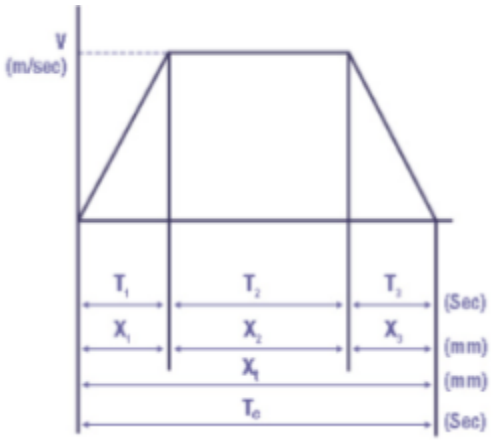

Figure 32: Trapezoidal Motion Profile

The velocity capability of our machine was taken directly from our metrics. 0.2g (2 m/sec^2) is typical acceleration for a CNC mill[28]. The total travel of 1056mm is estimated from our full assembly CAD. Using the below equations, a full travel time was calculated to be 3.127 seconds.

$$t_a(s) = \frac{V_{max}(m/s)}{a\,(m/s^2)}$$

$$d_a(m) = \frac{1}{2} * a * (t_a)^2$$

$$d_{Vmax}(m) = d_{total}(m) - 2 * d_a$$

$$t_{Vmax}(s) = \frac{d_{Vmax}}{V_{max}}$$

$$t = 2 * t_a + t_{Vmax}$$

Subtractive Machining Forces

The subtractive/DED station of the TRIPLE requires a separate set of forces to design around. We researched the machining forces associated with cutting Inconel 718 to inform our design for the subtractive frame and XY system. Our approach focused on finding the specific cutting force of Inconel 718 and approximating the max depth of cut to calculate the cutting force (Table 18). The specific cutting force of Inconel 718 was found to be 7000 N/mm[29], and our approximated cutting area was 0.9 mm[18], resulting in a tangential cutting force of 6300

[28] CADEM, "CNC acceleration ,deceleration and cycle time"
[29] Tsai et al., "An investigation on the cutting force of milling Inconel 718"

N. There is also a radial component to the cutting force, and a conservative estimate for this value is at half of the tangential cutting force[30], equating to 3150 N. The total cutting force is the resultant of these two perpendicular vectors, and comes out to 7044 N. With a safety factor of 1.3 to account for chatter and vibration, we will be designing for a cutting force of 9157 N. This value is directly important for the spindle and spindle motor selection which will be chosen by AMPL. For the other components of the machine, the radial cutting force, also known as the thrust force, dictates the forces acting on the subtractive station frame and XY ball screws. Therefore, our designed thrust force is 4578 N.

Table 18: Cutting Forces for Inconel 718

Material	Specific Cutting Force (N/mm2)	Axial Depth of Cut (mm)	Radial Depth of Cut (mm)	Ft/Fc ratio	Cutting Surface Area (mm2)	Fc (N)	Fr (N)	Resultant Force (N)	Factor of Safety	Designed Cutting Force (N)	Designed Thrust Force (N)
Inconel 718	7000	3	0.3	0.5	0.9	6300	3150	7044	1.3	9157	4578

These values are for forces in the XY plane. Our max forces in the Z direction come when drilling, and we have found the max value for a reasonable sized drill bit and feed rate is roughly 6000 N[31]. These values allow us to analyze the subtractive frame, however to analyze our motion system and build plate we need specific x and y force values. The cutting force was derived from our previously calculated thrust force of 7044 Newtons and a thrust-to-cutting force ratio of 0.5.

$$F_c = F_{xy} * ratio = 7044 * 0.5 = 3522\ Newtons$$

To ensure the design can withstand the most rigorous conditions, we modeled a worst-case scenario where the tool moves in both the X and Y axes simultaneously.

$$F_x = F_y = \frac{3522}{\sqrt{2}} = 2490\ Newtons$$

Our FEA analyses will be considered within safe operating limits if our factor of safety is above 1.3 when a load of 2490 Newtons is applied in both the x and y direction.

Frame Manufacturing Considerations

As we were designing this large machine, it was very important to keep manufacturability in mind. Given our initial engineering analysis, we found that the TRIPLE would need to withstand tremendously high forces during the press forging and subtractive operations without the rest of the machine deflecting excessively. In order to withstand these forces while remaining under our maximum allowed deformation metric, it was clear

[30] Prabhu et al., "COMPARATIVE STUDY ON THE MACHINING OF Ti-6Al-4V TITANIUM ALLOY AND INCONEL 718 SUPER ALLOY"

[31] Pervaiz et al., "Drilling Force Characterization during Inconel 718 Drilling: A Comparative Study between Numerical and Analytical Approaches"

that our frame would need to have a substantial mass to prevent any major deflections. Large, solid blocks would serve as a great basis for each of the major components of the machine because they would adequately limit the amount of deflection imposed by the excessive forces, but those pieces of metal would be too heavy and too large to reasonably transport and use to build the TRIPLE. In order to minimize cost and lead times, our goal is to make as many components in the Ford Prototyping Shop as possible.

Our main manufacturing considerations were the limitations of the shop's machine types and machine size. We have access to both manual and CNC mills and lathes. The manual milling machines have roughly 36"x12" travel while the largest CNC mill can have roughly 30"x16" of travel. The manual lathes can hold up to a 2" piece of material, while the CNC lathe can hold roughly 8" using standard collets or chucks. We also have a waterjet with a maximum cut area of 4' by 4', and several TIG welders with a large welding area. Components that reach the upper bounds of these capabilities pose a different issue: weight. Because the shop is in the Ford basement, we would need to move heavy stock materials with the shop's rear freight elevator. The entrance is in the back of the autobay past all the cars, and it exits into the CNC room. and which is hard to access behind other machines, and it is frequently filled with plywood or other large material. All these factors mean that we would need to outsource the manufacturing of our larger components to nearby machine shops or on demand manufacturing services like Xometry or SendCutSend.

The smaller machine parts, like X and Y frame components, can be made in house, but the larger frame pieces will need to be outsourced. There are a couple different options for outsourced components, either as welded or fastened metal pieces or custom cast frame components.

Metal Pieces

One method for designing and manufacturing the frame is to design it as many different individual plates or bars that can be welded together. Flat pieces could be waterjet here if they are smaller than the 4'x4' maximum, otherwise they would need to be outsourced. Assembling multiple flat pieces would be cheaper than machining out of a solid block, and it would reduce the size and weight of each component. Each piece could be moved separately and welded in the workspace, allowing us to design without the constraint of fitting through doorways.

Casting

The frame could also be manufactured with a custom made metal casting mold. This process would allow us complete flexibility in our design process, and create geometry that might be more difficult if we were to use flat plates alone. The downside is that getting any custom casting is incredibly expensive with a long lead time because the manufacturer has to make both the requested part and the mold required to make it. Additionally, the piece is completely solid so it would be incredibly heavy and would be difficult to ship, maneuver, and assemble. For these reasons, we chose to design the frame and all other components without using casting.

Forming Frame

Component Selection

The design process for the forming force applicator was started with two parallel actuator architectures: a hydraulic cylinder-driven press and a roller screw-driven press. However, safety concerns were expressed by the lab regarding the use of high-pressure hydraulic systems in proximity to molten metal and laser-based equipment. As a result, two roller screws apiece from Rollvis and Tolomatic were considered, with specifications and an alternatives matrix below.

Table 19: Roller Screw Specs and Alternatives Matrix

Specifications		**Rollvis RV60X15**		**Rollvis HRV60x15**		**Tolomatic RSX 25 RN10**		**Tolomatic RSX 33 RN10**	
Lead (mm)		15		15		10		10	
Backlash (mm)		0.04		0.04		0.03		0.03	
Static Load (kN)		415		654		222		294	
Dynamic Load (kN)		915		1512		442		442	
Selection Criteria	**Weight (%)**	Score	Weighted	Score	Weighted	Score	Weighted	Score	Weighted
Cost	0.15	4	0.6	3	0.45	2	0.3	2	0.3
Accuracy	0.10	3	0.3	3	0.3	4	0.4	4	0.4
Rigidity	0.10	2	0.2	3	0.3	4	0.4	4	0.4
Housing	0.15	1	0.15	1	0.15	4	0.6	4	0.6
Load Capacity	0.20	4	0.8	5	1	2	0.4	3	0.6
Lead Time	0.20	2	0.4	2	0.4	4	0.8	4	0.8
Weighted Total Score		2.45		2.6		2.9		3.1	

The Tolomatic RSX33 RN10 roller screw was our final selection. It has adequate force capacity (70kN more than required), has mounting and stroke configuration options, and is supplied in the midwest.

We evaluated several motor options to ensure the actuator could deliver the required forming forces. Lead, efficiency, and required torque options are below in Table 20.

Table 20: Motor Selection

Lead (mm/rev)	Efficiency (η)	Required Torque, Minimum, Nm	Required Power @300 rpm (kW)	Notes	Yaskawa Σ-7 G1EA	Siemens 1FW3	Parker TK0400
1	0.75	22.5	0.71	Lower torque, high precision, slow linear motion	Yes	Yes	Yes
1	0.9	18.8	0.59		Yes	Yes	Yes
5	0.75	112.8	2.95	Common balance between torque and speed	No	Yes	Yes
5	0.9	94	2.95		Yes	Yes	Yes
10	0.75	225.7	7.09	Higher speed, needs gearbox or torque motors	No	Yes	Yes
10	0.9	188.1	5.91		No	Yes	Yes
20	0.75	451.4	14.18	Large torque, direct drive torque motor range	No	Yes	Yes
20	0.9	376.1	11.81		No	Yes	No
50	0.75	1128.4	35.43	Extremely high torque consider hydraulics	No	No	No
50	0.9	940.4	29.52		No	No	No

Candidate motors included the Yaskawa Σ-7 G1EA, Siemens 1FW3, and two variants of the Parker TK0400. Each motor was compared across the criteria listed in Table 21 below.

Table 21: Roller Screw Motor Selection Matrix

	Yaskawa Σ-7 G1EA	Siemens 1FW3	Parker TK0400	Parker TK 0400
Cost (0.05)	4	2	5	4
Precision/Control (0.44)	5	5	2	2
Torque Margin (0.33)	2	4	3	5
Integration Ease (0.14)	5	3	3	3
Size (0.08)	4	2	4	2
Overall	4.21	4.16	3.14	2.93

The Yaskawa Σ-7 G1EA was chosen to drive the roller screw, providing the precision, reliability, and ease of integration required for forming operations. The Siemens 1FW3 offered similar positional control but slightly lower torque margin, which could limit performance under peak forming loads. The Parker TK0400 variants were rejected because one lacked sufficient positional precision for repeatable forming and the other presented mechanical integration challenges due to nonstandard housing geometry.

Bolt Selection

In-depth bolt stress analysis was conducted for both the roller screw/crossmember connection and the crossmember/upright connection. The following stress states were considered:

1. Primary shear stress due to the double shear configuration of all bolts
2. Secondary shear stress due to the moment about the bolt circle for the crossmember/upright connection
3. Appropriate preload and resultant axial tensile stress
4. Bending stress in the bolt itself
5. Bearing stresses in the bolt/surrounding structure

To be conservative, it was assumed that the bolts would be taking all of the pressing load. Standard methods from Shigley's[32] and online resources like Mechanicalc[33] were utilized. Metric hardware was required for the roller screw mounts, so all hardware was designed to metric sizes and classes (grades). Below is the analysis for the preload, shear, bearing, and bending stresses of the Class 12.9 M24 bolts used in the roller screw/crossmember connection. The full bolt analysis spreadsheet for the forming frame can be found here.

First, we have the critical size and strength information based on the class of bolt (Table 22).

Table 22: Bolt Size and Class Info[34]

Diameter (mm)	Length (mm)	Pitch (mm)	Class/ Grade	Min Tensile Strength (MPa)	Min Yield Strength (MPa)	Proof Strength (MPa)	Proof Load (N)	At (mm^2)
24	400	3	12.9	1220	1100	935	238000	352.5

A_t is the tensile stress area, taken from the major diameter and pitch. The Proof Strength is taken to be 85% of Yield strength. Next, we must find the preload and associated stress (Table 23).

Table 23: Bolt Preload

Nonpermanent Factor	Preload Force, based on Proof Load (N)	Kt	Preload Torque (N-m)	Preload Stress (MPa)
0.75	178500	0.2	856.8	506.4

The nonpermanent factor = 0.75 for reused joints. The preload force is that factor times the proof strength, and the preload torque is the preload force times a friction factor Kt (assumed to be 0.2 in this case) times the bolt diameter. Lastly, the preload stress is simply the preload force divided by the tensile stress area. Next, we find the shear and bearing stresses for the double shear arrangement (Table 24).

[32] Budynas and Nisbett, "Shigley's Mechanical Engineering Design," 10th Ed.
[33] Mechanicalc, "Bolted Joint Analysis"
[34] ASTM F568 12.9 Datasheet

Table 24: Bolt Shear Stresses

Forming Force (N)	# of Bolts	Forming force @ each bolt (N)	Avg Shear Stress (MPa)	Thickness of Plates t (mm)	Thickness of Mountings t1 (mm)	Bearing Stress @ Bolt/Plate Interface (MPa)	Bearing Stress @ Bolt/Roller Screw Mounting Interface (MPa)
224000	8	28000	30.9	25	100	23.3	11.7

These calculations assume the load is distributed evenly over all eight bolts. The average shear stress is half of the load each bolt takes, divided by the shank cross sectional area. The bearing stresses are the load each bolt takes divided by the mounting thickness times the shank diameter.

Our final stress component is now the bending stress (Figure 33, Table 25). Assuming a fixed-fixed beam with two point loads, as diagrammed below, gives:

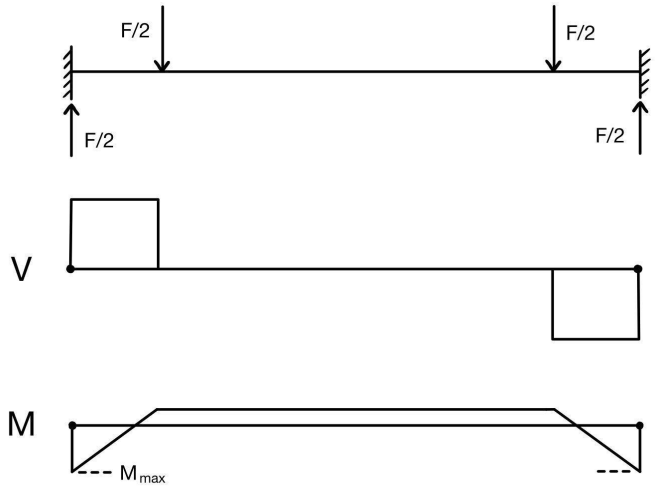

Figure 33: Bolt Bending Approximation

Table 25: Bolt Bending Stresses

Beam Length (mm)	Mmax (N-m)	Bending Stress (MPa)
345	467.9	344.8

From there, we combine all stresses to find von-Mises stress and our overall factor of safety. For bolts, a factor n is applied to all stress components except for the preload stress, and solved iteratively to give a factor of safety. See Table 26, below.

Table 26: Bolt Factor of Safety

n	**Von Mises Stress (MPa)**	**FoS**
1.69	1099.145739	1.69

From this analysis, we can conclude that Class 12.9 M24 bolts are adequate for the roller screw mounting. This is a conservative estimate, assuming bolts take all of the load and none of the interference features outlined in the design overview take any load.

For the roller screw/crossmember connection, the default mounting hardware from Tolomatic had to be modified to accommodate 8 larger M24 bolts compared to the designed M20 mounting. We wanted to run further analysis to see if accounting for the interference features would allow for unmodified mounting hardware to be used.

Assuming that the force from the roller screw is distributed proportionally across the area of interference and the bearing area of the bolts in each joint (#of bolts x diameter x plate thickness), each feature is able to take between ~45-48% of the applied load, considerably reducing the load on the bolts. Table 27 shows the resulting changes in FOS.

Table 27: Updates in bolt FOS considering interference

Upright Connections (8x **M30** Bolts)			Roller Screw Connection (8x **M24** Bolts)		
Grade	Old FOS	New FOS	Grade	Old FOS	New FOS
12.9	3.57	4.94	12.9	1.69	2.34
10.9	2.6	3.6	10.9	1.349	1.855
8.8	1.69	2.35	8.8	0.943	1.295

This updated analysis increases FOS for existing hardware, and adds capability to drop to lower grade hardware for the M24 bolts. Table 28 below displays FOS for smaller hardware, including the M20 bolts required for Tolomatic's stock mounting flanges.

Table 28: FOS for smaller bolts in each connection

Upright Connections (8x **M27** Bolts)		Roller Screw Connection (8x **M20** Bolts)	
Grade	FOS	Grade	FOS
12.9	2.28	12.9	1.045
10.9	1.38	10.9	0.775
8.8	0.83	8.8	0.525

For the upright connections, using smaller M27 bolts is only feasible with Grade 12.9 hardware. This would likely not result in cost savings compared with the larger but weaker Grade 8.8 M30 bolts that outperform them significantly. For the roller screw connection, M20 bolts of all grades are still too weak.

If accommodating manufacturer mounts is non-negotiable, a few design changes could be implemented:

1. Interference area could be significantly increased. To accomplish this, the upright tabs could widen or be supplemented with additional features, and the front mounting flange could be modified to be wider.
2. More welded joints/connections could be utilized. The lab was initially hesitant about having welded connections on the machine frames at all, but this stance has changed following a design review with other members of the HAMMER ERC.

FEA Setup and Results

Ideal Loading

Finite Element Analysis was conducted using Ansys Static Structural on a simplified version of the final frame assembly. All hardware was replaced with beam elements of proper strength, and a simplified version of the roller screw body replaced the detailed model of the roller screw and motor. Frictional contact definitions were used at inter-component interactions, but bonded contact was used for intra-component interactions. See Figures 34 and 35 below for details of the simulation preparation.

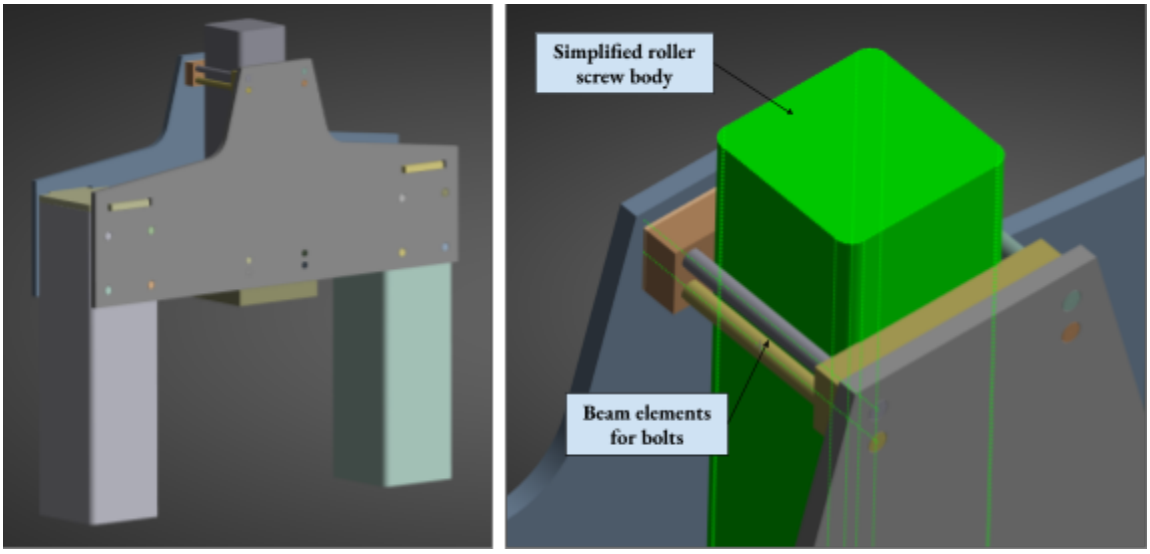

Figure 34: Simulation Geometry (left), Detailed View of Simplifications (right)

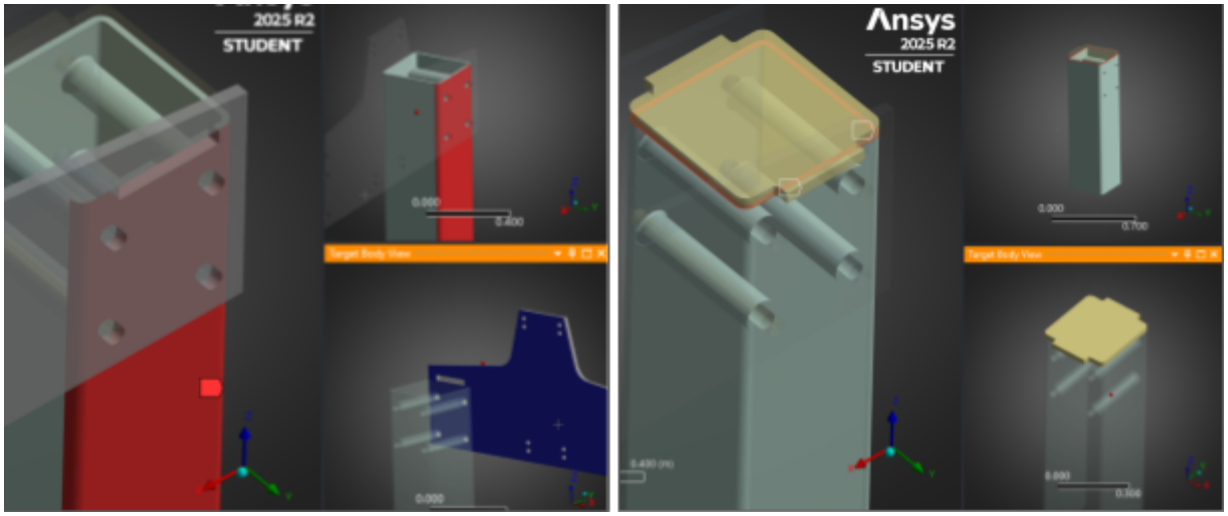

Figure 35: Frictional Contact at Upright and Crossmember (left), Bonded Contact at Upright and Cap (right)

Ansys mesh parameters are too exhaustive to list, but quad-dominant meshing was used with an element size of 0.02m. 41k nodes and 91k elements were generated. The student license was not able to compute results for a mesh that was appreciably finer. Figure 36 below shows the mesh.

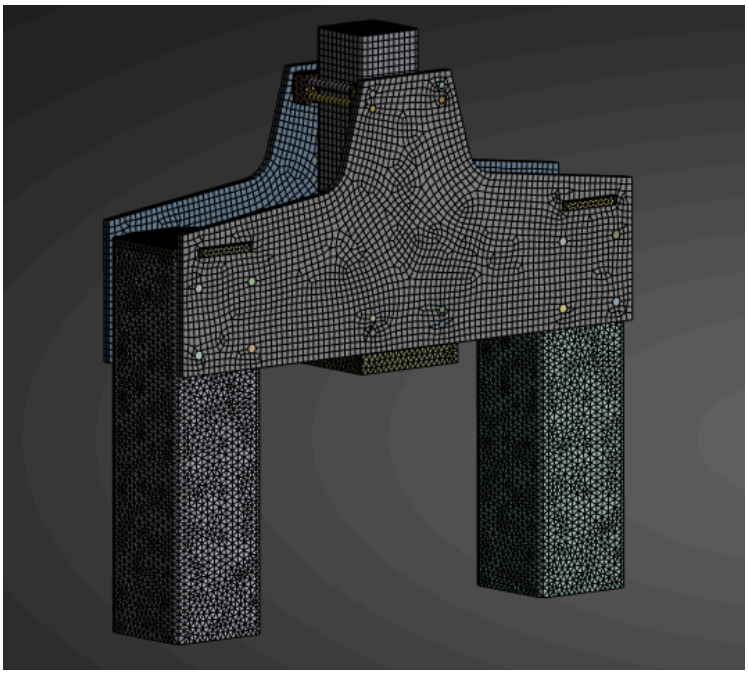

Figure 36: Ansys Mesh, Forming Frame

The forming load was distributed across the eight bolt holes that attach the roller screw to the frame, and the beam elements modeling the bolts were joined to the appropriate bolt holes with cylindrical joints. The base of either upright was fixed. Stress and deformation plots are below in Figures 37 and 38.

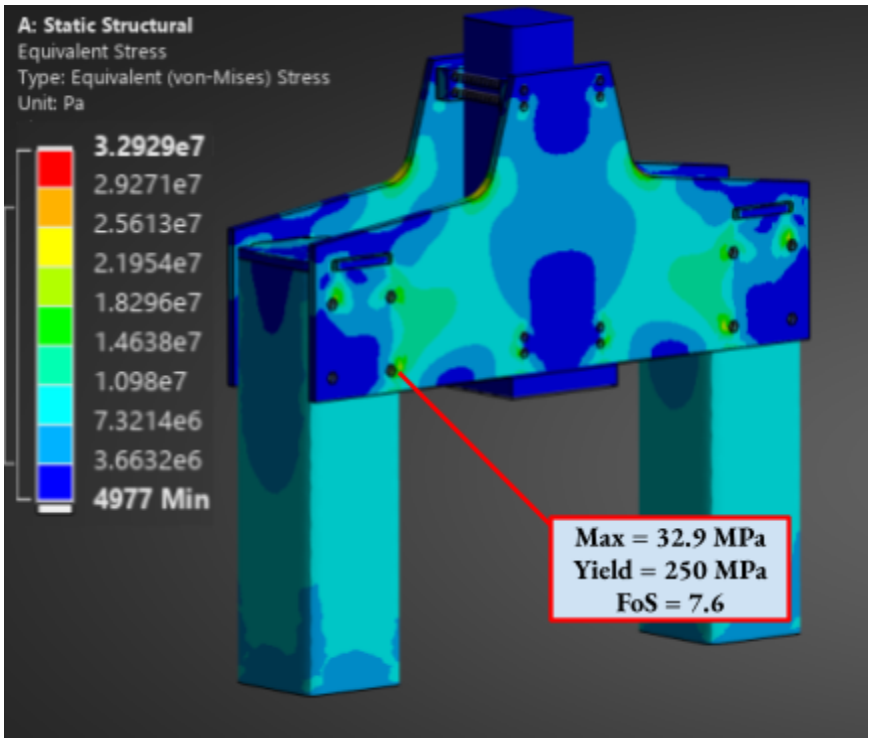

Figure 37: Forming Frame von-Mises Stress

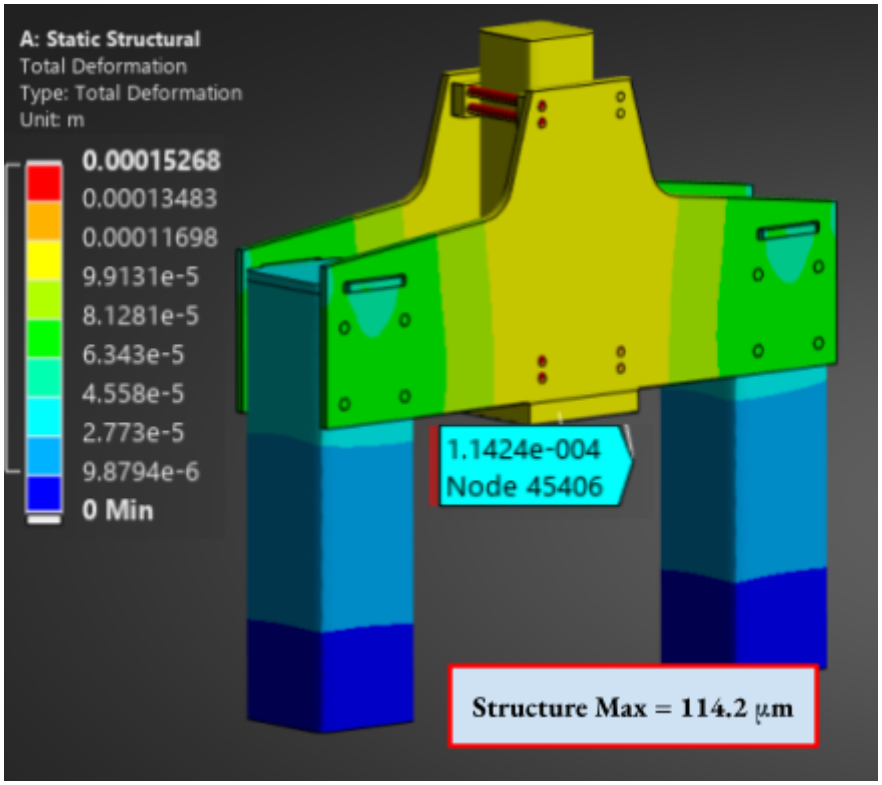

Figure 38: Forming Frame Deformation

The stress plot demonstrates that this design is safe with respect to yield, with a factor of safety of 7.6. The deformation plot shows some nonphysical behavior with respect to the bolt elements, but the maximum deformation of the structure itself is 114.2μm. This value takes up less than half of our 0.5mm ideal deflection budget, but is only one of two primary contributors to that budget. This deflection value and load gives a frame stiffness of 1970N/μm.

Nonideal Loading

The lab wanted to consider nonideal perturbations of the forming load to account for imperfect alignment or an off-axis reaction force from pressing on a slanted or stepped surface. For the forming frame, two load cases with 5-degree off-axis loads were considered; the first is out-of-plane with respect to the frame, and the second is in-plane. Remaining consistent with the ideal axially aligned analysis, a remote load of 224kN was distributed across the bolted connections at the specified angle. See Figure 39 for the setups of each load case.

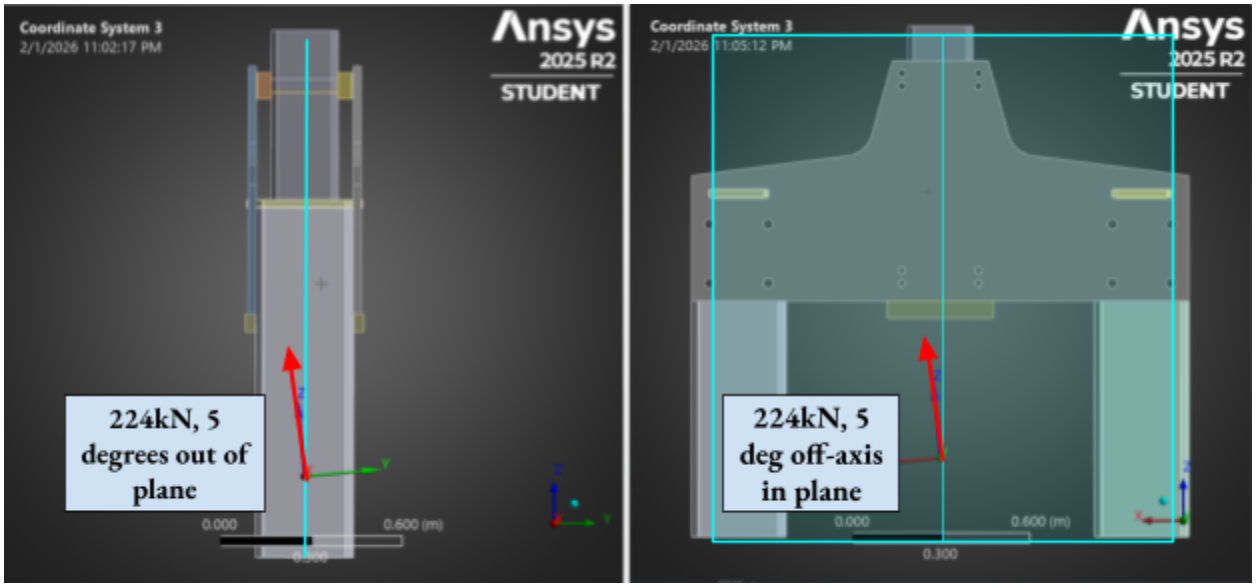

Figure 39: Setup, Out of Plane Case (Left) and In-plane Case (Right)

The results for the out-of-plane case are below in Figures 40 and 41. The stress distribution is asymmetric, with the crossmember that the load is angled towards (the “front”) experiencing more stress. This crossmember also experiences more deflection as the roller screw body twists. Maximum deflection in the out-of-plane case is 431 microns, which is approaching our deflection budget with just this component.

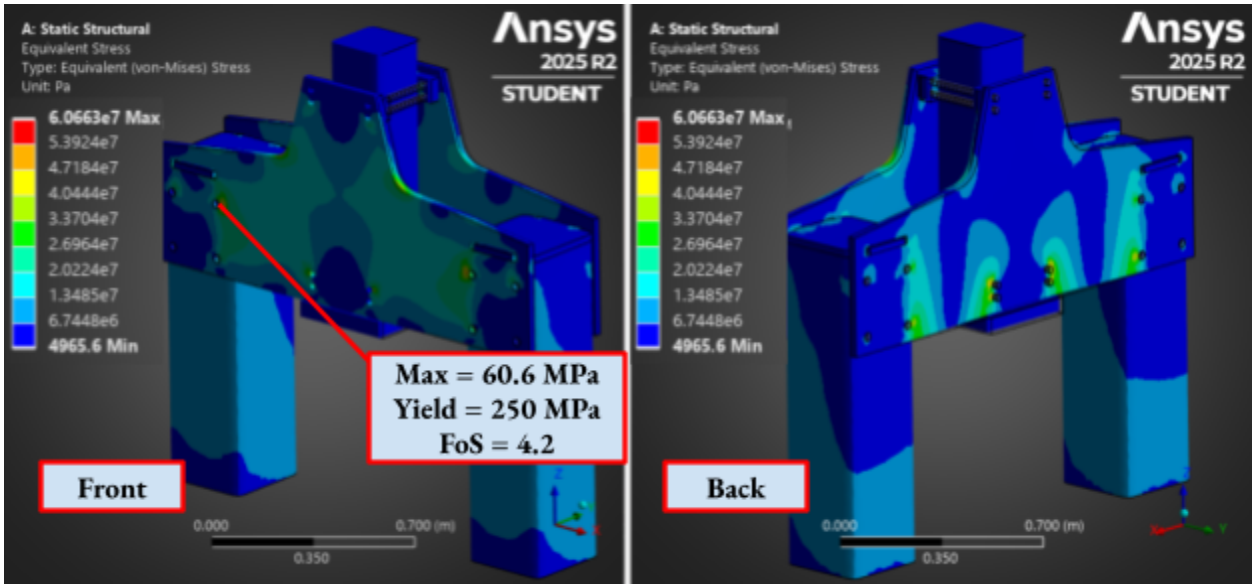

Figure 40: Out-of-plane case, Stress

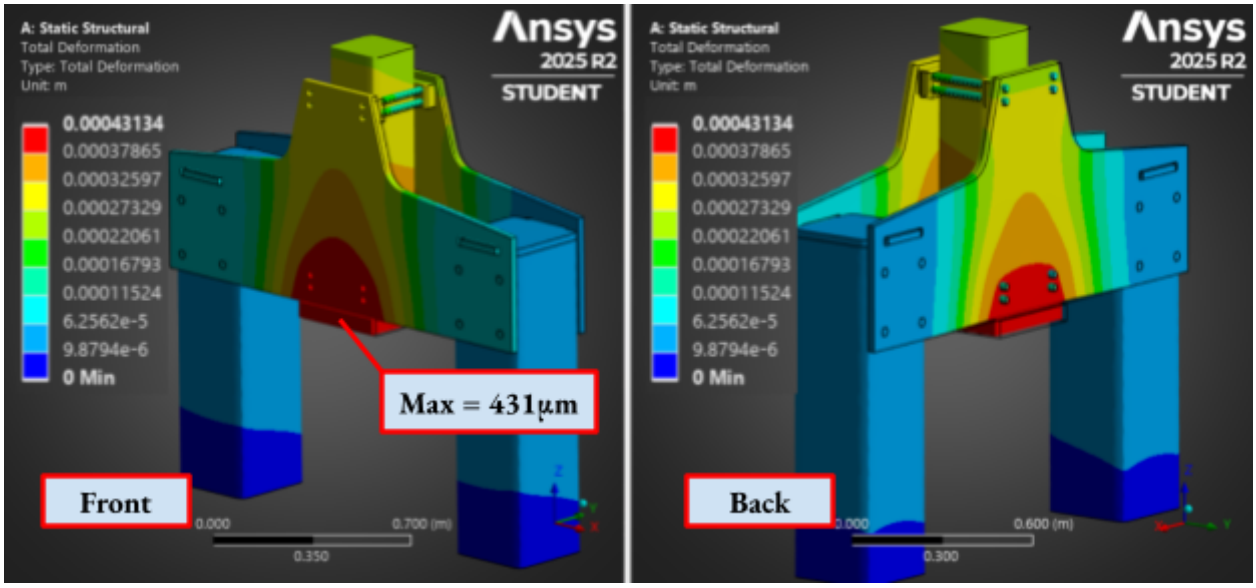

Figure 41: Out-of-plane case, deflection

The results for the in-plane case are below in Figure 42. The stress distribution is asymmetric again, but in this case it is left-right asymmetry. The stress and deflection results are symmetric front to back, so they are displayed in 2D for clarity. As expected, the side that the load points to experiences more stress and deflection. Maximum deflection in the in-plane case is 192 microns, which is only 40 microns more than the ideal axial load case.

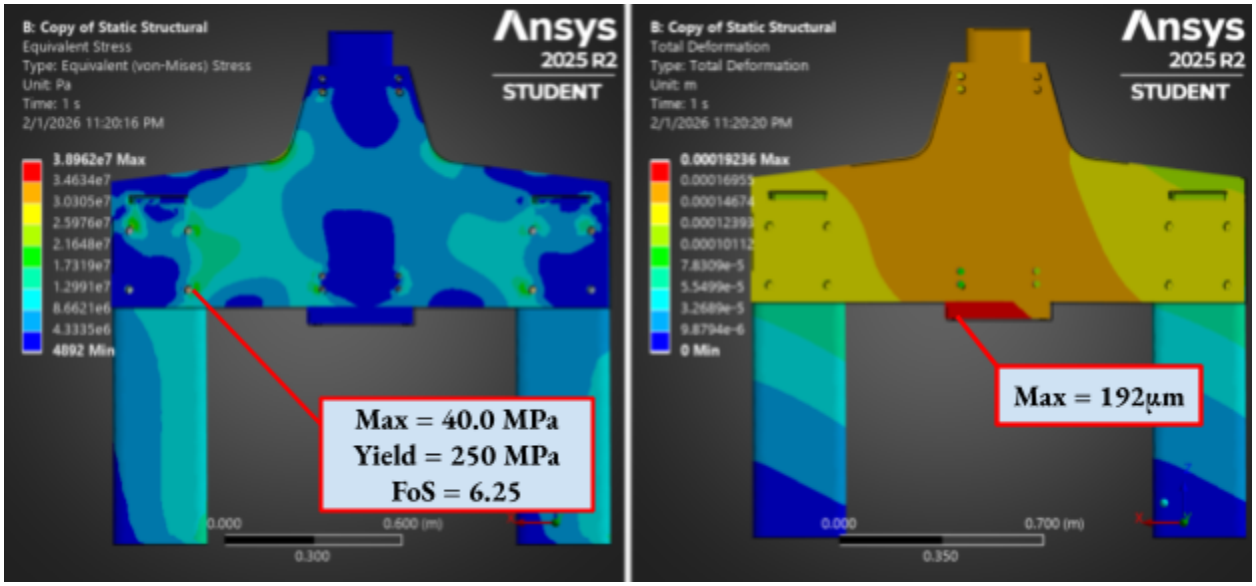

Figure 42: In-plane case, stress and deflection

The out-of-plane case is experiencing considerable deflection (approaching our 500 micron total deflection budget for forming). The lab expressed concern about this, and it is an area for future design work.

Subtractive Frame

SolidWorks FEA was performed on the subtractive frame. Simulations were run using remote loads applied at the tip of the stand-in subtractive spindle at the subtractive head mounting holes, and the bolt holes on the upright base were fixed. The subtractive machining forces for Inconel 718 were used to simulate worst case scenarios for milling forces:

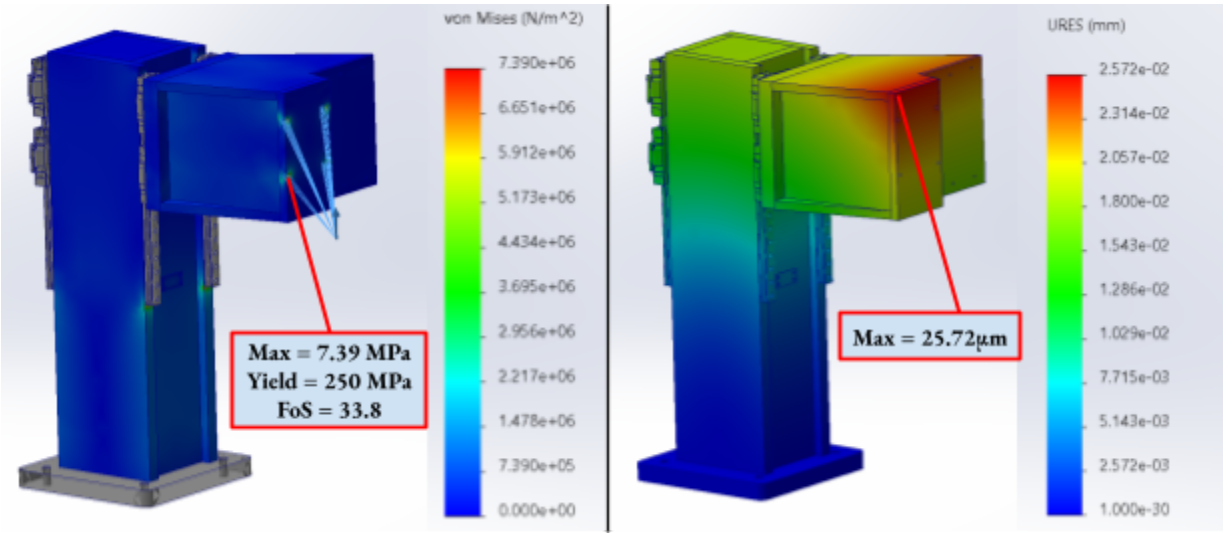

Figure 43: Subtractive frame response under 6000 N drilling force

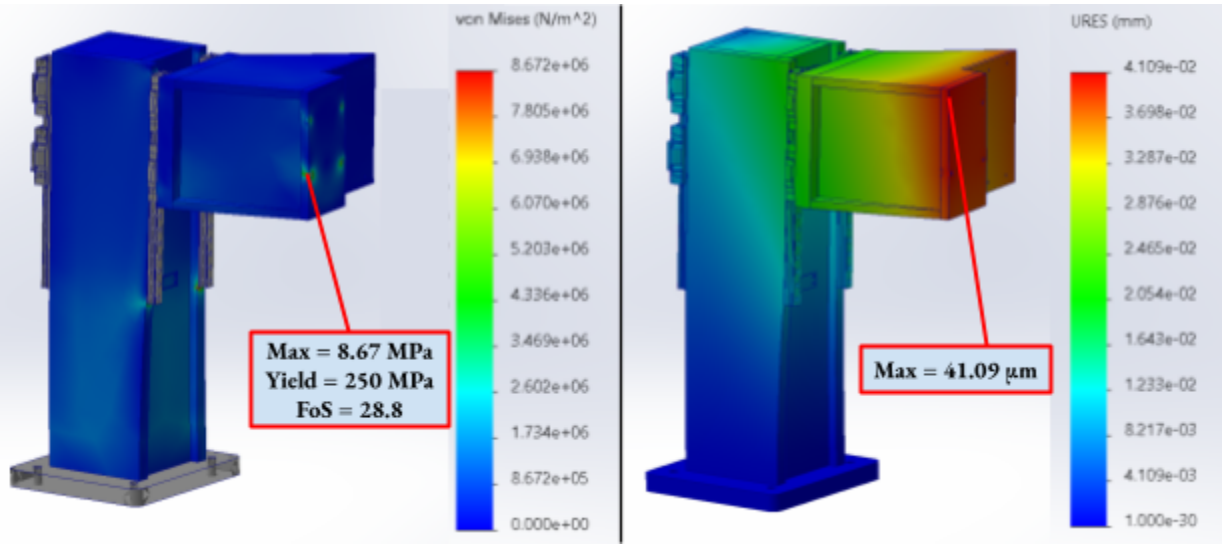

Figure 44: Subtractive frame response under 4592 N out of plane force

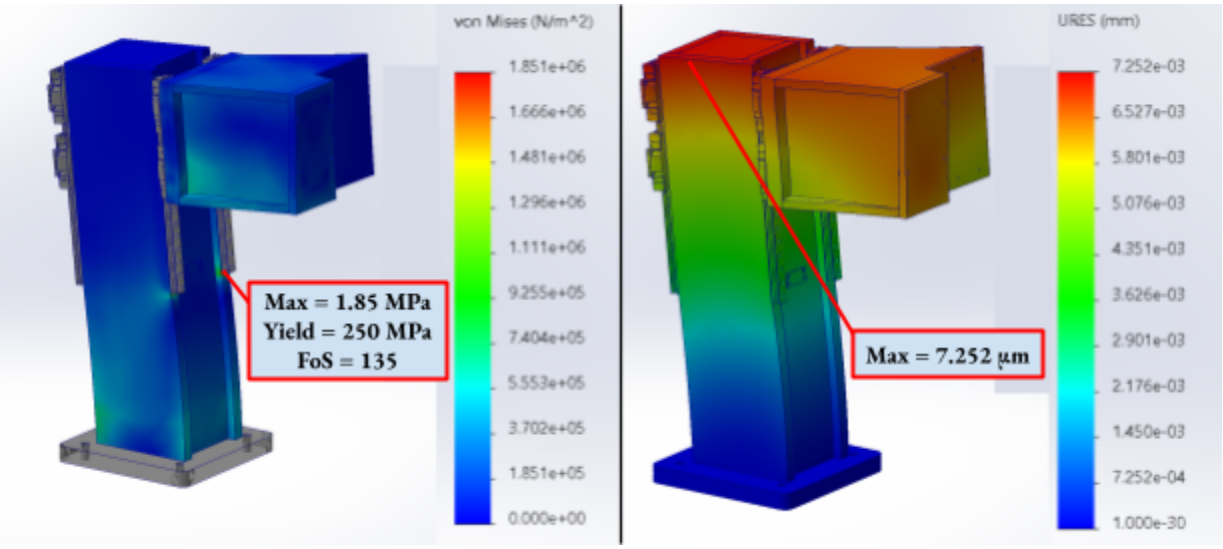

Figure 45: Subtractive frame response under 4592 N in plane force

Table 29: Subtractive Frame FEA Results Summary

Applied Force Direction	**Applied Force Magnitude (N)**	**Maximum Von Mises Stress (MPa)**	**Maximum Deflection (µm)**	**Stiffness (N/µm)**
Upwards (Fig X)	6000	7.39	25.7	233.3
Horizontal in Plane Toward upright (Fig X)	4592	1.85	7.25	633.4
Horizontal out of Plane	4592	8.67	41.1	111.7

(Fig X)				

This design meets the current stiffness metrics in all three loading directions, with the out of plane horizontal machining being the worst case. These results should still be treated as preliminary because a final spindle and DED head have not been selected by the AMPL lab. The geometry, mass, and mounting configuration of the process heads will significantly affect the load application points, cantilever bending moments, and the required counterweight mass.

The spindle and DED head selection will also determine the sizing of the counterweight rail system and chain/sprocket transmission components. For this reason, additional refinement and optimization of the subtractive frame is not yet justified, since spindles and DED heads vary wildly in size and weight and would invalidate any fine tuned analysis. Finally, the reported stiffness values represent only the subtractive frames stiffness, not the other parts of the machine in the load path (machine base, XY gantry system, etc) and solidworks FEA is known to overpredict stiffness.

XY Gantry Component Selection

In our selected layout for the TRIPLE, the workpiece must travel in both the X and Y directions. The primary function of the XY motion control system is to facilitate the seamless, repeatable sequence of DED followed by press forging. This requires a unique combination of high precision for DED, high precision and thrust force for subtractive machining, and extreme structural rigidity to manage high static forces generated by the press forging process.

Ideation for the XY gantry involved each team member sketching or using CAD to mock up various drive mechanisms ideas. The ideas ranged from ball screws to a robotic arm, with many other mechanisms considered. Ten unique ideas were ranked in an alternative matrix to identify the best layouts, the top three ideas are shown below in Table 30. The selection criteria and their corresponding weights were provided to us by the client. The full matrix with the ten ideas can be found in Appendix B.

Table 30: Alternatives Matrix for the Top Three XY Drive Mechanisms

		Ball Screws	**Linear Motors**	**Roller Screw (Planetary or Recirculating)**
Selection Criteria	**Weight (%)**	Score	Score	Score
Cost	10	3	1	2
Accuracy	20	4	5	5
Rigidity	20	3	3	3
Lifetime	10	4	4	3
Maintenance	5	2	4	2

Load Capacity	15	5	3	5
Speed	10	5	5	4
Footprint	5	3	4	3
Weighted Total Score		3.6	3.45	3.5
Rank		1	3	2

Researching these mechanisms and reviewing their weighted performance revealed that ball screws with linear guide rails were the best option for movement in the XY plane. Linear guide rails are used in nearly all modern high-precision machines due to their high load capacity and rigidity, and very low sliding friction. Most commercial CNC machines use ball screws for their linear drives.

Rail Selection

The linear guide rails are one of the more expensive and critical components of our motion system, and there are two main types of carriages for these rails: ball bearing carriages and roller bearing carriages. Roller bearings have a significantly higher static load rating, rigidity, and moment resistance than ball bearings due to their larger contact area. Due to our need for high rigidity and load capacity, they are the clear choice over ball bearing carriage with only a slight price increase.

A thorough analysis of the roller guide systems was conducted, with the following brands considered: THK, NSK, Rexroth, Schaeffler, Schneeberger, and IKO. These brands dominate the market share[35] and are exclusively used by the leading machine design companies.

There are two driving numbers for this product selection: the estimated vertical pressing force of 224 kN needed for the forming process at room temperature, and our metric for the elastic deflection of the system. The more rigid the better for the XY movement system, and higher rigidity rails allow for more leeway in the design of other components involved in the process. While the forces occurring during the subtractive process should not be ignored, and are a driving factor in ball screw selection, all of the rails investigated are rated for much higher lateral loads than those from milling, and the drilling force is less than our forming press.

First we identified rails with bearings that have a dynamic load rating higher than the 224 kN forming force. Later on in the process, we received advice from our correspondent at THK that we should consider the pressing as a static force on the bearing and aim for a safety factor of eight for the bearing ratings. However, the following research is still relevant as it helped us identify the brand that was best for our needs.

With all companies being able to withstand our press forging force, rigidity became the differentiator. THK, Schneeberger, and NSK have the best rigidity constants and were worth pursuing further, but even within this group, THK stood above the rest.

[35] Reports and Insights, "Linear Guide Market Size, Share, Growth | Trends 2025-2033"

Table 31: Benchmarking of Linear Rails

Brand & Model	Rail Width (mm)	Carriage Dimens. L x W x H (mm)	Static Load Rating (kN/Block)	Dynamic Load Rating (kN/block)	Radial Rigidity (µm/kN)	Lateral Rigidity (µm/kN)
THK - SRG65LC	65	303 x 170 x 90	599	278	0.164	0.317
NSK - RA65GM	65	302.5 x 170 x 90	756	288	0.234	Not Provided
Rexroth - FLS 65mm	65	255.3 x 170 x 90	606.3	295.9	0.288	0.433
Schaeffler - RUE65-E-L	65	261.9 x 170 x 90	640	270	0.308	0.45
Schneeberger - MR W 65-B	65	260 x 170 x 90	530	295	0.236	Not Provided

Quotes for the 65mm models from THK, Schneeberger, and NSK were requested, all with a rail length of 1000 mm, and all came back between $1,800 and $2,100 per rail. With all other factors being similar between these three models, rigidity was the deciding factor in choosing to source our roller guide rails from THK. Additionally, THK had been the most responsive and informative when communicating product details.

We identified three possible THK rail configurations that would meet or closely approach our safety factor of eight for the vertical forces (Table 23). Two configurations used two rails with one carriage each, and the third option used two carriages on each rail. Our updated metrics allow a maximum system-total deflection of 0.5 mm, and these rails will deflect a maximum of 0.025 mm or less at our full pressing force of 224 kN. We did not receive the exact rigidity constants for these models, but were assured that they were similar to our previously calculated values, or better in the case of the SRG85LC. The lead time for all models is roughly two months.

We eliminated the SRG85LC because the rigidity benefits did not justify the significant price and size increase. One SRG85LC rail was quoted at $4,400, over double the 65mm model. We then discussed the option of two carriages per rail, but ultimately chose to stick with one carriage per rail because the two-carriage option would increase our minimum rail length and buildplate dimensions by 110 mm in both the X and Y directions. The only benefit of two carriages is increased moment capability, which is unnecessary for our application. The SRG65SLC is the rail of choice for the TRIPLE.

Table 32: Benchmarking Rail Configurations

Brand & Model	Rail Width (mm)	Carriage Dimensions L x W x H (mm)	Static Load Rating (kN/Block)	Dynamic Load Rating (kN/block)	Radial Rigidity (µm/kN)	Lateral Rigidity (µm/kN)	Safety Factor for 224 kN Static Loading
2x THK - SRG65SLC	65	380 x 170 x 90	811	352	Upon Request	Upon Request	7.24
2x THK - SRG85LC	85	350 x 215 x 110	990	497	Upon Request	Upon Request	8.84

4x THK - SRG65C	65	245 x 170 x 90	441	219	Upon Request	Upon Request	7.88

The final step in selecting our exact roller guide rail was the carriage attachments. A THK correspondent suggested we choose the carriage attachments that include double end seals, side seals, inner seals, a metal scraper, and a self-lubricator. The three types of seals protect from dust and chips from all angles. The metal scraper hovers just above the top surface of the rail and will push away chips or welding splatter from the DED process. This will give us protection for anything that makes it through the telescoping steel covers that we intend to have covering the rails and ball screws. The self-lubricator will lengthen the lifespan of the carriages before human maintenance is required, and will ensure the roller bearings always have enough lubrication. Another customizable option that we have locked down is the preload on the carriages. We will go with the heaviest preload they offer, C0, which is at around 8% of the static load rating of the bearing. This greatly improves our rigidity, and we have room to spare with our static safety factor to accommodate this extra loading.

The seals add additional length to the carriages, increasing from 380 mm to 442.4 mm, but this is a necessary addition to protect the lifespan of the bearings. This change then reduces our maximum travel length, so to combat that, we had to increase the total length of X and Y rails.

A few options that we rejected were the fluorine seals, the laminated contact scraper, and the rail bellows. The fluorine seals are only necessary when working with extreme chemicals, and do not apply to our processes. The laminated contact scraper excels at removing minute foreign material from the rails, but we do not expect such material to be common in the machine, especially as we are using laser DED and not powder-based DED. And lastly, we opted to cover the whole drive system with telescoping steel covers or heat-resistant fabrics, instead of isolating just the rails themselves with the bellows for protection.

The majority of the work done on the XY axis consisted of validation of the previous design. AMPL wanted to change the designed forming force from 224 kN to 100 kN. Therefore the linear rails can be sized down and still maintain the same factor of safety as before. We have selected the SRG55LC rails from THK as our new linear motion component, replacing the SRG65SLC rails. The ball screws and coupler do not change because the dominant factor in their selection was the forces applied while using milling operations on Inconel 718, and those force expectations remain the same.

Ball Screw and Motor Selection

Ball screws were sourced from THK, which we chose as the best supplier because they have the widest range of products and were the most responsive. Other suppliers such as Thomson Linear or Rockford Ball Screw had fewer options, providing less design flexibility.

The loading of the ball screws combines the subtractive load case described above, with the inertial and friction loads due to the mass of the moving parts. Using our CAD models, the moving masses were estimated to be 400

kg for the X axis and 150 kg for the Y axis. The below equations are used to calculate the inertial and friction forces:

$$Inertial = Mass(kg) * Accel(m/sec^2)$$

$$Friction = Mass(kg) * Friction\ Coefficient$$

A friction coefficient of 0.001 was chosen from the maximum of THK's[36] published values, and the acceleration was chosen to be 2m/sec^2, as specified in the movement time subsection above.

Table 33: Total Motion Forces

	X Forces (N)	Y Forces (N)
Max Machining	9156.698	9156.698
Inertial	800.000	300.000
Friction	0.400	0.150
Total	9957.098	9456.848

THK recommends a factor of 5 for any conditions that may include vibrations or impact, shown below in Table 34. Though the goal is to isolate the ball screws from any forming forces, the nut and screw will still see vibrations and impacts in the axial direction due to subtractive machining forces.

Table 34: THK Recommended Safety Factors

Load Conditions	Recommended Safety Factor
Without vibrations or impacts	2
With vibrations or impacts	5

This safety factor brings the required ~50,000N static load rating. A lead of 10 or 12mm is chosen as it provides the best balance between torque and speed requirements for the motors. Shown below are possible THK models that achieve the required values.

Table 35: Possible THK Ball Screw Models

Category	Required Value	SDA 3110V-5	EPB 5010V-8	SBN 3610V-7	BIF 3612V-10
Static Load Rating (N)	49,785	57,100	54,300	53,200	52,700
Lead (mm)	10 or 12	10	10	12	10
Nut Mass (kg)		0.96	2.3	4.34	5.33

[36] THK, Ball Screw General Catalog, Login required

Nut Length (mm)		65	131	140	163
Nut Diameter (mm)		86	110	123	124
Screw Diameter (mm)		31	50	36	40
Screw Mass (kg/m)		5.02	14	7.99	8.87

The SDA 3110V-5 was chosen as the current option for both the X and Y axes, as it has the required load rating and is the smallest of the available options. THK sells this model as an assembly with the end supports and seals, with a choice between campus seals and thin film seals being offered. A quote for the required lengths of 1050 mm for the X axis and 675 mm for the Y axis has been requested. With a lead of 10mm, the required continuous torque and max speed of the driving motor needs to be 17.5Nm and 2120RPM, found using the equations below:

$$Torque = \frac{Lead^{*}\ Dynamic\ Load}{1800^{*}pi} \qquad RPM = \frac{Velocity\ (mm/min)}{Lead\ (mm/rev)}$$

Shown below are motors from select companies that surpass these requirements.

Table 36: Motor Options

Manufacturer	**Required Value**	**Yaskawa**	**Baldor**	**Moog**
Part Number		SGM7G-44	HDS180C-2540B	G-5-M8
Rated Torque (Nm)	17.6	28.4	25	22.35
Max Speed (RPM)	2150	3000	3500	2400
Weight (kg)		17.5	25.1	16
Body Length (mm)		184	297	271

The Yaskawa SGM7G-44 motor was chosen for both axes. This is the smallest motor length wise and the second smallest motor mass wise. Yaskawa motors are also used by Haas in the CNC machines. The motor driver has not been chosen, and will need to be selected before a quote can be requested.

Bolt Selection

We analyzed bolts by looking at how they resist shear force and compress components together. Due to the high run time and complexity of the motion system, the bolt strength was determined through the following considerations. Since forming involves applying only a downward force, the components should not separate unless there is slipping. Therefore, the bolts are primarily placed to provide stiffness and prevent the sliding/rotation of the plates and parts stacked on top of each other. In order to rigidly constrain the system but not cause too much stiffness where the system can't deflect (since deflection is preferable to yielding), we will

consider 50% of the 240kN load applied downward. This means on each plane of bolts we need a sum of 120kN of pretension. Using Grade 8.8, we end up with roughly 15 percent pretension on each bolt.

The primary function of the bolts in this motion system is to provide sufficient clamping force to achieve system rigidity and prevent relative motion (sliding or rotation) between stacked components under load.The system is designed for a forming operation that applies a maximum downward load of 240kN. To maintain a rigid constraint, the design assumes that 50% of this load must be resisted by the bolt pretension on each plane to prevent separation or slipping. Hence, the required total pretension per plane for the motion system is 120kN.

The design uses Grade 8.8 bolts. Table 37 lists the size, required pretension per bolt, and the resulting percentage of the Grade 8.8 proof load. The proof load is dependent on the diameter of the bolt. The percentage of proof load is the Pretension Percentage. Each layer is highlighted a different color, beginning from the top build plate (green) through to the bottom base (purple). The appropriate hardware is included in the Bill of Materials in Appendix C.

Table 37: Bolt Dimensions, Proof Loads, and Pretensions for XY Gantry

	Diameter Shank	Head Limit	Length w/o Nut	Count	Nut Limit	Grade 8.8 Proof Load (kN)	Required Pretension (kN)	Pretension Percentage
Build Plate to Carriage	16	n/a	65	4	n/a	94.2	11.78	12.5
Interference to Carriage	16	n/a	45	4	24	94.2	11.78	12.5
Top Adaptor	8	15	19	4	n/a	20.3	15.23	75
Total (120kN)							155.16	129.3
Top Rail to Top Plate	18	26	65	4	n/a	121.2	15.15	12.5
Top Rail to Top Plate	18	26	95	4	n/a	121.2	15.15	12.5
Total (120kN)							121.2	100
Top Plate to Carriage (thru mid and lower plate)	16	n/a	143	8	24	94.2	11.78	12.5
Bottom Adaptor	8	15	19	4	n/a	20.3	15.23	75
Total (120kN)							155.16	129.3
Bottom Rail to Base	18	26	103	8	n/a	121.2	15.15	12.5
Total (120kN)							121.1	100

In order to use a Grade 5.6 M16 or M18 bolt in the configurations above, they would have to get pretensioned to 63.7% and 52.1%, respectively. While these percentages are technically below the 100% point, they pose significant engineering problems. One problem being, there is a low margin of error. Tightening a bolt to 63.7% of its proof load leaves a very small margin for error in the tightening process (torque wrench inaccuracy, thread friction variation, etc.). Overtightening by even a small amount could cause the bolt to yield permanently. By contrast, the Grade 8.8 M16 bolts required only 12.5% of their proof load to achieve the same pretension, leaving a huge reserve of strength to handle uncertainties, dynamic spikes, and manufacturing variations. Additionally grade 8.8 is the most common used in CNC applications with 10.9 grade bolts being used in high stress areas. Using too stiff of a bolt (10.9) also poses the concern that the system may break before it deforms to its full capacity. By having the bolts pretensioned to 12.5%, each plane has a Factor of Safety of 8. This is the recommended factor of safety for forming, so we hit this requirement.

The bolts must also withstand the shear forces generated from machining. The worst-case force the system is expected to experience is a tool-breaking force of approximately 10kN. A Grade 8.8 M16 bolt has a shear yield strength of 480 MPa. This results has a factor of 7.4.

$$F_{shear} = Ultimate\ Shear\ Stress\ *\ Area\ = 480\ MPa\ *\ 157\ mm^2 = 75.36\ kN$$

$$FOS_{shear} = \frac{Failure\ Load}{Applied\ Load} = \frac{73.97kN}{10kN} = 7.4$$

Lastly, FEA was run without bolted connections and bolts were established afterwards. Due to low forces and stresses, we are able to select bolts without running an overcomplicated full system in ansys with bolted connection everywhere.

XY Gantry Analysis

The Finite Element Analysis (FEA) for the forming process was structured to simulate a conservative worst-case scenario. The primary load applied was a vertical force downwards, set at 240kN, which exceeds the worst-case force expectation (224kN) to provide a safety buffer . To simplify the system, the ball screw and its mounts were omitted, assuming they receive zero deflection. Drive motors were not modeled but their effect was captured by applying equivalent moments around their attachment points on the axis plates. The base of the motion system was given a critical boundary constraint of zero deflection. This restriction supports the design requirement that the base plate must be rigid, and it is necessary for the FEA software to solve the static structural analysis. This setup can be seen in Figure 46.

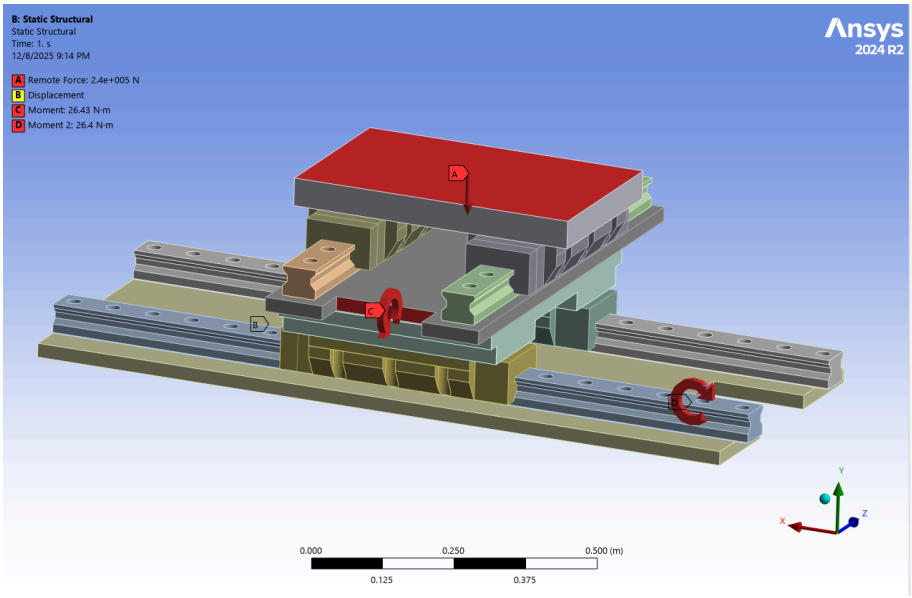

Figure 46: XY Gantry Forming Analysis Setup

Deflection of the 2 cases for forming can be seen in Figure 47 and 48 below.

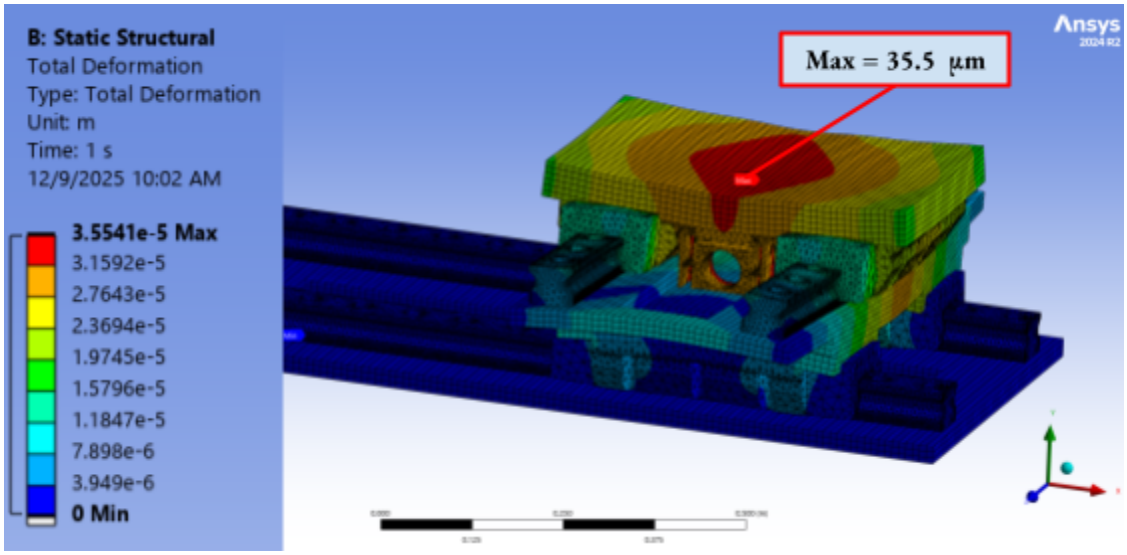

Figure 47: Center Forming Displacement (Maximum of 35.5 microns)

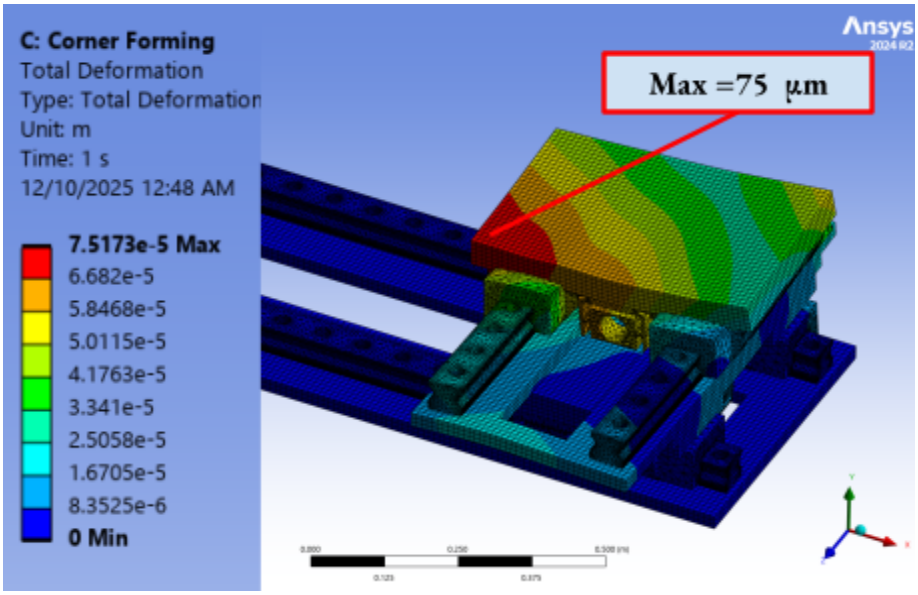

Figure 48: Corner Forming Displacement (Maximum of 75 microns)

The results obtained from the forming analysis validate the structural accuracy of the model. By applying the 240kN vertical force at the center of the system, we measured a vertical deflection of 20 microns in the top rails in the vertical-Y-direction using a probe check. This outcome is logical and serves as a strong indication that the model is accurately representing the system's behavior. Mechanically, the applied 240 kN force is split across the two supporting carriages, equating to approximately 120 kN per carriage. This calculated load precisely corresponds with the 20 microns deflection per carriage specified in the rail/carriage manufacturer's technical data, thus confirming the validity of the material refinement and the overall FEA setup.

Stress of forming cases can be seen in the Figure 49 panel. The three images on the left correspond to the center forming case and the three on the right correspond to the corner forming case. Note that the bottom two images show the factor of safety. There are noticeable singularities that are causing inaccurate maximum stress, however since the maximum stress is a singularity and it is happening on the carriage which we know from specs can withstand the impact we are delivering with a factor of safety of 8, we can disregard it. Additionally, the concern for the center forming factor of safety appears at the adaptor piece that will be getting analyzed independently and hence we can disregard. From this we know our motion system will not yield and actually survives forging with a factor of safety of 15.

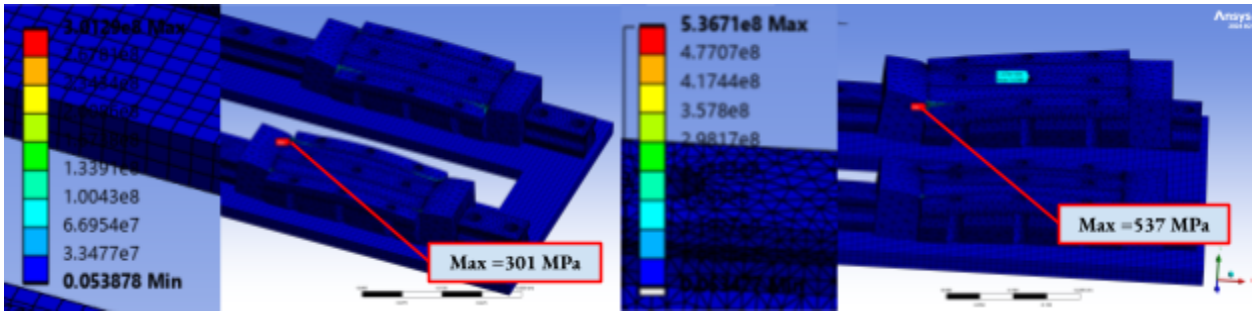

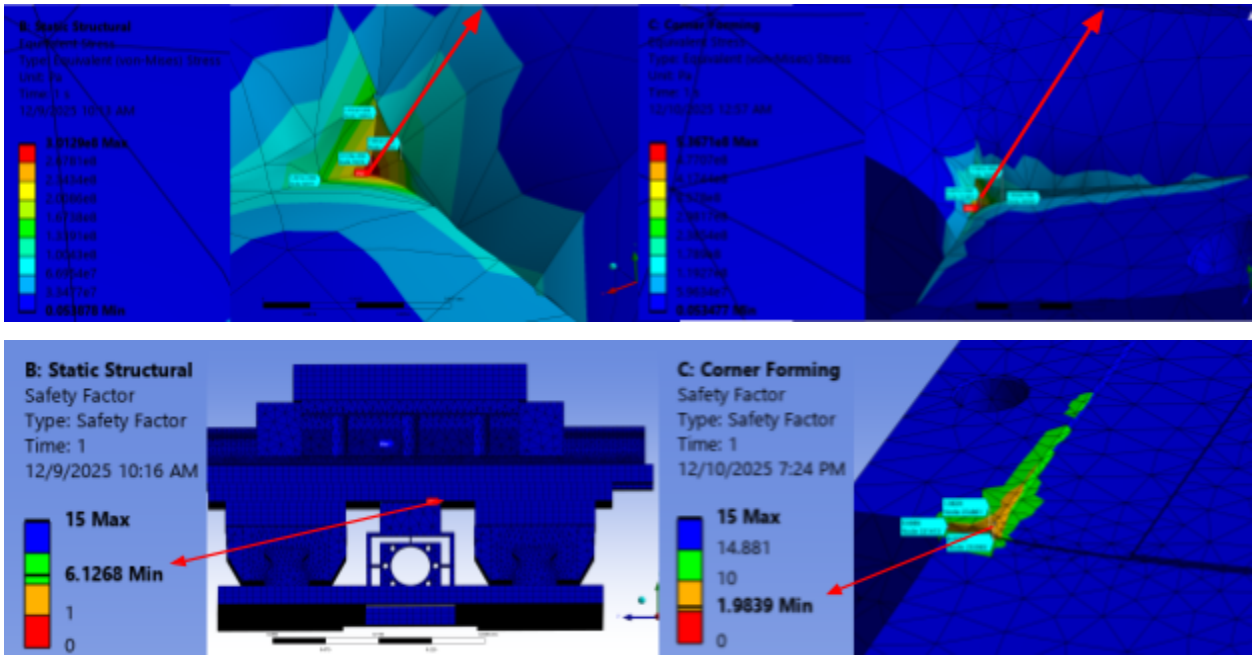

Figure 49: Stress of Forming (left is center case, right is corner case) and Factor of Safety (bottom row)

To explore potential improvements in deflection, we conducted experiments investigating the effects of both material selection and plate thickness on structural rigidity. Initial tests involving various steel alloys demonstrated that altering the material of the build/interference plate yielded a maximum deflection change of only 0.4 microns. This minimal improvement was deemed negligible, especially considering the associated trade-off of higher cost and the increased difficulty in machining the superior steel grade. Conversely, increasing the combined thickness of the interference and build plates by 0.5 inches (12.7 mm) from the current 2 inch total resulted in a more substantial improvement of nearly 2 microns in overall deflection. While this represents a five-fold increase in benefit compared to the material change, the 2 micron reduction is still considered marginal in the grand scheme of the system's performance, given that the current configuration already satisfies the required forming error budget.

AMPL also requested that we rerun the forming cases at a 5 degree angle to determine if the systems withstand an error in the application of the forming force. The motion system deflection from Ansys for these new cases in comparison to the original cases can be seen in Figure 50.

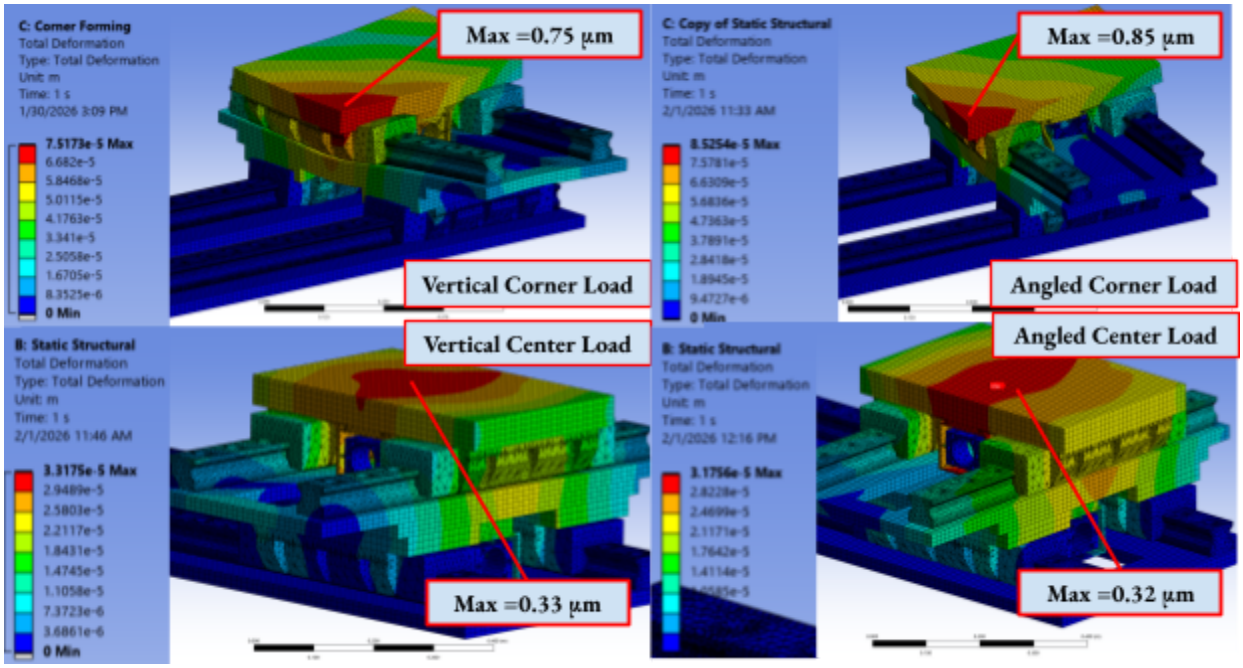

Figure 50: Deflection on Motion System

(Left: Vertical Load Case. Right: 5 degree angle Load Case, Top: Corner Forming, Bottom: Center Forming)

The total deflection for the 5 degree load case is within the acceptable range of deformation (0.5mm). This holds true for the two worst case scenarios in regard to the motion system - the force application at the center of the plate and at the corner of the workpiece. The specific deflection at the force location can be seen in Table 38.

Table 38: Deflection on Motion System in Microns

	Corner Vertical	Corner 5 Degree	Center Vertical	Center 5 Degree
Total	57	-8	26	26
X	-29	-9	-1	6
Y	-48	15	-26	-5
Z	11	62	0.3	6

Motion System Summary

Across all load cases analyzed, every component within the motion system achieved a minimum Factor of Safety (FOS) of 15. This high FOS confirms that the system is adequately designed for yield strength, ensuring reliability far exceeding typical operational requirements and allowing for unpredictable conditions and further adaptations of the machine.

A fundamental way of determining if a machine is within spec is looking at the stiffness rather than deflection since deflection on the same machine changes based on material. Stiffness k is calculated as the ratio of applied

force to the resulting deflection, expressed as k = F * δ. It is the primary metric for determining a machine's rigidity and is directly correlated with achievable machining accuracy. Our motion system stiffness in regards to different processes is shown in Table 39.

Table 39: Motion System Stiffness vs Case

	Forming Center	Forming Corner	Subtractive Center	Subtractive Corner	Subtractive Center (Lower F)	Subtractive Corner (Lower F)
Deflection (Z, μm)	28.0	48.3	0.44	2.0	0.74	-0.67
Deflection (Total, μm)	35.0	57.4	293.0	289	206	2.6
Stiffness (N/μm)	6860	4180	34	34.6	31.7	2497

The calculated stiffness values provide a strong indication of our TRIPLE system's performance capability across its two primary functions.

Machining Stiffness: Our motion system exhibits a machining stiffness of 34 N/μm. This value is good and positions the machine firmly within industry standards for high-quality production equipment. Per Slocum[37], "For production precision machines, stiffness values in the range of 15–50 N/μm are typically required." Our 34 N/μm falls perfectly into the required range for reliably achieving tight tolerances associated with high-precision manufacturing. However, it is important for us to note that this value is below the threshold for true Ultra-Precision machines, which "demand stiffness values greater than 50 N/μm."

Forming Stiffness and Comparison to Forging: The motion system's forming stiffness, which ranges from 4,180 to 6,860 N/μm, is 4 to 6 times the stiffness of the forming frame alone. This magnitude is exceptionally high and beneficial for the forming application. While this is not directly comparable to the immense stiffness of dedicated, large-scale industrial forging presses (which can be in the hundreds of thousands of N/μm), this value ensures that our hybrid machine possesses a highly rigid platform for micro-forging and forming operations. High stiffness minimizes structural deflection under extreme tonnage, guaranteeing efficient energy transfer and dimensional consistency, which is critical for precision forming processes.

To evaluate the machining load, two approaches were considered. First, using a calculated cutting force of 9157 N, the components were distributed evenly along the X and Y axes, with an additional Z component applied to simulate a spiral trajectory. This resulted in a total magnitude of approximately 10 kN, a value deliberately

[37] Slocum, “Precision Machine Design”

chosen since most machining tools are not designed to withstand forces beyond this threshold. Recognizing that this assumption might be overly conservative, the force was subsequently reduced to 6551 N (with components of 4578 N, 1000 N, and 4578 N).

Interestingly, the reduction in applied force revealed nonlinear stiffness behavior in the system. For the center case, stiffness decreased, suggesting an element of elasticity during the initial deformation of the motion system. Conversely, in the corner case, stiffness increased under the reduced load. This contrasting behavior indicates that the system's stiffness response is not uniform and may depend on load distribution and boundary conditions. Such findings warrant further investigation, as they suggest complex interactions between structural elasticity, load paths, and machine geometry.

Engineering Analysis - Workpiece Fixturing System

ANSYS Thermal Simulations

In preparation for running test DED prints on a miniature-sized build plate, we ran additional ANSYS DED simulations to obtain test results to compare with temperature data collected during the actual print. These simulations were run on two designs: the build plate with a one-inch-thick aluminum standoff layer and the build plate with a quarter-inch-thick alumina plate.

Aluminum Standoffs Design

We began with simulating a print of a one-layer, 75mm square of Inconel 718. This size fills a large portion of the build plate with room left for the mounting holes, and is our marginal specification for build area. The simulation parameters can be seen below in Table 40, and the G-code for the tool pathing can be found in Appendix F. An adiabatic constraint was applied to the bottom face of the build plate to prevent convective heat transfer, as this surface will be mounted to the linear rail carriages. Seen below in Figure 51 are the results. The thermal gradient of the structure shows that the area directly under the most recent printed material is the hottest, while earlier areas of the print have begun to cool down. The plate area under the latest deposited material ended at 110℃, whereas the area under the beginning of the build had cooled to 52℃. However, our primary interest is in the temperature of the bottom face of the build plate. Figure 52 includes a graph of the max temperature over time on this face, maxing out at 63℃. Notably, the max temperature follows a nearly linear trend over the progression of the print.

Table 40: Two-Layer DED Simulation Parameters

Parameter	**Value w/ Units**
Material	Inconel 718
Process Temperature (derived from material)	1260 ℃
Deposition Rate	30 mm^3/s (derived from ideal spec, density

	of IN718)
Convection Coefficient k, part	10 W/m^2 ℃
Convection Coefficient k, build plate	10 W/m^2 ℃
Room Temperature	23 ℃

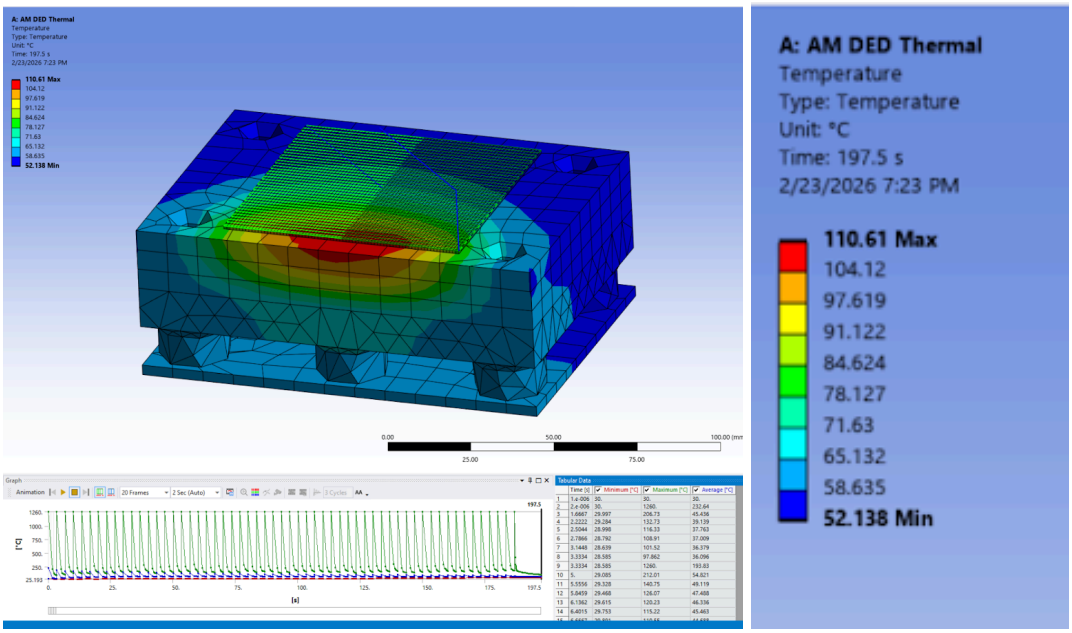

Figure 51: Thermal gradient after one-layer DED simulation on the build plate with standoffs.

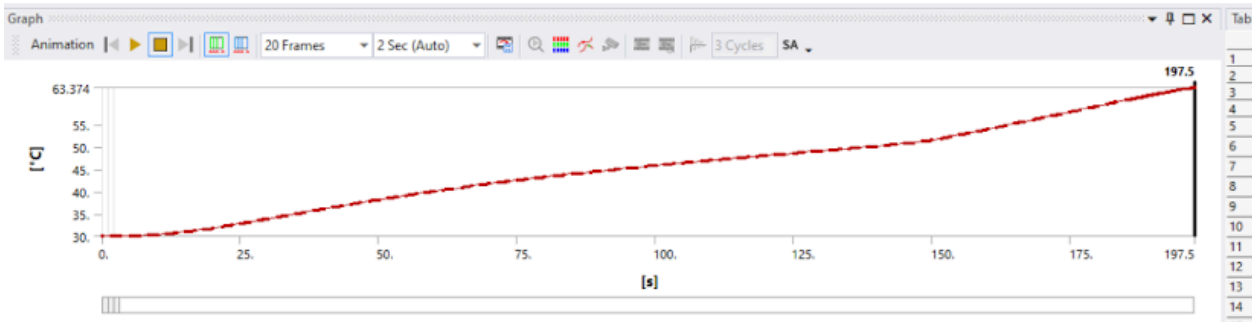

Figure 52: Max temperature at the bottom of the thermocouple plate over time. Reaches 63℃ after one layer.

Next, a simulation of a five-layer, 75mm square of Inconel 718 was run, with all of the printing parameters in Table 40 remaining the same. Additionally, heat transfer through radiation was enabled in an attempt to get more accurate results, although at the cost of increased computational time. Emissivity values of 0.15 and 0.6 were used for the aluminum and the Inconel, respectively. Finally, a dwell time of 60 seconds in between layers was added. Figure 53 displays the thermal results of this simulation after five layers. In this case, the whole build

plate heated up far above room temperature, with the hottest point ending at 184℃ and the coolest at 164℃. Figure 54 includes a graph of the max temperature over time at the bottom of our build plate, maxing out at 181℃. The bottom of the build plate only reached 55℃ after one deposited layer, compared to the 63℃ from the previous simulation. 181℃ is far above the marginal value of 80℃ that we were designing to meet, so adjustments in process parameters and build plate design were thought to be necessary.

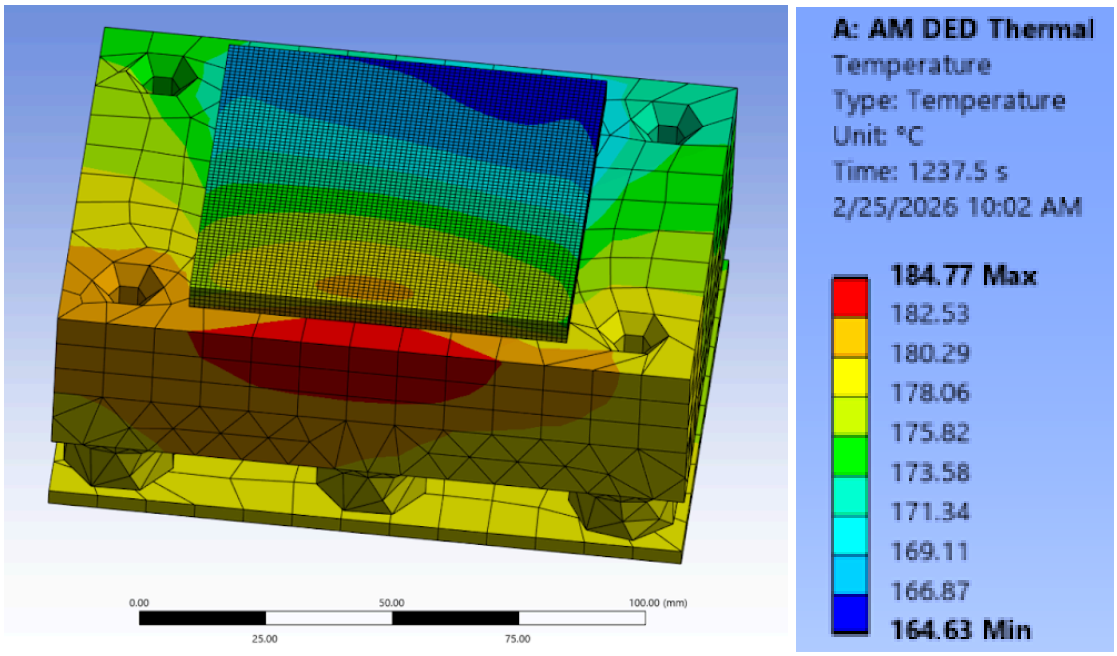

Figure 53: Thermal gradient after five-layer DED simulation on build plate with standoffs.

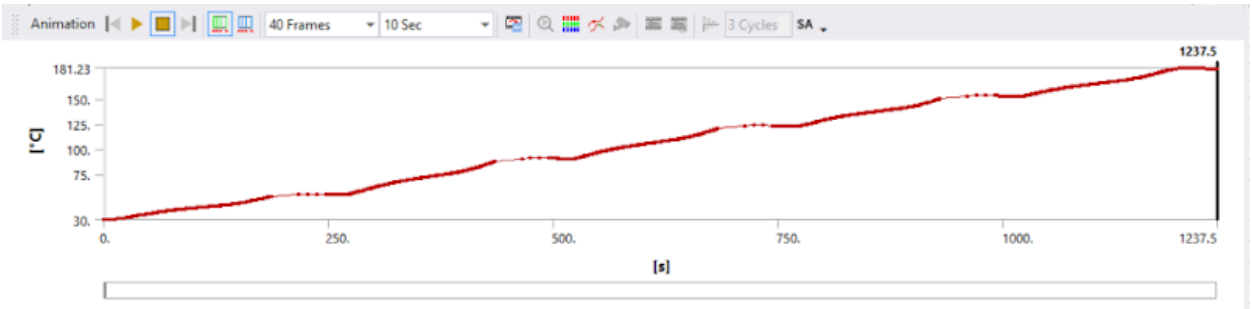

Figure 54: Max temperature at the bottom of the thermocouple plate over time. Reaches 55℃ after one layer, 181℃ after five layers.

Alumina Plate Design

Similar simulations were also run for the alumina plate design. Figure 55 shows the results for a five-layer part with the same settings as the print shown above. The major takeaway from this simulation was the higher max temperatures reached compared to the standoff design, with the maximum temperature of the whole plate

reaching 364℃, and even the outer corners ending above 250℃. As seen in Figure 56, the bottom of the build plate broke the 300℃ barrier by the end of the print.

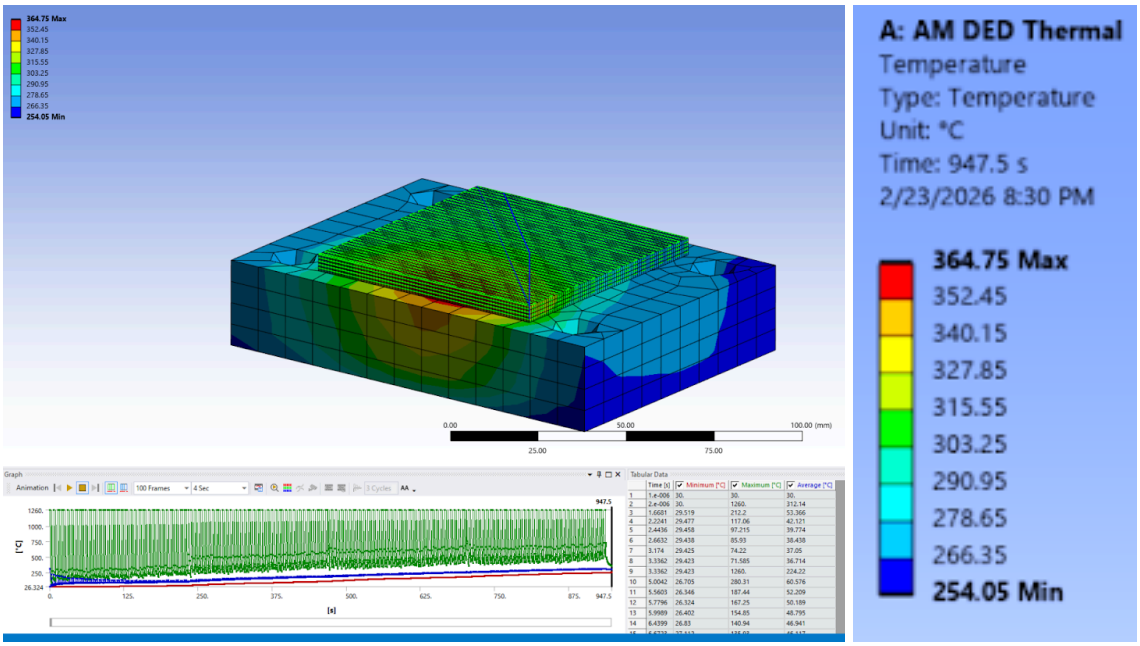

Figure 55: Thermal gradient after five-layer DED simulation on the alumina plate design.

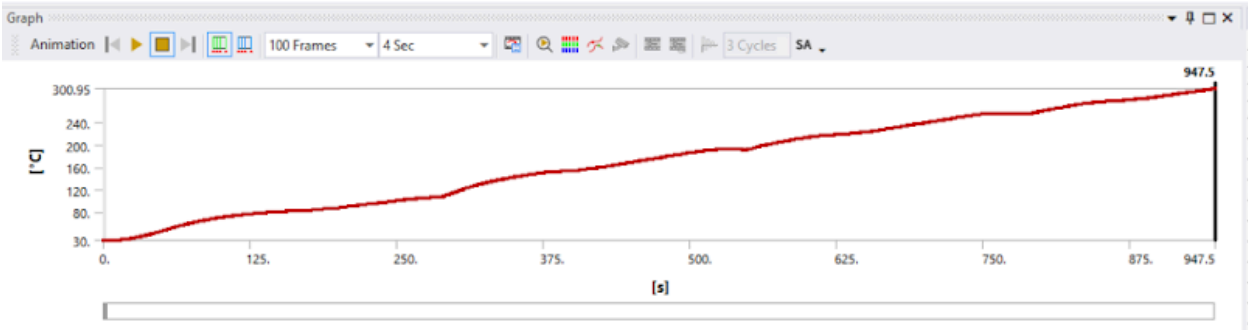

Figure 56: Max temperature of the bottom face of the build plate over time. Reaches 300℃ after five layers.

Revised Thermal Simulations

Then, following the first physical DED test of our miniature build plates, simulation parameters were adjusted in an attempt to match the empirical results, specifically the near-constant temperature throughout the later layers of the print. Discussion of the physical test setup can be found in the Thermal Testing section later in the report. For our simulation, the same diagonal-hatching infill pattern, and associated G-code (Appendix F), from the physical test was input into ANSYS. The convection coefficients were adjusted to 50 W/M^2K for the Inconel part to account for the shielding gas spray during deposition, and 30 W/M^2K for the rest of the build plate to simulate the air flow from the swirling shielding gas. The results, seen in Figure 57, showed an improvement, but still not close to our empirical values. The max temperature that the build plate reached by the end of printing

was 213℃, with the coldest area being at 137℃. The temperature at the base of the build plate, shown in Figure 58, climbed linearly again during the process, reaching 154℃ at its hottest point. This is still far above our specification of 80℃, and nearly three times the temperature seen during our physical print. This adjusted analysis was only done for the build plate with standoffs, as it was determined to be the final design following testing.

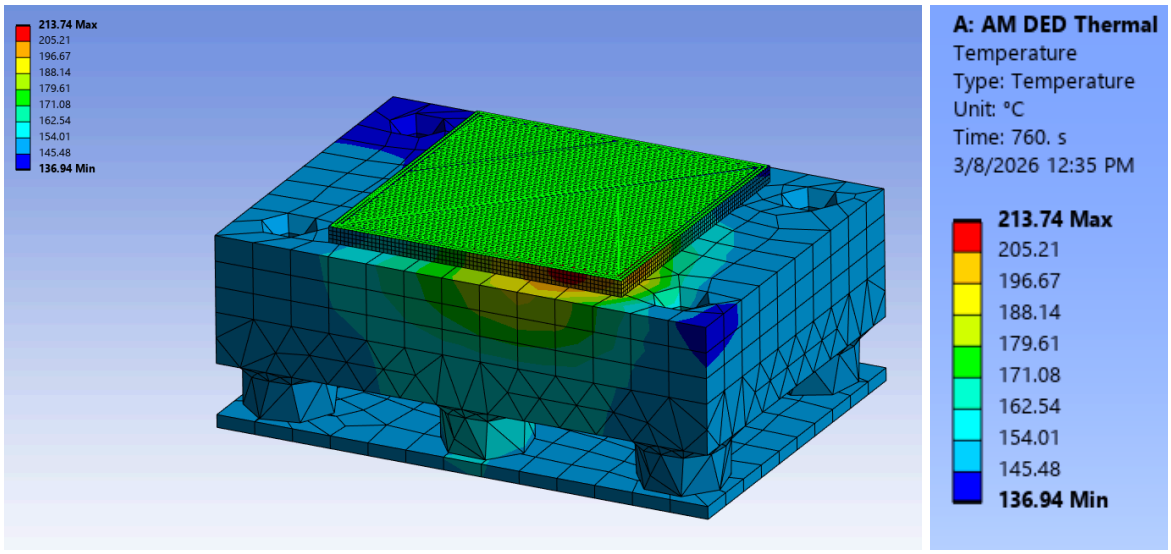

Figure 57: Thermal gradient after a four-layer DED simulation with adjusted infill pattern and convection coefficients.

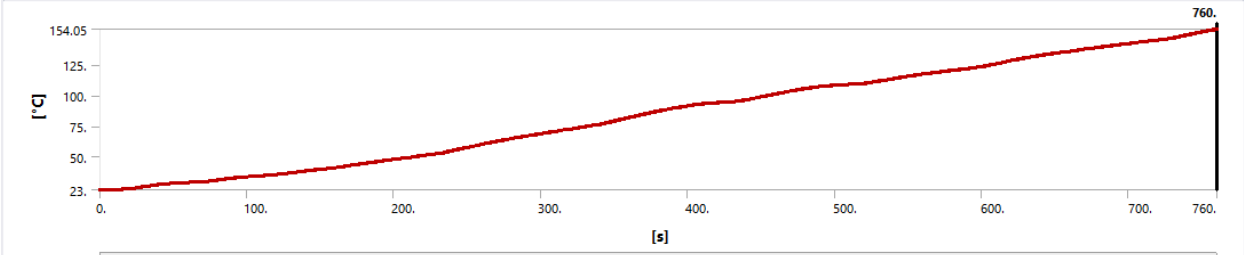

Figure 58: Maximum temperature on the bottom of the build plate after a four-layer DED simulation with adjusted infill pattern and convection coefficients.

The last aspect of the physical print that needed to be matched was the total process time. The Meltio machine took 55 minutes for the four-layer part, and the simulation built the part in 12 minutes. This proved to be a more difficult task than expected. We tried setting time commands in the G-code, implementing the laser feed speeds from AMPL's G-code file, and manually setting the time for each layer in the analysis settings. However, each of these has caused errors or was just ignored by the software. Finally, the parameter that got us the desired print time was changing the material deposition rate from 30 mm^3/s to 7.5 mm^3/s. After a 12-hour simulation, the results in Figures 59 and 60 were obtained. Unfortunately, they still did not match our empirical data, as the temperature at the bottom of the build plate still followed a close to linearly increasing trend, and reached 126℃ by the end of the fourth layer.

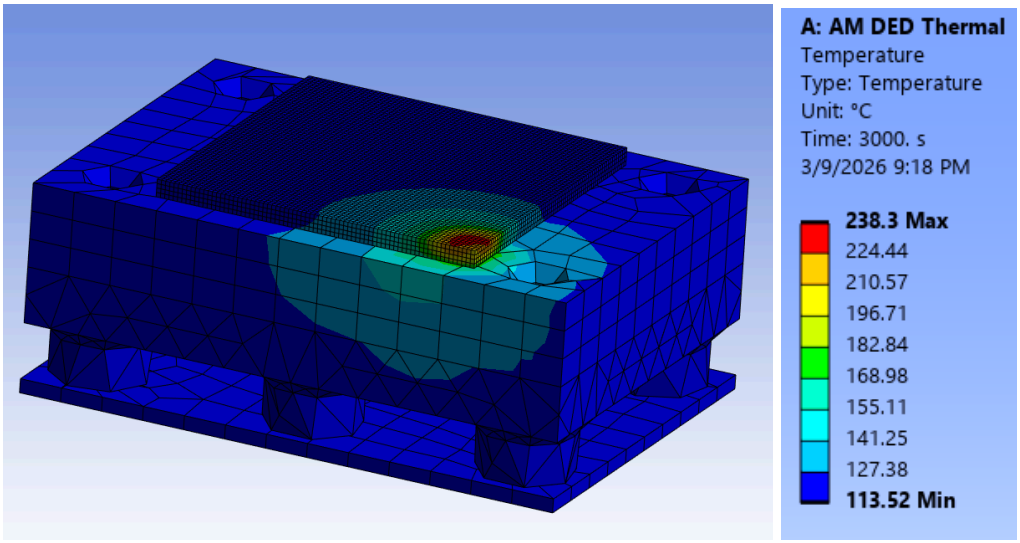

Figure 59: Thermal results after matching DED process duration

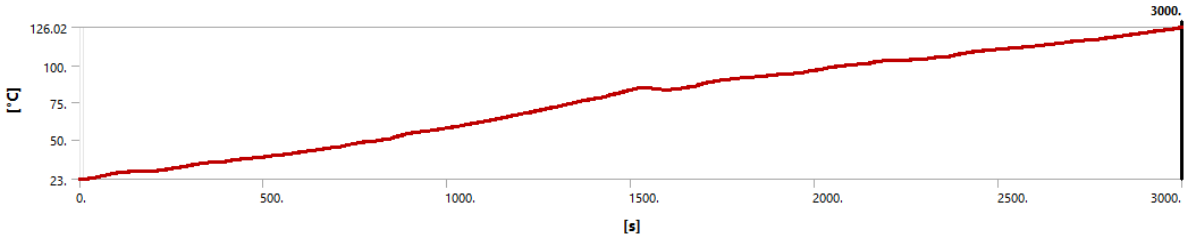

Figure 60: Maximum temperature on the bottom of the build plate after matching DED process duration

In a final effort to match the empirical results, the convection coefficients were increased to an unreasonably high value of 300 W/M^{2}K, and the adiabatic constraint on the bottom face was removed, yet the temperature trend was still close to linear throughout the whole process (Figure 61). Note that this was just a two-layer simulation in order to reduce computational time for repeated simulations.

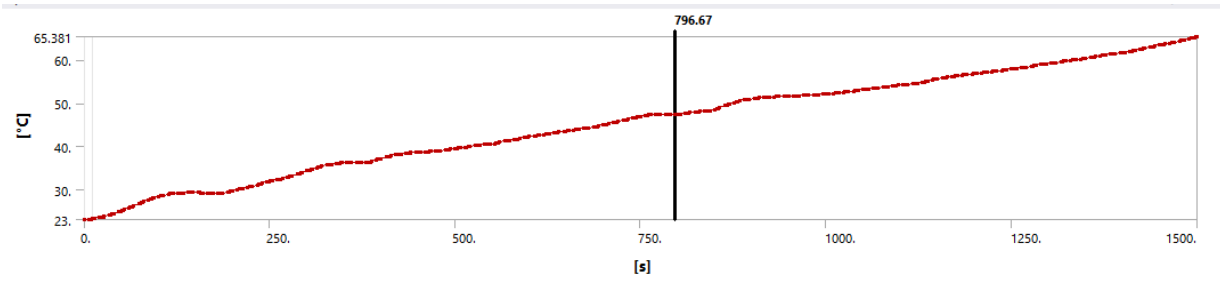

Figure 61: Maximum temperature on the bottom of the build plate after two layers with increased convection coefficients

Overall, the simulations were a good exercise for learning the effects of changing DED process parameters on the thermal results of the print. Although the outputs did not mirror the empirical data, the most important result

is that the physical test passed our metrics. Future work can be done to hone in these simulations, but they are not imperative to machine success.

Small Build Plate Structural Simulations

In preparation for running test forming testing after printing on the miniature-sized build plates, we ran additional structural simulations to obtain test results that can be compared with data collected. We ran these simulations on two designs: the build plate with a one-inch-thick aluminum standoff layer and the build plate with a quarter-inch-thick alumina plate.

The most important part of these simulations was matching the material properties to those of the materials we bought, since different vendors have drastically different properties, as we learned recently from our alumina purchase, and hence can not use default ANSYS materials. The properties used can be seen in Table 41 below. The McMaster 304 stainless steel had equivalent properties to Stainless Steel 304L Annealed from the Ansys material database, so we used the given material.

Alumina material properties were the ones we had to carefully analyze from McMaster data. The starred data in Table 41 indicates material properties that were defined differently in name on McMaster. Flexural Strength was given, however Ansys does not have a flexural strength property. We assigned this property as the Ultimate Yield Strength. Furthermore, Tensile Strength was imputed as Tensile Yield Strength. Lastly, Poisson's Ratio and Young's Modulus were not given, so we got these values from Matweb. If simulation results do not line up well with testing results, the Alumina material properties would be a good starting place to investigate errors.

Table 41: Material Properties used in Material Assignment in Ansys Structural Simulations

Material	Density (kg/m^3)	Young's Modulus (GPa)	Yield Strength (MPa)	Ultimate Yield Strength (MPa)	Poisson's Ratio	Compressive Strength (MPa)
Aluminum 6061	2713	69	240	300	0.33	N/A
304 Stainless Steel	7904	190	200	530	N/A	N/A
Alumina Silicate	2491	*10	*17	*69	*0.2	170

The forming test was modeled in Ansys by applying a downward force of 100 kN through a 1-inch diameter contact area, simulating the maximum load requirements our three-process machine must withstand. The 1-inch specification was chosen to directly match the physical tooling available in the laboratory where our empirical testing will occur. For the boundary conditions, the bottom surface of the assembly was constrained with zero deflection. We have intentionally omitted the rail setup from this simulation, as the test piece will maintain a solid contact surface during the procedure, and our primary objective is the validation of the structural simulations against the physical forming data.

Aluminum Standoffs Design

Simulations for the small testing version of the Aluminum Standoff design focused on characterizing the deflection and stress distribution under forming forces. As shown in Figure 62, the central forming force results in a maximum deflection of 41 microns at the center of the plate, while the underside shows a more distributed deflection of 26 microns.

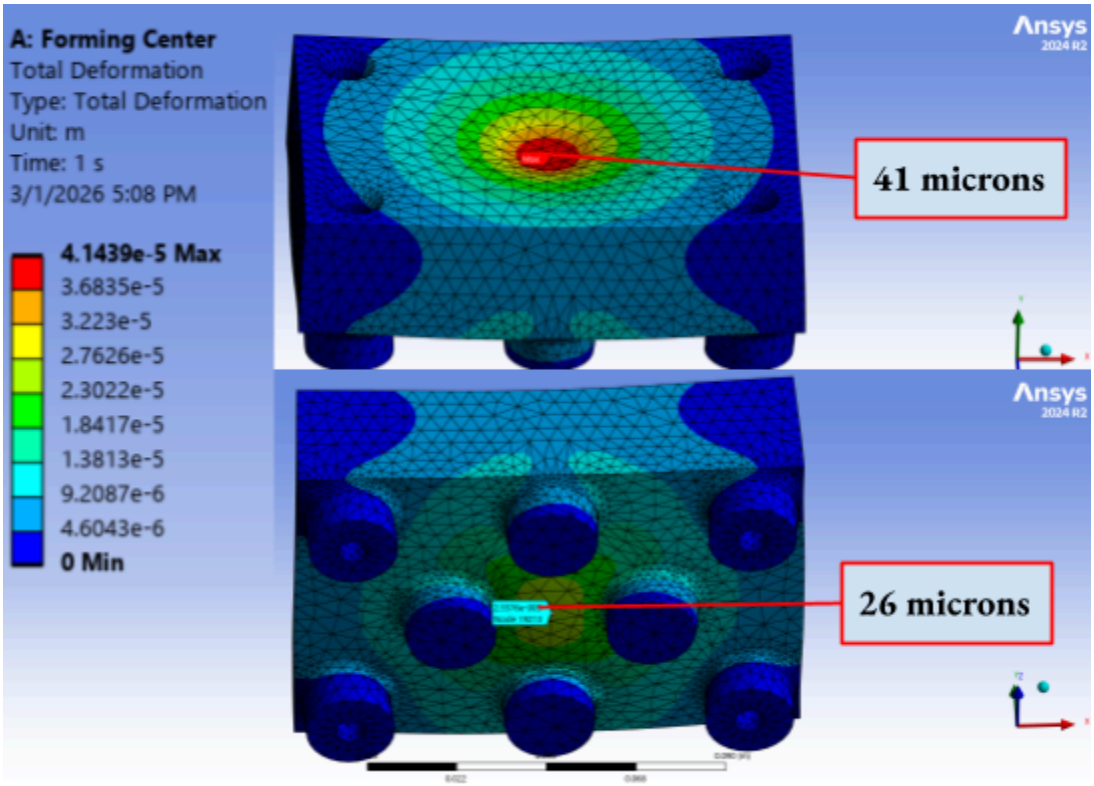

Figure 62: Standoff Forming Force - Maximum Total Deflection
Top: Build Plate; Bottom: Standoff Underside

The Aluminum Standoff design had a maximum stress of 100 GPa on the top surface and 180 GPa on the lower structural features, as seen in Figure 63. When compared against the material's Yield Strength of 240 GPa, the design remains within the elastic region. The stress concentration is highest at the fillet areas, indicating that a simple increase in fillet size can solve any stress issues.

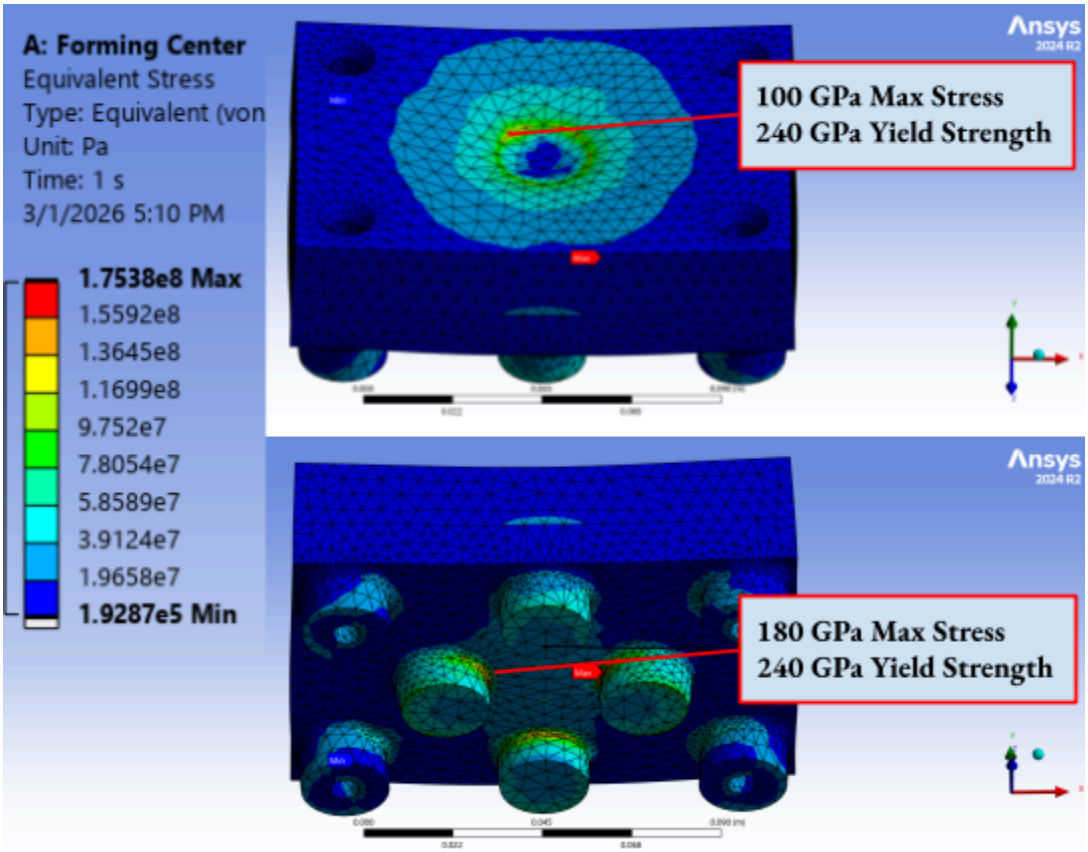

Figure 63: Standoff Forming Force - Maximum Stress
Top: Build Plate; Bottom: Standoff Underside

The Factor of Safety (FoS) analysis in Figure 64 highlights the same information - that while the overall standoff design is robust, the minimum FoS is localized at the fillets.

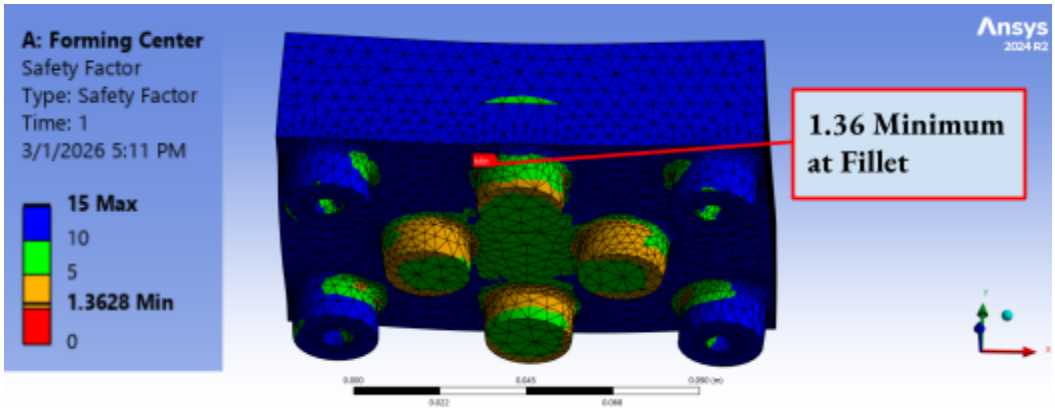

Figure 64: Standoff Forming Force Factor of Safety

Alumina Insulation Design

The second design investigated for the small testing stack was the Alumina insulation design. Figure 65 below shows a maximum deflection of 36 microns at the center of the plate, which is an improvement in stiffness over the aluminum standoff design of 41 microns.

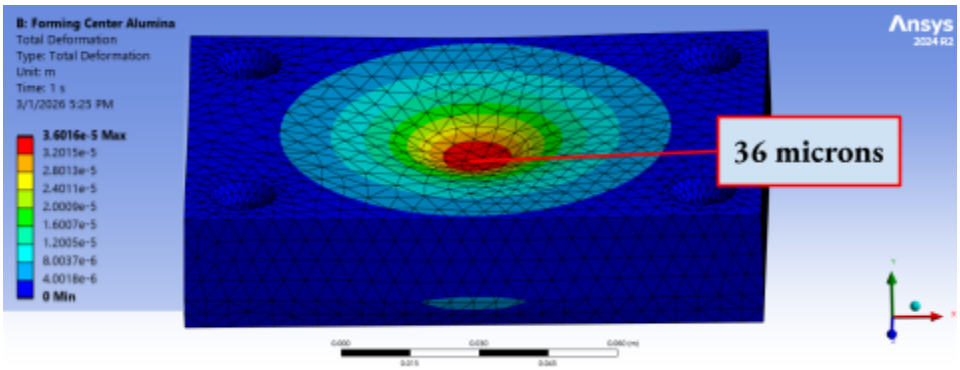

Figure 65: Insulation Forming Force Maximum Total Deflection

Despite the improved deflection characteristics and superior thermal performance, the Alumina Insulation design presents a significant structural risk at the current state. The Factor of Safety (FoS) analysis, as seen in Figure 66 reveals a minimum value of 0.41, indicating that the ceramic plate is predicted to fail under the current forming force loads.

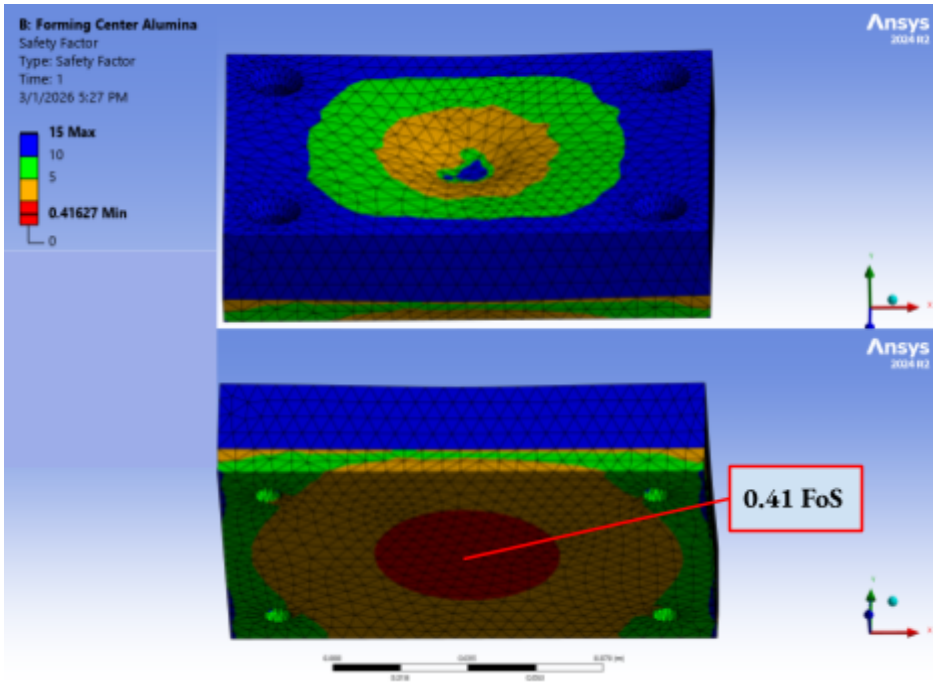

Figure 66: Insulation Forming Force Factor of Safety (0.41)

Workpiece Fixturing System Testing

Preliminary Testing

Thermal Testing

Setup & Procedure

We conducted two DED test prints with the help of PhD student Xingyang Li and the lab's Meltio M450 DED printer. For both prints, four 75x75mm solid square layers of Inconel 718 were printed onto our 304 stainless steel test build plates, one atop our 6061 aluminum alloy standoff design and the other with an alumina silicate insulation layer underneath. For each, temperature readings were recorded from a thermocouple inserted into a separate 0.25" thick 6061 aluminum alloy plate underneath the temperature control layer. Figure 67, below, shows the experimental setup for the standoff design test.

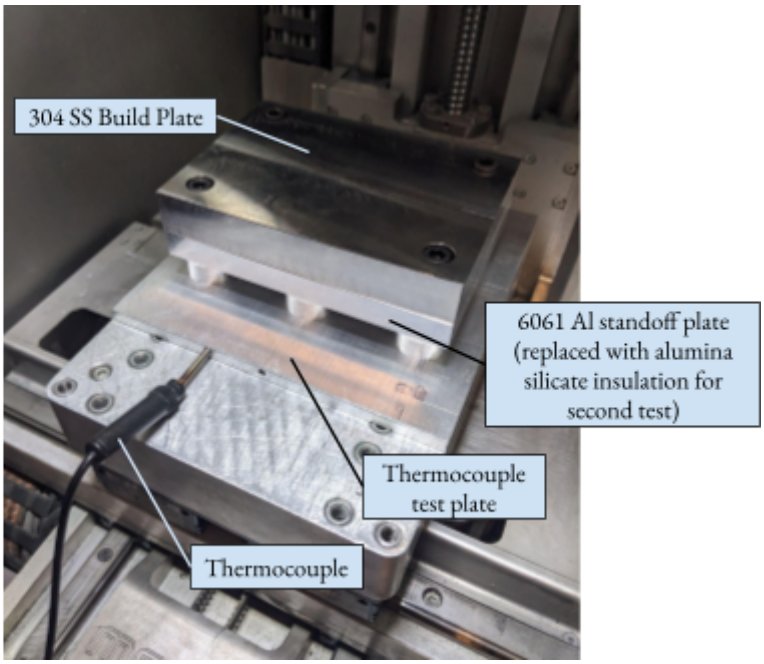

Figure 67: DED test setup, standoff design

There were several minor issues that we had to resolve before the first test, primarily with the thermocouple and thermocouple plate. The original thermocouple plate design protruded out from the M450's mounting block and interfered with the walls of the build chamber during the machine's homing procedure. This was fixed by bandsawing off the sides of the thermocouple plate to match the width of the mounting block. The end of the thermocouple would also hit the door during the homing procedure, which was addressed by taping it down to the mounting block. The thermocouple lead was passed through the door seal, and the body was taped to the outside of the machine (see Figure 68). Data had to be manually recorded from the digital readout, and the device would occasionally enter sleep mode.

Figure 68: Thermocouple mounting

While not ideal, this setup worked well enough to get good data. If the lab should choose to do similar testing in the future, a thermocouple that can output data to an SD card and mount inside the machine would be preferable.

For the first test, Xingyang had to swap the wire and align the lasers to it with an alignment camera. For later tests, this was skipped since the inconel wire was not changed out. Before each print, the machine prompted several pre-print checks (making sure the chiller, argon, etc. was all in good working order). The print settings were set to a default profile for Inconel 718. Each layer was printed with two perimeter tracks, alternating diagonal infill, and ~3 seconds of dwell time between layers. Below is an image of the live camera feed during the print, and a visualization of the current layer's progress.

Figure 69: Meltio dashboard and thermocouple reading mid-print

We recorded data every thirty seconds for an hour for each print. The actual print time was around 55 minutes, and we continued recording data after the print was done with the door closed for another 5 minutes to see the thermal behavior at the end of the print. Below is an image of the finished print from the insulation test.

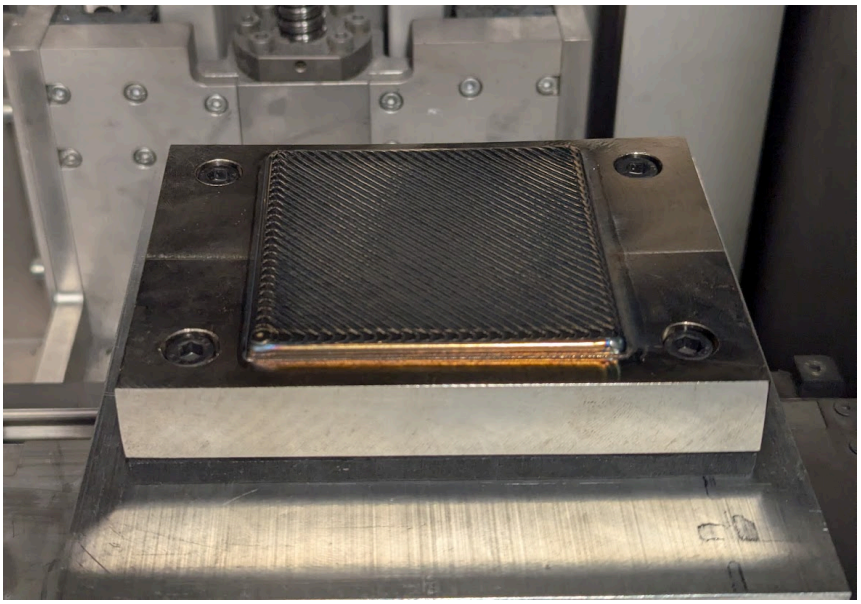

Figure 70: Completed test print, insulation design

The build plate was easy to remove (took ~45 seconds), despite warping significantly.

Results

Complete data from both prints can be found here. First, we'll take a look at the temperature vs time data for the standoff design:

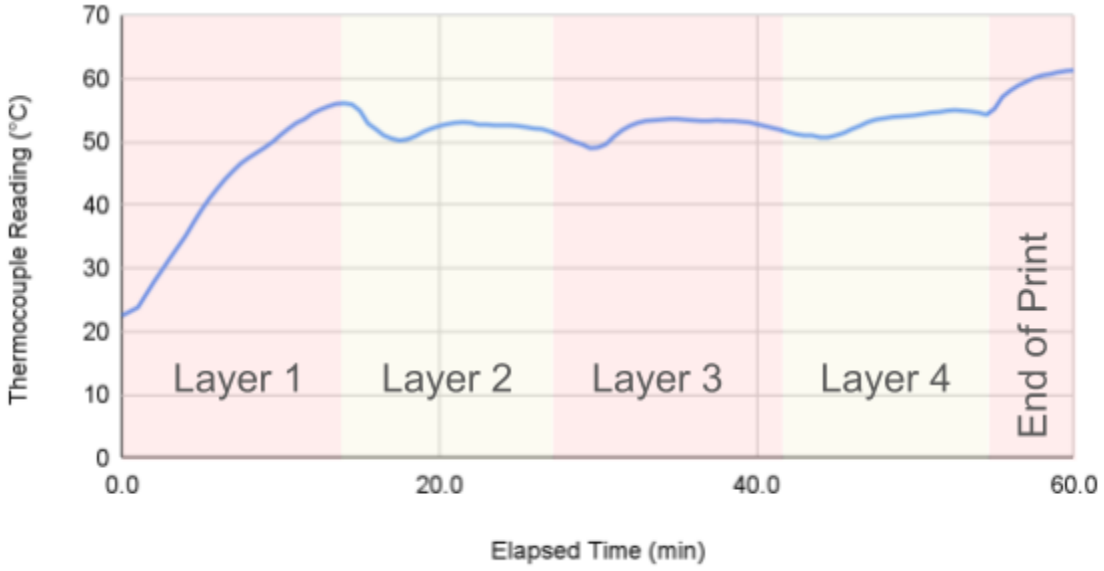

Figure 71: Aluminum Standoff Temperature vs Time

Data from this test displays a steady, nearly linear increase in temperature during the first layer. Temperature then decreases during the first 5 minutes of layer 2, before increasing to a quasi-equilibrium around 52.7℃. This pattern repeats for layers 3 and 4, although the initial temperature decrease is less pronounced and the quasi-equilibrium temperature increases slightly for each successive layer (53.4℃ and 54.5℃ for 3 and 4, respectively). At the end of the print, the temperature increases sharply before beginning to level out around 61.5℃.

We attribute the initial decrease in temperature at the start of layers 2-4 to a decreased heat flux as the perimeter tracks and initial infill are deposited. More heat is put into the part when the deposition track turns back on itself, which happens more during infill deposition. The slight increase in equilibrium temperature layer after layer is thought to be due to a "heatsoak" effect, where the heat from previously deposited layers more gradually moves through the assembly. The increase in temperature at the end of print is explained by the shutoff of shielding gas flow, drastically altering the convection conditions in the build chamber and resulting in a new, higher temperature equilibrium.

We will now take a look at the data from the insulation design:

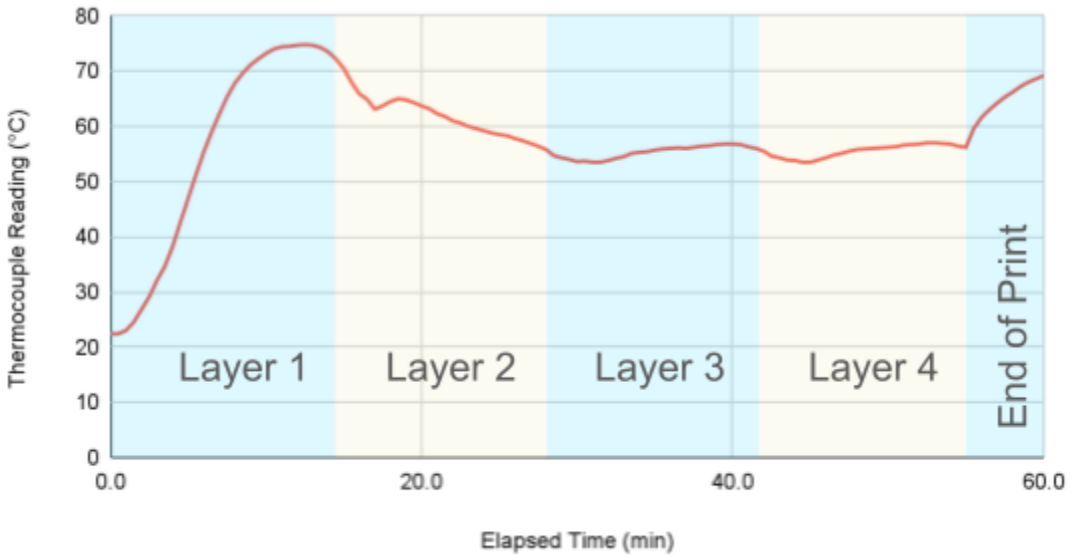

Figure 72: Alumina Insulation Temperature vs Time

General trends are shared between the two tests; the sharpest increase is in the first layer, temperature decreases at the start of layers 2-4, quasi-equilibrium conditions exist at the end of later layers, and there's an asymptotic increase to a new equilibrium after the print ends. However, the increase in the first layer is more nonlinear, approaching 74.5℃ asymptotically at the end of the layer. Layer 2 displays a general decrease, and equilibrium is not reached again until layer 3. Generally, the temperature is higher for the insulation design compared to the standoff design, as seen below in Figure 73.

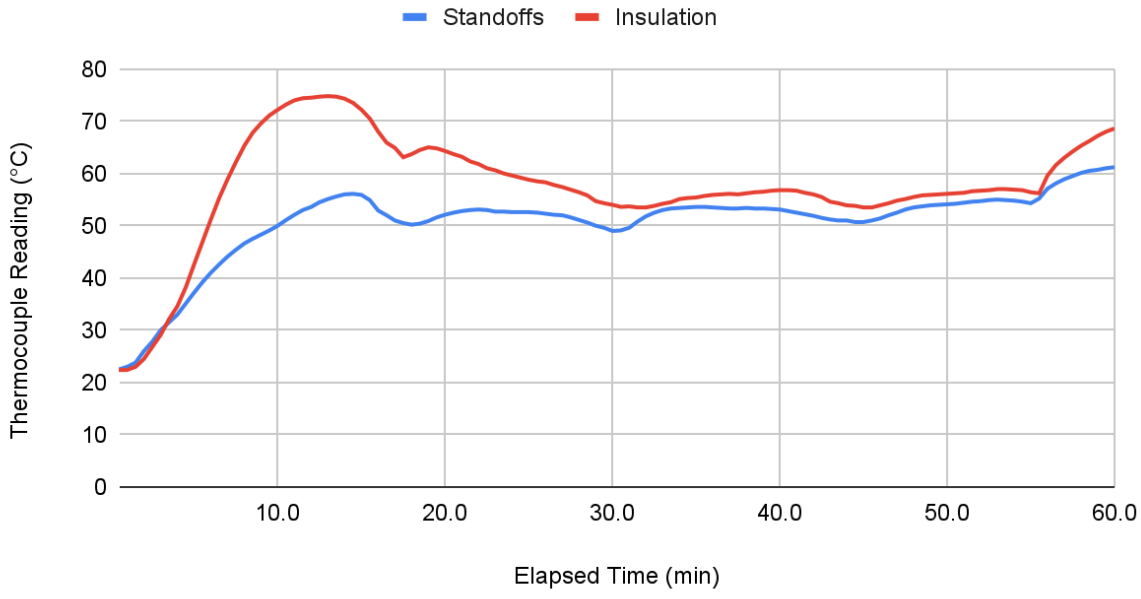

Figure 73: Temperature Over Time, Standoff vs Insulation

Both designs remain promising and perform within our marginal specification of limiting temperature at the motion components to 80°C. With an overall lower and more stable temperature profile, the standoff design emerges as a slight favorite; we also expect the standoff design to perform better as we scale it up to the full-size M450 build area, as there will be more thermal mass and more standoffs to dissipate heat. We do not expect the same benefits of scale with the insulation layer, since the primary driver of the design's performance is the thickness of the insulation layer, and that will remain unchanged.

Forming Testing

To prepare for the build plate forming tests, the team coordinated with Carla Shute, the facility manager of the CLaMMP Lab. The facility contains the instrumentation required for the 100 kN forming load test, specifically an Instron universal testing machine like the one shown in Figure 74. This system is capable of performing controlled deflection rate compression cycles up to our expected load.

Figure 74: Instron Universal Testing Machine

The moving crosshead can accommodate various toolhead diameters, ranging from 2 to 5 inches. The team has selected the 2-inch diameter tool to simulate the most concentrated load case. They are currently verifying the structural limits of this specific toolhead. If the 100 kN target exceeds its safety factor, the maximum test load will be adjusted to approximately 95 kN. The exact allowable load will be confirmed prior to testing.

The machine's lower pressurized surface consists of a flat plate approximately 18 inches wide. The build plate assembly will rest directly on this surface.

While the team initially identified that this flat-plate setup would not capture bending effects caused by the spacing of the final x-y system rails, the specific dimensions of those rails have not yet been finalized by the lab. Consequently, the current objective is to establish a baseline for the build plate's independent structural integrity. This data remains critical for the final design hand-off. No additional fixtures were used, as the primary goal was to evaluate the deflection and performance of the plate assembly itself.

The forming test was conducted as a standard compression sequence. The crosshead descended at a controlled rate of 10μm/s, applying load through the 2-inch tool until reaching the target force threshold of 100 kN. The Instron system provides real-time force and displacement readouts, which were used to monitor instantaneous deflection.

Post-test analysis involved extracting the load-vs-displacement data to characterize:

1. Stiffness: The slope of the linear-elastic region.
2. Linearity: Identification of any unexpected compliance or non-linear behavior.
3. Structural Integrity: Verification that the assembly withstands 100 kN without permanent deformation or damage.

Upon successful completion of the first press, the test was repeated for a total of five cycles per build plate. This iterative approach ensured reliability of our results and provided a preliminary assessment of whether the system experiences degradation or weakening under low-cycle loading while also showing on which cycle the majority of the plastic deformation occurs.

Alumina Materials Testing

We anticipated that our alumina insulation would fail under maximum loads, so we conducted a preliminary test to determine its failure threshold. We placed a spare piece of alumina underneath a stainless steel jaw as shown in Figure 75 and ran the test at a displacement rate of 5 microns per second.

Figure 75: Alumina Material Compression Test

Interestingly, the material did not fail as expected, which prompted a re-evaluation of the theoretical material limits. By doing some basic hand calculations to calculate the compressive strength of 25,000 psi over a surface area of 8 square inches, we determined that the theoretical failure load is approximately 1957kN, which would give us a factor of safety of around 20.

$$\sigma = 25,000\,psi\,; A = 17.6\,in^2\,; F = \sigma * A = 25,000 * 17.6 = 440,000\,lbf = 1957kN$$

This confirmed that our simulation discrepancies were primarily due to the material properties being inputted incorrectly and that the alumina design should survive forming.

Scaled Design Testing

Following the alumina tests, we moved to testing our test-scale designs. We attached a 0.857” screw and compressed the approximate center of the print area to 100kN for five cycles to simulate the forming process. The location was estimated visually, which may result in some discrepancy in the data. We increased the rate of movement to 10 microns per second to optimize our testing time after noticing that the slower rate was unnecessary. The center forming setup can be seen in Figure 76.

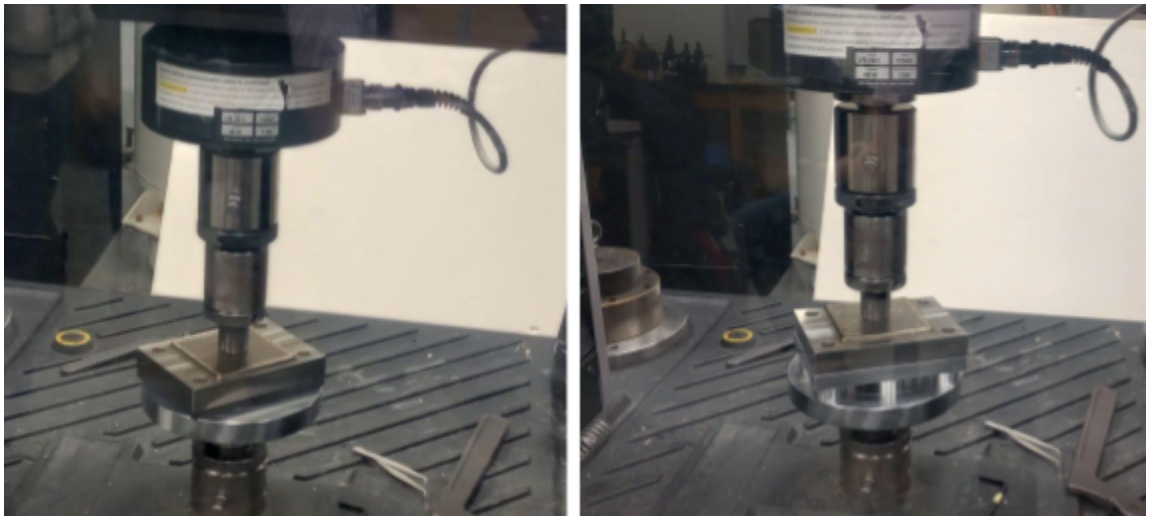

Figure 76: Center Forming Setup for Insulation (Left) and Standoff (Right) Test Designs

We observed significant initial deflection during the first press, followed by minimal changes in subsequent cycles. For the alumina insulated buildplate, the load in the first cycle begins to rise noticeably at around 0.005 mm of displacement, while in the second cycle, the corresponding rise does not occur until roughly 0.052 mm.

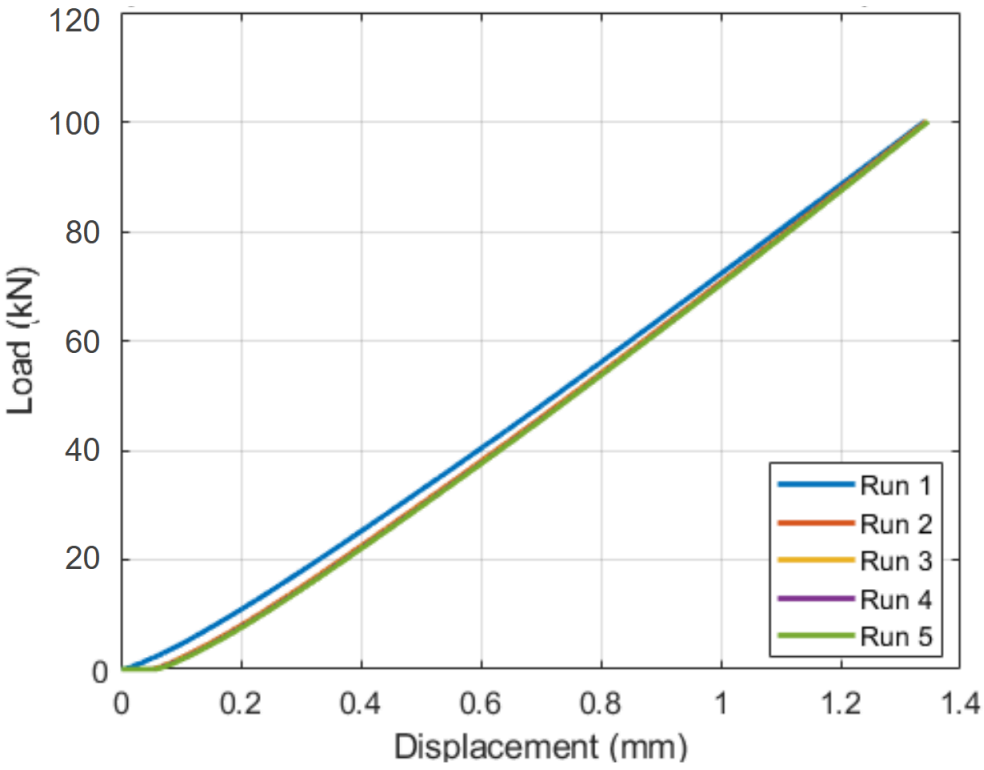

Figure 77: Compression Test: Alumina Insulated Build Plate (Zoomed In)

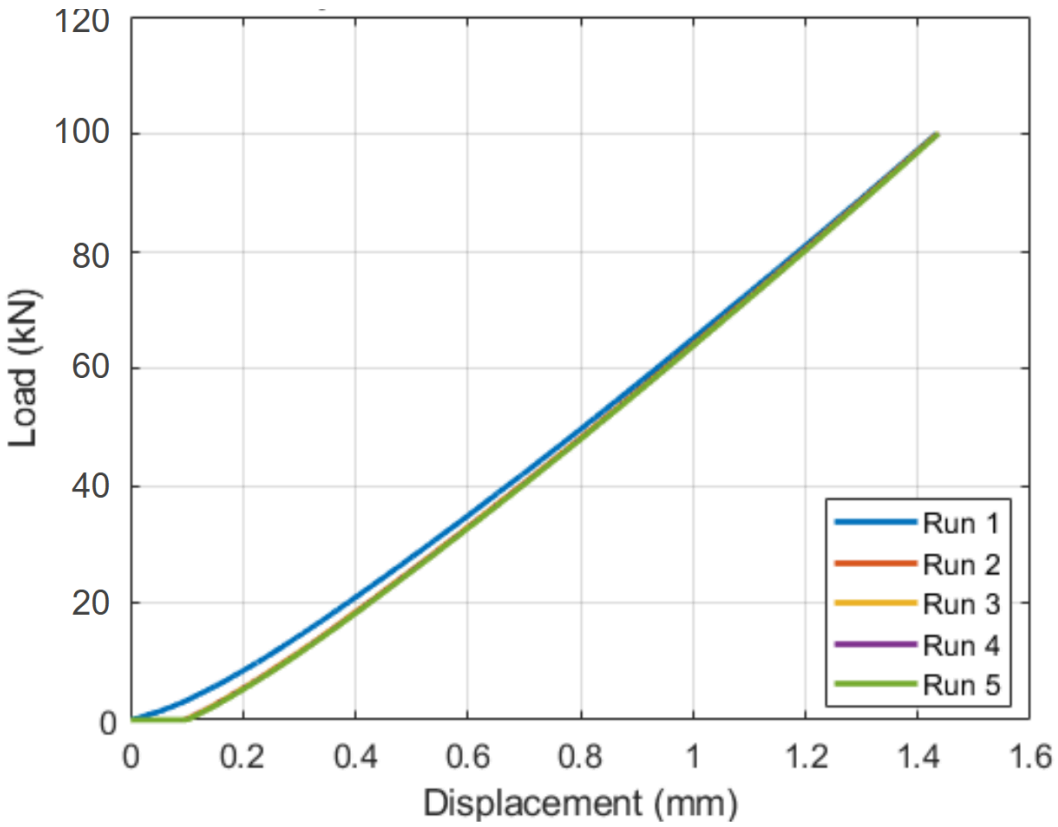

Figure 78: Compression Test: Alumina Insulated Build Plate (Zoomed In)

This difference of about 0.047 mm represents the horizontal displacement shift seen on the graph at the start of the test, which represents the plastic deformation due to the first compression cycle of the setup. The displacement at which the load starts to increase sharply marks when the sample is fully engaged with the compression tool. By comparing the contact points across cycles, we can see that after the second cycle, there is no noticeable increase in this horizontal displacement relative to the previous cycle. We assume from this that the inconel layers plastically deform during the first press, and not during subsequent presses. For the aluminum standoffs build plate, the plastic deformation we calculated based on the data resulted in 0.052 mm. This is likely due to the aluminum being more compliant than the alumina, but could also be due to variance in the print.

From the data, we also determined the stiffness of alumina build plate assembly to be 80 kN/mm. The stiffness of the standoff assembly was, interestingly, also nearly exactly 80 kN/mm. It is important to note that these deflection values cannot be used directly to validate the deflection data from our simulations. This is because the Inconel structure collapses first, accounting for the large initial deflections, before the build plate itself begins to deflect. To accurately validate the simulation data, a secondary test would be required using a pre-formed Inconel structure to isolate the deflection of the plate.

We proceeded to do a forming test at the corner of the plate and performed two additional presses to simulate worst-case forming at the corner. The setup can be seen in Figure 79.

Figure 79: Corner Forming Setup for Insulation (Left) and Standoff (Right) Mini Designs

It took a significant amount of time for the machine to register a significant load after zeroing during these tests because the stainless steel plate was warped, causing it to move before making full contact at the corner. The gap from the warping can be seen in Figure 80. Testing results are shown in the graphs below.

Figure 80: Corner forming gap between build plate and insulation due to warped build plate

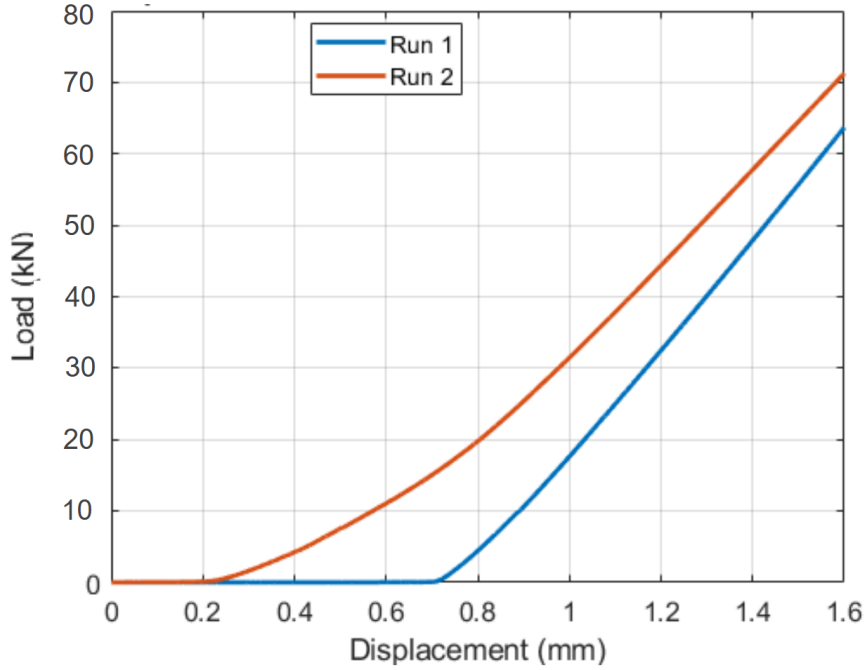

Figure 81: Compression Test: Alumina Insulated Build Plate Corner (Zoomed In)

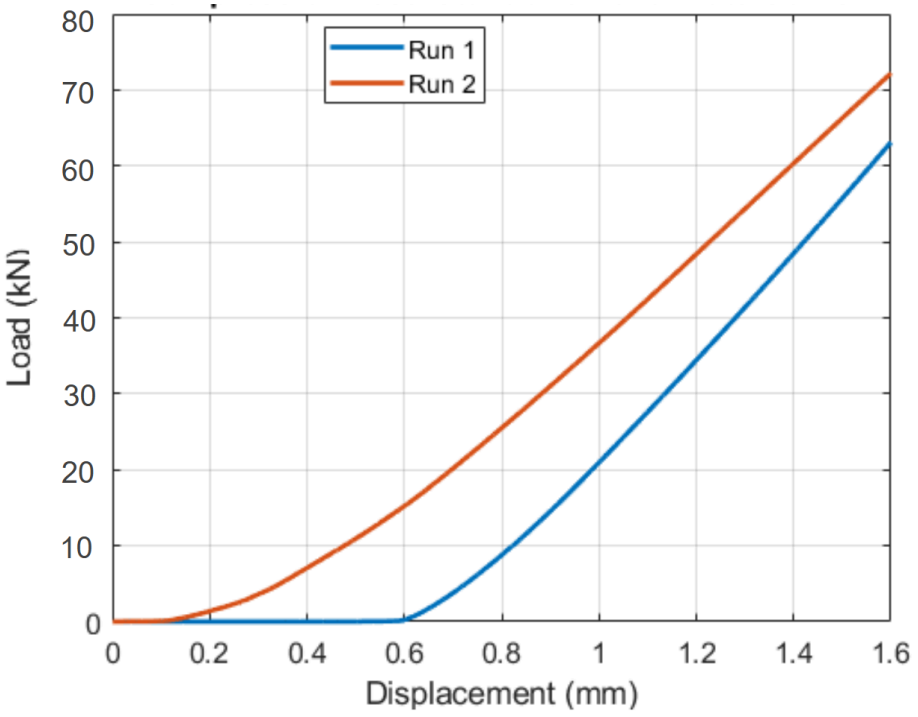

Figure 82: Compression Test: Standoffs Insulated Build Plate Corner (Zoomed In)

After the testing, we observed that the Inconel was indeed formed with the corner being affected more, as shown in Figure 83 for the insulation design and Figure 84 for the standoff design. We believe this is because the edges are slightly elevated, meaning a smaller surface was receiving the load, and hence the load was more concentrated. This gives our team hope that a smaller tool should be able to form better. For further testing, our team made an adaptor for a 9.5mm tool size.

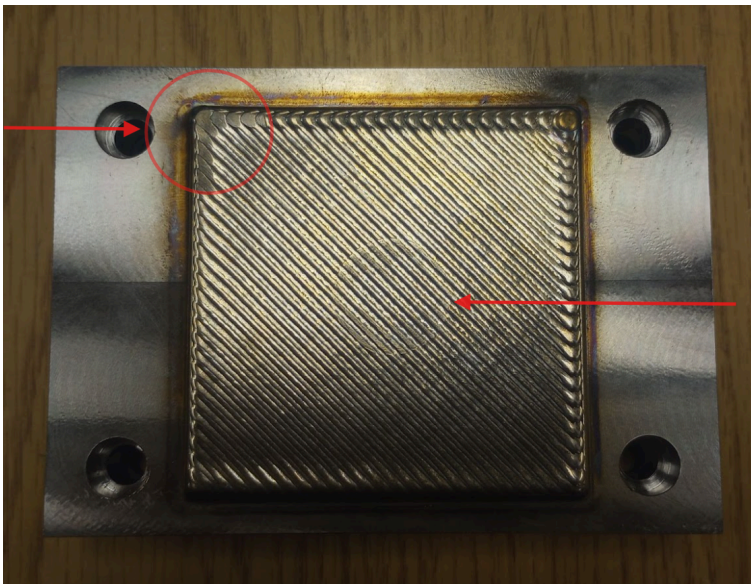

Figure 83: Formed Build Plate with highlighted formed areas of Insulation Mini Design

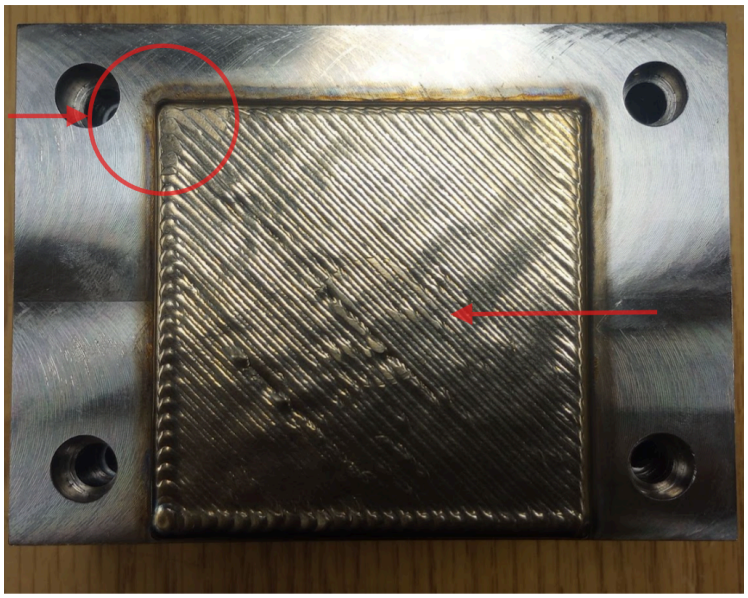

Figure 84: Formed Build Plate with highlighted formed areas of Standoff Mini Design

Through both quantitative data and qualitative observations, we confirmed that the Inconel was successfully formed in both the insulation and standoff designs. However, we did notice minor artifacts from the corner

pressing process, specifically chipping on the alumina at the concentrated line of the corner press, as shown in Figure 85. This was likely caused by the warped steel plate and raises some concerns regarding the brittleness of the alumina.

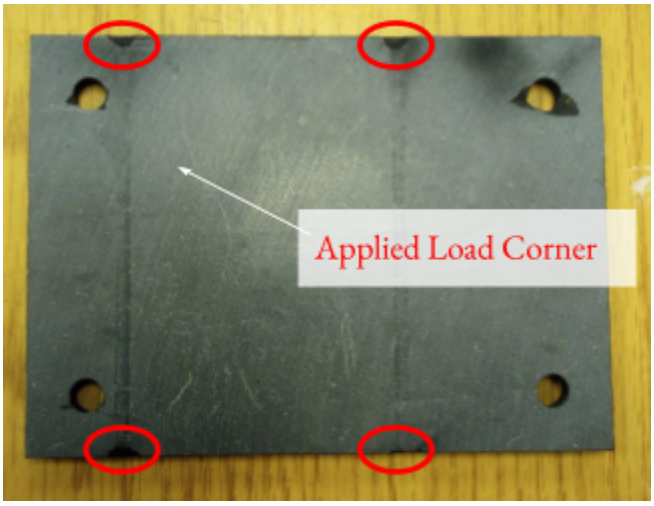

Figure 85: Alumina Insulation Sheet Chipped during corner forming due to warped Build Plate

Additionally, the aluminum standoff became warped during testing as seen in Figure 86.

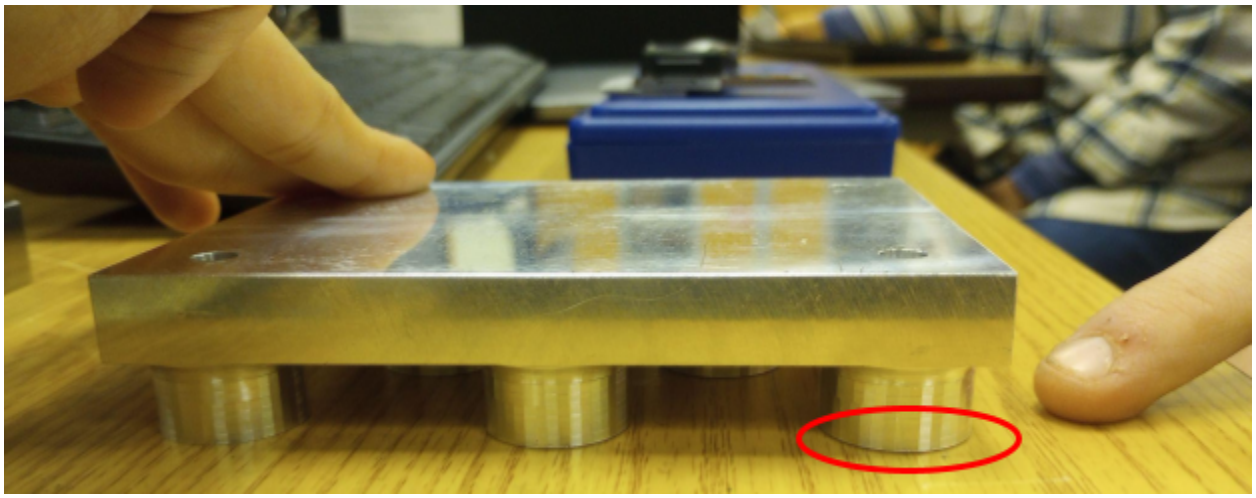

Figure 86: Aluminum Standoff warped/permanently deformed during corner forming

Since the plates were not fixed down during these corner tests, it is reasonable to conclude that full contact was never achieved and that this testing is not representative of a properly clamped test environment, where we expect the chipping and warping would be mitigated.

Furthermore, we noticed circular indents in our alumina in Figure 87 which we initially thought were from the forming tool imprint, but realized were from the bottom plate pattern. This is important to note since it may

affect results minimally so for a true forming test we would have to place a solid piece of metal underneath for full plate contact. We don't anticipate these circles affecting data significantly.

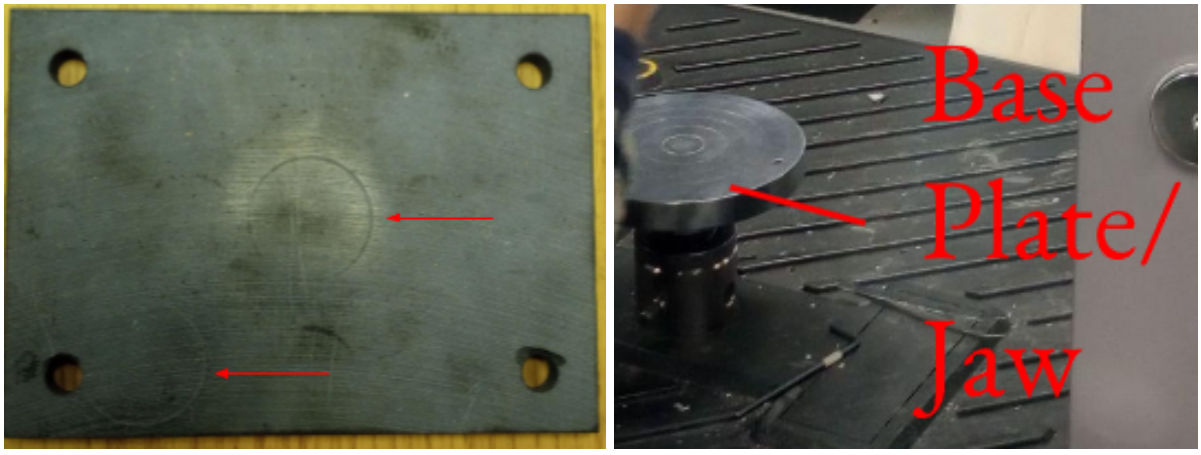

Figure 87: Alumina Sheet shows circular indents from the center ring of the Base Plate / Jaw

Subtractive Testing

Setup and Procedure

To test whether our buildplates could withstand subtractive machining operations, we designed and manufactured an adapter plate to bolt the buildplate assemblies into a HAAS CNC mill. This setup enabled facing and side milling operations to be performed directly on the printed and formed Inconel 718 parts. The goal of this test was to determine whether the buildplates could tolerate the shear forces and vibrations introduced during machining without structural failure.

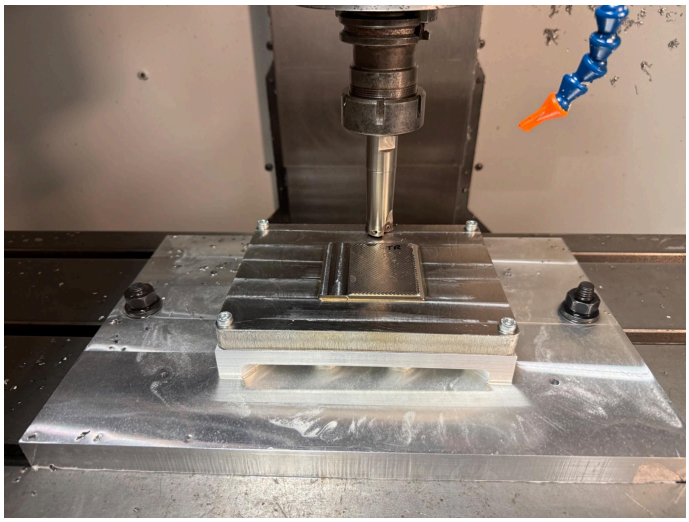

Figure 88: Machining Test Setup

The intended cutting tool was a Mitsubishi WJX09UR1602FA16S (Figure 89), a ¾-inch two-flute indexable end mill equipped with VP15TF inserts designed for heat-resistant alloys. The recommended cutting parameters used for the test are shown in Table 42 and come from Mitsubishi's specifications for cutting Inconel 718 with these inserts.[38]

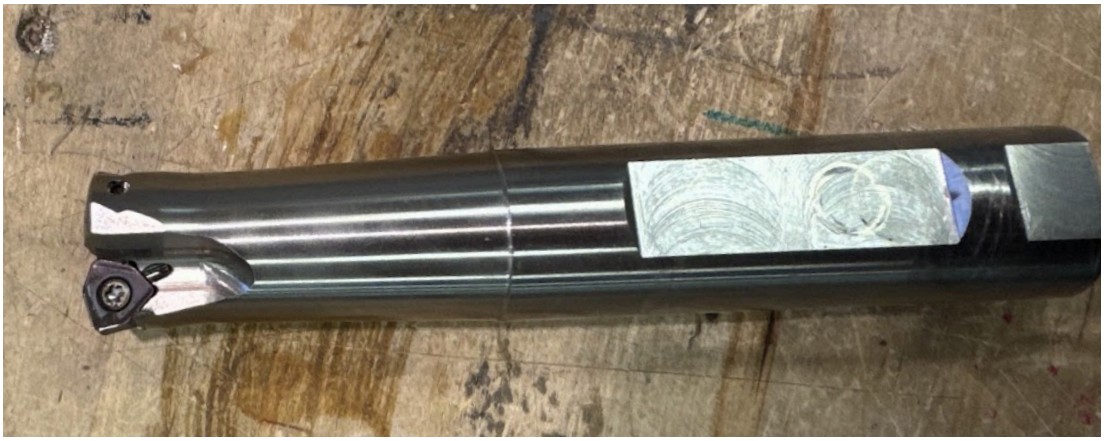

Figure 89: 3/4-inch two-flute indexable endmill with VP15TF inserts

Table 42: Subtractive Test Cutting Parameters

Operation	**Cutting Speed (SFM)**	**Feed Per Tooth (IPR)**	**RPM (n)**	**Table Feed (inch/min)**	**Radial Depth of Cut (in)**	**Axial Depth of Cut (in)**
Face Milling	130	0.006	662	7.9	0.375	0.02
Side Milling	130	0.006	662	7.9	0.25	0.1

When machining Inconel 718, the key challenge is work hardening. The material becomes harder in the region directly affected by the cutting tool, so the feed and speed must ensure the cutter removes material deeper than the work-hardened region during each engagement. During this test, qualitative observations were collected regarding machining performance after which the buildplate was removed and analyzed. The primary objective was to determine whether one buildplate design performed better than the other under the shear and vibrational loads induced during milling, and if catastrophic failure could occur.

Standoff Design

Although the machining was intended to use the indexable end mill shown in Figure 89, a different ¾-inch end mill without the correct inserts was used while maintaining the same feed and speed parameters. This mistake was not ideal, but both the facing and side milling operations proceeded smoothly (Figure 90).

[38] PDV coated grade for milling Miracle VP15TF

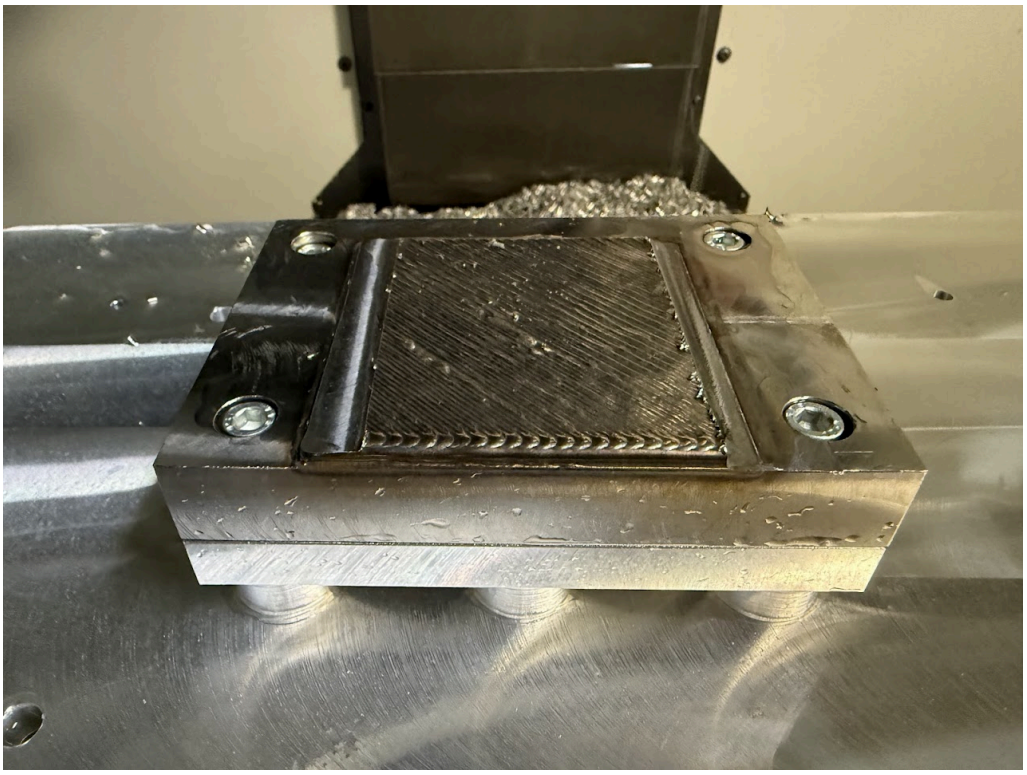

Figure 90: Aluminum standoff design with facemilling (left) and side milling (right)

The resulting surface finish was very smooth and the part machined well, some burrs were produced while side milling. The cutting process produced a consistent and stable sound, indicating favorable cutting conditions, and no visible damage to the cutting tool was observed. Additionally, the four M6 bolts successfully secured the entire buildplate stack during machining.

Insulation Design

Using the same incorrect end mill, the alumina–silicate insulated buildplate design was machined. During this operation, a noticeably higher-pitched sound was observed. Although the final cut surfaces appeared smooth, the edges of the machined regions contained more burrs.

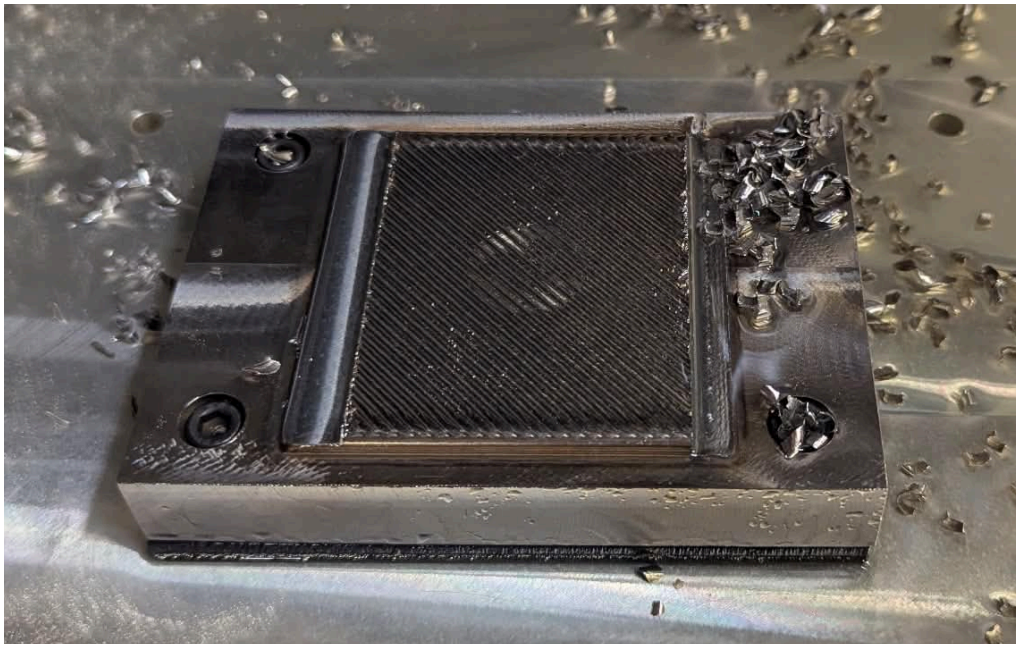

Figure 91: Alumina Silicate design with facemilling (left) and side milling (right)

Upon further inspection, the end mill inserts had sustained visible damage during this operation, which may partially explain the sound and increased burrs (Figure 92).

Figure 92: Damaged endmill insert, with damage circled in red

Additional damage was also observed in the alumina–silicate plate after machining. Marks from the forming process appeared more pronounced and possible hairline cracks were identified in the material, but it was unknown at the time whether the increased visibility was due to another factor like wetting from coolant. Furthermore, some chips had not been fully cleared before the buildplate was bolted down, resulting in them becoming embedded in the alumina layer and causing localized chipping.

Initial testing did not show a meaningful difference in machinability, but since the alumina silicate plate was easily damaged from the bolting down and its possible hairline cracks formed/were worsened by the process, the aluminum standoff design is preferred for subtractive machining.

Preliminary Testing Summary and Design Recommendation

Initial results from thermal testing showed that both designs reached quasi-equilibrium conditions after the first print layer, with the alumina insulation design experiencing a much greater temperature spike during the first layer and higher temperatures throughout. No conclusive decision was reached based on the initial DED thermal testing, but the standoff design emerged as a slight favorite as it passed our ideal temperature metric throughout the whole print.

Initial results from forming testing were that both the alumina insulated and standoff build plate designs are capable of withstanding direct low-cycle 100 kN compressive loading and that the full build plate assemblies are robust enough to survive forming. The build plates assembled were not fixed down and are not fully representative of the expected final machine setup. Chipping on the edges of the alumina due to the stress concentrations from the warped build plate raised concerns concerning the brittleness of alumina.

Initial results from subtractive testing indicated that the aluminum standoff design performed slightly better. The alumina design was damaged because the buildplate area was not properly cleaned before part mounting, and it is possible hairline cracks propagated during the test but not confirmed. For machining, both designs performed similarly and differences were likely due to using a worn tool on the alumina design.

After the subtractive testing was performed, the buildplate designs were handled by the team and advisors over the next couple of hours. Over time hairline cracks became increasingly pronounced, and the alumina sheet eventually fractured during normal handling by the team.

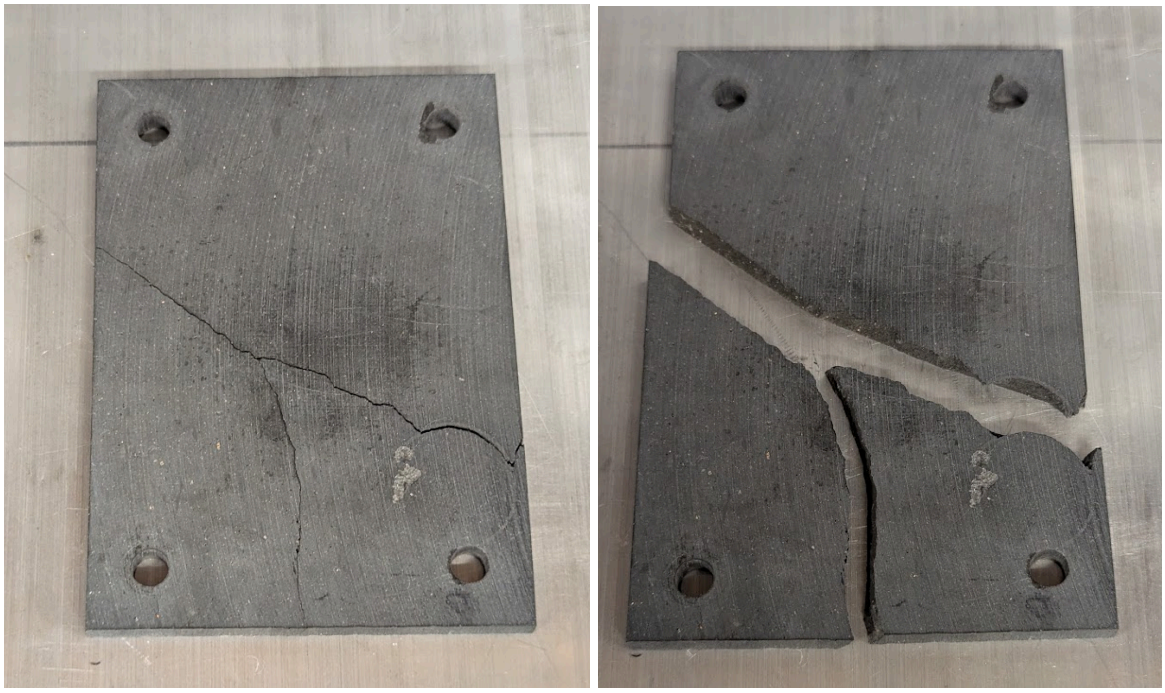

Figure 93: Fractured alumina insulation plate

Due to the failure of the alumina plate after the three processes occurred, we determined that the aluminum standoff design would be what we recommended for our client. For the final standoff design, we kept the same standoff diameter, standoff height, and block height. The overall footprint was scaled up to the full size of the M450 build area, with provisions to ensure that the thermocouple could still be inserted.

Etching and Polishing

Although the material grain structure validation and refinement is part of the research expected to be done by AMPL, we still wanted to gather some baseline information of what our post-testing workpiece looks like on a microscopic scale to identify any potential improvements in grain structure. After completing the DED, forming, and subtractive testing, we asked AMPL to cut one of our plates in half, directly through the forming area, using the wire EDM machine in the research shop. This allowed us to reveal the cross-section of the steel and Inconel workpiece and to understand the effect the large forming tool had on the grain structure of the deposited Inconel when compared with the grain structure of an unformed area.

We reached out to Dr. Carla Shute at Northwestern's CLaMMP lab for help preparing and analyzing our sample. In order to view the grain structure under a microscope, a sample must first be sanded and polished to a flat, mirror finish, and then be etched to reveal the individual grains. While the sanding should be done automatically by a machine with a spinning sanding plate, our sample was too big to safely and accurately hold flat. Instead, we manually wet sanded the cross-section side of the cut workpiece, stepping up from 180-grit sanding sheets to 800 grit. After bringing the surface to a near mirror finish, we continued polishing using

3-micron and then 1-micron diamond polishing solutions. Once polished, we etched the workpiece using Marble's reagent solution consisting of distilled water, hydrochloric acid, and copper (II) sulfate, by applying it briefly with a swab and rinsing within 2–3 seconds using water and isopropyl alcohol to stop the reaction. Finally, we examined the piece under a high-resolution image-stitching microscope.

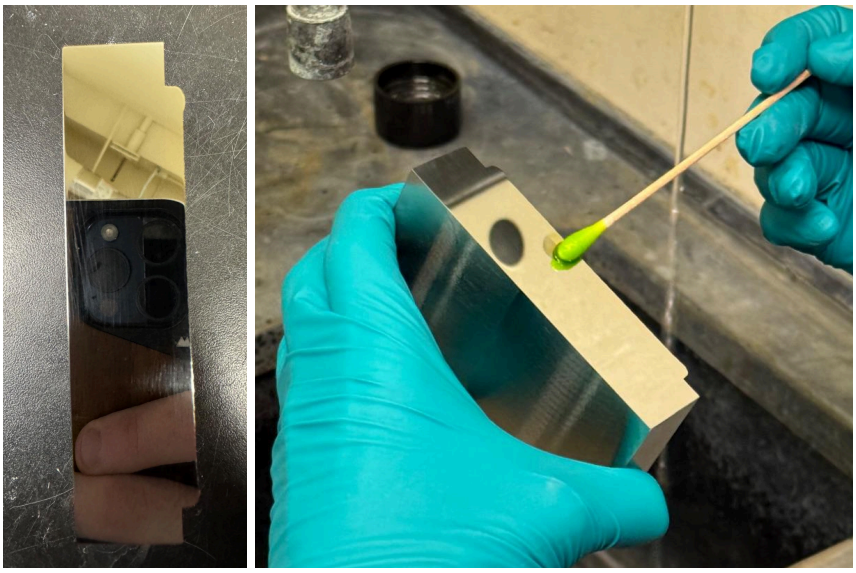

Figure 94: Polished Cross-Section and Marble's Etching Compound Applied to the Inconel

From the resulting images, it was difficult to observe a significant difference between the formed and non-formed sections. This is likely due to the large size of the 21.8mm diameter forming tool (we later scaled down the tool diameter for final testing to a 9.5mm diameter to better match the expected size for the final machine). Figure 95 below shows a side by side comparison of the formed and not formed grain structure without any noticeable difference..

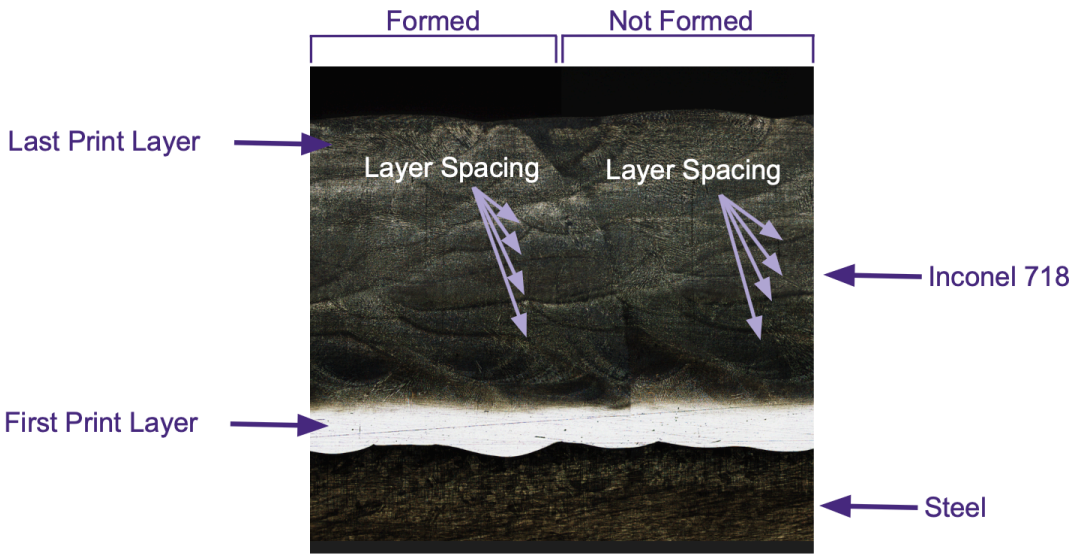

Figure 95: Polished and Etched Workpiece under Microscope, Formed and Unformed Region

The forming process seems to have flattened the arc-shaped grains on the right side, making the layer boundaries look much more compressed on the left compared to the rounded print pools on the right. Even though the overall thickness hasn't changed much, the first layer shows a much clearer indentation into the steel build plate on the formed side. This suggests the forming pressure didn't just compress the Inconel material, but forced the Inconel to interlock more tightly with the stainless steel build plate.

As next steps, the lab will further investigate the effects of forming on the Inconel grain structure post-DED printing using more advanced methods. Performing electron backscatter diffraction (EBSD) across the full region (both within and outside the formed area) and analyzing Orientation Distribution Functions would provide more quantifiable insights. Additionally, for improved polishing quality and more reliable results, we recommend cutting the workpiece/build plate into a much smaller section (around 1.5 cm × 1 cm × 1 cm) to allow better control during polishing, as working with the full plate proved challenging due to its size. Finally, repeating this process on the final tested build plate, where a smaller forming tool was used, would likely yield more noticeable results.

Final Design Testing

Final DED Testing

We repeated the identical DED testing procedure with the larger build plate design, printing 4 75x75mm solid square layers onto the build plate and recording thermocouple measurements every thirty seconds for an hour. The finished test, still in the machine, is below in Figure 96.

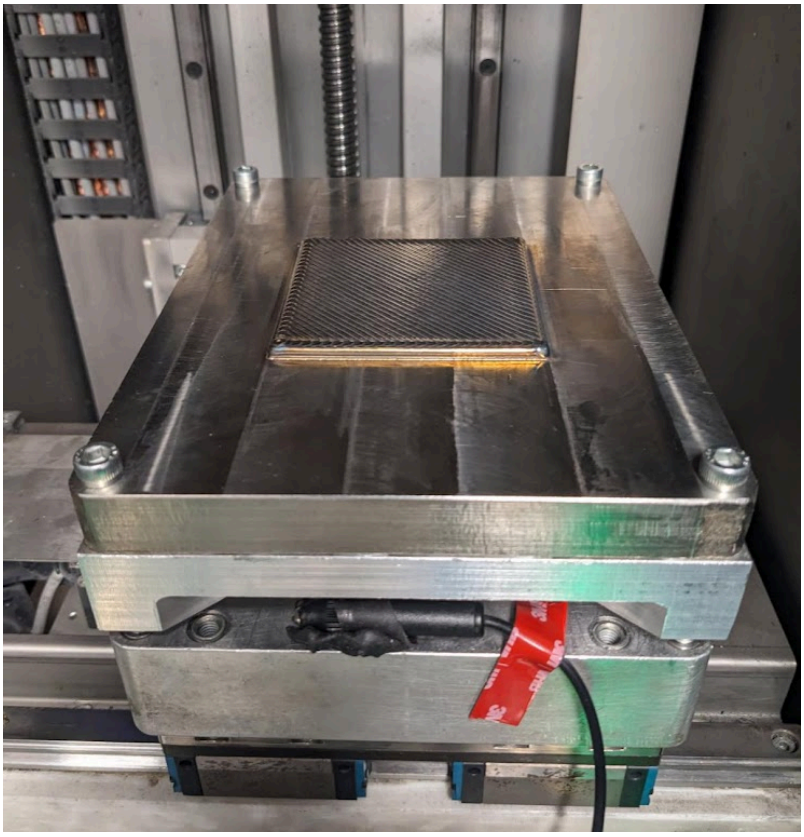

Figure 96: Final Design, DED Test

The temperature vs time data for the final DED test is below in Figure 97.

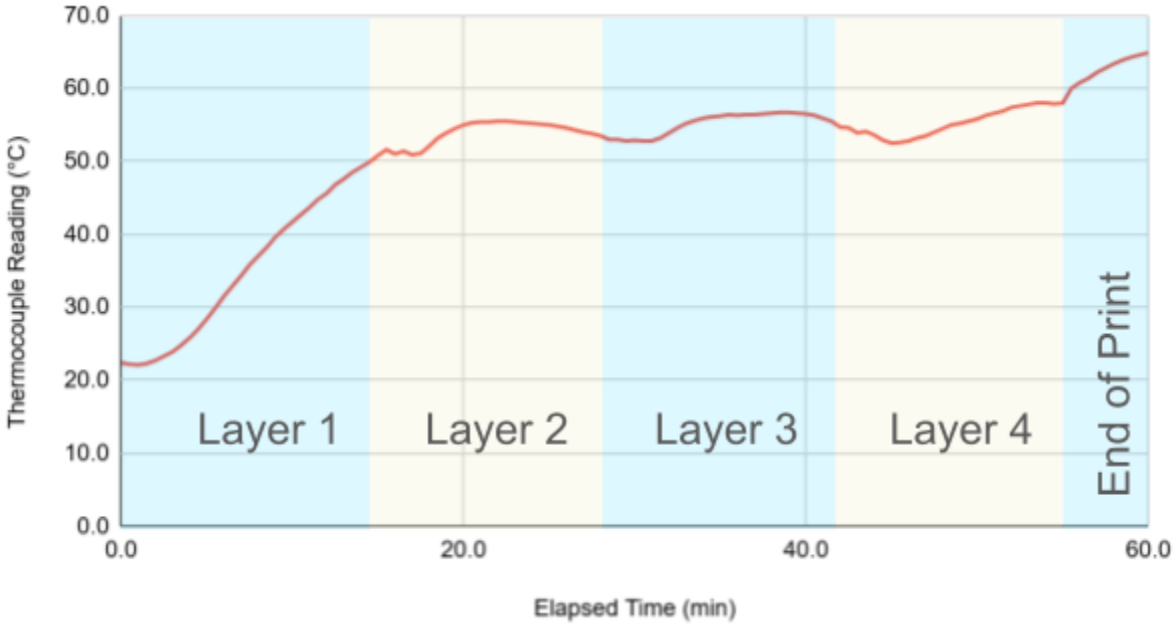

Figure 97: Temperature vs Time, Final DED Test

Compared to the smaller standoff test design, we see less a more gradual rise in layer 1, minimal cooling between layers 1 and 2, slightly higher equilibrium temperatures in layers 2-4, and diminished inter-layer cooling overall. We attribute the decreased cooling between layers and the more gradual first layer temperature increase to the increased thermal mass of the larger system. The decrease in cooling and increased equilibrium temperature is also attributed to the fact that the larger plate blocks the shielding gas flow from reaching the standoffs, decreasing convection. The thermocouple temperature during the print remains below 60°C, passing our ideal specification and giving a 20°C buffer to the maximum service temperature of our motion components. We recommend that our client incorporate forced air convection through the standoffs for optimal performance in the final machine.

Final Forming Testing

Using the larger standoff buildplate design, compressive testing at 100 kN was performed. In comparison to the earlier compressive testing we did with the smaller build plates, our large build plate compressive testing was performed using a much smaller 9.5 mm tool to yield a much more significant forming deformation result on the workpiece.

Once again, we used the Instron compressive testing system to perform our testing. Given that the moving crosshead can only accommodate built in tool diameters as low as 2 inches, we fabricated a 9.5 mm (3/8 inch) tool, approximating the laboratory's 10 mm target size (Figure 98). This tool was fabricated by grinding a dowel pin using a surface grinder. To isolate part deflection from tool compression, the setup was preloaded as shown in Figure 99. However, this resulted in localized indentation on both the threaded 0.857-inch tool above the dowel pin and the steel substrate.

Figure 98: Dowel pin surface is grinded down for full contact as a forming tool

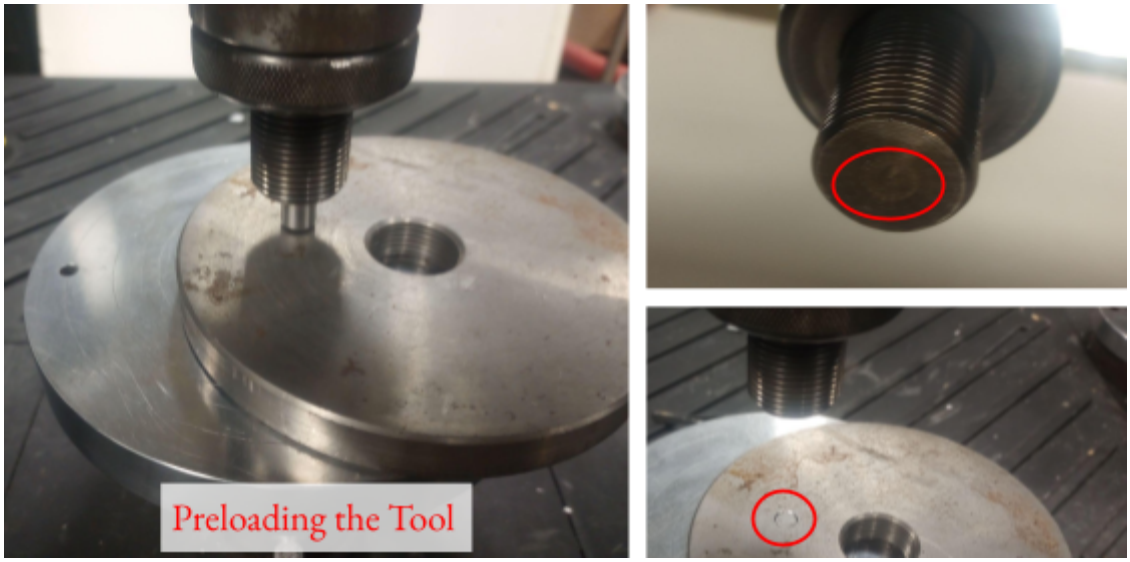

Figure 99: Tool was preloaded under a steel plate that resulted in plate and tool deformation

The forming test was conducted as a standard compression sequence. The crosshead descended at an increased rate of 20μm/s, applying load through the 9.5 mm tool until reaching the target force threshold of 100 kN. The Instron system provides real-time force and displacement readouts, which were used to monitor instantaneous deflection. Once again, The machine's lower pressurized surface consists of a flat plate approximately 18 inches wide. The large build plate assembly rested directly on this surface.

Our previous compression tests with the small build plates cycled the 100 kN load 5 times, from which we learned that most of the plastic deformation occurs with the first cycle. With the 2nd to 5th cycles showing negligible additional plastic deformation. For our compression tests with the large build plates we ran the first test 3 times and saw the same behavior, so for the next tests we only ran two cycles.

In Table 43, the first center run recorded an Inconel deformation of 0.32 mm. We believe this value is artificially high due to tool seating and compression of the tool when used on the hard inconel top surface. Subsequent runs (2–4) were more consistent, yielding values of 0.22 mm, 0.18 mm, and 0.17 mm, respectively.

Table 43: Deformation of prototype at 6 locations

All Units (mm)	**Center 1**	**Center 2**	**Center 3**	**Center 4**	**Edge**	**Corner**
Deformation of Inconel	0.32	0.22	0.18	0.17	-	-
Total Deflection	1.81	1.75	1.70	1.69	3.2	3.1
Deflection Of Build Plate	1.49	1.48	1.52	1.52	-	-

Graphs of the individual runs can be seen in Appendix A. The deflection of the build plate remained consistent across the four primary center runs. Based on the data collected, the average build plate deflection was 1.5 mm with a standard deviation of 0.018. This means we have a 95% Confidence Interval of 1.46 - 1.54 mm. At approximately 1500 microns, this deflection is 30 times the currently allocated budget. While the lab has expressed a willingness to expand this tolerance, this metric requires formal reevaluations. These findings provide a data-driven baseline for the lab to establish a more feasible deflection budget moving forward.

To ensure edge and corner forming are possible, we ran one press for each case. Edge and corner forming exhibited a larger total deflection (total deflection being combined Inconel deformation and build plate deflection) at around 3.2 mm. The value is higher likely due to the reduced surface area at the tool plate boundary which creates a higher force concentration. The lab may wish to further evaluate the consistency of presses across different regions of the part, however the center presses seemed promising in producing repeatable results.

A notable outcome due to our tool being fixed by compression only as opposed to being a threaded insert was that the edge press resulted in tool failure at around 98kN. This can be seen in Figure 100 where the force displacement graph is shown. The broken tool and setup are shown in Figure 101.

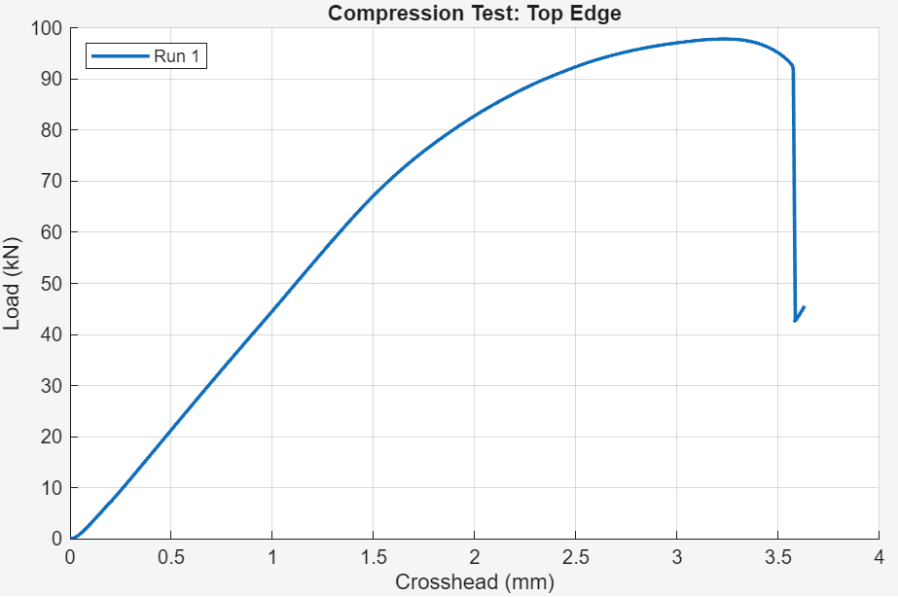

Figure 100: Compression Test of Top Edge resulting in Tool Failure

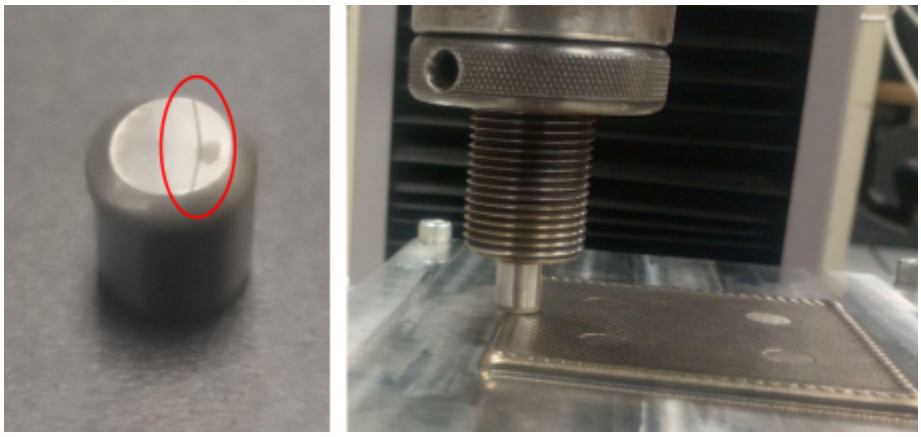

Figure 101: Tool failure (left) during edge pressing (right)

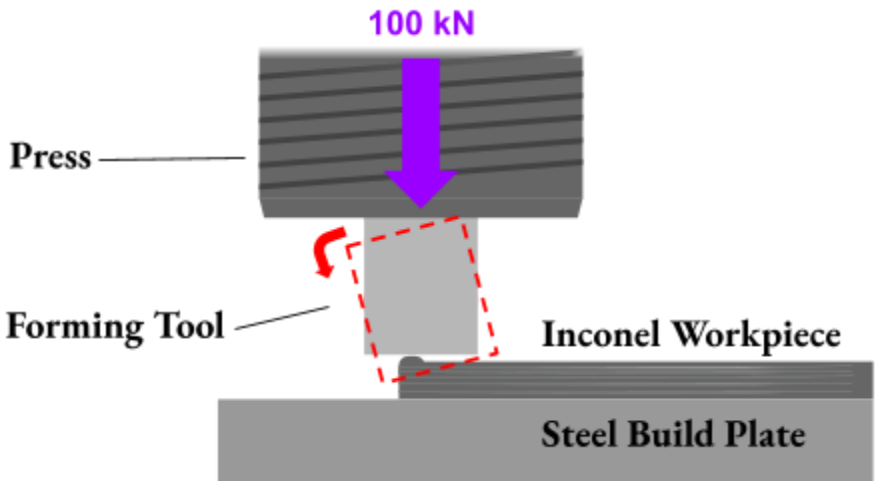

Figure 102: Unfixed Compression Testing Tool Failure Diagram

We believe that the overhang of the tool along with the dome-shaped inconel ridge left by the edge layer of the Laser DED process caused the tool to press at an angle and create the deformation shown in Figure 103. The angling of the tool caused the compression load to be applied through a corner rather than across the full flat surface, concentrating the force at a small point and leading to tool failure. In the final forming machine setup, this failure mode is unlikely because the tool will be rigidly fixed rather than simply stacked under the applied load. This incident highlights the need for the lab to ensure the tool is strong enough and positioned properly especially at the worst load scenario around the edge.

Figure 103: Edge pressing resulted in an angled deformation due to improper tool setup

Overall, we were able to successfully form the inconel on the full size standoff design, meeting the binary metric of successfully forming. The forming indentations left on the piece can be seen in Figure 104.

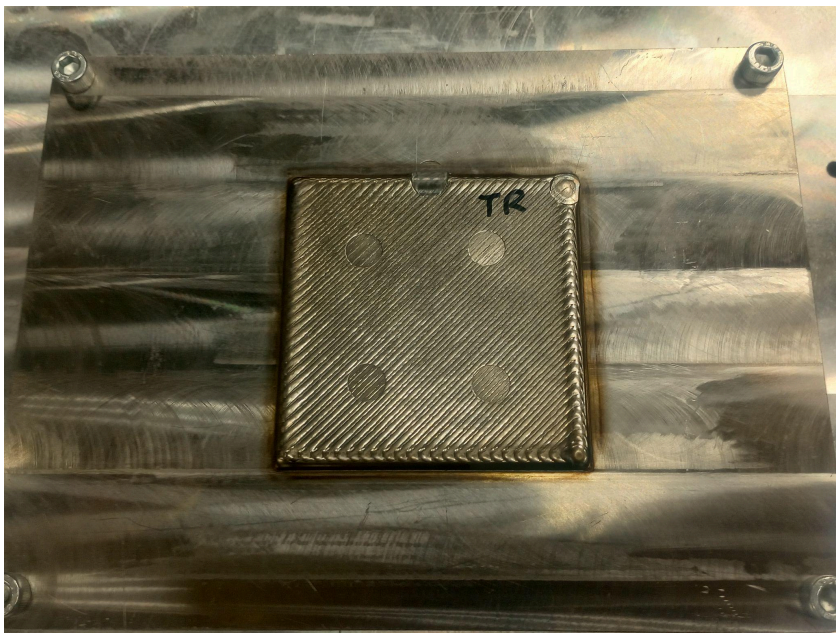

Figure 104: All forming marks on Full Size standoff design with TR marking Top Right of the piece

Looking at the overall forming performance in terms of plastic deflection, although we aren't able to completely isolate the workpiece deformation from the build plate and standoff deformation, we saw a significant plastic deformation in the workpiece (visible in Figure 104) and, based on the plotted crosshead deflection grafts, the plastic deformation is evident with the shift in the x-axis between the first and the second test, the zero slope in the beginning of the second test before the force starts ramping up shows the amount that the crosshead moved until making contact with the surface. Clearly the first run resulted in notable workpiece deformation. We saw an average of 0.21 mm of plastic deformation, a significant improvement over the initial small build plate tests due to the size reduction of the tool head.

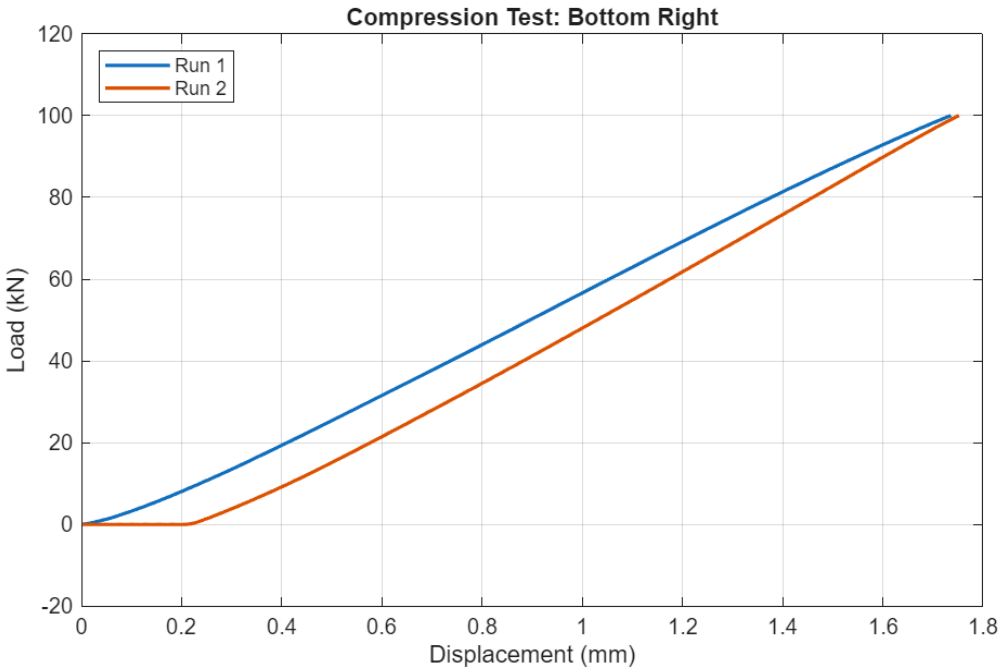

Figure 105: Compression Test - Bottom Right

Final Subtractive Testing

Using the larger standoff buildplate design, subtractive machining tests were performed. Face milling and side milling operations were carried out using the same procedure as the smaller buildplates (see Subtractive Testing section), but this time with the correct inserts installed in the end mill.

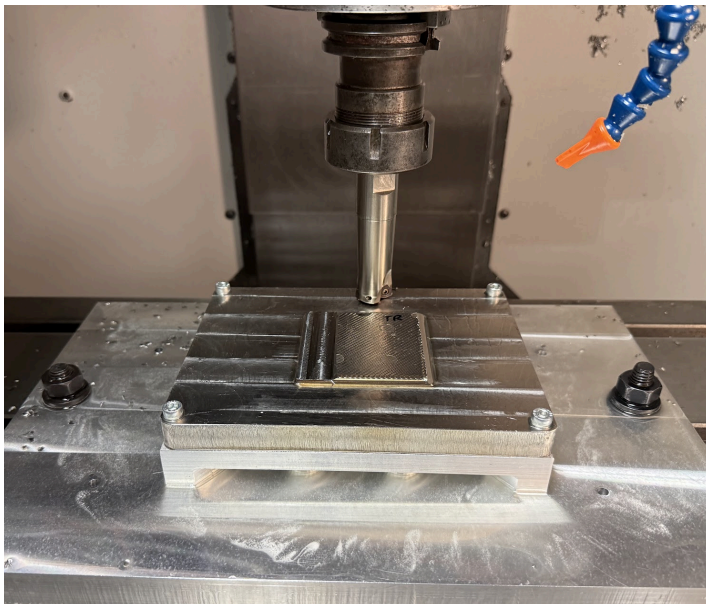

Figure 106: Aluminum standoff recommended design with facemilling (left) and side milling (right)

More regions of the part had been plastically deformed during the forming experiments, so the machining operations were intentionally performed through these formed regions to evaluate whether formed material affects machining behavior.

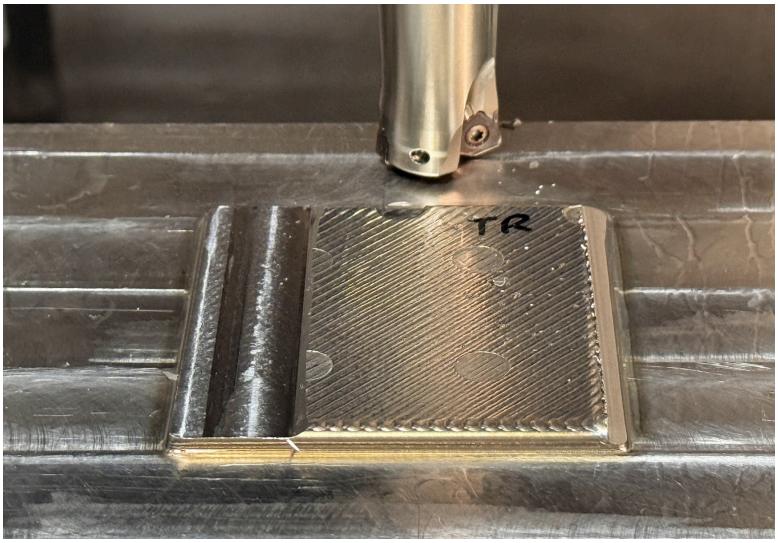

Figure 107: Closeup of subtractive testing through formed regions (circular depressions in the print)

No observable changes in machining behavior or in the final machined surface were detected when cutting through the formed regions. The tool engagement remained stable and the resulting surfaces were comparable to those produced in unformed areas. Additionally, using the correct end mill inserts improved the overall cutting performance, producing a smoother machining sound and an improved surface finish after cutting.

Cost Analysis

This project consists of designing a single machine intended for laboratory testing and analysis, so a traditional per-unit manufacturing cost breakdown is not really relevant. Instead, we are evaluating expected operating costs over the machine's service life. For this analysis, we focused on the variable costs of running the machine, given that the cost of the final design is still unknown.

We estimated the cost per hour of each of the three machine processes, and then estimated the hours of use per year for each process to determine the yearly cost of running this machine.

Table 44: Operating Cost Analysis

Variable Cost - General				
Category	**Unit**	**Usage Per Print**	**Price ($/unit)**	**Cost Per Print ($)**
Build Plates	Number	0.2	10	2

Variable Costs - Laser Wire DED				
Category	**Unit**	**Usage Per Hour**	**Price ($/unit)**	**Cost Per Hour ($)**
Electricity	kWh	8	0.15	1.2
Wire Feedstock	kg	0.876	60	52.56
Shielding Gas (Argon)	L	1200	0.05	60
Nozzle/Optics Wear	hr	1	3	3
Total DED Variable Cost/hr	-	-	-	**116.76**

Variable Costs - CNC Milling				
Category	**Unit**	**Usage Per Hour**	**Price ($/unit)**	**Cost Per Hour ($)**
Electricity	kWh	6	0.15	0.9
Endmills/Inserts	hr	1.5	45	67.5
Coolant	L	2	0.02	0.04
Total Milling Variable Cost/hr	-	-	-	**68.44**

Variable Costs - Forming				
Category	**Unit**	**Usage Per Hour**	**Price ($/unit)**	**Cost Per Hour ($)**
Electricity	kWh	1	0.15	0.15
Die Wear	hr	1	15	15
Lubricant	L	0.1	5	0.5
Total Forming Variable Cost/hr	-	-	-	**15.65**

Parameter	**Value**
Operating Hours	20 hours/week
Operating Weeks	50 weeks/year
Total Hours	1000 hours/year

Process Allocation	Percent Use	Hours per Year	Cost Per Year ($)
Laser Wire DED	50%	500	58380
Subtractive Machining	30%	300	20532
Forming	20%	200	3130

The cost of running this machine is primarily driven by the Inconel 718 material used, specifically the price of wire feedstock in the laser wire DED process. Inconel also contributes greatly to tool wear in the subtractive process resulting in a higher cost there as well. We do not know how much Inconel printing the lab would do, and we know the lab currently prints and forms with other steel materials which only cost ~10$/kg. Making things from less expensive alloys would significantly reduce the cost of running this machine for additive and subtractive processes.

Patent Claim Analysis

We conducted a preliminary patent claim analysis to assess potential infringement risks and define the novelty of the TRIPLE manufacturing system. One of the patents we analyzed was CN114833353A[39], a Chinese patent titled *"Composite additive manufacturing method and device"*. We chose to review it because it describes a process architecture that integrates two of TRIPLE's three manufacturing processes. The independent claim of the patent describes a composite additive manufacturing method where the DED head deposits a layer, and then the material is roll-pressed layer-by-layer. The device is shown in Figure 108.

[39] CN114833353A

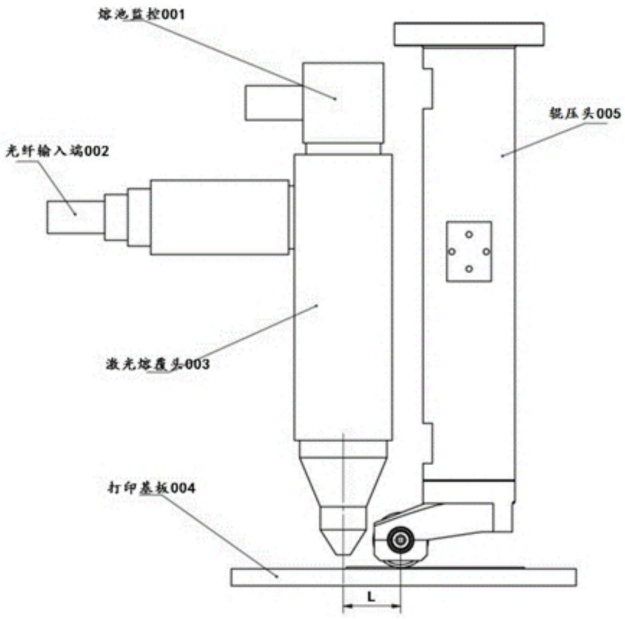

Figure 108. Patent CN114833353A's drawing of a DED head (left) and roller press (right)

To evaluate the TRIPLE for potential patent infringement, we analyzed each element of the patent's independent claim separately, as shown in Table 45. If all of the patent's elements are present in the TRIPLE, then we are infringing the patent.

Table 45: Evaluating TRIPLE Relative to Patent CN114833353A

Claim Element	**Presence in TRIPLE**	**Description**
Path Generation from Digital Model	Present	TRIPLE utilizes control software to generate toolpaths from digital models, which is functionally identical to the patent's requirement for a mathematical model. Although this software has not yet been developed/chosen for our system and is relatively standard across additive manufacturing setups.
Layer-by-Layer DED Deposition	Present	TRIPLE utilizes a laser-wire DED head for material deposition, which is functionally identical to the patent's layer-by-layer "fusion deposition".
Simultaneous Rolling Forming	Absent	TRIPLE utilizes a forming process driven by a vertical roller screw press that activates after each layer, contrary to the patent's simultaneous horizontal rolling press.
Substrate Stripping	Partially	TRIPLE requires post-processing to remove the finished part from the buildplate, similar to the patent's composite

		substrate stripping, albeit using different mechanics.

Because our system does not use simultaneous roll-pressing, it does not contain every element of the patent's independent claim. As a result, our system is not likely to infringe on their claim.

We also considered whether our forming method could be considered equivalent under the doctrine of equivalents. While the functions of both systems are similar, the methods and results differ significantly. Rolling relies on friction and continuous movement under the rollers, whereas our design uses localized, incremental forming through a high-force press. Our approach utilizes a unique machine architecture that provides different forming capabilities. Because the method and resulting geometries differ, our system is furthermore unlikely to be considered equivalent to the patented system.

Finally, we evaluated the novelty of the TRIPLE. Our system is novel because the patent does not disclose everything that our system does. Our system is also non-obvious, because our specific integration of milling and high-precision press forming into an additive process cannot be created by simply combining this patent with another related patent.

TRIPLE Patent Draft

After evaluating CN114833353A (and other patents) for infringement risks, we turned to draft our own broad claim for the TRIPLE. Our Independent Claim 1 is as follows. The TRIPLE is "an integrated hybrid manufacturing apparatus for producing high-performance metal components, an apparatus comprising:

- **Element 1:** A station with a cantilevered frame supporting a DED toolhead and a subtractive machining spindle.
- **Element 2:** A separate station with a high-stiffness frame supporting a localized compressive forming press driven by a roller-screw.
- **Element 3:** A shared multi-axis motion system configured to translate a buildplate between the two stations.
- **Element 4:** A control system configured to perform a sequential manufacturing cycle on a layer-by-layer basis, directing the material deposition, press forming, and subtractive finishing."

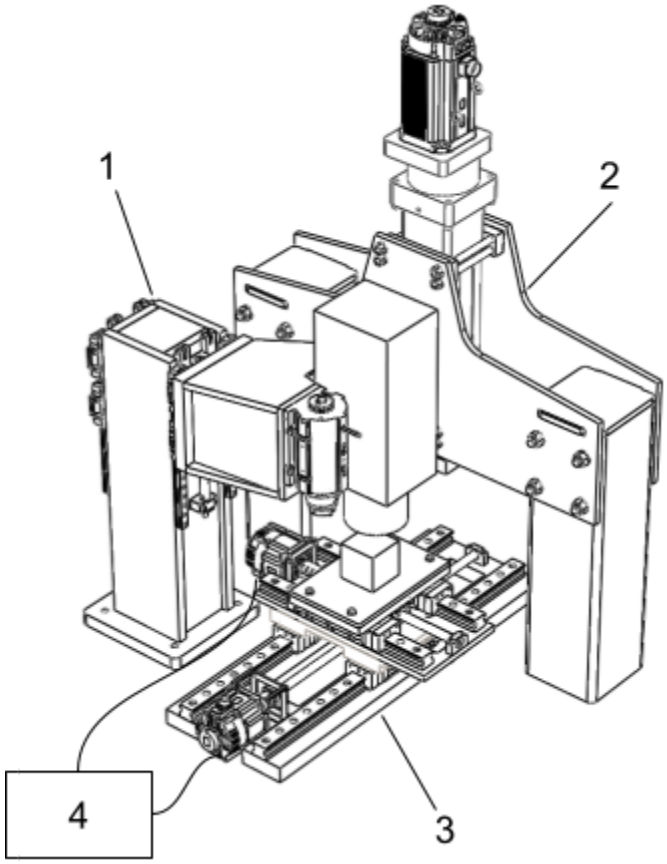

Figure 109: Patent Claim Elements

To strengthen the TRIPLE's patent claim, we predicted which modifications a competitor would make to avoid infringement. To avoid literal infringement, a competitor could modify the machine architecture or force application method in the following ways:

1. **Component Substitution:** The most direct method would be to replace the roller-screw actuator with a hydraulic cylinder or pneumatic hammer. This modification would remove a primary structural limitation of the claim while potentially achieving similar material property results.
2. **Station Consolidation:** A competitor could utilize a single-station design where all the toolheads are mounted on the same frame, either fixed next to each other or rotated using a tool changer. This would dodge our multi-station element and the requirement to translate the buildplate between stations.
3. **Process Transition:** By implementing simultaneous accompanying forming (as described in patent CN114833353A), a competitor could bypass our sequential process element, which relies on incremental rather than continuous forming.
4. **Distributed Manufacturing Workflow:** A competitor could separate the additive, forming, and machining processes into individual machines connected by an automated part transfer and alignment

system. This setup would allow the part to go through all the steps in sequence while avoiding the claim element, requiring a single integrated system with multiple stations.

Future work & recommendations

Further design and development of the TRIPLE hybrid manufacturing system are required prior to full implementation. The team recommends that AMPL proceed with the current design direction, while acknowledging that alternative machine layouts are under consideration. If the two-station architecture is maintained, several critical subsystems must be further developed.

Key next steps include the design and integration of process-specific tooling. A forming tool must be developed, including an adapter to interface with the existing press system. In parallel, a subtractive spindle and laser wire DED process head must be selected. Integration of these process heads will require updates to the subtractive frame and motion system to ensure secure mounting and full access to the intended build volume.

Additional engineering analysis is necessary to validate system performance. Structural simulations should be expanded to confirm the subtractive frame can withstand machining forces without excessive deflection, and vibrational analysis should be conducted to ensure the system's natural frequencies do not interfere with subtractive machining operations. If extraneous materials are of interest, we recommend that the lab purchase small samples and do material testing themselves, as we noticed concerning discrepancies in material properties with our alumina usage. A properly designed and sourced machine base will also be required, with careful consideration given to mounting strategy and overall system rigidity.

The workpiece fixturing system should be further developed to a full scale model.

In addition to mechanical development, the electronics and control architecture must be designed for the TRIPLE. This includes motion control, process sequencing, and safety systems necessary for multi-process operation.

Finally, a detailed manufacturing and assembly plan should be established. A suitable space for machine assembly must be identified, and large structural components should be fabricated and welded on-site where feasible. Procurement of components, system integration, and staged assembly should be planned to ensure efficient and successful implementation of the full hybrid manufacturing system.

Acknowledgements

The team would like to thank our client, specifically Professor Cao, at Northwestern University's AMPL group for providing the opportunity to work on this project and further the lab's research. We would like to thank PhD students Carter Taylor, Peter Li, and Malachi Landis for their continuous design feedback and support, as well as Masters students Jakob Schaeffer and Colin Balke for their design work on other machine components.

We would also like to thank the Ford Shop professionals Eric Capper, Bob Taglia, Heidi Huckabay, Kazuki Guzmán, and Josh Lantzy for their manufacturing guidance. Dr. Carla Shute at Northwestern's CLaMMP lab and PhD student Xingyang Li in the Fast-AM lab provided invaluable assistance and machine access to enable our testing.

In addition, we would like to thank Professor Gatchell, Professor Beltran, and Professor Keys for their guidance and support throughout the past two quarters.

Appendices

Appendix A: Full Scale Compression Test

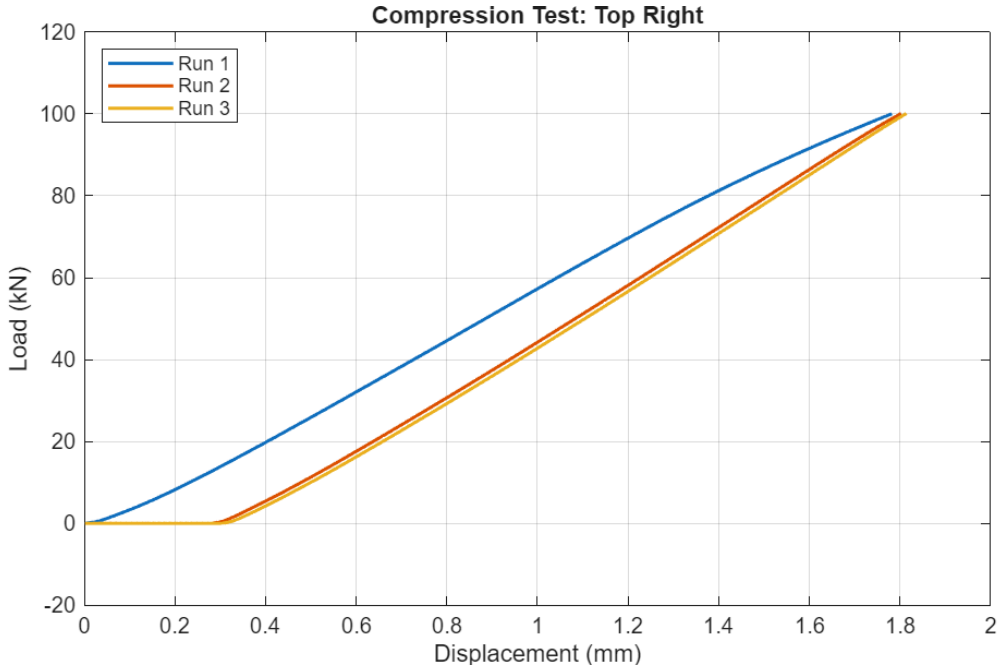

Figure A1: Compression Test of Center located at the Top Right

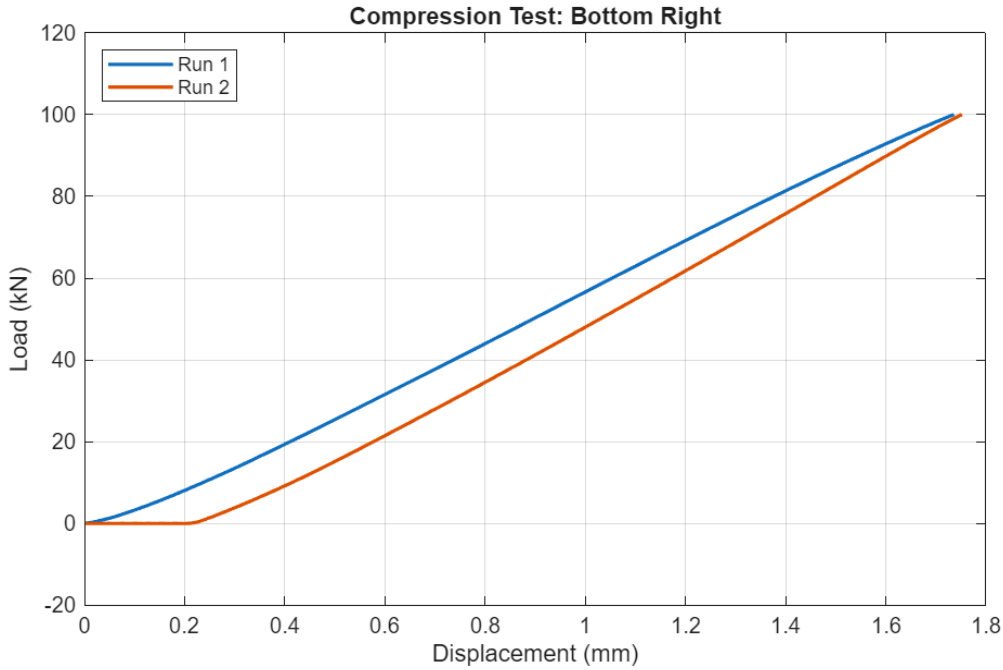

Figure A2: Compression Test of Center located at the Bottom Right

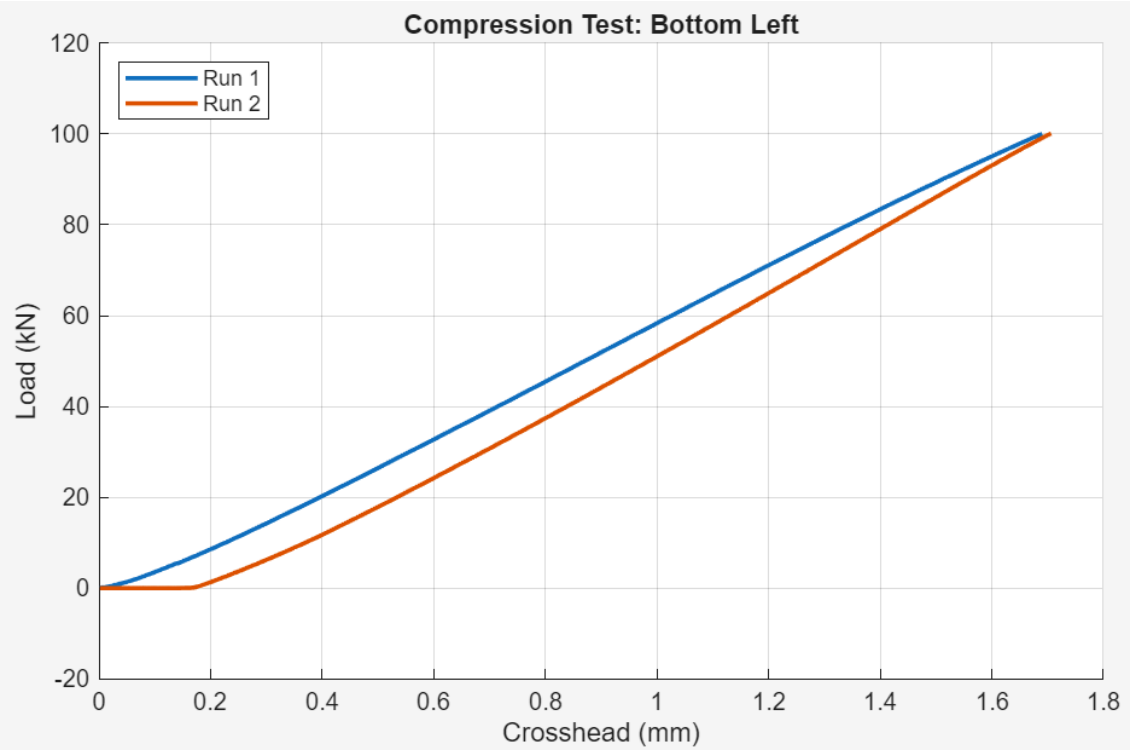

Figure A3: Compression Test of Center located at the Bottom Right

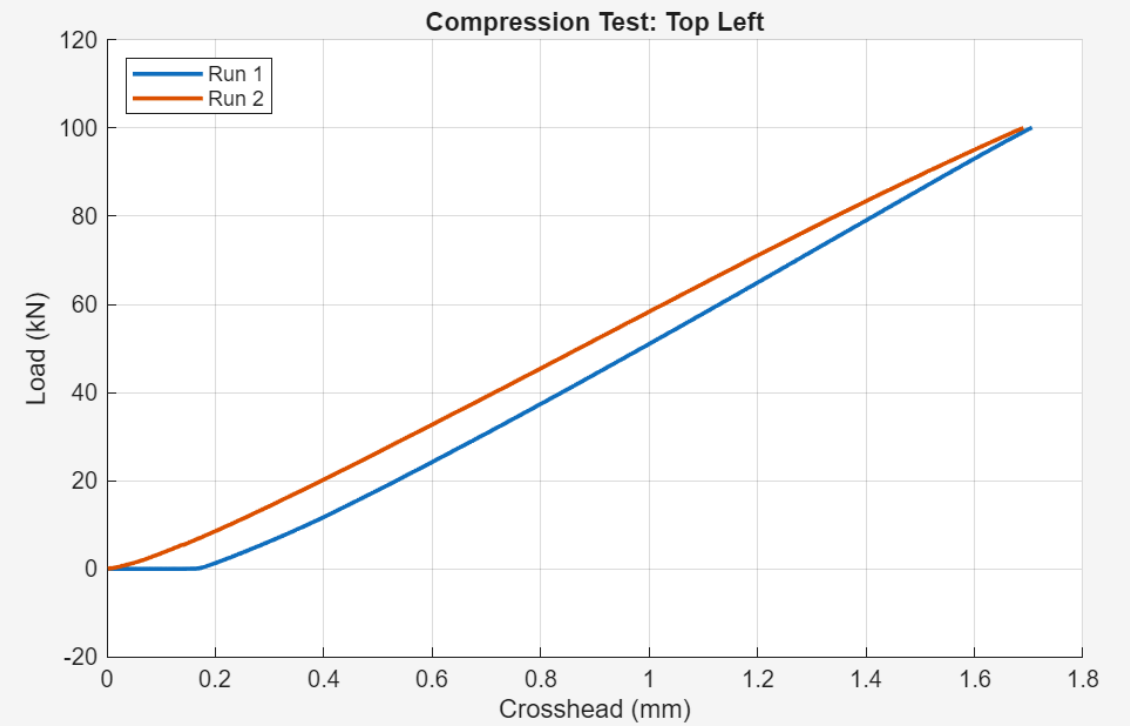

Figure A4: Compression Test of Center located at the Top Left

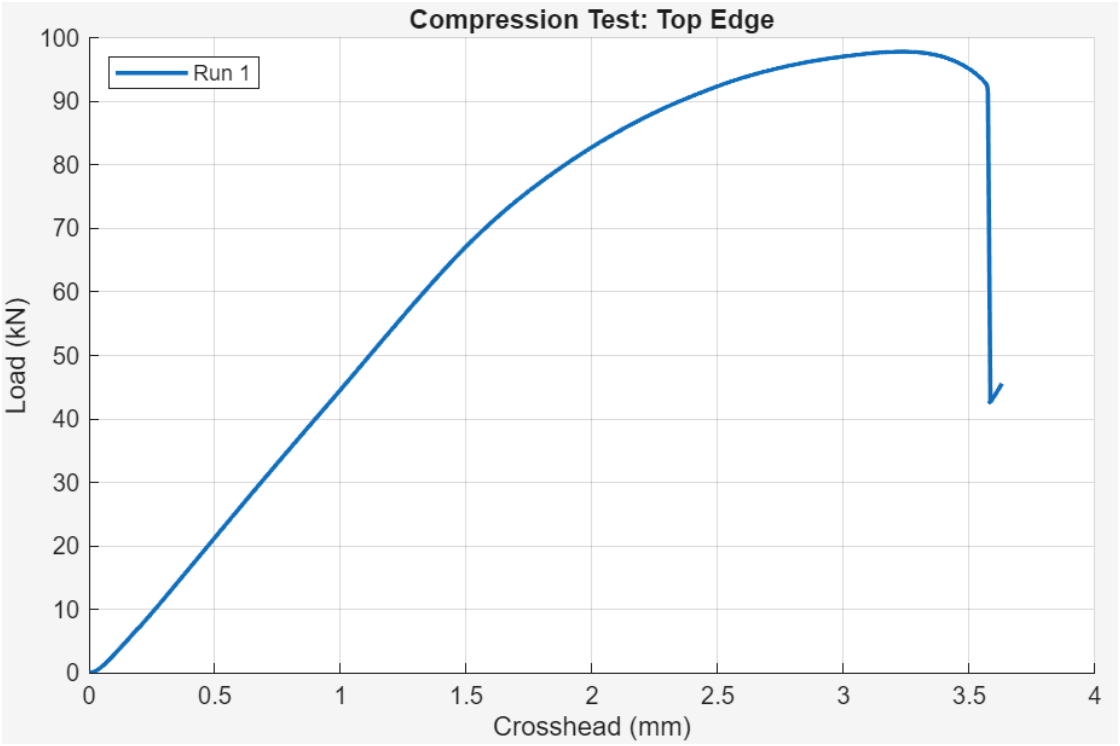

Figure A5: Compression Test of Top Edge resulting in Tool Failure

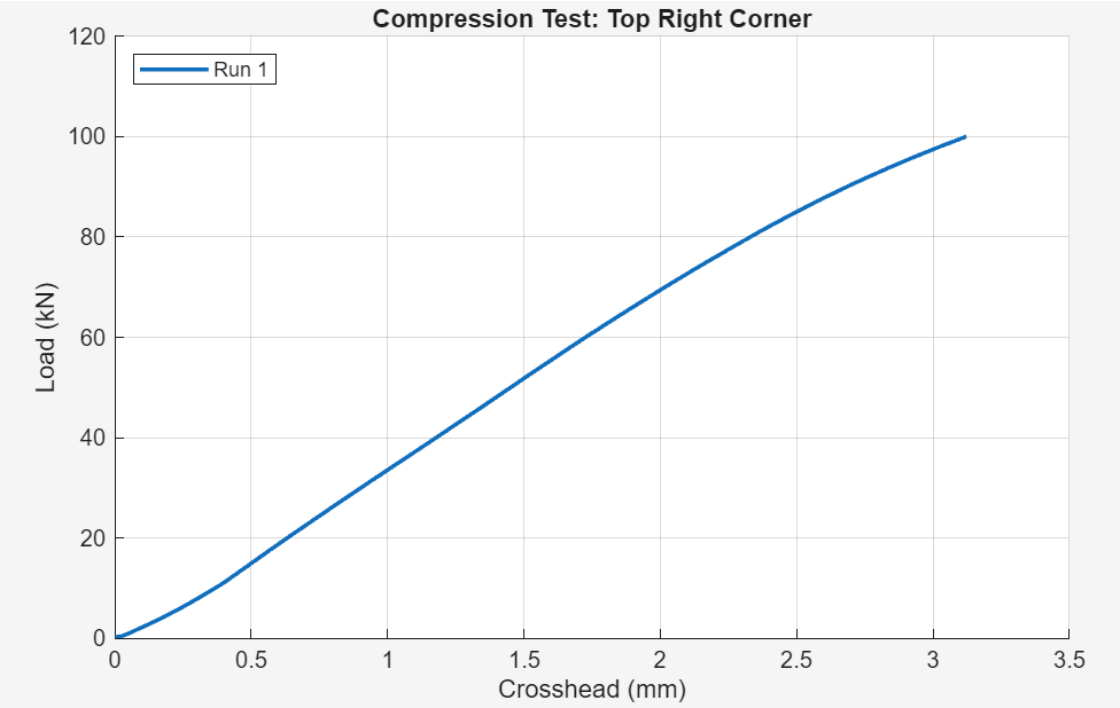

Figure A6: Compression Test of Center located at the Top Right Corner

Appendix B: Motion System Alternative Matrix

Table B1: Motion System Alternatives Matrix

		Ball Screws	Helical Rack & Pinion	Linear Motors	Belt Drive (Timing Belts)	Robotic Arm	Direct-Drive Linear Motor Stages	Roller Screw (Planetary or Recirculating)	Direct-Drive Rotary Motors (Rotary Torque Motors)	Gearbox/Reducer with Ball Screw/Rack	Hydraulic
Selection Criteria	**Weight (%)**	Score	Score	Score	Score	Score	Score	Score	Score	Score	Score
Cost	10	3	4	1	5	1	1	2	1	2	1
Accuracy	20	4	2	5	3	5	5	5	2	3	4
Rigidity	20	3	3	3	1	2	2	3	3	3	3
Lifetime	10	4	3	4	2	4	4	3	3	3	3
Maintenance	5	2	3	4	4	3	4	2	1	2	1
Load Capacity	15	5	5	3	2	2	2	5	5	5	5
Speed	10	5	4	5	5	3	5	4	5	4	3
Footprint	5	3	3	4	3	2	3	3	2	2	1
Weighted Total Score		3.6	3.15	3.45	2.65	2.75	3.05	3.5	2.8	3.05	2.95
Rank		1	4	3	10	9	5	2	8	5	7

Appendix C: Bill of Materials

Table C1: Bill of Materials

	Part Number	Name/Description	Amount	Cost/Item	Total Cost	Retailer	Link
X-Y Gantry	SDA3110V-5CCG0+1250LC2-J1K(1050G00BK 20 BF 200)	X Axis Ball Screw Assembly	1	Awaiting Quote	Awaiting Quote	THK	Link
	SDA3110V-5CCG0+675LC2-J1K(475G00BK 20BF 200)	Y Axis Ball Screw Assembly	1	Awaiting Quote	Awaiting Quote	THK	Link
	SRG65SLC1QZKKC0-1500LP_G37-5	X Axis Linear Rail Assembly	2	$2,500	$5,000	THK	Link
	SRG65SLC1QZKKC0-775LP_G12-5	Y Axis Linear Rail Assembly	2	$2,500	$5,000	THK	Link
	SGM7G-44	Motor	2	Awaiting Quote	Awaiting Quote	Yaskawa	Link
	60inx22inx2.5in Steel Plate Stock	Baseplate Stock	1	$1,370.96	$1,370.96	Midwest Steel	Link
	7inx5.75inx2in Steel Plate Stock	X Axis Ball Nut Mount Stock	1	$90.33	$90.33	Midwest Steel	Link
	22.5inx16inx2.5in Steel Plate Stock	X Axis Mounting Plate Stock	1	$394.56	$394.56	Midwest Steel	Link
	32inx16inx1in Steel Plate Stock	Y Axis Baseplate	1	$225.00	$225.00	Midwest Steel	Link
	5.75inx3inx2in Steel Plate Stock	Y Axis Ball Nut Mount Stock	1	$46.13	$46.13	Midwest Steel	Link
	20.5inx13inx1.5in Steel Plate Stock	Y Axis Mounting Plate Stock	1	$178.90	$178.90	Midwest Steel	Link

	20.5inx13inx0.75in Steel Plate Stock	Build Plate Stock	1	$206.28	$206.28	Midwest Steel	Link
	7.5inx2.5in Steel Round Bar Stock	Coupler Stock	1	$45.10	$45.10	Midwest Steel	Link
	91290A056	Steel Socket Head Screw M18 x 2.5, 120mm	8	$4.28	$34.24	McMaster	Link
	91290A050	Steel Socket Head Screw M18 x 2.5, 90mm	4	$3.22	$12.88	McMaster	Link
	91290A048	Steel Socket Head Screw M18 x 2.5, 80mm	4	$2.86	$11.44	McMaster	Link
	91290A842	Steel Socket Head Screw M16 x 2, 100mm, Partially Threaded, Pack of 5	2	$15.68	$31.36	McMaster	Link
	91290A825	Steel Socket Head Screw M16 x 2, 55mm, Pack of 5	1	$10.38	$10.38	McMaster	Link
	91280A850	Class 8.8 Steel Hex Head Screw, M16 x 2mm Thread, 80mm, Partially Threaded, Pack of 5	1	$12.41	$12.41	McMaster	Link
	91280A183	Class 8.8 Steel Hex Head Screw, M12 x 1.75, 85mm, Pack of 10	1	$17.02	$17.02	McMaster	Link
	91280A724	Class 8.8 Steel Hex Head Screw, M12 x 1.75, 50mm, Pack of 10	1	$9.26	$9.26	McMaster	Link
	91280A712	Class 8.8 Steel Hex Head Screw, M12 x 1.75, 20mm, Pack of 25	1	$20.99	$20.99	McMaster	Link

	91290A472	Steel Socket Head Screw M8 x 1.25, 120mm, Pack of 5	2	$5.16	$10.32	McMaster	Link
	91290A466	Steel Socket Head Screw M8 x 1.25, 90mm, Partially Threaded, Pack of 10	1	$7.71	$7.71	McMaster	Link
	91290A462	Steel Socket Head Screw M8 x 1.25, 80mm, Partially Threaded, Pack of 25	1	$15.49	$15.49	McMaster	Link
	91280A554	Class 8.8 Steel Hex Head Screw, M8 x 1.25, 70mm, Partially Threaded, Pack of 25	1	$16.29	$16.29	McMaster	Link
	91290A252	Steel Socket Head Screw M5 x 0.8, 25mm, Pack of 50	1	$10.96	$10.96	McMaster	Link
	94645A260	M18 x 2.5 Locknut, Pack of 5	3	$12.98	$38.94	McMaster	Link
	94645A230	M12 x 1.75 Locknut, Pack of 10	1	$9.25	$9.25	McMaster	Link
	94645A210	M8 x 1.25 Locknut, Pack of 50	1	$11.16	$11.16	McMaster	Link
	94645A102	M5 x 0.8 Locknut, Pack of 50	1	$15.66	$15.66	McMaster	Link
	93475A315	M18 Washer, Pack of 10	2	$8.27	$16.54	McMaster	Link
	93475A290	M12 Washer, Pack of 25	1	$11.22	$11.22	McMaster	Link
	93475A270	M8 Washer, Pack of 100	1	$12.52	$12.52	McMaster	Link
	93475A310	M16 Washer, Pack of 25	1	$19.34	$19.34	McMaster	Link

Forming	NMFC#52200	Carbon Steel Square Tube, 4' of 300x300mm, 12.5mm wall	2	$2,033.22	$4,066.44	Parker Steel International	
	NMFC#106140	Steel Plate 25mm, 96x67in	1	$4,004.31	$4,004.31	Parker Steel International	
		Packaging, Handling and Freight			$557.00	Parker Steel International	
	HB30-3.5CL12.9BL	M30 x 440mm Hex Bolt Class 12.9	8	$111.00	$888.00	DMS Fasteners	Link
	31161518	M24 x 400mm Hex Bolt Class 12.9	8	$116.36	$930.88	Fastenal	Link
				TOTAL:	$23,359.27		

Appendix D: Manufacturing Drawings

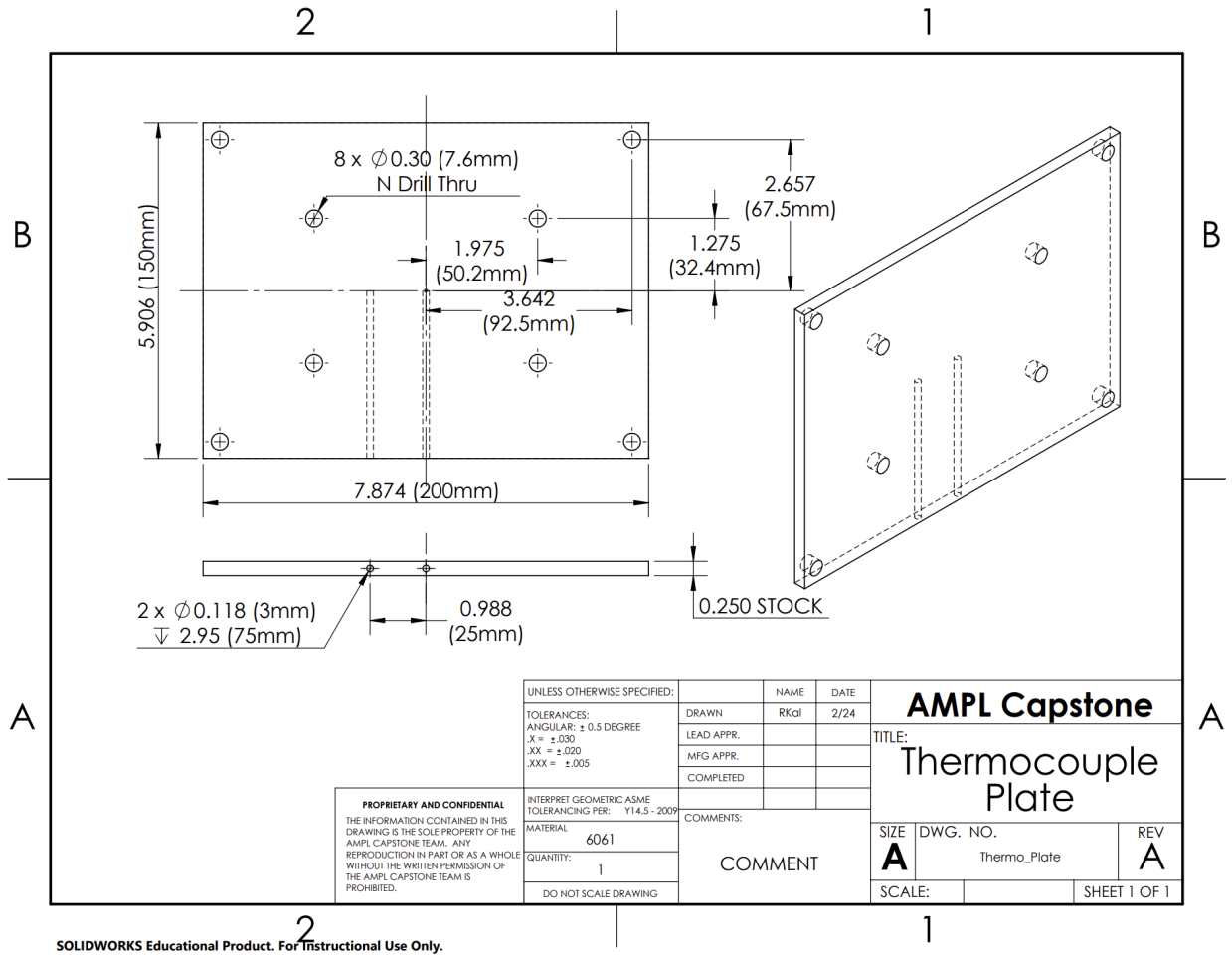

Figure D1: Thermocouple Plate Drawing

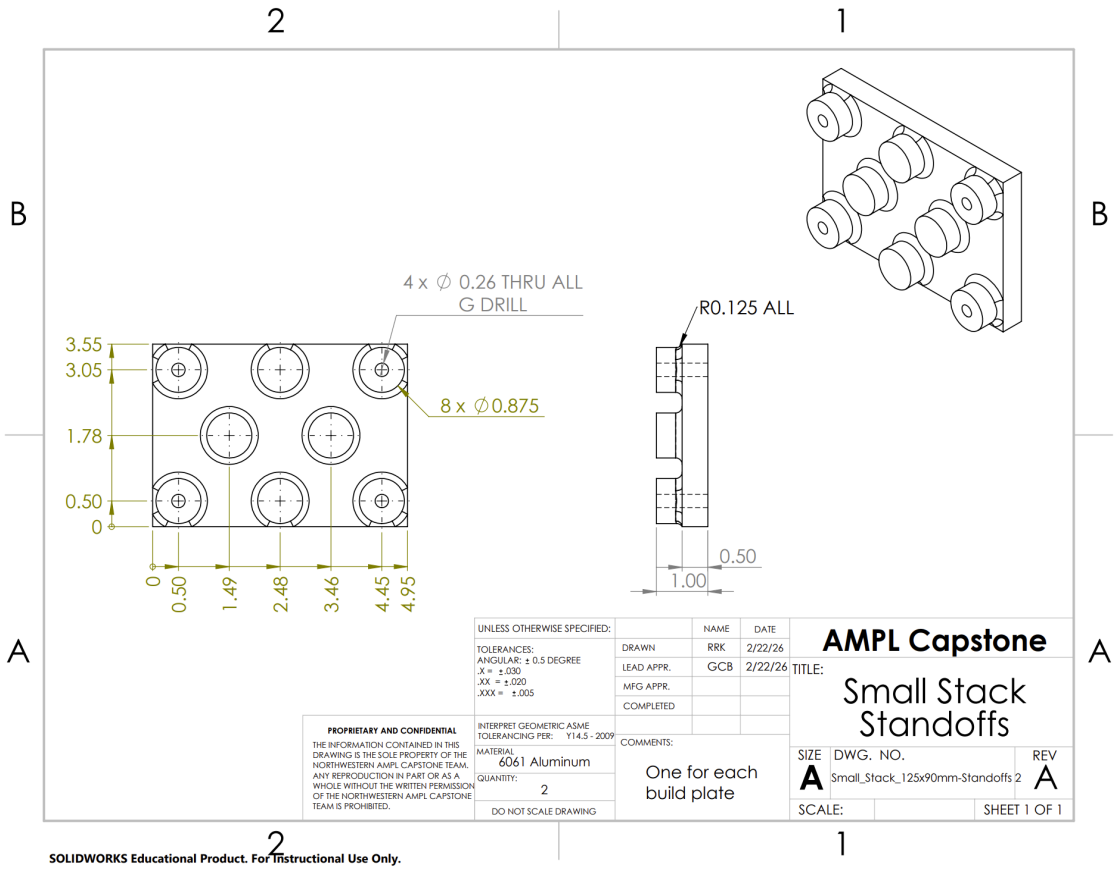

Figure D2: Standoff Plate Mini Design Drawing

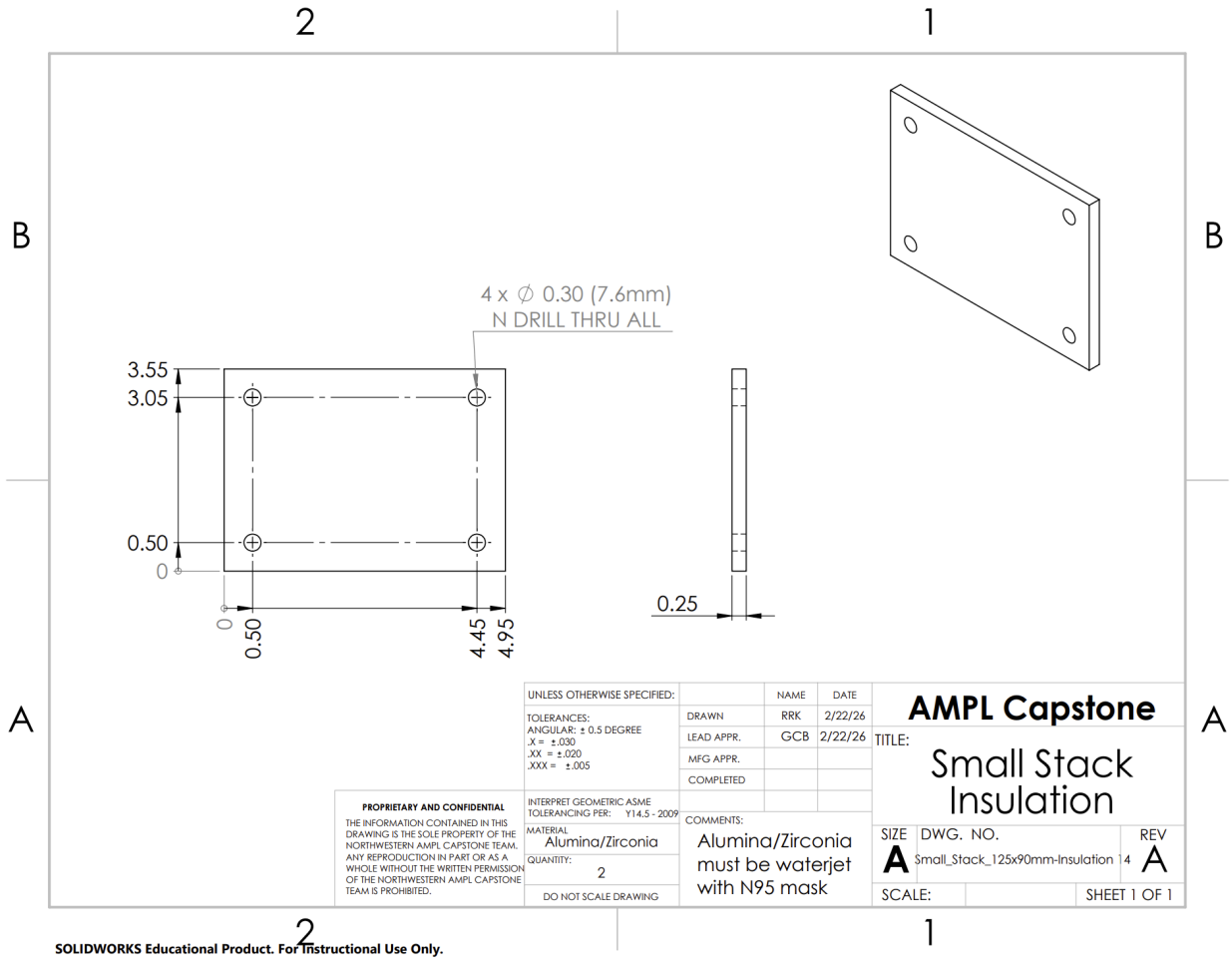

Figure D3: Alumina Plate Mini Design Drawing

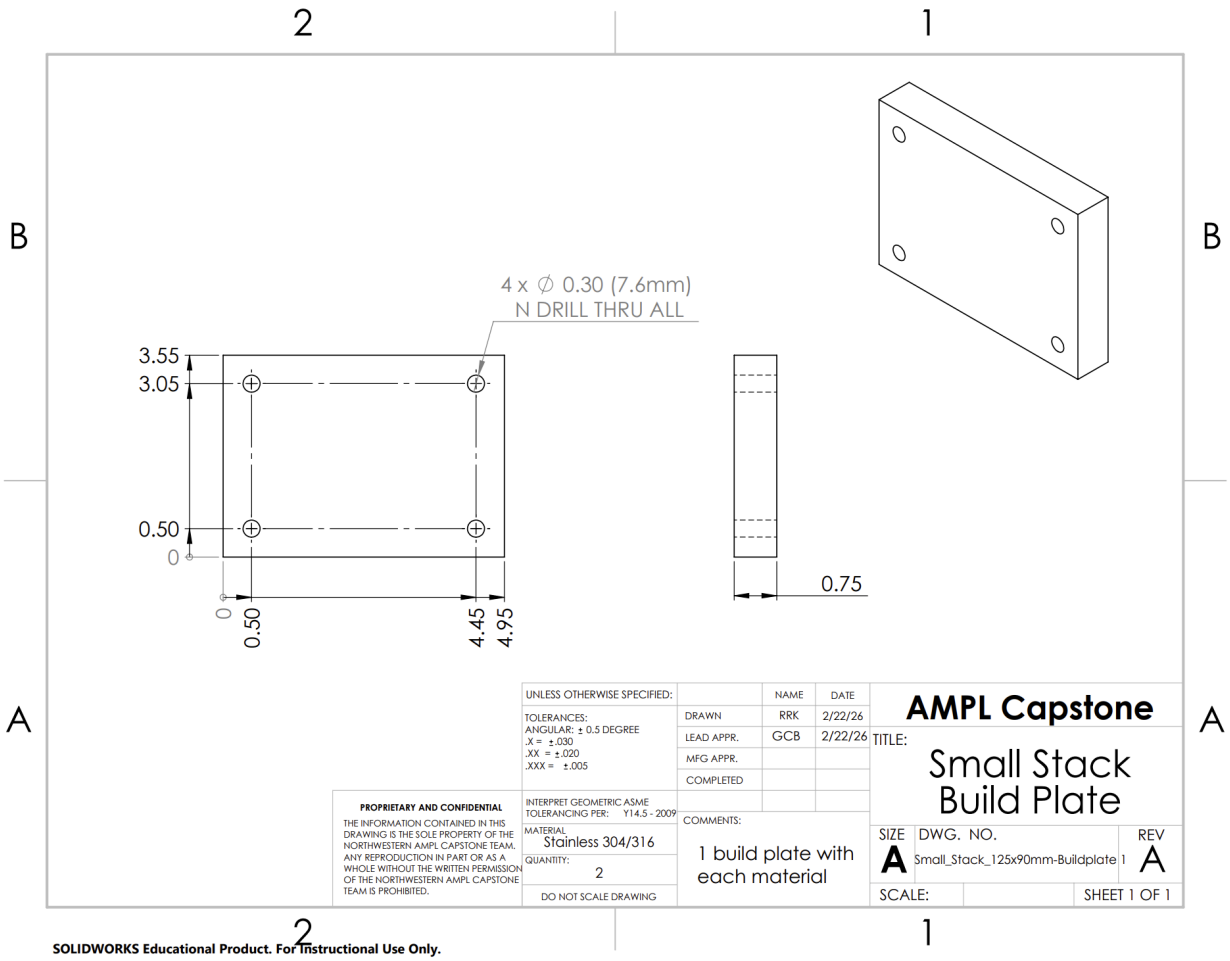

Figure D4: Stainless Buildplate Mini Design Drawing

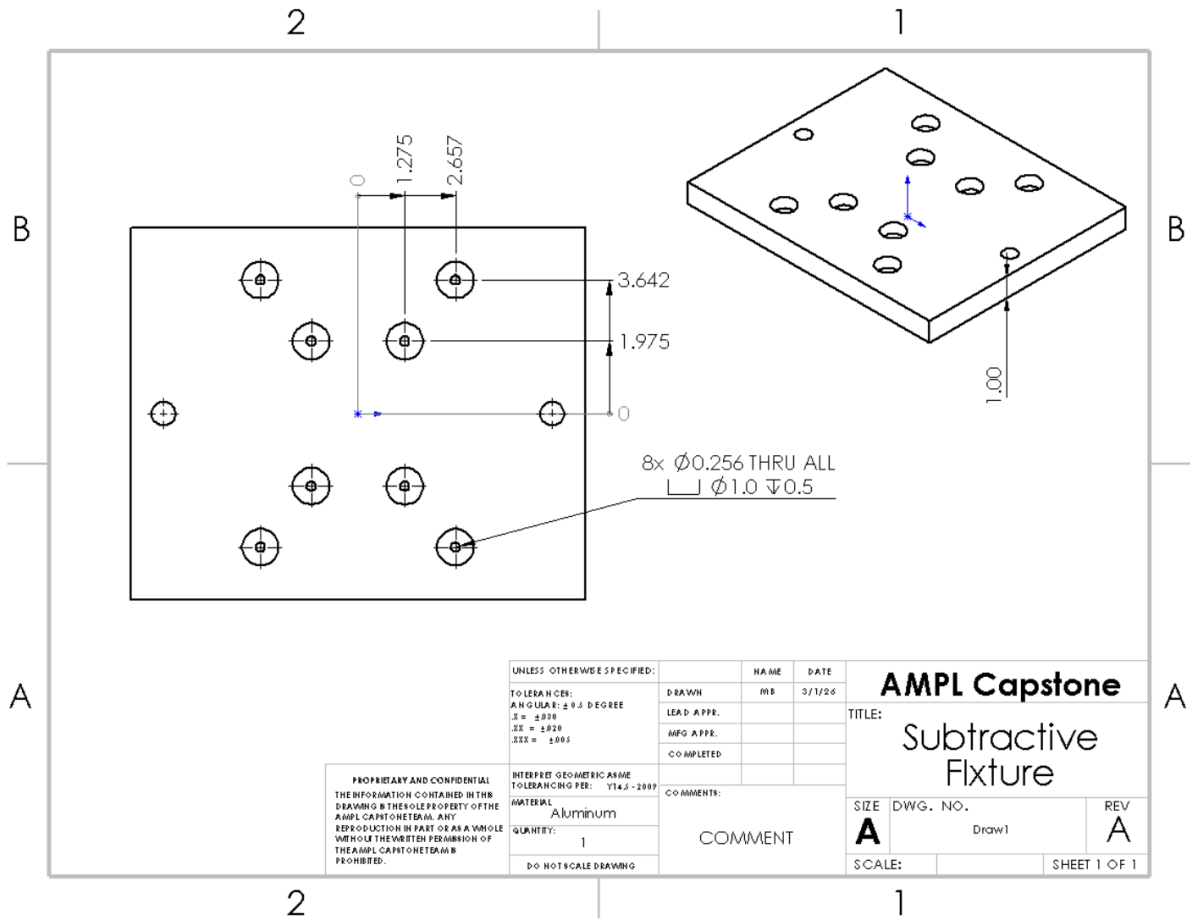

Figure D5: Subtractive Testing Fixture Plate

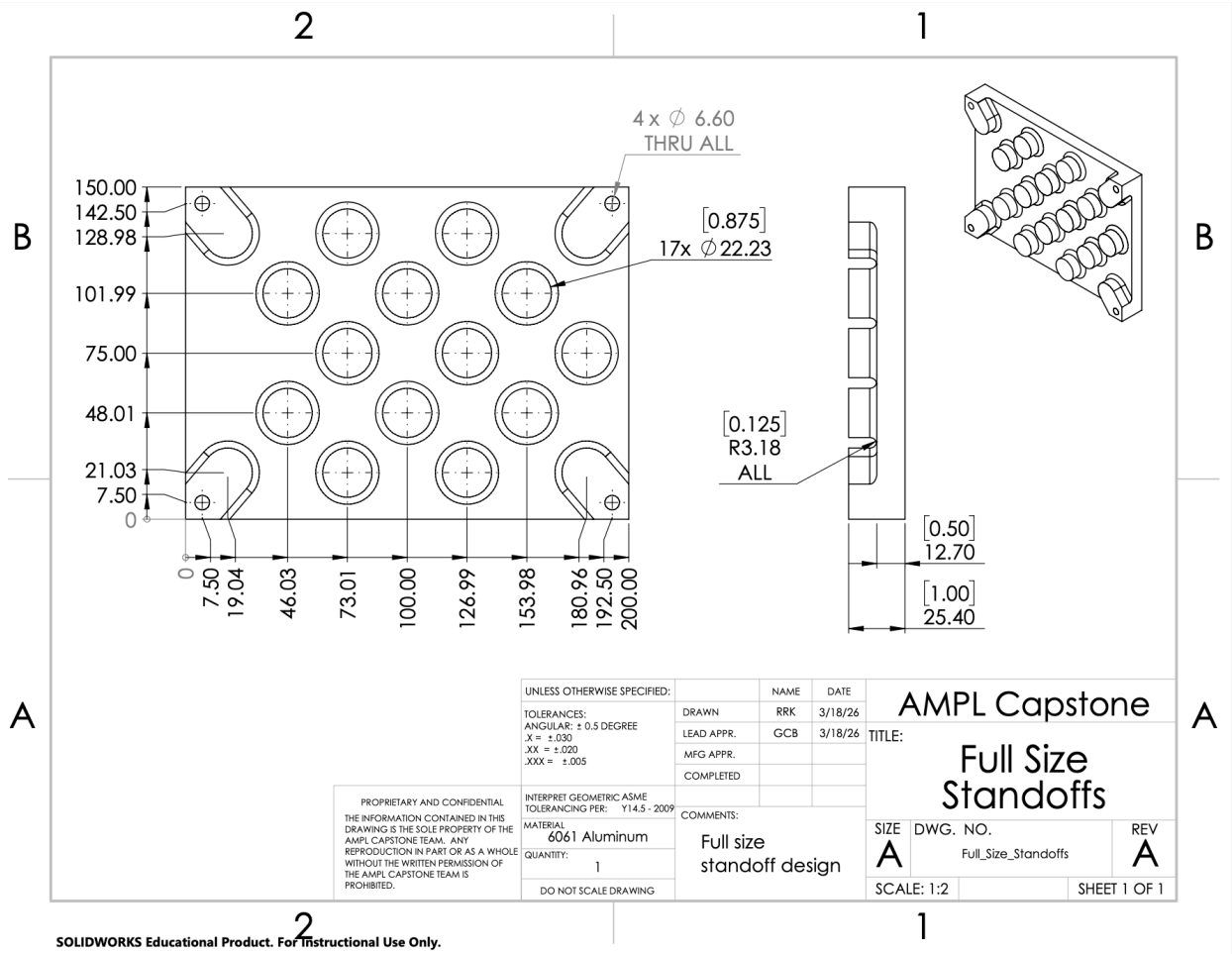

Figure D6: Full Size Standoff Plate Drawing

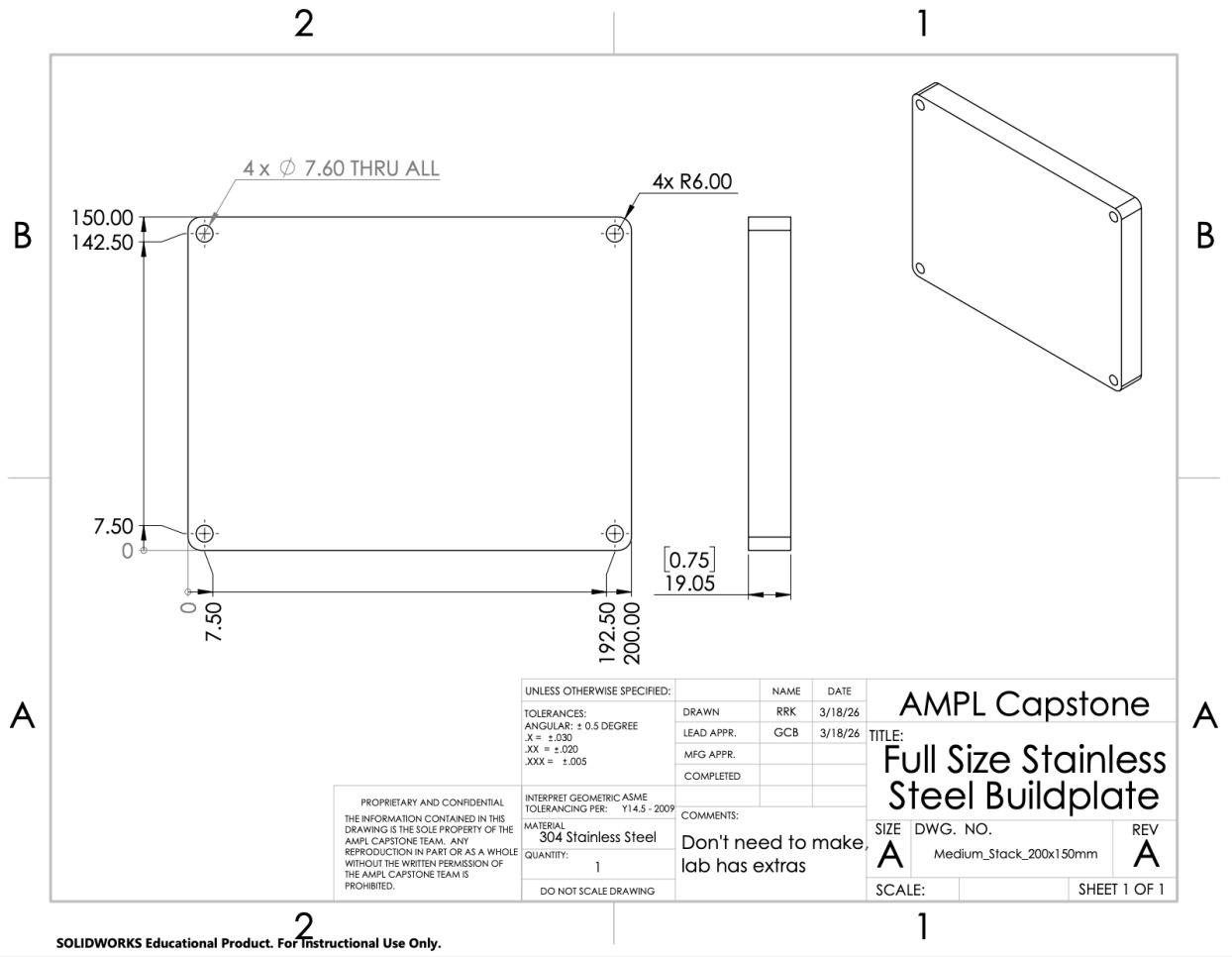

Figure D7: Full Size Stainless Steel Buildplate Drawing

Appendix E: CNC Setup Sheets

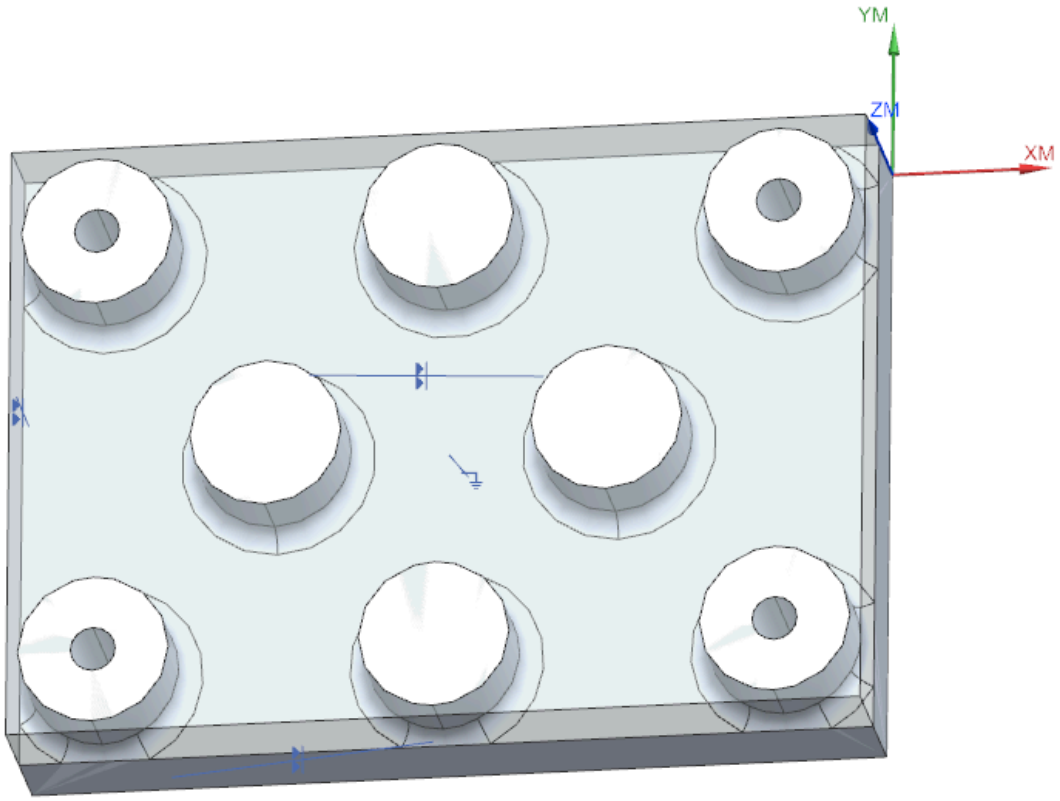

Figure E1: Standoff Plate Mini Design MCS Setup

Table E1: Standoff Plate Mini Design CNC Tool Table

Tool Number	Tool	Shortest Length
12	Spot Drill	0.23in
13	G Drill	1.31in
14	1in End Mill	0.59in
15	0.5in End Mill	0.62in
16	0.25in End Mill	0.56in
17	0.25in Ball Mill	0.68in

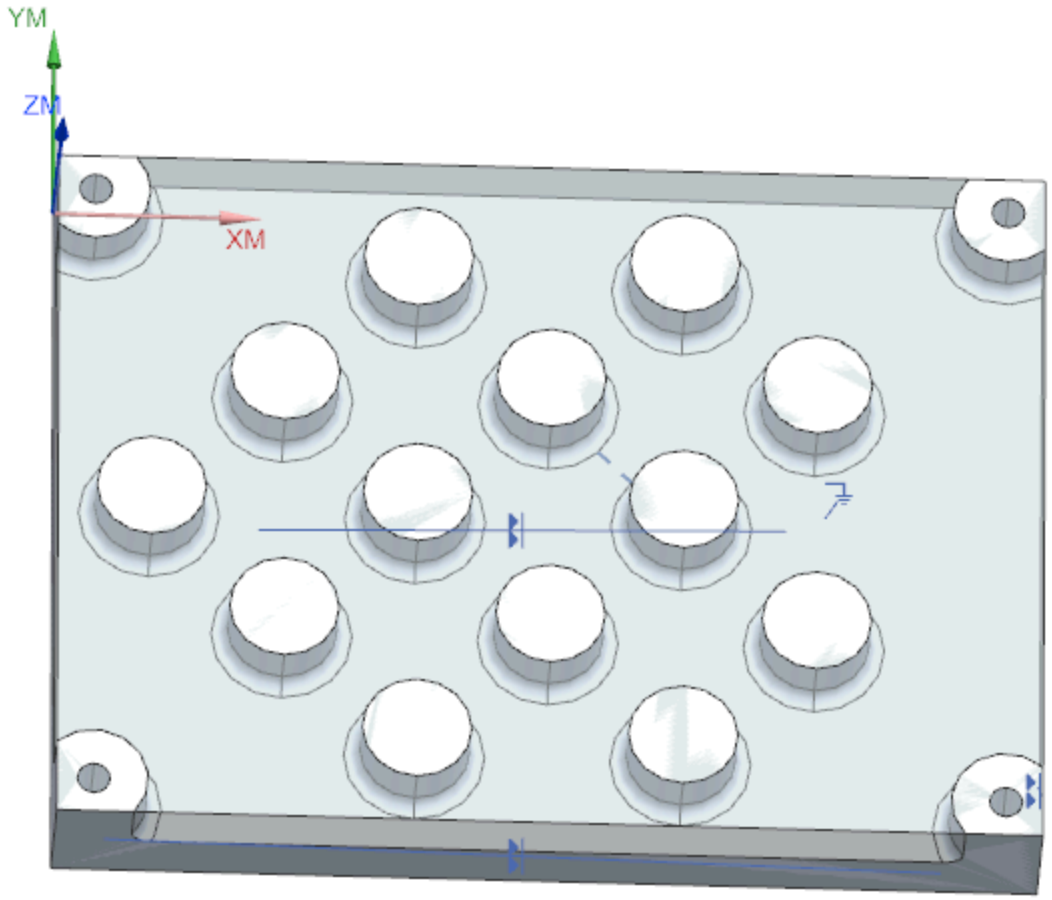

Figure E2: Standoff Plate Full Design MCS Setup

Table E2: Standoff Plate Full Design CNC Tool Table

Tool Number	Tool	Shortest Length
12	Spot Drill	0.23in
13	G Drill	1.31in
14	1in End Mill	0.59in
15	0.5in End Mill	0.59in
17	0.375in End Mill	0.52in
18	0.25in End Mill	0.57in
19	0.25in Ball Mill	0.61in

Appendix F: ANSYS DED Simulation G-Code

One Layer Linear Infill

%

(Snake raster through 150mm square, origin at center)

(Square bounds: X[-75,75], Y[-75,75])

(Line spacing: 2mm)

G21 (mm units)

G90 (absolute positioning)

G17 (XY plane)

F1000 (feed rate)

(Move to start position)

G0 X-75 Y-75; G1 X75 Y-75; G1 X75 Y-73; G1 X-75 Y-73; G1 X-75 Y-71; G1 X75 Y-71; G1 X75 Y-69; G1 X-75 Y-69; G1 X-75 Y-67; G1 X75 Y-67; G1 X75 Y-65; G1 X-75 Y-65; G1 X-75 Y-63; G1 X75 Y-63; G1 X75 Y-61; G1 X-75 Y-61; G1 X-75 Y-59; G1 X75 Y-59; G1 X75 Y-57; G1 X-75 Y-57; G1 X-75 Y-55; G1 X75 Y-55; G1 X75 Y-53; G1 X-75 Y-53; G1 X-75 Y-51; G1 X75 Y-51; G1 X75 Y-49; G1 X-75 Y-49; G1 X-75 Y-47; G1 X75 Y-47; G1 X75 Y-45; G1 X-75 Y-45; G1 X-75 Y-43; G1 X75 Y-43; G1 X75 Y-41; G1 X-75 Y-41; G1 X-75 Y-39; G1 X75 Y-39; G1 X75 Y-37; G1 X-75 Y-37; G1 X-75 Y-35; G1 X75 Y-35; G1 X75 Y-33; G1 X-75 Y-33; G1 X-75 Y-31; G1 X75 Y-31; G1 X75 Y-29; G1 X-75 Y-29; G1 X-75 Y-27; G1 X75 Y-27; G1 X75 Y-25; G1 X-75 Y-25; G1 X-75 Y-23; G1 X75 Y-23; G1 X75 Y-21; G1 X-75 Y-21; G1 X-75 Y-19; G1 X75 Y-19; G1 X75 Y-17; G1 X-75 Y-17; G1 X-75 Y-15; G1 X75 Y-15; G1 X75 Y-13; G1 X-75 Y-13; G1 X-75 Y-11; G1 X75 Y-11; G1 X75 Y-9; G1 X-75 Y-9; G1 X-75 Y-7; G1 X75 Y-7; G1 X75 Y-5; G1 X-75 Y-5; G1 X-75 Y-3; G1 X75 Y-3; G1 X75 Y-1; G1 X-75 Y-1; G1 X-75 Y1; G1 X75 Y1; G1 X75 Y3; G1 X-75 Y3; G1 X-75 Y5; G1 X75 Y5; G1 X75 Y7; G1 X-75 Y7; G1 X-75 Y9; G1 X75 Y9; G1 X75 Y11; G1 X-75 Y11; G1 X-75 Y13; G1 X75 Y13; G1 X75 Y15; G1 X-75 Y15; G1 X-75 Y17; G1 X75 Y17; G1 X75 Y19; G1 X-75 Y19; G1 X-75 Y21; G1 X75 Y21; G1 X75 Y23; G1 X-75 Y23; G1 X-75 Y25; G1 X75 Y25; G1 X75 Y27; G1 X-75 Y27; G1 X-75 Y29; G1 X75 Y29; G1 X75 Y31; G1 X-75 Y31; G1 X-75 Y33; G1 X75 Y33; G1 X75 Y35; G1 X-75 Y35; G1 X-75 Y37; G1 X75 Y37; G1 X75 Y39; G1 X-75 Y39; G1 X-75 Y41; G1 X75 Y41; G1 X75 Y43; G1 X-75 Y43; G1 X-75 Y45; G1 X75 Y45; G1 X75 Y47; G1 X-75 Y47; G1 X-75 Y49; G1 X75 Y49; G1 X75 Y51; G1 X-75 Y51; G1 X-75 Y53; G1 X75 Y53; G1 X75 Y55; G1 X-75 Y55; G1 X-75 Y57; G1 X75 Y57; G1 X75 Y59; G1 X-75 Y59; G1 X-75 Y61; G1 X75 Y61; G1 X75 Y63; G1 X-75 Y63; G1 X-75 Y65; G1 X75 Y65; G1 X75 Y67; G1 X-75 Y67; G1 X-75 Y69; G1 X75 Y69; G1 X75 Y71; G1 X-75 Y71; G1 X-75 Y73; G1 X75 Y73; G1 X75 Y75;

(End)

G0 X0 Y0

M30

%

Four Layer Diagonal Hatching Infill

G90; M83; G21; G92 X0 Y0 Z0; @TIME 0; G1 Y0.0000 F1000; G1 X-36.000 Z-36.000 F3010; M101; G1 X36.000 Z-36.000 E100.84057 F324; G1 X36.000 Z36.000 E100.84057; G1 X-36.000 Z36.000 E100.84057; G1 X-36.000 Z-36.000 E100.84057; M103; G1 X-37.000 Z-37.000 F3010; M101; G1 X37.000 Z-37.000 E103.64170 F267; G1 X37.000 Z37.000 E103.64170; G1 X-37.000 Z37.000 E103.64170; G1 X-37.000 Z-37.000 E103.64170; M103; G1 X34.196 Z-35.100 F3010; M101; G1 X35.100 Z-34.196 E1.61076 F405; G1 X35.100 Z-32.782 E1.78263; G1 X32.782 Z-35.100 E4.13177; G1 X31.368 Z-35.100 E1.78262; G1 X35.100 Z-31.368 E6.65278; G1 X35.100 Z-29.954 E1.78262; G1 X29.954 Z-35.100 E9.17380; G1 X28.540 Z-35.100 E1.78263; G1 X35.100 Z-28.540 E11.69481; G1 X35.100 Z-27.125 E1.78263; G1 X27.125 Z-35.100 E14.21583; G1 X25.711 Z-35.100 E1.78262; G1 X35.100 Z-25.711 E16.73684; G1 X35.100 Z-24.297 E1.78263; G1 X24.297

Z-35.100 E19.25785; G1 X22.883 Z-35.100 E1.78263; G1 X35.100 Z-22.883 E21.77887; G1 X35.100 Z-21.468 E1.78263; G1 X21.468 Z-35.100 E24.29988; G1 X20.054 Z-35.100 E1.78263; G1 X35.100 Z-20.054 E26.82090; G1 X35.100 Z-18.640 E1.78263; G1 X18.640 Z-35.100 E29.34192; G1 X17.226 Z-35.100 E1.78263; G1 X35.100 Z-17.226 E31.86294; G1 X35.100 Z-15.812 E1.78262; G1 X15.812 Z-35.100 E34.38394; G1 X14.397 Z-35.100 E1.78263; G1 X35.100 Z-14.397 E36.90496; G1 X35.100 Z-12.983 E1.78263; G1 X12.983 Z-35.100 E39.42597; G1 X11.569 Z-35.100 E1.78262; G1 X35.100 Z-11.569 E41.94698; G1 X35.100 Z-10.155 E1.78263; G1 X10.155 Z-35.100 E44.46799; G1 X8.741 Z-35.100 E1.78263; G1 X35.100 Z-8.741 E46.98901; G1 X35.100 Z-7.326 E1.78263; G1 X7.326 Z-35.100 E49.51003; G1 X5.912 Z-35.100 E1.78263; G1 X35.100 Z-5.912 E52.03105; G1 X35.100 Z-4.498 E1.78263; G1 X4.498 Z-35.100 E54.55206; G1 X3.084 Z-35.100 E1.78263; G1 X35.100 Z-3.084 E57.07308; G1 X35.100 Z-1.670 E1.78262; G1 X1.670 Z-35.100 E59.59408; G1 X0.255 Z-35.100 E1.78262; G1 X35.100 Z-0.255 E62.11509; G1 X35.100 Z1.159 E1.78263; G1 X-1.159 Z-35.100 E64.63612; G1 X-2.573 Z-35.100 E1.78262; G1 X35.100 Z2.573 E67.15712; G1 X35.100 Z3.987 E1.78263; G1 X-3.987 Z-35.100 E69.67814; G1 X-5.402 Z-35.100 E1.78263; G1 X35.100 Z5.402 E72.19915; G1 X35.100 Z6.816 E1.78263; G1 X-6.816 Z-35.100 E74.72017; G1 X-8.230 Z-35.100 E1.78263; G1 X35.100 Z8.230 E77.24119; G1 X35.100 Z9.644 E1.78263; G1 X-9.644 Z-35.100 E79.76221; G1 X-11.058 Z-35.100 E1.78262; G1 X35.100 Z11.058 E82.28322; G1 X35.100 Z12.473 E1.78262; G1 X-12.473 Z-35.100 E84.80423; G1 X-13.887 Z-35.100 E1.78263; G1 X35.100 Z13.887 E87.32524; G1 X35.100 Z15.301 E1.78263; G1 X-15.301 Z-35.100 E89.84626; G1 X-16.715 Z-35.100 E1.78262; G1 X35.100 Z16.715 E92.36727; G1 X35.100 Z18.129 E1.78263; G1 X-18.129 Z-35.100 E94.88828; G1 X-19.544 Z-35.100 E1.78262; G1 X35.100 Z19.544 E97.40930; G1 X35.100 Z20.958 E1.78263; G1 X-20.958 Z-35.100 E99.93031; G1 X-22.372 Z-35.100 E1.78263; G1 X35.100 Z22.372 E102.45133; G1 X35.100 Z23.786 E1.78263; G1 X-23.786 Z-35.100 E104.97235; G1 X-25.201 Z-35.100 E1.78263; G1 X35.100 Z25.201 E107.49336; G1 X35.100 Z26.615 E1.78262; G1 X-26.615 Z-35.100 E110.01437; G1 X-28.029 Z-35.100 E1.78263; G1 X35.100 Z28.029 E112.53539; G1 X35.100 Z29.443 E1.78263; G1 X-29.443 Z-35.100 E115.05640; G1 X-30.857 Z-35.100 E1.78262; G1 X35.100 Z30.857 E117.57742; G1 X35.100 Z32.272 E1.78262; G1 X-32.272 Z-35.100 E120.09843; G1 X-33.686 Z-35.100 E1.78263; G1 X35.100 Z33.686 E122.61945; G1 X35.100 Z35.100 E1.78263; G1 X-35.100 Z-35.100 E125.14027; G1 X-35.100 Z-33.686 E1.78263; G1 X33.686 Z35.100 E122.61925; G1 X32.272 Z35.100 E1.78263; G1 X-35.100 Z-32.272 E120.09824; G1 X-35.100 Z-30.857 E1.78264; G1 X30.857 Z35.100 E117.57722; G1 X29.443 Z35.100 E1.78262; G1 X-35.100 Z-29.443 E115.05621; G1 X-35.100 Z-28.029 E1.78263; G1 X28.029 Z35.100 E112.53520; G1 X26.615 Z35.100 E1.78263; G1 X-35.100 Z-26.615 E110.01418; G1 X-35.100 Z-25.200 E1.78262; G1 X25.200 Z35.100 E107.49316; G1 X23.786 Z35.100 E1.78262; G1 X-35.100 Z-23.786 E104.97215; G1 X-35.100 Z-22.372 E1.78263; G1 X22.372 Z35.100 E102.45114; G1 X20.958 Z35.100 E1.78263; G1 X-35.100 Z-20.958 E99.93012; G1 X-35.100 Z-19.544 E1.78263; G1 X19.544 Z35.100 E97.40911; G1 X18.129 Z35.100 E1.78263; G1 X-35.100 Z-18.129 E94.88809; G1 X-35.100 Z-16.715 E1.78263; G1 X16.715 Z35.100 E92.36708; G1 X15.301 Z35.100 E1.78263; G1 X-35.100 Z-15.301 E89.84606; G1 X-35.100 Z-13.887 E1.78262; G1 X13.887 Z35.100 E87.32505; G1 X12.473 Z35.100 E1.78263; G1 X-35.100 Z-12.473 E84.80404; G1 X-35.100 Z-11.058 E1.78263; G1 X11.058 Z35.100 E82.28302; G1 X9.644 Z35.100 E1.78262; G1 X-35.100 Z-9.644 E79.76201; G1 X-35.100 Z-8.230 E1.78263; G1 X8.230 Z35.100 E77.24100; G1 X6.816 Z35.100 E1.78263; G1 X-35.100 Z-6.816 E74.71998; G1 X-35.100 Z-5.401 E1.78263; G1 X5.401 Z35.100 E72.19896; G1 X3.987 Z35.100 E1.78263; G1 X-35.100 Z-3.987 E69.67795; G1 X-35.100 Z-2.573 E1.78263; G1 X2.573 Z35.100 E67.15693; G1 X1.159 Z35.100 E1.78263; G1 X-35.100 Z-1.159 E64.63591; G1 X-35.100 Z0.255 E1.78263; G1 X-0.255 Z35.100 E62.11490; G1 X-1.670 Z35.100 E1.78263; G1 X-35.100 Z1.670 E59.59389; G1 X-35.100 Z3.084 E1.78263; G1 X-3.084 Z35.100 E57.07288; G1 X-4.498 Z35.100 E1.78262; G1 X-35.100 Z4.498 E54.55187; G1 X-35.100 Z5.912 E1.78263; G1 X-5.912 Z35.100 E52.03085; G1 X-7.326 Z35.100 E1.78263; G1 X-35.100 Z7.326 E49.50984; G1 X-35.100 Z8.741 E1.78263; G1 X-8.741 Z35.100 E46.98882; G1 X-10.155 Z35.100 E1.78262; G1 X-35.100 Z10.155 E44.46781; G1 X-35.100 Z11.569 E1.78263; G1 X-11.569 Z35.100 E41.94679; G1 X-12.983 Z35.100 E1.78263; G1 X-35.100 Z12.983 E39.42577; G1 X-35.100 Z14.398 E1.78262; G1 X-14.398 Z35.100 E36.90477; G1 X-15.812 Z35.100 E1.78263; G1 X-35.100 Z15.812 E34.38375; G1 X-35.100 Z17.226 E1.78263; G1 X-17.226 Z35.100 E31.86273; G1 X-18.640 Z35.100 E1.78262; G1 X-35.100 Z18.640 E29.34172; G1 X-35.100 Z20.054 E1.78262; G1 X-20.054 Z35.100 E26.82071; G1 X-21.469 Z35.100 E1.78263; G1 X-35.100 Z21.469 E24.29969; G1 X-35.100 Z22.883 E1.78263; G1 X-22.883 Z35.100 E21.77868; G1 X-24.297 Z35.100 E1.78262; G1 X-35.100 Z24.297 E19.25766; G1 X-35.100 Z25.711 E1.78263; G1 X-25.711 Z35.100 E16.73664; G1 X-27.125 Z35.100 E1.78262; G1 X-35.100 Z27.125 E14.21564; G1 X-35.100 Z28.540 E1.78263; G1 X-28.540 Z35.100 E11.69462; G1 X-29.954 Z35.100 E1.78263; G1 X-35.100 Z29.954 E9.17361; G1 X-35.100 Z31.368 E1.78263; G1 X-31.368 Z35.100 E6.65259; G1 X-32.782 Z35.100 E1.78263; G1 X-35.100 Z32.782 E4.13157; G1 X-35.100 Z34.197 E1.78262; G1 X-34.197 Z35.100 E1.61057; M103; G1 Y1.0000 F1000; G1 X-36.000 Z36.000 F3010; M101; G1 X-36.000 Z-36.000 E100.84057 F360; G1 X36.000 Z-36.000 E100.84057; G1 X36.000 Z36.000 E100.84057; G1 X-36.000 Z36.000 E100.84057; M103; G1 X-37.000 Z37.000 F3010; M101; G1 X-37.000 Z-37.000 E103.64170 F297; G1 X37.000 Z-37.000 E103.64170; G1 X37.000 Z37.000 E103.64170; G1 X-37.000 Z37.000 E103.64170; M103; G1 X-35.100 Z-34.196 F3010; M101; G1 X-34.196 Z-35.100 E1.61100 F450; G1 X-32.782 Z-35.100 E1.78263; G1 X-35.100 Z-32.782 E4.13202; G1 X-35.100 Z-31.368 E1.78262; G1 X-31.368 Z-35.100 E6.65303; G1 X-29.954 Z-35.100 E1.78263; G1 X-35.100 Z-29.954 E9.17405; G1 X-35.100 Z-28.539 E1.78262; G1 X-28.539 Z-35.100 E11.69506; G1 X-27.125 Z-35.100 E1.78262; G1 X-35.100 Z-27.125 E14.21607; G1 X-35.100 Z-25.711 E1.78263; G1 X-25.711 Z-35.100 E16.73709; G1 X-24.297 Z-35.100 E1.78263; G1 X-35.100 Z-24.297 E19.25811; G1 X-35.100 Z-22.883 E1.78262; G1 X-22.883 Z-35.100 E21.77912; G1 X-21.468 Z-35.100 E1.78262; G1 X-35.100 Z-21.468 E24.30013; G1 X-35.100 Z-20.054 E1.78262; G1 X-20.054 Z-35.100 E26.82115; G1 X-18.640 Z-35.100 E1.78263; G1 X-35.100 Z-18.640 E29.34216; G1 X-35.100 Z-17.226 E1.78263; G1 X-17.226 Z-35.100

E31.86318; G1 X-15.811 Z-35.100 E1.78262; G1 X-35.100 Z-15.811 E34.38419; G1 X-35.100 Z-14.397 E1.78263; G1 X-14.397 Z-35.100 E36.90521; G1 X-12.983 Z-35.100 E1.78263; G1 X-35.100 Z-12.983 E39.42622; G1 X-35.100 Z-11.569 E1.78263; G1 X-11.569 Z-35.100 E41.94724; G1 X-10.155 Z-35.100 E1.78263; G1 X-35.100 Z-10.155 E44.46825; G1 X-35.100 Z-8.740 E1.78262; G1 X-8.740 Z-35.100 E46.98926; G1 X-7.326 Z-35.100 E1.78263; G1 X-35.100 Z-7.326 E49.51027; G1 X-35.100 Z-5.912 E1.78263; G1 X-5.912 Z-35.100 E52.03129; G1 X-4.498 Z-35.100 E1.78263; G1 X-35.100 Z-4.498 E54.55231; G1 X-35.100 Z-3.084 E1.78263; G1 X-3.084 Z-35.100 E57.07332; G1 X-1.669 Z-35.100 E1.78263; G1 X-35.100 Z-1.669 E59.59434; G1 X-35.100 Z-0.255 E1.78263; G1 X-0.255 Z-35.100 E62.11536; G1 X1.159 Z-35.100 E1.78262; G1 X-35.100 Z1.159 E64.63637; G1 X-35.100 Z2.573 E1.78262; G1 X2.573 Z-35.100 E67.15738; G1 X3.987 Z-35.100 E1.78263; G1 X-35.100 Z3.987 E69.67840; G1 X-35.100 Z5.402 E1.78262; G1 X5.402 Z-35.100 E72.19940; G1 X6.816 Z-35.100 E1.78263; G1 X-35.100 Z6.816 E74.72042; G1 X-35.100 Z8.230 E1.78263; G1 X8.230 Z-35.100 E77.24143; G1 X9.644 Z-35.100 E1.78263; G1 X-35.100 Z9.644 E79.76245; G1 X-35.100 Z11.059 E1.78263; G1 X11.059 Z-35.100 E82.28347; G1 X12.473 Z-35.100 E1.78263; G1 X-35.100 Z12.473 E84.80448; G1 X-35.100 Z13.887 E1.78263; G1 X13.887 Z-35.100 E87.32550; G1 X15.301 Z-35.100 E1.78262; G1 X-35.100 Z15.301 E89.84650; G1 X-35.100 Z16.715 E1.78263; G1 X16.715 Z-35.100 E92.36753; G1 X18.130 Z-35.100 E1.78262; G1 X-35.100 Z18.130 E94.88854; G1 X-35.100 Z19.544 E1.78263; G1 X19.544 Z-35.100 E97.40955; G1 X20.958 Z-35.100 E1.78263; G1 X-35.100 Z20.958 E99.93056; G1 X-35.100 Z22.372 E1.78263; G1 X22.372 Z-35.100 E102.45158; G1 X23.786 Z-35.100 E1.78263; G1 X-35.100 Z23.786 E104.97259; G1 X-35.100 Z25.201 E1.78263; G1 X25.201 Z-35.100 E107.49361; G1 X26.615 Z-35.100 E1.78263; G1 X-35.100 Z26.615 E110.01463; G1 X-35.100 Z28.029 E1.78262; G1 X28.029 Z-35.100 E112.53564; G1 X29.443 Z-35.100 E1.78262; G1 X-35.100 Z29.443 E115.05665; G1 X-35.100 Z30.858 E1.78263; G1 X30.858 Z-35.100 E117.57766; G1 X32.272 Z-35.100 E1.78263; G1 X-35.100 Z32.272 E120.09868; G1 X-35.100 Z33.686 E1.78263; G1 X33.686 Z-35.100 E122.61970; G1 X35.100 Z-35.100 E1.78262; G1 X-35.100 Z35.100 E125.14002; G1 X-33.686 Z35.100 E1.78263; G1 X35.100 Z-33.686 E122.61900; G1 X35.100 Z-32.271 E1.78262; G1 X-32.271 Z35.100 E120.09799; G1 X-30.857 Z35.100 E1.78263; G1 X35.100 Z-30.857 E117.57697; G1 X35.100 Z-29.443 E1.78263; G1 X-29.443 Z35.100 E115.05595; G1 X-28.029 Z35.100 E1.78262; G1 X35.100 Z-28.029 E112.53494; G1 X35.100 Z-26.615 E1.78263; G1 X-26.615 Z35.100 E110.01393; G1 X-25.200 Z35.100 E1.78263; G1 X35.100 Z-25.200 E107.49291; G1 X35.100 Z-23.786 E1.78263; G1 X-23.786 Z35.100 E104.97190; G1 X-22.372 Z35.100 E1.78263; G1 X35.100 Z-22.372 E102.45088; G1 X35.100 Z-20.958 E1.78263; G1 X-20.958 Z35.100 E99.92987; G1 X-19.543 Z35.100 E1.78262; G1 X35.100 Z-19.543 E97.40885; G1 X35.100 Z-18.129 E1.78262; G1 X-18.129 Z35.100 E94.88784; G1 X-16.715 Z35.100 E1.78263; G1 X35.100 Z-16.715 E92.36682; G1 X35.100 Z-15.301 E1.78263; G1 X-15.301 Z35.100 E89.84581; G1 X-13.887 Z35.100 E1.78263; G1 X35.100 Z-13.887 E87.32479; G1 X35.100 Z-12.472 E1.78263; G1 X-12.472 Z35.100 E84.80378; G1 X-11.058 Z35.100 E1.78262; G1 X35.100 Z-11.058 E82.28276; G1 X35.100 Z-9.644 E1.78262; G1 X-9.644 Z35.100 E79.76175; G1 X-8.230 Z35.100 E1.78262; G1 X35.100 Z-8.230 E77.24074; G1 X35.100 Z-6.816 E1.78263; G1 X-6.816 Z35.100 E74.71972; G1 X-5.401 Z35.100 E1.78263; G1 X35.100 Z-5.401 E72.19871; G1 X35.100 Z-3.987 E1.78263; G1 X-3.987 Z35.100 E69.67770; G1 X-2.573 Z35.100 E1.78263; G1 X35.100 Z-2.573 E67.15668; G1 X35.100 Z-1.159 E1.78263; G1 X-1.159 Z35.100 E64.63567; G1 X0.256 Z35.100 E1.78263; G1 X35.100 Z0.256 E62.11465; G1 X35.100 Z1.670 E1.78263; G1 X1.670 Z35.100 E59.59363; G1 X3.084 Z35.100 E1.78263; G1 X35.100 Z3.084 E57.07262; G1 X35.100 Z4.498 E1.78263; G1 X4.498 Z35.100 E54.55160; G1 X5.912 Z35.100 E1.78263; G1 X35.100 Z5.912 E52.03058; G1 X35.100 Z7.327 E1.78263; G1 X7.327 Z35.100 E49.50957; G1 X8.741 Z35.100 E1.78262; G1 X35.100 Z8.741 E46.98856; G1 X35.100 Z10.155 E1.78264; G1 X10.155 Z35.100 E44.46754; G1 X11.569 Z35.100 E1.78263; G1 X35.100 Z11.569 E41.94653; G1 X35.100 Z12.983 E1.78262; G1 X12.983 Z35.100 E39.42552; G1 X14.398 Z35.100 E1.78262; G1 X35.100 Z14.398 E36.90450; G1 X35.100 Z15.812 E1.78262; G1 X15.812 Z35.100 E34.38349; G1 X17.226 Z35.100 E1.78263; G1 X35.100 Z17.226 E31.86247; G1 X35.100 Z18.640 E1.78263; G1 X18.640 Z35.100 E29.34146; G1 X20.055 Z35.100 E1.78263; G1 X35.100 Z20.055 E26.82044; G1 X35.100 Z21.469 E1.78263; G1 X21.469 Z35.100 E24.29942; G1 X22.883 Z35.100 E1.78263; G1 X35.100 Z22.883 E21.77841; G1 X35.100 Z24.297 E1.78263; G1 X24.297 Z35.100 E19.25740; G1 X25.711 Z35.100 E1.78263; G1 X35.100 Z25.711 E16.73638; G1 X35.100 Z27.126 E1.78263; G1 X27.126 Z35.100 E14.21537; G1 X28.540 Z35.100 E1.78263; G1 X35.100 Z28.540 E11.69435; G1 X35.100 Z29.954 E1.78262; G1 X29.954 Z35.100 E9.17334; G1 X31.368 Z35.100 E1.78263; G1 X35.100 Z31.368 E6.65232; G1 X35.100 Z32.782 E1.78262; G1 X32.782 Z35.100 E4.13131; G1 X34.197 Z35.100 E1.78263; G1 X35.100 Z34.197 E1.61030; M103; G1 Y2.0000 F1000; G1 X36.000 Z36.000 F3010; M101; G1 X-36.000 Z36.000 E100.84057 F360; G1 X-36.000 Z-36.000 E100.84057; G1 X36.000 Z-36.000 E100.84057; G1 X36.000 Z36.000 E100.84057; M103; G1 X37.000 Z37.000 F3010; M101; G1 X-37.000 Z37.000 E103.64170 F297; G1 X-37.000 Z-37.000 E103.64170; G1 X37.000 Z-37.000 E103.64170; G1 X37.000 Z37.000 E103.64170; M103; G1 X-34.197 Z35.100 F3010; M101; G1 X-35.100 Z34.197 E1.61057 F450; G1 X-35.100 Z32.782 E1.78262; G1 X-32.782 Z35.100 E4.13157; G1 X-31.368 Z35.100 E1.78263; G1 X-35.100 Z31.368 E6.65259; G1 X-35.100 Z29.954 E1.78263; G1 X-29.954 Z35.100 E9.17361; G1 X-28.540 Z35.100 E1.78263; G1 X-35.100 Z28.540 E11.69462; G1 X-35.100 Z27.125 E1.78263; G1 X-27.125 Z35.100 E14.21564; G1 X-25.711 Z35.100 E1.78262; G1 X-35.100 Z25.711 E16.73664; G1 X-35.100 Z24.297 E1.78263; G1 X-24.297 Z35.100 E19.25766; G1 X-22.883 Z35.100 E1.78262; G1 X-35.100 Z22.883 E21.77868; G1 X-35.100 Z21.469 E1.78263; G1 X-21.469 Z35.100 E24.29969; G1 X-20.054 Z35.100 E1.78263; G1 X-35.100 Z20.054 E26.82071; G1 X-35.100 Z18.640 E1.78262; G1 X-18.640 Z35.100 E29.34172; G1 X-17.226 Z35.100 E1.78262; G1 X-35.100 Z17.226 E31.86273; G1 X-35.100 Z15.812 E1.78262; G1 X-15.812 Z35.100 E34.38375; G1 X-14.398 Z35.100 E1.78263; G1 X-35.100 Z14.398 E36.90477; G1 X-35.100 Z12.983 E1.78262; G1 X-12.983 Z35.100 E39.42577; G1 X-11.569 Z35.100 E1.78263; G1 X-35.100 Z11.569 E41.94679; G1 X-35.100 Z10.155 E1.78263; G1 X-10.155 Z35.100 E44.46781; G1 X-8.741 Z35.100 E1.78262; G1

X-35.100 Z8.741 E49.50984; G1 X-35.100 Z7.326 E1.78263; G1 X-7.326 Z35.100 E52.03085; G1 X-5.912 Z35.100 E1.78263; G1 X-35.100 Z5.912 E54.55187; G1 X-35.100 Z4.498 E1.78262; G1 X-4.498 Z35.100 E57.07288; G1 X-3.084 Z35.100 E1.78263; G1 X-35.100 Z3.084 E59.59389; G1 X-35.100 Z1.670 E1.78263; G1 X-1.670 Z35.100 E62.11490; G1 X-0.255 Z35.100 E1.78263; G1 X-35.100 Z0.255 E64.63591; G1 X-35.100 Z-1.159 E1.78263; G1 X1.159 Z35.100 E67.15693; G1 X2.573 Z35.100 E1.78263; G1 X-35.100 Z-2.573 E69.67795; G1 X-35.100 Z-3.987 E1.78263; G1 X3.987 Z35.100 E72.19896; G1 X5.401 Z35.100 E1.78263; G1 X-35.100 Z-5.401 E74.71998; G1 X-35.100 Z-6.816 E1.78263; G1 X6.816 Z35.100 E77.24100; G1 X8.230 Z35.100 E1.78263; G1 X-35.100 Z-8.230 E79.76201; G1 X-35.100 Z-9.644 E1.78263; G1 X9.644 Z35.100 E82.28302; G1 X11.058 Z35.100 E1.78262; G1 X-35.100 Z-11.058 E84.80404; G1 X-35.100 Z-12.473 E1.78263; G1 X12.473 Z35.100 E87.32505; G1 X13.887 Z35.100 E1.78263; G1 X-35.100 Z-13.887 E89.84606; G1 X-35.100 Z-15.301 E1.78262; G1 X15.301 Z35.100 E92.36708; G1 X16.715 Z35.100 E1.78263; G1 X-35.100 Z-16.715 E94.88809; G1 X-35.100 Z-18.129 E1.78263; G1 X18.129 Z35.100 E97.40911; G1 X19.544 Z35.100 E1.78263; G1 X-35.100 Z-19.544 E99.93012; G1 X-35.100 Z-20.958 E1.78263; G1 X20.958 Z35.100 E102.45114; G1 X22.372 Z35.100 E1.78263; G1 X-35.100 Z-22.372 E104.97215; G1 X-35.100 Z-23.786 E1.78262; G1 X23.786 Z35.100 E107.49316; G1 X25.200 Z35.100 E1.78262; G1 X-35.100 Z-25.200 E110.01418; G1 X-35.100 Z-26.615 E1.78263; G1 X26.615 Z35.100 E112.53520; G1 X28.029 Z35.100 E1.78263; G1 X-35.100 Z-28.029 E115.05621; G1 X-35.100 Z-29.443 E1.78262; G1 X29.443 Z35.100 E117.57722; G1 X30.857 Z35.100 E1.78264; G1 X-35.100 Z-30.857 E120.09824; G1 X-35.100 Z-32.272 E1.78263; G1 X32.272 Z35.100 E122.61925; G1 X33.686 Z35.100 E1.78263; G1 X-35.100 Z-33.686 E125.14027; G1 X-35.100 Z-35.100 E1.78263; G1 X-33.686 Z-35.100 E122.61945; G1 X-32.272 Z-35.100 E1.78263; G1 X35.100 Z33.686 E120.09843; G1 X35.100 Z32.272 E1.78262; G1 X-30.857 Z-35.100 E117.57742; G1 X-29.443 Z-35.100 E1.78262; G1 X35.100 Z30.857 E115.05640; G1 X35.100 Z29.443 E1.78263; G1 X-28.029 Z-35.100 E112.53539; G1 X-26.615 Z-35.100 E1.78263; G1 X35.100 Z28.029 E110.01437; G1 X35.100 Z26.615 E1.78262; G1 X-25.201 Z-35.100 E107.49336; G1 X-23.786 Z-35.100 E1.78263; G1 X35.100 Z25.201 E104.97235; G1 X35.100 Z23.786 E1.78263; G1 X-22.372 Z-35.100 E102.45133; G1 X-20.958 Z-35.100 E1.78263; G1 X35.100 Z22.372 E99.93031; G1 X35.100 Z20.958 E1.78263; G1 X-19.544 Z-35.100 E97.40930; G1 X-18.129 Z-35.100 E1.78262; G1 X35.100 Z19.544 E94.88828; G1 X35.100 Z18.129 E1.78263; G1 X-16.715 Z-35.100 E92.36727; G1 X-15.301 Z-35.100 E1.78262; G1 X35.100 Z16.715 E89.84626; G1 X35.100 Z15.301 E1.78263; G1 X-13.887 Z-35.100 E87.32524; G1 X-12.473 Z-35.100 E1.78263; G1 X35.100 Z13.887 E84.80423; G1 X35.100 Z12.473 E1.78262; G1 X-11.058 Z-35.100 E82.28322; G1 X-9.644 Z-35.100 E1.78262; G1 X35.100 Z11.058 E79.76221; G1 X35.100 Z9.644 E1.78263; G1 X-8.230 Z-35.100 E77.24119; G1 X-6.816 Z-35.100 E1.78263; G1 X35.100 Z8.230 E74.72017; G1 X35.100 Z6.816 E1.78263; G1 X-5.402 Z-35.100 E72.19915; G1 X-3.987 Z-35.100 E1.78263; G1 X35.100 Z5.402 E69.67814; G1 X35.100 Z3.987 E1.78263; G1 X-2.573 Z-35.100 E67.15712; G1 X-1.159 Z-35.100 E1.78262; G1 X35.100 Z2.573 E64.63612; G1 X35.100 Z1.159 E1.78263; G1 X0.255 Z-35.100 E62.11509; G1 X1.670 Z-35.100 E1.78262; G1 X35.100 Z-0.255 E59.59408; G1 X35.100 Z-1.670 E1.78262; G1 X3.084 Z-35.100 E57.07308; G1 X4.498 Z-35.100 E1.78262; G1 X35.100 Z-3.084 E54.55206; G1 X35.100 Z-4.498 E1.78263; G1 X5.912 Z-35.100 E52.03105; G1 X7.326 Z-35.100 E1.78263; G1 X35.100 Z-5.912 E49.51003; G1 X35.100 Z-7.326 E1.78263; G1 X8.741 Z-35.100 E46.98901; G1 X10.155 Z-35.100 E1.78263; G1 X35.100 Z-8.741 E44.46799; G1 X35.100 Z-10.155 E1.78263; G1 X11.569 Z-35.100 E41.94698; G1 X12.983 Z-35.100 E1.78262; G1 X35.100 Z-11.569 E39.42597; G1 X35.100 Z-12.983 E1.78263; G1 X14.397 Z-35.100 E36.90496; G1 X15.812 Z-35.100 E1.78263; G1 X35.100 Z-14.397 E34.38394; G1 X35.100 Z-15.812 E1.78262; G1 X17.226 Z-35.100 E31.86294; G1 X18.640 Z-35.100 E1.78263; G1 X35.100 Z-17.226 E29.34192; G1 X35.100 Z-18.640 E1.78263; G1 X20.054 Z-35.100 E26.82090; G1 X21.468 Z-35.100 E1.78263; G1 X35.100 Z-20.054 E24.29988; G1 X35.100 Z-21.468 E1.78263; G1 X22.883 Z-35.100 E21.77887; G1 X24.297 Z-35.100 E1.78263; G1 X35.100 Z-22.883 E19.25785; G1 X35.100 Z-24.297 E1.78263; G1 X25.711 Z-35.100 E16.73684; G1 X27.125 Z-35.100 E1.78262; G1 X35.100 Z-25.711 E14.21583; G1 X35.100 Z-27.125 E1.78263; G1 X28.540 Z-35.100 E11.69481; G1 X29.954 Z-35.100 E1.78263; G1 X35.100 Z-28.540 E9.17380; G1 X35.100 Z-29.954 E1.78262; G1 X31.368 Z-35.100 E6.65278; G1 X32.782 Z-35.100 E1.78262; G1 X35.100 Z-31.368 E4.13177; G1 X35.100 Z-32.782 E1.78263; G1 X34.196 Z-35.100 E1.61076; M103; G1 Y3.0000 F1000; G1 X36.000 Z-36.000 F3010; M101; G1 X36.000 Z36.000 E100.84057 F360; G1 X-36.000 Z36.000 E100.84057; G1 X-36.000 Z-36.000 E100.84057; G1 X36.000 Z-36.000 E100.84057; M103; G1 X37.000 Z-37.000 F3010; M101; G1 X37.000 Z37.000 E103.64170 F297; G1 X-37.000 Z37.000 E103.64170; G1 X-37.000 Z-37.000 E103.64170; G1 X37.000 Z-37.000 E103.64170; M103; G1 X35.100 Z34.197 F3010; M101; G1 X34.197 Z35.100 E1.61030 F450; G1 X32.782 Z35.100 E1.78263; G1 X35.100 Z32.782 E4.13131; G1 X35.100 Z31.368 E1.78262; G1 X31.368 Z35.100 E6.65232; G1 X29.954 Z35.100 E1.78263; G1 X35.100 Z29.954 E9.17334; G1 X35.100 Z28.540 E1.78262; G1 X28.540 Z35.100 E11.69435; G1 X27.126 Z35.100 E1.78263; G1 X35.100 Z27.126 E14.21537; G1 X35.100 Z25.711 E1.78263; G1 X25.711 Z35.100 E16.73664; G1 X24.297 Z35.100 E1.78263; G1 X35.100 Z24.297 E19.25740; G1 X35.100 Z22.883 E1.78263; G1 X22.883 Z35.100 E21.77841; G1 X21.469 Z35.100 E1.78263; G1 X35.100 Z21.469 E24.29942; G1 X35.100 Z20.055 E1.78263; G1 X20.055 Z35.100 E26.82044; G1 X18.640 Z35.100 E1.78263; G1 X35.100 Z18.640 E29.34146; G1 X35.100 Z17.226 E1.78263; G1 X17.226 Z35.100 E31.86247; G1 X15.812 Z35.100 E1.78263; G1 X35.100 Z15.812 E34.38349; G1 X35.100 Z14.398 E1.78262; G1 X14.398 Z35.100 E36.90450; G1 X12.983 Z35.100 E1.78262; G1 X35.100 Z12.983 E39.42552; G1 X35.100 Z11.569 E1.78262; G1 X11.569 Z35.100 E41.94653; G1 X10.155 Z35.100 E1.78263; G1 X35.100 Z10.155 E44.46754; G1 X35.100 Z8.741 E1.78264; G1 X8.741 Z35.100 E46.98856; G1 X7.327 Z35.100 E1.78262; G1 X35.100 Z7.327 E49.50957; G1 X35.100 Z5.912 E1.78263; G1 X5.912 Z35.100 E52.03058; G1 X4.498 Z35.100 E1.78263; G1 X35.100 Z4.498 E54.55160; G1 X35.100 Z3.084 E1.78263; G1 X3.084 Z35.100 E57.07262; G1 X1.670 Z35.100 E1.78263; G1 X35.100 Z1.670 E59.59363; G1 X35.100 Z0.256 E1.78263; G1 X-0.256 Z35.100 E62.11465; G1 X-1.670 Z35.100 E1.78263; G1

X35.100 Z-1.670 E59.59389; G1 X35.100 Z-3.084 E1.78263; G1 X-3.084 Z35.100 E57.07288; G1 X-4.498 Z35.100 E1.78262; G1 X35.100 Z-4.498 E54.55187; G1 X35.100 Z-5.912 E1.78263; G1 X-5.912 Z35.100 E52.03085; G1 X-7.326 Z35.100 E1.78263; G1 X35.100 Z-7.326 E49.50984; G1 X35.100 Z-8.741 E1.78263; G1 X-8.741 Z35.100 E46.98882; G1 X-10.155 Z35.100 E1.78262; G1 X35.100 Z-10.155 E44.46781; G1 X35.100 Z-11.569 E1.78263; G1 X-11.569 Z35.100 E41.94679; G1 X-12.983 Z35.100 E1.78263; G1 X35.100 Z-12.983 E39.42577; G1 X35.100 Z-14.398 E1.78262; G1 X-14.398 Z35.100 E36.90477; G1 X-15.812 Z35.100 E1.78263; G1 X35.100 Z-15.812 E34.38375; G1 X35.100 Z-17.226 E1.78263; G1 X-17.226 Z35.100 E31.86273; G1 X-18.640 Z35.100 E1.78262; G1 X35.100 Z-18.640 E29.34172; G1 X35.100 Z-20.054 E1.78263; G1 X-20.054 Z35.100 E26.82071; G1 X-21.469 Z35.100 E1.78263; G1 X35.100 Z-21.469 E24.29969; G1 X35.100 Z-22.883 E1.78262; G1 X-22.883 Z35.100 E21.77868; G1 X-24.297 Z35.100 E1.78262; G1 X35.100 Z-24.297 E19.25766; G1 X35.100 Z-25.711 E1.78263; G1 X-25.711 Z35.100 E16.73638; G1 X-27.125 Z35.100 E1.78263; G1 X35.100 Z-27.125 E14.21564; G1 X35.100 Z-28.540 E1.78263; G1 X-28.540 Z35.100 E11.69462; G1 X-29.954 Z35.100 E1.78263; G1 X35.100 Z-29.954 E9.17361; G1 X35.100 Z-31.368 E1.78263; G1 X-31.368 Z35.100 E6.65259; G1 X-32.782 Z35.100 E1.78263; G1 X35.100 Z-32.782 E4.13157; G1 X35.100 Z-34.197 E1.78262; G1 X-34.197 Z35.100 E1.61030; M103; G1 X35.100 Z-35.100 F3010; M101; G1 X33.686 Z-35.100 E1.78262; G1 X-35.100 Z33.686 E122.61970; G1 X-35.100 Z32.272 E1.78263; G1 X32.272 Z-35.100 E120.09868; G1 X30.858 Z-35.100 E1.78263; G1 X-35.100 Z30.858 E117.57766; G1 X-35.100 Z29.443 E1.78263; G1 X29.443 Z-35.100 E115.05665; G1 X28.029 Z-35.100 E1.78262; G1 X-35.100 Z28.029 E112.53564; G1 X-35.100 Z26.615 E1.78262; G1 X26.615 Z-35.100 E110.01463; G1 X25.201 Z-35.100 E1.78263; G1 X-35.100 Z25.201 E107.49361; G1 X-35.100 Z23.786 E1.78263; G1 X23.786 Z-35.100 E104.97259; G1 X22.372 Z-35.100 E1.78263; G1 X-35.100 Z22.372 E102.45158; G1 X-35.100 Z20.958 E1.78263; G1 X20.958 Z-35.100 E99.93056; G1 X19.544 Z-35.100 E1.78263; G1 X-35.100 Z19.544 E97.40955; G1 X-35.100 Z18.130 E1.78263; G1 X18.130 Z-35.100 E94.88854; G1 X16.715 Z-35.100 E1.78262; G1 X-35.100 Z16.715 E92.36753; G1 X-35.100 Z15.301 E1.78263; G1 X15.301 Z-35.100 E89.84650; G1 X13.887 Z-35.100 E1.78262; G1 X-35.100 Z13.887 E87.32550; G1 X-35.100 Z12.473 E1.78263; G1 X12.473 Z-35.100 E84.80448; G1 X11.059 Z-35.100 E1.78263; G1 X-35.100 Z11.059 E82.28347; G1 X-35.100 Z9.644 E1.78263; G1 X9.644 Z-35.100 E79.76245; G1 X8.230 Z-35.100 E1.78263; G1 X-35.100 Z8.230 E77.24143; G1 X-35.100 Z6.816 E1.78263; G1 X6.816 Z-35.100 E74.72042; G1 X5.402 Z-35.100 E1.78263; G1 X-35.100 Z5.402 E72.19940; G1 X-35.100 Z3.987 E1.78262; G1 X3.987 Z-35.100 E69.67840; G1 X2.573 Z-35.100 E1.78263; G1 X-35.100 Z2.573 E67.15738; G1 X-35.100 Z1.159 E1.78262; G1 X1.159 Z-35.100 E64.63637; G1 X-0.255 Z-35.100 E1.78262; G1 X-35.100 Z-0.255 E62.11536; G1 X-35.100 Z-1.669 E1.78263; G1 X-1.669 Z-35.100 E59.59434; G1 X-3.084 Z-35.100 E57.07332; G1 X-35.100 Z-3.084 E57.07332; G1 X-35.100 Z-4.498 E1.78263; G1 X-4.498 Z-35.100 E54.55231; G1 X-5.912 Z-35.100 E1.78263; G1 X-35.100 Z-5.912 E52.03129; G1 X-35.100 Z-7.326 E1.78263; G1 X-7.326 Z-35.100 E49.51027; G1 X-8.740 Z-35.100 E1.78263; G1 X-35.100 Z-8.740 E46.98926; G1 X-35.100 Z-10.155 E1.78262; G1 X-10.155 Z-35.100 E44.46825; G1 X-11.569 Z-35.100 E1.78263; G1 X-35.100 Z-11.569 E41.94724; G1 X-35.100 Z-12.983 E1.78263; G1 X-12.983 Z-35.100 E39.42622; G1 X-14.397 Z-35.100 E1.78263; G1 X-35.100 Z-14.397 E36.90521; G1 X-35.100 Z-15.811 E1.78263; G1 X-15.811 Z-35.100 E34.38419; G1 X-17.226 Z-35.100 E1.78262; G1 X-35.100 Z-17.226 E31.86318; G1 X-35.100 Z-18.640 E1.78263; G1 X-18.640 Z-35.100 E29.34216; G1 X-20.054 Z-35.100 E1.78263; G1 X-35.100 Z-20.054 E26.82115; G1 X-35.100 Z-21.468 E1.78262; G1 X-21.468 Z-35.100 E24.30013; G1 X-22.883 Z-35.100 E1.78262; G1 X-35.100 Z-22.883 E21.77912; G1 X-35.100 Z-24.297 E1.78262; G1 X-24.297 Z-35.100 E19.25811; G1 X-25.711 Z-35.100 E1.78263; G1 X-35.100 Z-25.711 E16.73609; G1 X-35.100 Z-27.125 E1.78263; G1 X-27.125 Z-35.100 E14.21607; G1 X-28.539 Z-35.100 E1.78262; G1 X-35.100 Z-28.539 E11.69506; G1 X-35.100 Z-29.954 E1.78262; G1 X-29.954 Z-35.100 E9.17405; G1 X-31.368 Z-35.100 E1.78263; G1 X-35.100 Z-31.368 E6.65303; G1 X-35.100 Z-32.782 E1.78262; G1 X-32.782 Z-35.100 E4.13202; G1 X-34.196 Z-35.100 E1.78263; G1 X-35.100 Z-34.196 E1.61100; M103; M103; G91; G1 Y20 F1000; G90; M30;